University of Cambridge

Reversible Directed Phase Transfer of $M_4^{II}L_4$ and $M_4^{II}L_6$ Cages

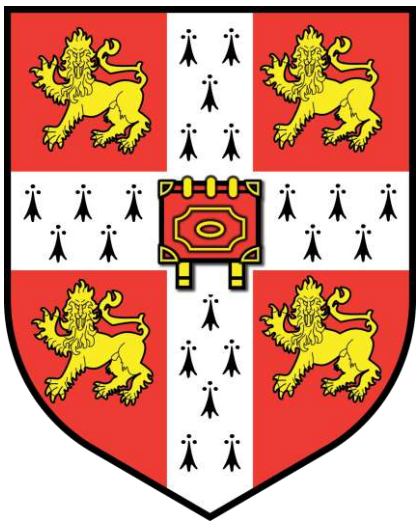

Maureen Claire Alma GEORGES

Darwin College

August 2017

A dissertation submitted to the University of Cambridge in partial fulfilment of the requirements for the degree of Master of Philosophy

Declaration

I hereby declare that this dissertation is the result of work that I have undertaken in the University Chemical Laboratory at the University of Cambridge between October 2016 and August 2017. Credit for results obtained through collaboration with other parties is referenced directly in the text and in the Acknowledgements section. Except where stated to the contrary, this dissertation is the result of my own work. This dissertation has not been, nor is currently being submitted for any other degree, diploma or other academic qualification at the University of Cambridge or any other University or similar institution, and does not exceed 15,000 words in length, as required by the degree committee.

Maureen Georges

August 2017

Acknowledgements

Firstly, I would like to thank my supervisor Prof. Jonathan Nitschke for inviting me to come to Cambridge as his student, where I have enjoyed a wonderful year.

Special thanks to Dr Arnaud Tron who spent a lot of his time teaching me. I really appreciated his gracious comport through the scientific and professional experiences we have had to overcome.

I would especially like to thank:

Angela Grommet for her guidance and kindness,

Alex Plajer for always cheering me up by turning on techno music in the bay,

Dr Edmundo Guzman-Percastegui for his support and wise advice throughout the year,

Marion Kieffer for her valuable and constructive suggestions as well as rowing discussions,

Duncan Howe for his gentle help and discussion about NMR experiments,

...but this list is non-exhaustive.

Total's "Bourse d'excellence" is acknowledged for funding this work.

Abstract

A major function assessed by Nature is the transport of a cargo between two different media, such as anions through cell membranes. Mimicking this function using complex systems is one of the biggest challenge of supramolecular chemistry. Metallo-organic cages are an important breakthrough in the encapsulation and transport of small molecules, providing a crucial platform for the development of systems chemistry.[1] Binding a network member within a tetrahedral cage allows it to be hidden and then revealed upon receipt of a release signal, or transported as a cargo between spatially distant parts of a network. Larger capsules may also isolate subsystems from each other in the manner of vesicles. These dynamic architectures are synthesised by self-assembly, which involves the simultaneous formation of multiple coordinative and dynamic covalent linkages during the same overall synthetic process.[2] Their shape and binding properties can be tuned by changing the subcomponents such as metals or ligands.

Great progress has been reported in recent years in the development of three-dimensional cages[3] that can interact with specific guest species, but there are limitations associated with the transport of these systems. Recent work by Nitschke et al.[4] have successfully addressed practical separations problems by transporting a tetrahedral cage and its cargo from water into an ionic liquid layer. However, this system is not ideal as the process is triggered by an anion exchange not by a direct stimulus.

This thesis reports the synthesis of an ionic liquid inspired tetrahedral system achieving reversible transport between water and an immiscible organic solvent driven by a change in temperature. Once the switchable capsules were obtained and characterised, their ability to move between different solvent phases upon heating was investigated. A capsule-mediated transport system as developed that is both directional and reversible. The flow of the capsule and its encapsulated cargo is directed using stimuli such as temperature modification. Ultimately an apparatus that allows the switchable capsules to move along a channel has been developed.

[1] Wilson, A.; Gasparini, G.; Matile, S. *Chem Soc Rev* **2014**, *43*, 1948.
[2] Nitschke, J.R. *Acc. Chem Res* **2007**, 40, 130.
[3] a) Pasquale, S.; Sattin, S.; Escudero-Adán, E.C.; Martínez-Belmonte, M.; de Mendoza, J. *Nat. Commun* **2012**, *3*, 785; b) Zhang, G.; Mastalerz, M. *Chem. Soc. Rev.* **2014**, *43*, 1934; c) Henkelis, J. J.; Carruthers, C.J.; Chambers, S.E.; Clowes, R.; Cooper, A.I. *et al. J. Am. Chem.Soc.* **2014**, *136*, 14393; d) Gütz, C.; Hovorka, R.; Klein, C.; Jiang, Q.-Q.; Bannwarth, C. *et al. Angew. Chem. Int. Ed.* **2014**, *53*, 1693.
[4] Grommet, A.; Nitschke, J. R. *J. Am. Chem. Soc.* **2017**, *139*, 2176.

Abbreviations

calcd	Calculated
CD_3CN	Deuterated acetonitrile
CDC	Constitutional dynamic chemistry
$CDCl_3$	Deuterated chloroform
CD_2Cl_2	Deuterated dichloromethane
CH_2Cl_2	Dichloromethane
$CHCl_3$	Chloroform
CH_3CN	Acetonitrile
C_2	2-fold rotational symmetry
C_3	3-fold rotational symmetry
COSY	Correlation spectroscopy
d	Doublet
dd	Doublet of doublets
D_2O	Deuterated water
DCL	Dynamic combinatorial library
DCM	Dichloromethane
DMF	Dimethylformamide
DOSY	Diffusion-ordered spectroscopy
eq.	Equivalents
ESI	Electrospray ionisation
Et	Ethyl
EtOAc	Ethyl acetate

EtOH	Ethanol
Et_2O	Diethyl Ether
g	Gram
h	Hour
HMBC	Heteronuclear multiple bond correlation
HPLC	High pressure liquid chromatography
KOH	Potassium hydroxide
HSQC	Heteronuclear single quantum coherence
Hz	Herz
J	Joules
K	Kelvin
LC-MS	Liquid chromatography-mass spectrometry
mL	Milliliter
mM	Millimolar
mmol	Millimole
Me	Methyl
MeOH	Methanol
MHz	Megahertz
min	Minute
MS	Mass spectrometry
m/z	Mass to charge ratio
PEG	Poly(ethylene) glycol
µL	Microlitre

µM	Micromolar
NMR	Nuclear magnetic resonance
NTf_2^-	Bis(trifluoromethylsulfonyl)amide anion
s	Singlet
t	Triplet
ppm	Parts per million
UV-vis	Ultra violet-visible
^oC	Degrees centigrade

Contents

1 – Introduction

1.1 Supramolecular chemistry and coordination cages

Multi-component systems, artificial or biological, rely on cooperation to be functional. Base pairs have few applications before they assemble into DNA; likewise, a circuit board cannot calculate an equation before being integrated into a computer. The assembly of pieces leads to function as a whole that can have a greater potential than its individual constituents. The way these components assemble consequently is crucial as it determines their purpose. The ability for molecules to cooperate, aggregate and combine allows them to achieve functions otherwise unachievable in their solitary state.

Traditionally defined as "chemistry beyond the molecule",[1] supramolecular chemistry explores the intramolecular and intermolecular interactions which lead to complex systems. Research in supramolecular chemistry draws much of its inspiration from nature and it is believed that a better understanding of this field will help solve some big questions that scientists face.

In 1894, Fischer proposed the lock and key model of enzyme-substrate binding[2] in which concepts of molecular recognition and host-guest chemistry are combined. However, the field of supramolecular chemistry truly emerged much later. Supramolecular chemistry developed rapidly after 1987 when the Nobel prize was awarded to Pedersen,[3] Cram[4] and Lehn[1] acknowledging their achievements and the importance of this area of science. More recently, Sauvage, Stoddart and Feringa were awarded the Nobel Prize in 2016 for their work on nanoscale molecular machines.[5]

It is important to know the complexities involved in self-assembly in order to create shapes for specific functions at a molecular level. Molecular cages are defined as any macromolecules possessing an internal cavity, with the possibility to host other molecules in its insides. These hosts can be either organic[6] or metal-organic[7] while the guests can be templating[8] or only stored[9]. The environments inside the cavity of the cages are interesting media in which reactions can occur[10] or be catalysed;[11] the cage can also act as a whole molecule protecting group[9] that prevents a reaction from occurring when a guest is encapsulated.

When dynamic reversible bonds are formed, the reaction will reach an equilibrium with time. The bonds formed are then under thermodynamic control and will generally lead to the thermodynamic product. The one with the lowest free energy will be obtained in case the mixture contains several compounds that can react reversibly. The composition may be influenced by external factors as structural groups can be rearranged and exchanged in solution in Constitutional Dynamic Chemistry (CDC) systems. This interchange of components is key to the self-assembly of large structures.[12]

Dynamic combinatorial chemistry (DCC) uses reversible covalent bond forming reactions such as imine exchange or ester formation. All reactions from *scheme 1* are dynamic bond formation reaction that are reversible hence their use in DCC. The following scheme, for example, illustrates how imines and amines can exchange their substituents, acetic acids and alcohols can reversibly lead to esters and ligand exchange can take place in coordination complexes.

Imine exchange

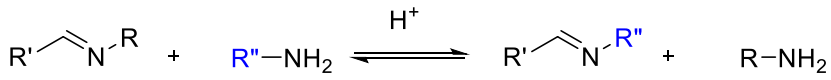

Ester formation and exchange

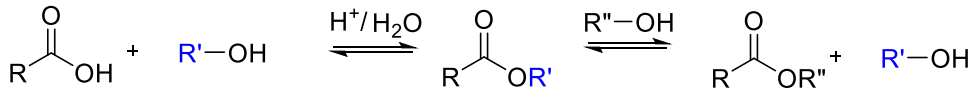

Ligand exchange

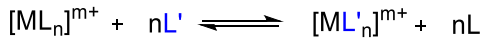

Scheme 1: Example of dynamic linkage commonly used in DCC.

1.2 Design of macromolecular architectures

To form macromolecular systems, it is possible to use the same non-covalent forces that nature exploits for many biological processes. Hydrogen bonds, π-π interactions and Van der Waals interactions are interactions that require little energy (2-40 kJ/mol) and are easily broken which makes them attractive for supramolecular chemistry. Different types of architectures have been synthesised using these intramolecular forces, including catenanes[13] and rotaxanes,[14] interlocking knots[15] and molecular motors (*fig 4*).[16] Metal-organic bonds are also appealing for supramolecular chemistry as they are stronger than other non-covalent bonds (60-200 kJ/mol). These bonds are labile and thus enable facile synthesis of discrete macromolecules; generally, these reactions proceed under thermodynamic control. Non-covalent bonds have been widely used to form structures like binuclear helicates, catenanes or polyhedra.[17] Structures such as catenanes, rotaxanes and knots have found application in the field of nanotechnology. Container molecules, on the other hand, play an important role in the encapsulation of guests.

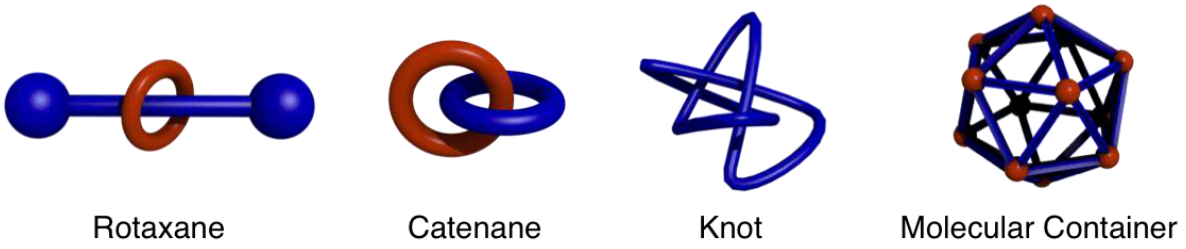

Figure 1: Supramolecular architectures.

In the reaction between linear and angular units, the product will depend on the size of each component, the stoichiometry in which components are combined, and the number of symmetry planes each unit possesses. The different geometries of bonding angle, variations of ligand length or the environment of the metal coordination can thus be used to form specific shapes.

Different approaches exist for the formation of 3D architectures. A possible one is the *directional bonding approach* where organic ligands and metal-containing precursors are designed to occupy the edges and vertices of the desired shape[17] (*fig 2*). Only if the denticity of the ligands and their angle match the geometry of the metal can they coordinate the metal centre. M. Fujita[18] and P.J. Stang[19] used this approach in the assembly of Pt^{II} or Pd^{II} salts and monodentate multi-branched, pyridine- or cyano-based ligands.

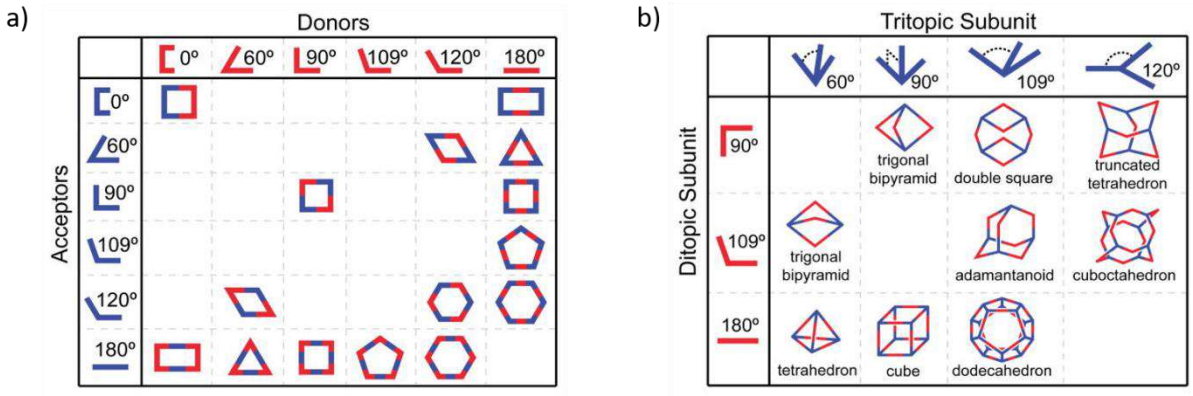

Figure 2: Directional bonding approach where a) ditopic building blocks generated a suite of 2D convex polygons and b) the combination of ditopic and tritopic building blocks resulted in 3D polygons. Figures reproduced from ref.[19]

Additionally, it is also possible to use the geometry of the metal coordination and the orientation of the interaction sites in a specific ligand to assemble the architectures. This second approach is the *symmetry interaction approach,* which provides instructions for the self-assembly of the structure, as defined by D. L. Caulder and K. N. Raymond.[20] Generally, when the metal, ligand and anion react, the product obtained is the entropically and enthalpically most stable architecture that satisfies both the coordination geometry of the metal cation and the coordinate vector of the organic molecule.

For a monodentate ligand, the coordinate vector is the vector directed from the coordinating atom to the metal center and for a bidentate ligand, it is the vector that bisects the coordinating atoms and is directed towards the metal center (*fig 3*).

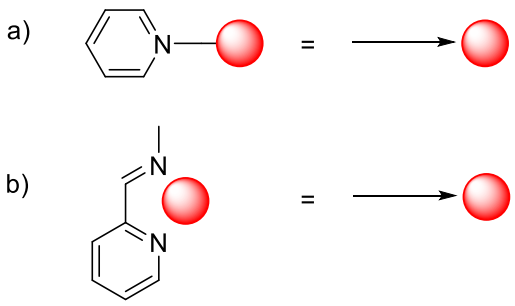

Figure 3: Example of coordinate vector of a) a monodentate ligand, b) a bidentate ligand.

An example is the formation of a helicate or a tetrahedron around a metal template with an octahedral coordination environment. The final structure depends on the coordinate vector of the twofold symmetric bis(bidentate) ligand. For example, the structure obtained with parallel coordinate vectors and a rigid ligand is most likely to be a triple helicate, whereas a tetrahedral shape may be formed in the case of an offset coordination vectors and ligands that are able to twist (*fig 4*).

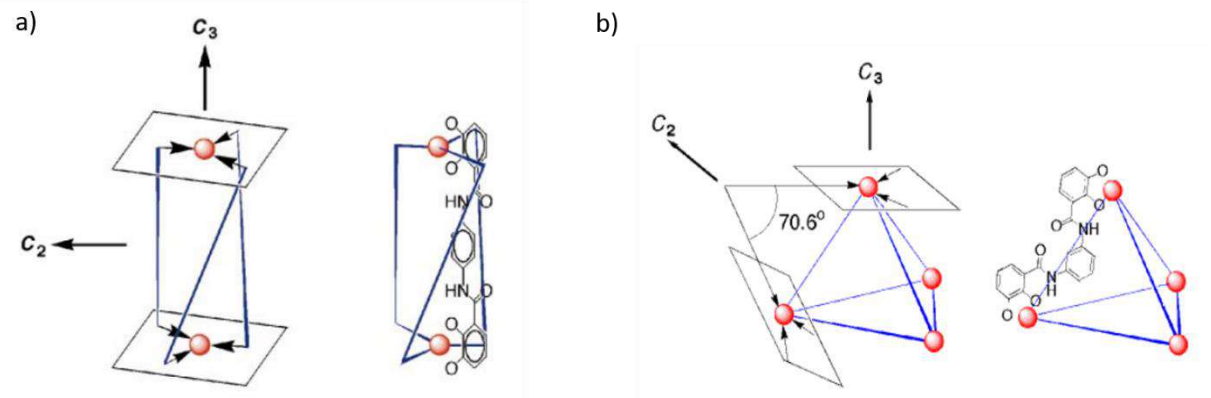

Figure 4: Symmetry interaction approach for a C3 chelate plane and a C2 coordinate vector in the case of a) parallel coordinate vectors yielding a triple helicate and b) offset coordinate vectors yielding a tetrahedron. Figures reproduced from ref.[20]

1.3 Container molecules

Container molecules are of interest in supramolecular chemistry as they show the ability to create host-guest systems. The structure of container molecules presents an inner cavity with interesting chemical and physical reactivity properties. The ligands, which may be either facial or form the edges of the container, defines the geometry of the architecture.[21] The environment inside the container molecules is different form the one outside and has been exploited to stabilise and contain reactive molecules[9] and catalyse chemical reactions.[22]

Furthermore, host-guest complexes have been shown to promote reactivity in specific cases. The rate and the selectivity of intermolecular reaction between two compounds can be increased as the cavity provides an increased concentration and regulated disposition of the compounds. As such, [2+2] photodimerisation of olefins could be promoted by a bowl-shaped coordination complex which determined the stereochemistry of the product formed as well (*fig 5*).[23] Upon irradiation with light, no dimerisation of acenaphthylene was observed at low concentration. However, dimers were formed in low yields (36%) and with no stereoselectivity (syn: 52%, anti: 48%) at higher concentration. For the increased concentration, the addition of a container molecule led to the syn-dimer in 98% yield.

The cavity brings two molecules of acenaphthylene together. The dimerisation is thus promoted as π-π interactions with the faces of the complex blocks the monomers in a manner that the syn-isomer will form preferentially over the anti (fig 5).

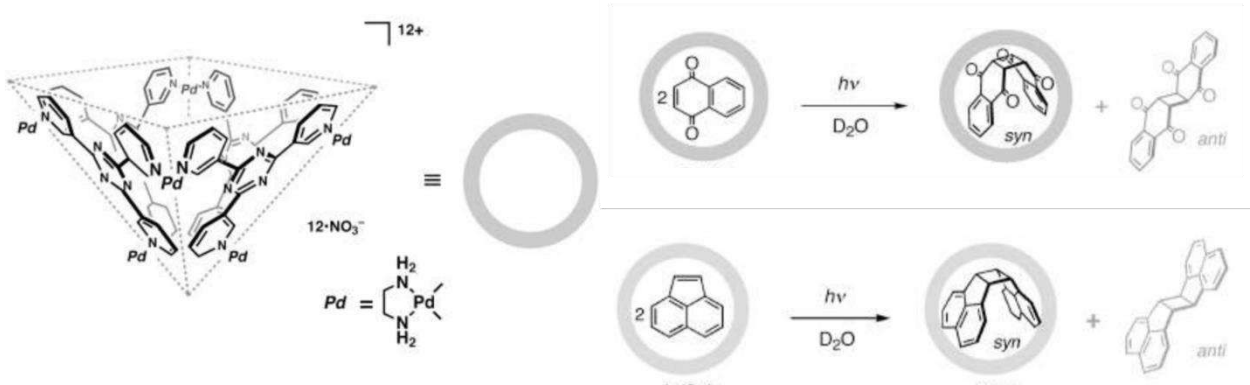

Figure 5: Bowl shaped cage promoting syn [2+2] photodimerisation of olefins[23]. Figures reproduces from ref[23].

Additionally, preparing nanoparticles within a narrow size distribution appears as a major challenge of materials chemistry. Indeed, the size of the nanoparticles has a major influence on their physical and chemical properties. A sphere composed of 12 metal ions and 24 ligands functionalised with sugar components has been used in the formation of monodisperse silica nanoparticles with a size that can be modified by tuning the length of the ligands (*scheme 2*).[24] Research on molecular capsules draws attention because of their interesting applications. Many different methods have thus been developed for the synthesis of metallo-supramolecular cages. However, the most common method remains molecular self-assembly. As the spontaneous association of molecules into stable and structurally well-defined aggregates, self-assembly will be further discussed in the next section.

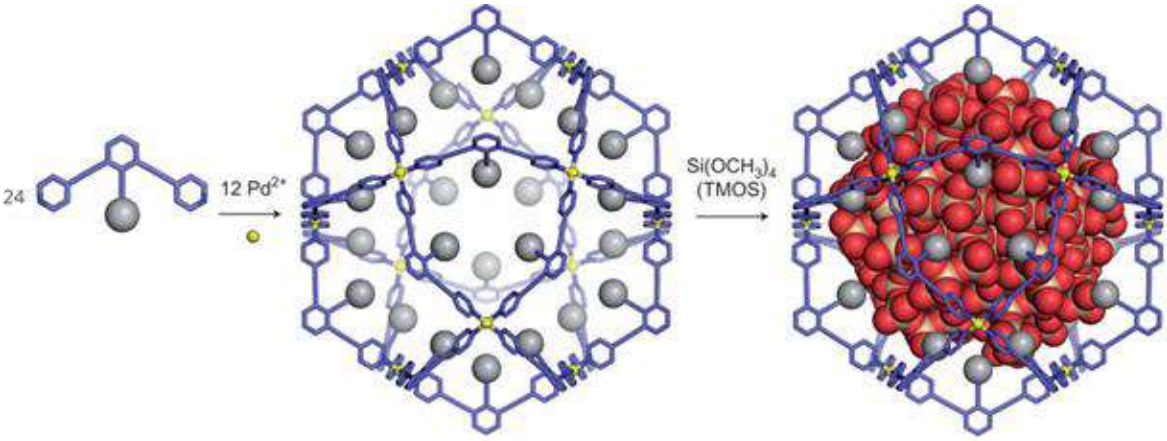

Scheme 2: Use of an $M_{12}L_{24}$ spherical cage in the preparation of silica nanoparticles.[24] Figures reproduced from ref [24].

1.4 Subcomponent self-assembly

Subcomponent self-assembly is the process by which subcomponents, building blocks, can reversibly assemble in order to form complex structures. Both dynamic covalent bonds and coordinative bonds are formed to build the supramolecular system. Specifically, condensation of an amine and an aldehyde to form an imine has been widely used in the formation of complex architectures in supramolecular chemistry. Because imines are dynamic covalent bonds, the amine can be recovered by hydrolysis of the imine species.

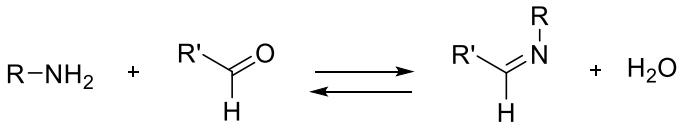

Scheme 3: Formation of an imine bond through the condensation of a primary amine and an aldehyde.

Initial research by Nitschke *et al.* focused on the stabilisation of copper imine complexes in an aqueous environment. In water, the Schiff base equilibrium would lie in favour of the amine formation and no imine species would thus be expected. Likewise, Cu(I) is often seen to disproportionate to Cu(II) in aqueous solution. Nevertheless, the Cu(I) complex and the imine bond can be stabilised by the formation of two imine bonds around the copper ion.[25]

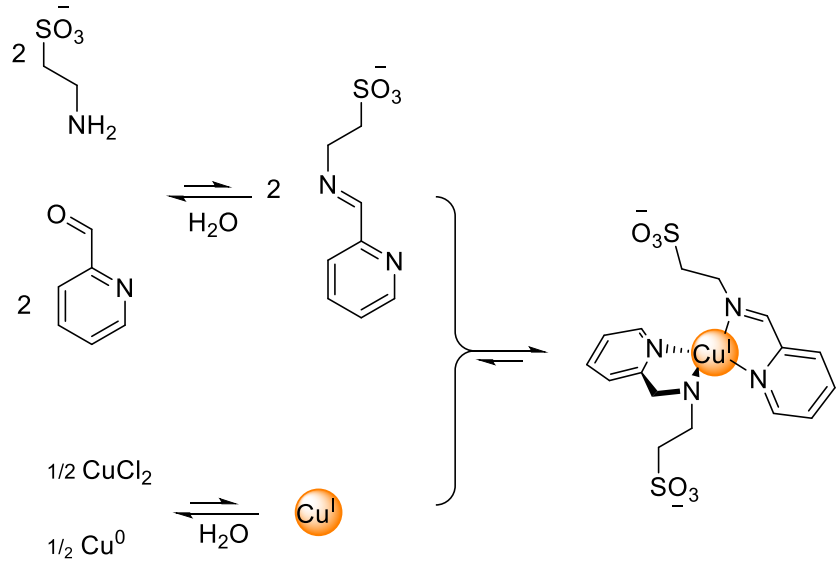

Scheme 4: Mutual stabilisation of copper imine system in water. Figure taken from ref[25]

This initial result oriented subsequent research towards a better understanding in different areas such as the construction of new supramolecular systems. For example, the above motif can be used as a corner for a cage by self-assembly.

Similarly, self-assembly can be exploited in the formation of molecular containers. An example of synthesis is shown in *scheme 5*. Tetrahedron **A** was synthesised by self-assembly of 4,4'-diaminobiphenyl-2,2'-disulfonic acid, 2-formylpyridine and $FeSO_4$ in the presence of a base, leading to a M_4L_6 tetrahedron soluble in water.[26]

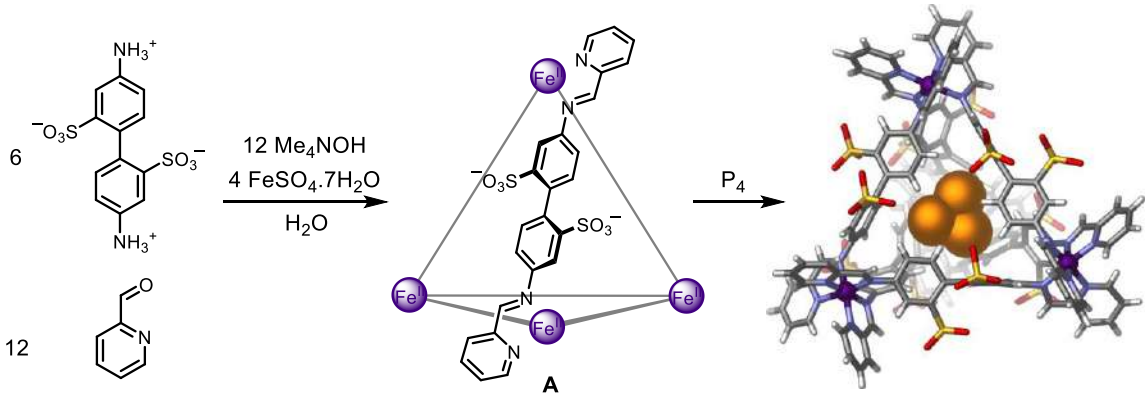

Scheme 5: Self-assembly of a $Fe^{II}_4L_4$ tetrahedron and crystal structure of the host-guest complex after encapsulation of P_4. Figure reproduced from ref[9]

Tetrahedron **A** has been shown to possess rich and varied host-guest chemistry. Small cyclic molecules can bind inside the hydrophobic cavity. Likewise, the inner void is able to capture and stabilise harmful greenhouse gases.[9, 27] White phosphorus P_4 is thermodynamically unstable and can slowly degrades into red phosphorus. Moreover, it is highly flammable and pyrophoric when exposed to air. Tetrahedron **A** has been shown to bind P_4 within its cavity in an aqueous solution, which leads to solubility of P_4 in water, but also stability of the phosphorus compound.

1.5 Previous work in the Nitschke group

Nitschke *et al.* reported the synthesis of face capped $Fe^{II}_4L_4$ cages by subcomponent self-assembly. [28] Interestingly, the solubility preferences of the tetrahedral component can be tuned by changing the counter anion of the cage. Indeed, the cage is soluble in acetonitrile with trifluoromethanesulfonate ($CF_3SO_3^-$) counterions whereas it is water soluble if synthesised with $FeSO_4$, in which case SO_4^{2-} would counter balance the charge from the cage. Moreover, the system has different guest binding properties depending on the solubilising solvent. In water, both aliphatic and aromatic guests were bound inside the cage cavity. In acetonitrile, a smaller range of guests were encapsulated as only aliphatic molecules bind. This system is thus an example of metal-organic architectures soluble in two different solvents with solvent-dependent binding properties depending on the counter anion.

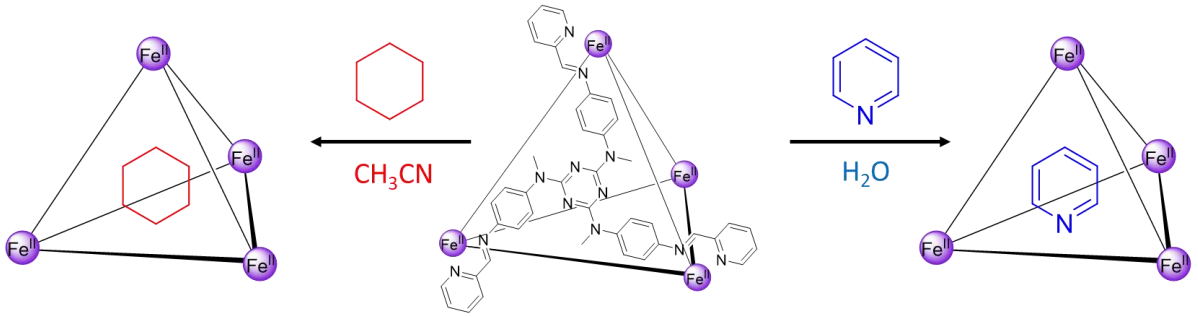

Figure 6: Tetrahedral cage with solvent-dependent guest binding properties in water and acetonitrile.[28]

The same tetrahedron with bis(trifluoromethylsulfonyl)amine anion (NTf_2^-) was studied regarding to guest binding in neat ionic liquids. Ionic Liquids (ILs) are proposed as an alternative for conventional organic solvents as less harmful and more environmentally friendly solvent.[29] Room-temperature ILs have attracted considerable interest as substitutes for volatile organic solvents. They consist of organic cations (imidazolium, pyridinium, sulfonium, phosphonium, etc.) and organic or inorganic anions. Because ionic liquids cover the entire spectrum of polarity, they have been used as solvents for many different types of molecules. As well as dissolving small organic, inorganic, and organometallic compounds, ionic liquids also have the ability to solubilise polymers,[30] enzymes,[31] and carbon nanotubes.[32] Additionally, as nonflammable, non-volatile and recyclable solvent, they are designated as green solvents and their solvating potential,[33] thermal stability[34] and tunable properties by suitable choices of ions[35] make their favourable media for chemical syntheses.

The work in *figure 7* investigates a triphasic system of water and two immiscible hydrophobic ionic liquids where three different coordination cages are selectively dissolved in a separate layer from Nitschke and coworkers.[36] Three guests are added to the mixture and each is specifically bound to a host in one phase. The system can thus be described as a triphasic sorting system with one cage and its guest in each phase. Ionic liquid appear as good solvents for metal-organic architectures and interesting regarding to separation systems.

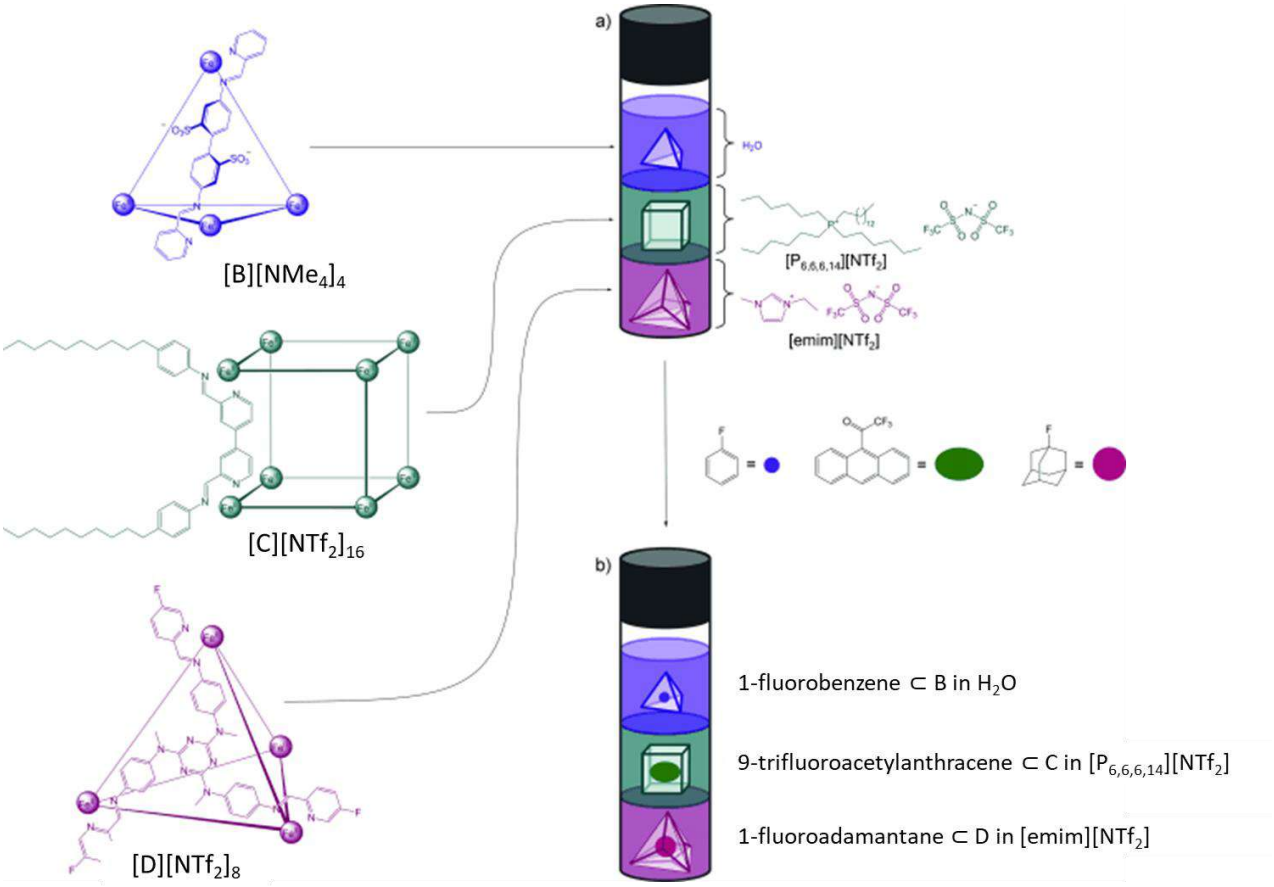

Figure 7: Triphasic sorting system of three cages and their cargos in immiscible phases. Figures reproduced from ref [36].

This work showed the need for alternative solvents such as ionic liquids and demonstrate the possibility to access to new functionalities by using ionic liquids. Furthermore, a unique combination of alkyl substituents and counteranions facilitates the tuning of the properties of the ionic liquid to fit the requirements the application.

Work in the Nitschke group also tackled the transport of cages and their cargo, as delivering molecules is a major function in nature. Indeed, in living organisms dissolved molecules often exist at a higher concentration inside the cell than outside, because the organism needs these molecules, they still must be absorbed against a concentration gradient. Container molecules are present to help the transport of these molecules between two different media.

For example, carrier proteins bind specific molecules to be transported on one side of the membrane. They then undergo conformational changes that allow the molecule to pass through the membrane and be released on the other side. Such an example establishes the importance of transporting cargos between two immiscible layers.

Recent work by Nitschke *et al.*[37] has successfully addressed practical separations problems by transporting a tetrahedral cage and its cargo from water into an ionic liquid layer. An anion exchange from SO_4^{2-} to BF_4^- drives this movement. The coordination cage and its guest can be transported back into the aqueous layer after exchanging the anion back to SO_4^{2-} (*fig 8*).

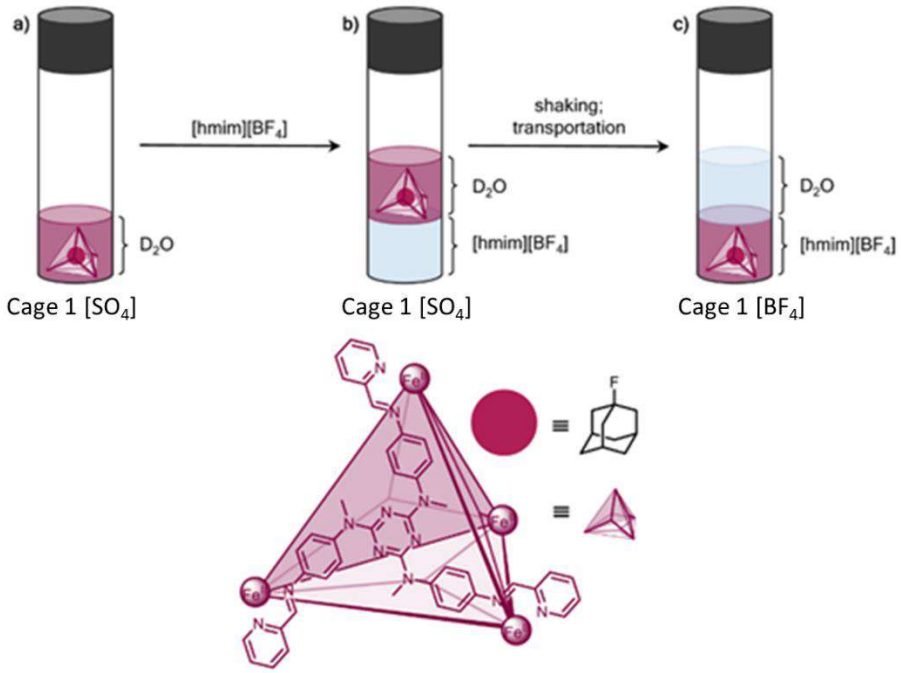

Figure 8:Phase transfer of a cage and its cargo between a water layer and an ionic liquid layer by anion exchange. Figure taken from ref [37]

However, this system is not ideal as the process is triggered by an anion exchange. Indeed, the transport does not occur by itself and the cage needs to undergo a reaction for it to move between phases. Likewise, it is also not fully reversible and cannot travel against a concentration gradient.

1.6 Reversible phase transfer of an imidazolium ionic liquid

Coupled with the previous work on phase transfer, the main inspiration for this project comes from work by Wang *et al*.[38] They reported the synthesis of ionic liquids $[PEG_n(mim)_2][NTf_2]_2$ (*fig 9*), n ranging from 4 to 22, that successfully transferred between two immiscible phases upon a change in temperature.

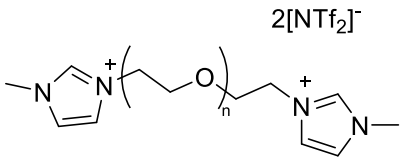

Figure 9: Structure of ionic liquid $[PEG_n(mim)_2][NTf_2]_2$ reproduced from ref [38]

The bis(trifluoromethylsulfonyl)amide anion (NTf_2^-) is very hydrophobic and the poly(ethylene) glycol chain is hydrophilic.[39, 40, 41] Wang *et al*. demonstrated that it is thus possible to tune the ratio hydrophilicity/hydrophobicity in the IL with the number of repeat units of the PEG chain and by careful selection of the anion. The PEG-based ILs, which are dissolved in water at 25°C, transfer to EtOAc after increasing the temperature to 50°C. The IL transfers back to the aqueous layer upon cooling to ambient temperature.

The transfer observed between the phases is due to a conformational change of the PEG chain. Indeed, at low temperature, the chain is coiled and has a hydrophobic interior and an hydrophilic exterior. As such, the ionic liquid can interact with water molecules which makes it water soluble. At high temperature, the conformation of the PEG chain changes and the chain becomes less coiled (*fig 10*). Indeed, a high temperature increases the entropy of the system and the PEG chain gains more degrees of freedom. As a result, the chain adopts the conformation of a strand where the hydrophobic interior is exposed. The polymer becomes then less hydrophilic as the interactions between the ionic liquid and the water decreases. The solubility of the ionic liquids thus changes and it transfers to the EtOAc layer.

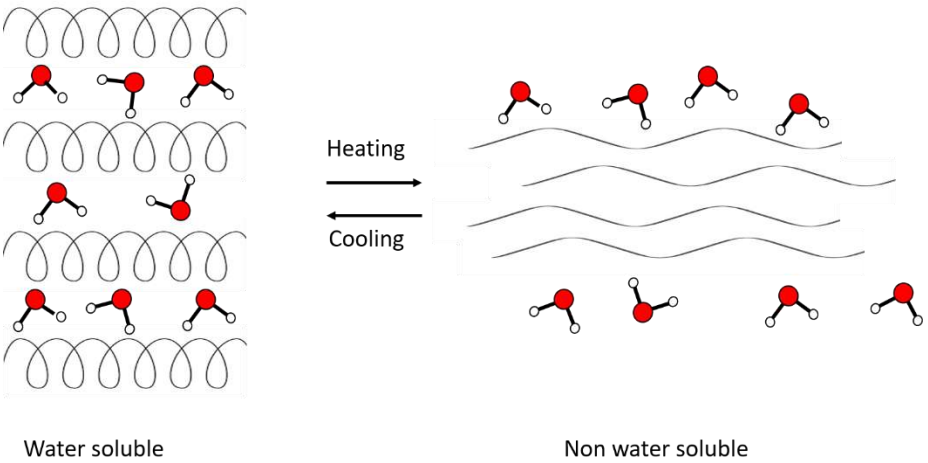

Figure 10 : Conformational change of PEG chains with temperature. At low temperature the ionic liquid is water soluble. At high temperature the ionic liquid transfers to organic phase.

Different PEG chain lengths have been studied and a reversible transfer between water and organics was observed only for PEG chains with a molecular weight of 800 and 1000. Lower molecular weight chains remained in the organic layer after a change of temperature. Wang *et al*. thus developed a strategy by which the hydrophilicity and the hydrophobicity of imidazolium functionalised ionic liquids can be tuned by varying the length of the PEG chain and the anion. These systems undergo reversible phase transfer between water and EtOAc upon temperature variations.

1.7 Project aims

The aim of this project is to achieve fully reversible transport of a coordination cage between water and an immiscible organic solvent driven by a change in temperature (*fig 11*). To transfer between phases, the subcomponents of the cage will be functionalised with arms similar to the ionic liquid developed by Wang et *al.*

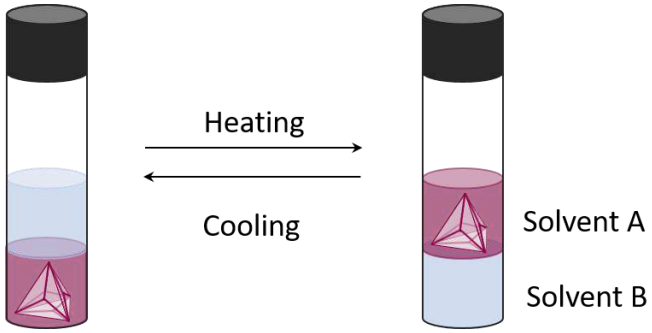

Figure 11: Phase transfer upon temperature variations.

For the purpose of studying the transfer properties of metallo-organic systems, the following systems will be investigated:

1-non-functionalised cages assisted by ionic liquid,

2-short PEG chain functionalised cages with and without ionic liquid,

3-long PEG chain functionalised cages in the presence or not of an ionic liquid.

Table 1: Steps for reversible phase transfer investigated in this project.

Cages	No IL	IL
Non-functionalised	No transport	?
Short PEG chain functionalised	?	?
Long PEG chain functionalised	?	?

The final goal is to develop a capsule-mediated transport system that is both directional and reversible, where the flow of the capsule and its encapsulated cargo is directed using stimuli such as temperature changes. Ultimately an apparatus that allows the switchable capsules to move along a channel will be developed and will enable the transport of a cage and its cargo against their gradient of concentration.

2-Results and discussion

It was shown by the Nitschke group that **cage 1** has the same solubility properties as the counter anions.[37] It is interesting to probe if the presence of the ionic liquid is enough to change the solubility properties of the molecular capsules. Moreover, different anions can be investigated for their influence on the solubility of the cage in the presence or not of the ionic liquid.

2.1 Synthesis of the ionic liquid

In order to study the transfer properties of $[PEG_{1000}(mim)_2][NTf_2]_2$, **ILA** was synthesised using a modified procedure[38] to obtain an increased yield. The final ionic liquid **ILA** $[PEG_n(mim)_2][NTf_2]_2$ was obtained in three steps.

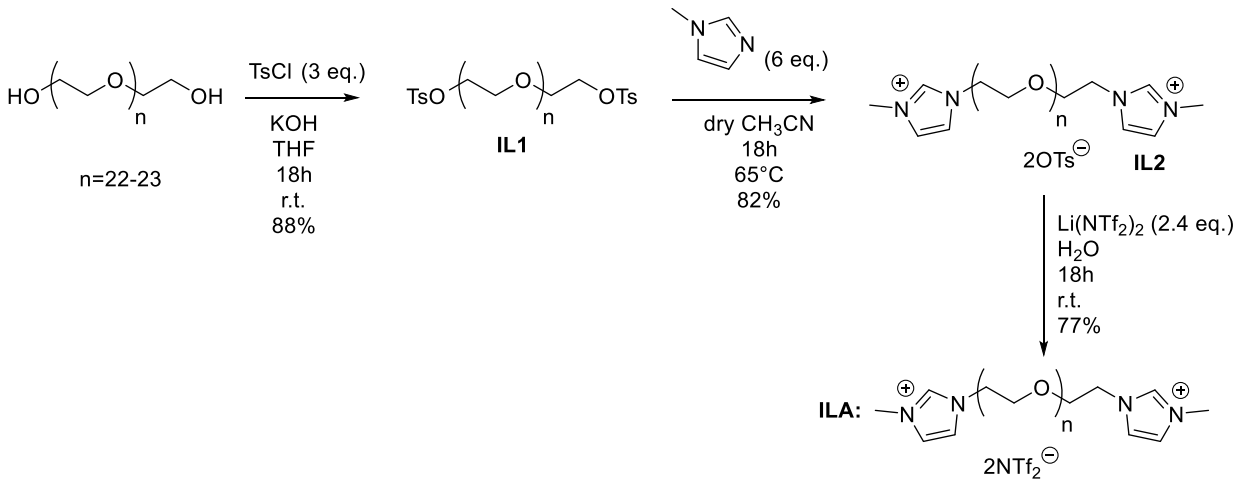

Scheme 6 : Procedure for the synthesis of ionic liquid ILA.

Poly(ethylene) glycol (1000 MW) reacted with p-toluenesulfonyl chloride affording the tosylated PEG IL1. An intermediate ionic liquid $[PEG_{1000}(mim)_2][OTs]_2$ was obtained by the reaction of 1-methylimidazole with **IL1**. Anion exchange using bis(trifluoromethylsulfonyl)amine lithium salt in water afforded the ionic liquid $[PEG_{1000}(mim)_2][NTf_2]_2$ **ILA** as a colourless oil in 77% yield and high purity as confirmed by ^1H and ^{19}F-NMR spectroscopy and ESI-MS spectrometry**.**

The procedure has been modified from the original paper for purification reasons. Indeed, with the procedure from the paper where the PEG undergo a double chlorination, it was difficult to separate the starting material, the monosubstituted product and the desired product. The substitution by TsCl prevented a mixture of products and facilitated the isolation of the desired ditosylated product, which was confirmed by ESI-MS.

Both the +1 and the +2 charged molecules were observed by ESI-MS (*appendix fig S4*). The spectrum showed a distribution that corresponds to the different lengths of the chains. Species between n=15 to n=32 were observed. In the +1 species spectrum, the peaks are separated by 44 units which corresponds to a (CH_2-CH_2-O) repeat unit. This gap was observed in the +2 species spectrum as 44/2= 22. The mean value of m/z for the +1 species is 1264.4 which represents molecules of 1544.4 MW for n=22.

At room temperature, the ionic liquid $[PEG_{1000}(mim)_2][NTf_2]_2$ was observed to be soluble in water. The addition of a second solvent, EtOAc, led to a separation where three phases were formed: the bottom phase was mainly constituted of water, the middle phase was IL and the top phase was EtOAc. Cooling the solution to 10°C allowed the solubilisation of **ILA** in water. Partitioning experiments of **ILA** between water and EtOAc were performed to confirm the transfer ability of $[PEG_{1000}(mim)_2][NTf_2]_2$. A solution of 15% wt. **ILA** in 250uL ml of H_2O was prepared and the same volume of EtOAc were combined at 10°C leading to a biphasic system. At low temperature, **ILA** was soluble in the aqueous phase. After 10 min at 60°C, **ILA** transferred to the top EtOAc layer. The solution was cooled using an ice bath, driving a reversible transfer to the water layer.

The transport of the ionic liquid between water and EtOAc was monitored by slice-selective ^{19}F-NMR. Using this method, we were able to observe the distribution of the (NTf_2^-) anions throughout both layers. ^{19}F-NMR was chosen instead of ^{1}H-NMR because it is easier to follow the anion peak than broad peaks from the ^{1}H experiment.

Slice-selective NMR allows the investigation of spectral information from different physical locations within a sample.[42] To select the slice to be excited, a long radiofrequency pulse is applied in the presence of a magnetic field gradient. On the majority of NMR probes, a field gradient (B_o) is applied along the direction of the external magnetic field. During the application of B_o, the resonance frequencies have an offset Θ. This offset varies with the external field gradient and the vertical position. To excite a certain slice, a soft pulse with a bandwidth large enough to include an entire ^{1}H-NMR spectrum or 10-20 ppm from a ^{19}F-NMR spectrum is used at the offset Θ. Changing the offset of the pulse enables the investigation of different slices of the sample along in the direction of the applied gradient (generally vertical). Slice-selective NMR has been used to measure diffusion[43], monitor reactions[44] or analyse a sample.[45]

Here, slice-selective NMR, was used to collect spectra of thin slices (1 mm) throughout the total sample. This experiment was used to study, noninvasively, how the ionic liquid partitioned between the two layers. ^{19}F-NMR experiments were run on both layers at 10°C, 60°C and once again at 10°C to monitor the location of the (NTf_2^-) anions in the ionic liquid. Between each set of experiments, the NMR tube was inverted to facilitate the phase transfer. For a total volume of 500 µL in an NMR tube, the program measured 21 equidistant slices.

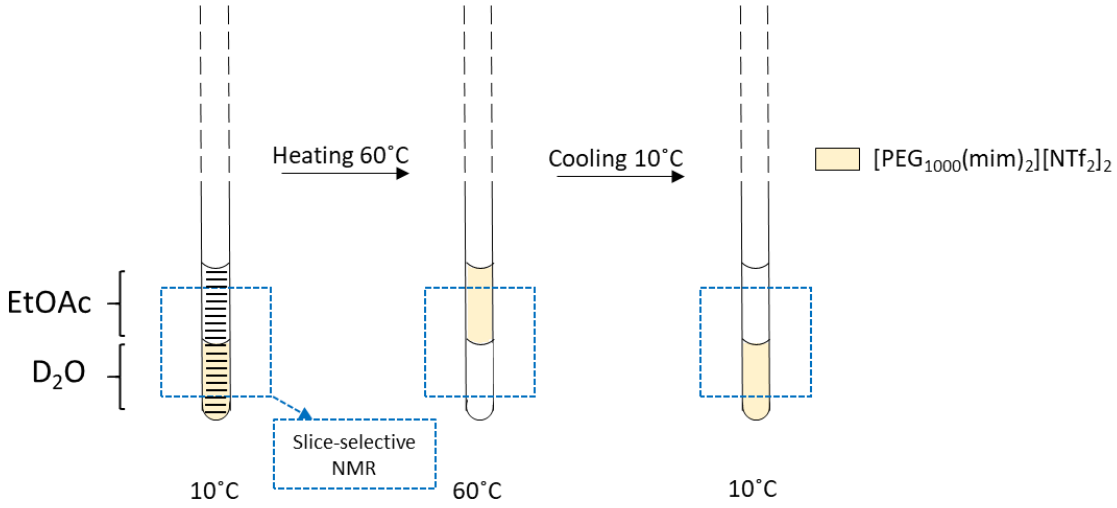

Figure 12 : Principle of the slice-selective NMR on biphasic samples of deuterated water and EtOAc between 10°C and 60°C.

This slice-selective ^{19}F-NMR experiment was carried out to investigate the transfer of **ILA** between water and EtOAc with temperature variations. For this purpose, the peak of the anion (NTf_2^-) was followed in the two phases. It was possible to obtain 3D spectra of the experiment indicating the location of the anions (*fig 13*). The presence of the (NTf_2^-) anions was represented by the orange curve. The intensity of the signal is represented on the F1 axis which is the vertical axis of the NMR tube. The F2 axis is the chemical shift axis.

Fig 13, a) shows the repartition of the (NTf_2^-) anions in both the water layer and the EtOAc layer at 10°C. The majority of the anions were located in the bottom phase, which corresponds to the D_2O. No peaks were observed in the EtOAc layer. So at 10°C, **ILA** was located in the aqueous phase.

It was possible to extract 1D ^{19}F-NMR spectra from the slice-selective experiment (*fig 13, b)*), in which each spectra was taken from a 1 mm slice of the sample. *Fig 13, b)* shows the ^{19}F-NMR spectra of slice 17 in the EtOAc layer (top) and of slice 6 in the water layer (bottom). No fluorinated peak can be seen in slice 17 whereas a peak representing the (NTf_2^-) anions of the ionic liquid is present in slice 6. This confirms the presence of the ionic liquid **ILA** in the water layer at 10°C.

The slice-selective ^{19}F-NMR experiment was repeated after heating the biphasic system to 60°C (*fig 14*). The 3D spectra shows the curve corresponding to the (NTf_2^-) anions in the upper part of the NMR tube. It reveals that most of the (NTf_2^-) anions are located in the top phase of EtOAc at 60°C. The water phase at the bottom shows a slight trace of fluorinated compound, probably a residue of ionic liquid.

The extracted 1D ^{19}F-NMR spectra for slices 6 (H_2O) and 17 (EtOAc) are shown in (*fig 14, b)*). A ^{19}F-NMR peak corresponding to the (NTf_2^-) anions was observed in slice 17 while the spectrum of the water layer displays no peak at 60°C. The absence of (NTf_2^-) anions in the aqueous phase and their presence in the organic phase suggests that **ILA** transferred from water to EtOAc upon heating to 60°C.

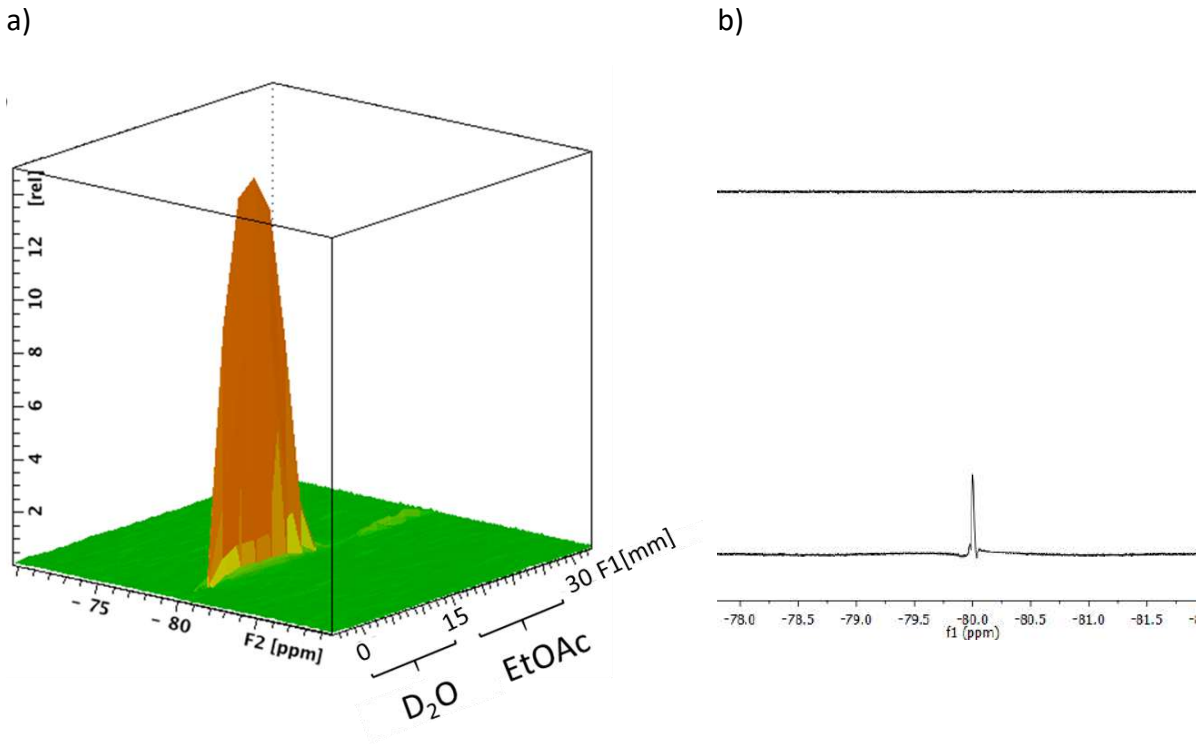

Figure 13 : Slice selective ^{19}F-NMR of ILA in deuterated water and EtOAc at 10°C. a): 3D ^{19}F-NMR spectra of the tube, F1 represents the height of the tube (mm) and F2 is the ppm axis. The orange peak represents the (NTf_2^-) anions of the ionic liquid. b) Slice 17 (top, EtOAc) and slice 6 (bottom, D_2O).

a) b)

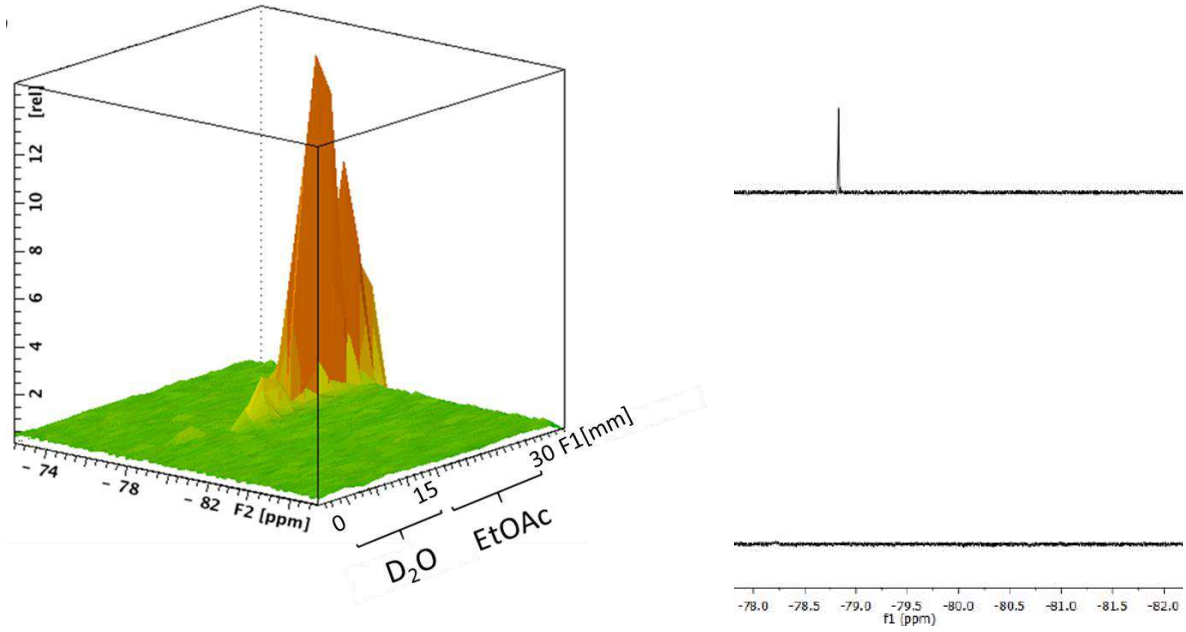

Figure 14 : Slice selective ^{19}F-NMR of ILA in deuterated water and EtOAc after heating to 60°C. a): 3D spectra of the tube, F1 represents the height (mm) and F2 is the ppm axis. The orange peak represents the (NTf_2^-) anions of the ionic liquid.b) Slice 17 (top, EtOAc) and slice 6 (bottom, D_2O). ILA is located in the organic layer.

a) b)

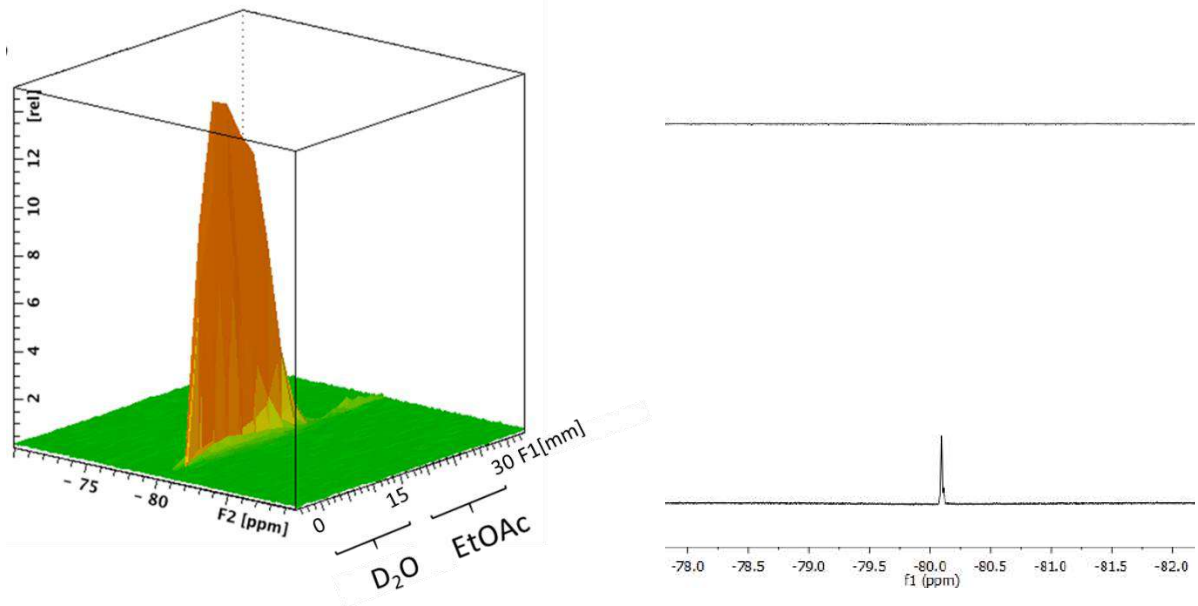

Figure 15 : Slice selective ^{19}F-NMR of ILA in deuterated water and EtOAc after cooling to at 10°C. a): 3D spectra of the tube, F1 represents the height (mm) and F2 is the ppm axis. b) Slice 17 (top, EtOAc) and slice 6 (bottom, D_2O). The orange peak represents the (NTf_2^-) anions of the ionic liquid. ILA transferred back to the aqueous layer.

The NMR tube was then cooled back to 10°C and the location of the (NTf_2^-) anions was probed by slice selective $_{19}$F-NMR. The 3D spectra shows that most of the anions are located in the bottom aqueous phase while only traces remain in the EtOAc. The ^{19}F-NMR spectra of slices 6 and 17 after cooling to 10°C reveal the presence of a fluorinated species in the water layer but none in the EtOAc. The peak observed corresponds to the counteranions of the ionic liquid. After cooling to 10°C, the majority of the ionic liquid transferred back to the water layer. To summarise, **ILA**, water soluble at 10°C, was observed to undergo phase transfer from water to EtOAc upon heating to 60˚C by slice-selective ^{19}F-NMR. The transfer was reversible as the $[PEG_{1000}(mim)_2][NTf_2]_2$ transferred back to the water layer after cooling down to 10˚C.

Given the previous results by Wang *et al.*, these results were expected. Nevertheless, in the previously reported case, the ionic liquid was soluble in water at room temperature. The same behavior was not observed for the IL synthesised in this project. Indeed, at ambient temperature, the ionic liquid was not water soluble and a triphasic system was formed with water, ionic liquid and EtOAc. To further investigate the separation, slice-selective ^{19}F-NMR was used to study the three phases which formed upon addition of EtOAc to the water at 25°C (*fig 16*).

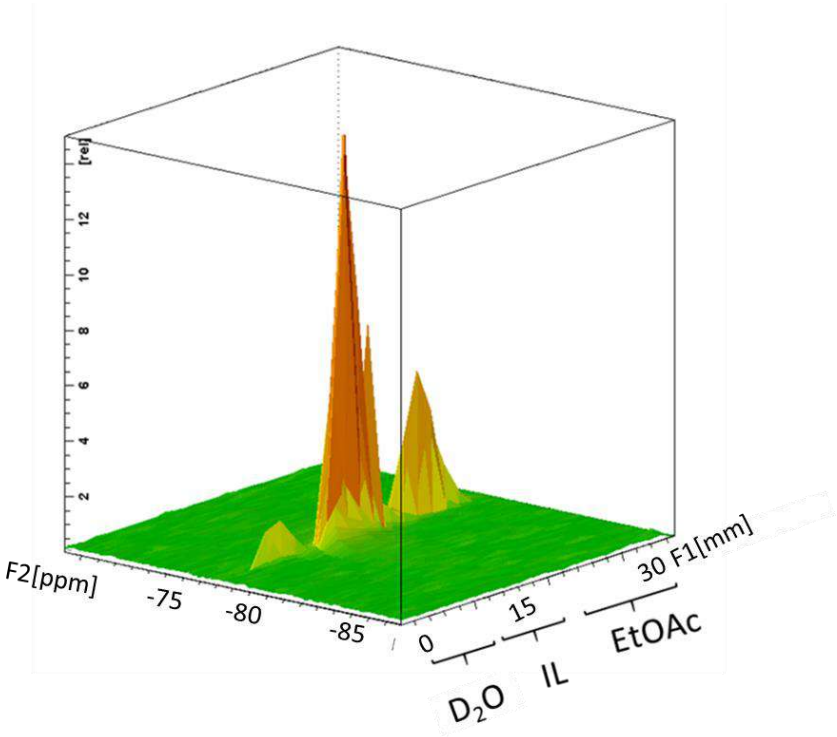

Figure 16 : 3D slice selective ^{19}F-NMR of ionic liquid a in water and EtOAc at 25°C where three layers are formed, F1 represents the height (mm) and F2 is the ppm axis. The orange peak represents the (NTf_2^-) anions of the ionic liquid.

At room temperature, the 3D ^{19}F-NMR spectrum shows that the majority of the anions from **ILA** are in the middle phase. Nevertheless, (NTf_2^-) anions are also present in the bottom layer (D_2O) and in the top layer (EtOAc). Because the presence of the anions is linked to the location of the ionic liquid **ILA,** we conclude that **ILA** is primarily located in the middle phase hence the system must necessarily be cooled to 10˚C to solubilise the **ILA** in water. The slice selective experiment showed however that **ILA** was soluble in both D_2O and EtOAc at ambient temperature thus indicating that the ionic liquid possess intermediate solubility.

2.2 Study of a non-functionalised cage – Project aim 1

The ionic liquid $[PEG_{1000}(mim)_2][NTf_2]_2$ was observed to transfer between two immiscible solvents upon a change in temperature. The first part of the project aims at investigating the transfer properties of a non-functionalised cage with and without ionic liquid. A Fe_4L_4 iron tetrahedron previously reported by Nitschke et al[28] was chosen for this experiment. Indeed, Fe_4L_4 tetrahedral cage with N2,N4,N6-tris(4-aminophenyl)-N2,N4,N6-trimethyl-1,3,5-triazine-2,4,6-triamine as panel was previously studied for its solubility in water and acetonitrile and its solvent-dependent guest binding properties.[28] This cage will be used as a model cage for this project. As discussed in introduction, (SO_4^{2-}) anions are highly hydrophilic, which makes the cage reported hydrophilic. The cage is soluble in water and will never go into an organic solvent.

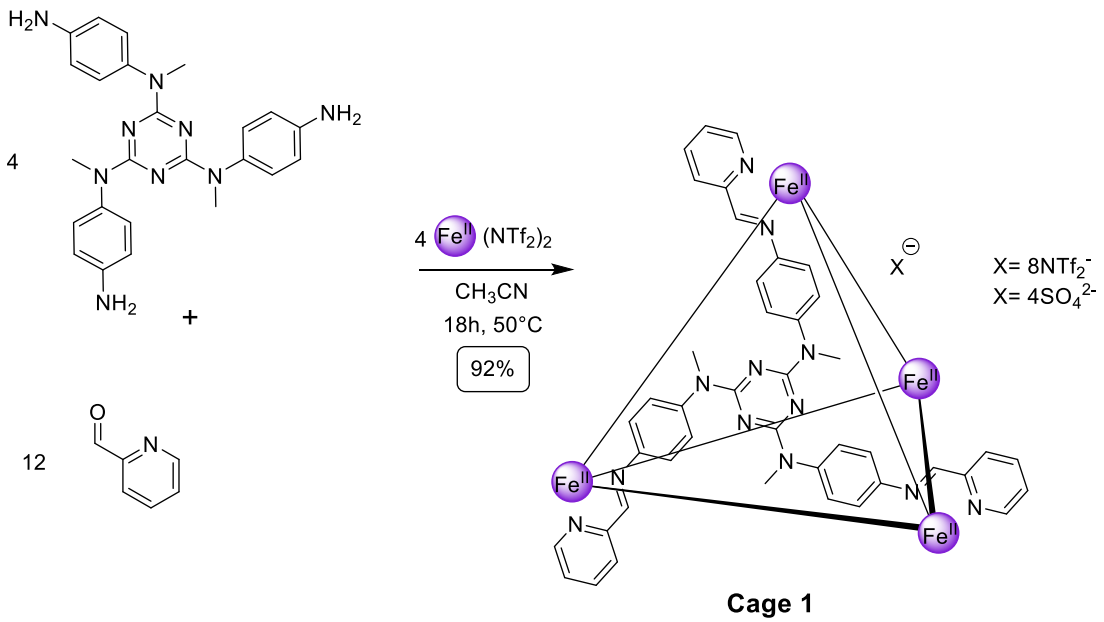

Scheme 7 : Self-assembly of cage 1 in acetonitrile.

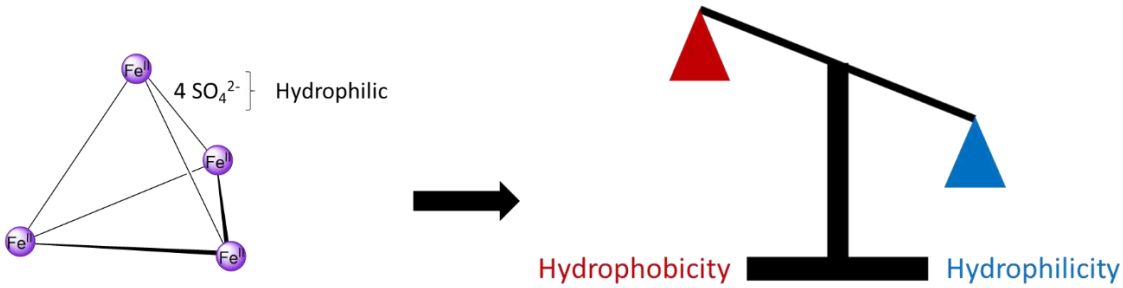

Figure 17: Effect of the SO_4^{2-} anions on the hydrophilicity of cage 1.

The cage with (NTf_2^-) anions was synthesised so the anion would be identical to the anion in **ILA**. The hydrophobicity of the counteranion makes **cage 1** not soluble in water by itself. In pursuit of project aim 1, the ionic liquid was used in an attempt to solubilise the cage in either water or EtOAc. Nevertheless, **cage 1** remained insoluble.

A system of an aqueous solution of **ILA** (15%wt., 0.5 mL), EtOAc (0.5 mL) and **cage 1** (1 mg, 0.19 µmol, 190 µM) was prepared. **Cage 1** was observed to be slightly soluble in **ILA**, sparingly soluble in EtOAc and insoluble in H_2O.

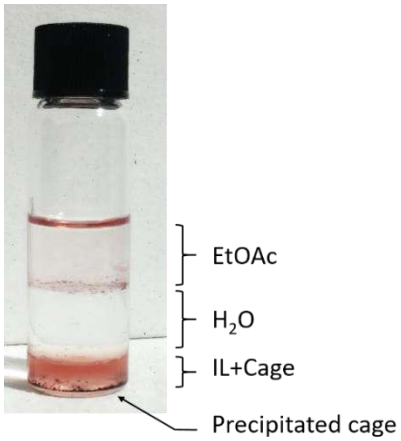

Figure 18 : Partitioning experiment vial of cage 1 in a triphasic system of ILA, water and EtOAc. Most of the cage precipitated and a small fraction was soluble in the ionic liquid.

As was observed for **ILA** in section 2.1, **cage 1** exhibits intermediate hydrophilicity and hydrophobicity at ambient temperature. The coordination complex is not soluble in H_2O because the (NTf_2^-) anions make it too hydrophobic but it is also not hydrophobic enough to be soluble in EtOAc. No transfer of the cage or the ionic liquid was observed after heating the system to 60°C or cooling it to 10°C with an ice bath. Notably, the cage influenced the transfer properties of the ionic liquid: the presence of **cage 1** thus stabilises the triphasic system.

Even though no transport was observed, this cage structure remains a good candidate due to its wide range of solubility and ability to accommodate guests. Evidently, intermediate hydrophobicity and hydrophilicity immobilise the system {cage + **ILA**}. To achieve transfer, thermoswitchable groups need to be added on the cage.

2.3 Design of functionalised cages for project aims 2 & 3

2.3.1 Balancing hydrophilicity and hydrophobicity of the cages

The necessity to adjust the balance between the hydrophilicity and the hydrophobicity to achieve successful transport was shown in section 2.2. Indeed, the cage must be water soluble at low temperature and soluble in EtOAc at high temperature. **Cage 1** presented in section 2.2 has intermediate solubility due to combination of factors. In this section, enhancing the hydrophilicity at low temperature will be accomplished by synthesising a ligand with poly(ethylene) glycol chains terminated by an imidazolium.

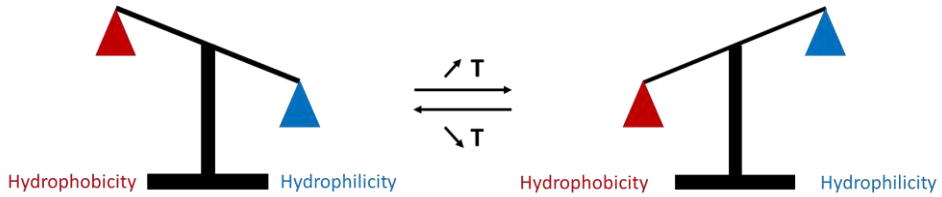

Figure 19: Ideal case of balanced hydrophilicity and hydrophobicity with temperature variations.

In order to achieve reversible transport between two immiscible phases (water and an organic solvent), a coordination cage should comprise a hydrophilic part as well as a hydrophobic part. Because intermediate solubility will make the cage insoluble in both phases, the solubility of the cage in both phases can be enhanced by functionalising the periphery of the cage with a thermoswitchable ionic liquid (*fig 20*).

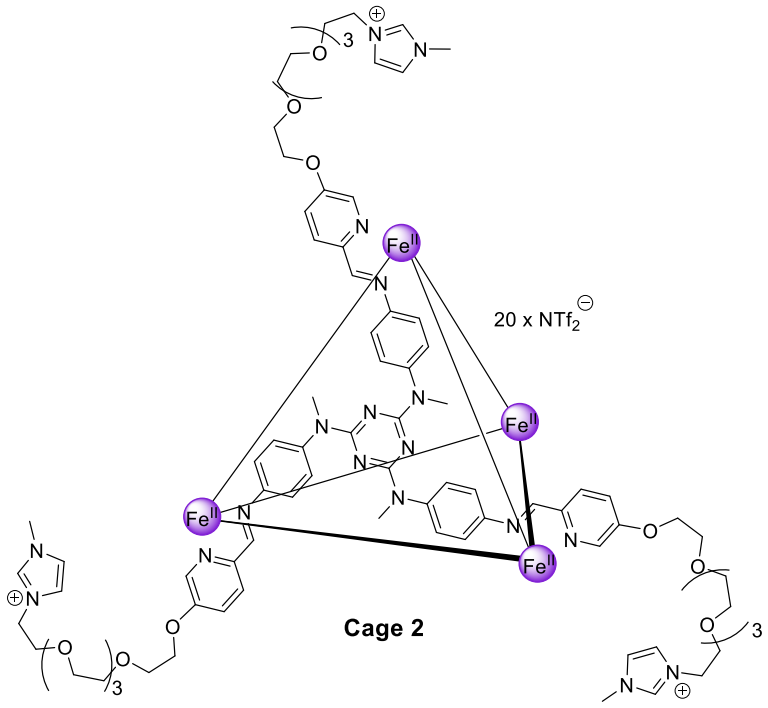

Figure 20 : Design of a tetrahedral iron II cage with imidazolium cations pending.

The peripheral groups for the cage will have a similar structure to **ILA** with a hydrophilic poly(ethylene) glycol chain (1 000 MW) and n hydrophobic counteranion (NTf_2^-). As discussed in Project aims, in this design, the length of the poly(ethylene) glycol chain is of paramount importance. Chains with few repeat units (n=5) and high repeat unit (1 000 MW, n~22) will be studied to determine the importance of the hydrophilicity of the peripheral arms for phase transfer.

The metal-organic cage will be synthesised by subcomponent self-assembly for the ease of synthesis. The formation of cages will be very similar to previous work by Nitschke et *al.* with functionalised peripheral arms. Initially, **cage 1** will be used as a scaffold upon which to attach arms. The phase transfer of functionalised cages will be monitored by slice-selective NMR and UV-Vis experiments. We hypothesise that a conformational change of the polymer chain from random coil to elongated strand will assist the phase transfer of the cage. Transporting a coordination cage using heat as a stimulus represents a significant progression from existing transport systems. No additional reaction would be needed to move the cages. Indeed, a change in temperature would be sufficient to transport cages and their cargos reversibly between two immiscible phases against a gradient.

Two different subcomponents with two different ethylene glycol chain lengths have been studied for this project: **A** has a short chain with 5 repeat units and **B** has a longer polymer chain with a mean value of repeat units of 22 (PEG_{1000}). The investigation of two different chain lengths allows the elucidation of the effect of the hydrophilicity of the chain on the transfer between water and EtOAc. The subcomponents with 5 repeat units will be referred to as PEG_{SHORT} and the subcomponents with long polymer chain (1 000 MW, approximately 22 repeat units) will be named PEG_{1000}. Upon successful synthesis of PEG-imidazolum subcomponents and cage assembly, partitioning experiments were carried out. While penta(ethylene) glycol chains were observed to transport to EtOAc, cages with longer chain could reversibly transfer between water and EtOAc.

2.3.2 General procedure for subcomponent synthesis

In order to study the formation of metal-organic cages, subcomponents **A** and **B** were synthesised according to the synthetic route designed by Dr. Arnaud Tron. Two different routes were followed depending on the length of the chain to produce tosylated aldehydes **A1** and **B3** *(scheme 3).*

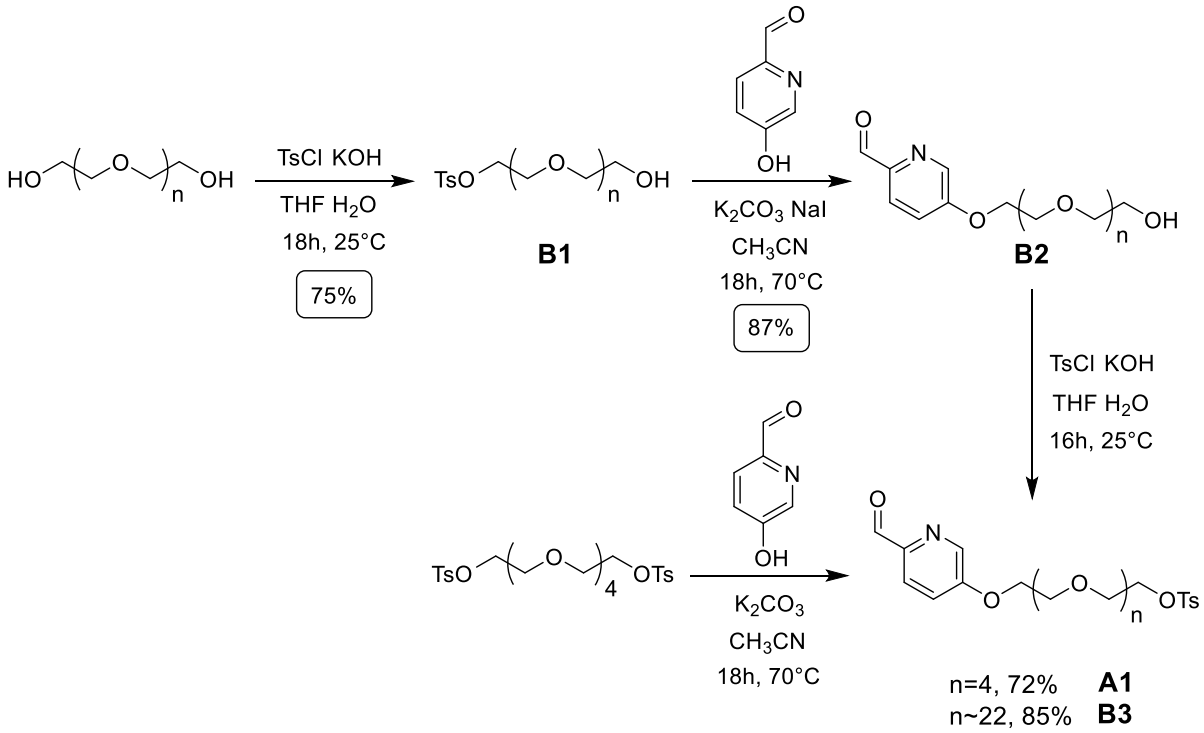

Scheme 8 : Synthesis of intermediate compounds A1 and B3.

Ditosylated compounds were used for the synthesis of the subcomponent **A**. The 3,6,9,12-tetraoxatetradecane-1,14-diol,1,14-bis(4-methylbenzenesulfonate) reacted with 5-hydroxypicolinaldehyde in dry acetonitrile affording the monocoupled product. Nevertheless, the same route could not be used for the PEG_{1000} species for purification reasons, and monotosylation was carried out in THF before coupling with the hydroxypicolinaldehyde. A second tosylation was performed to afford intermediate compound **B3**.

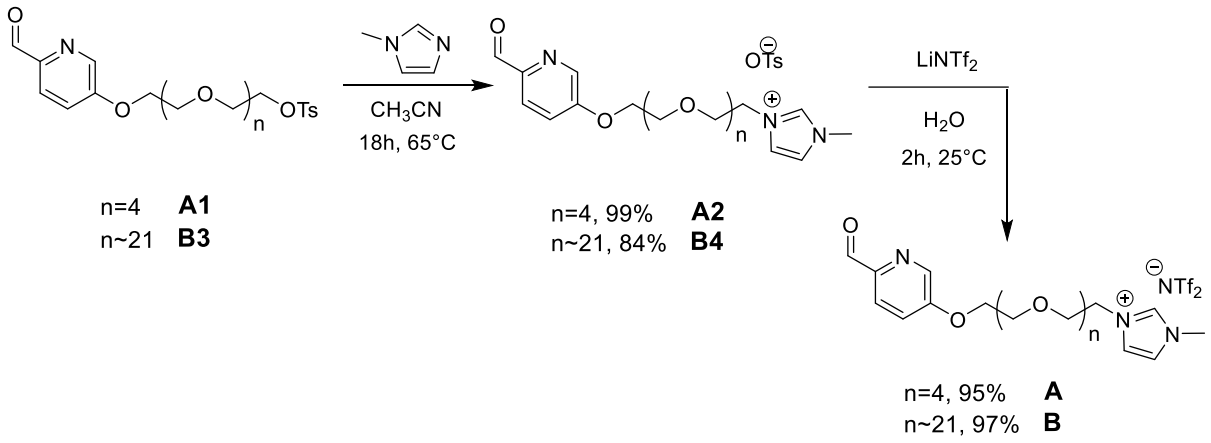

Figure 21 : Final steps of the synthesis of aldehyde subcomponents A and B.

1-Methylimidazole was added in acetonitrile to the ethylene glycol substituted aldehydes to obtain an imidazolium tosylate salt. Anion exchange with $Li(NTf_2)_2$ in water afforded the desired subcomponents A and B as light yellow oils in good yields and high purities. The formation of each compound was confirmed by ^{1}H-NMR in $CDCl_3$ or CH_2Cl_2 and MS-ESI. Final subcomponents **A** and **B** were characterised by ^{1}H-NMR, ^{19}F-NMR, COSY, DOSY, HSQC and HMBC, all confirming the structure of the final products.

2.3.3 General procedure for the self-assembly of metal-organic cages

To study partitioning experiments of metal-organic cages, 9 supramolecular cages were synthesised by varying the aniline, the length of the ethylene glycol chain and the metal salt.

The procedures for the formation of these complex structures are similar and can be described as follow: a stoichiometric amount of imidazolium aldehyde subcomponent (A or B), an aniline ligand (C_2 symmetric or C_3 symmetric), and a metal salt ($Fe(NTf_2)_2$, $Zn(NTf_2)_2$ or $Co(NTf_2)_2$) were dissolved in acetonitrile in a sealed reaction tube and three cycles of freeze-pump-thaw were performed. The solutions were stirred at 50°C for 18h. The solution was then cooled and concentrated under a flow of nitrogen. Addition of diethyl ether precipitated the cages as sticky solids that were isolated, dried and then dissolved in deuterated acetonitrile for further characterization. Each cage was characterised by ^{1}H-NMR spectroscopy, ^{19}F-NMR spectroscopy and ^{13}C-NMR spectroscopy. The stability of the coordination cages and their ability to transfer phase along with the ionic liquid **ILA** was then studied.

Table 2: Scope of functionalised cages self-assembled in this project.

Metal centres used for self-assembly with:	**Short ligand PEG_{SHORT}**	**Long ligand PEG_{1000}**
Aniline 1: N2,N4,N6-tris(4-aminophenyl)-N2,N4,N6-trimethyl-1,3,5-triazine-2,4,6-triamine 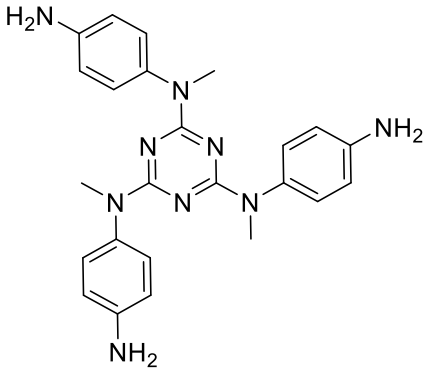	Fe	Fe Zn Co
Aniline 2: 1,5-bis(4-aminophenyl)anthracene 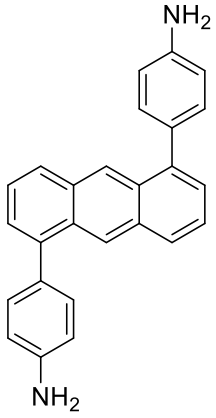	Fe	Fe

2.4 - Cages and partitioning

2.4.1 $Fe_4^{II}L_4$ tetrahedron with PEG_{SHORT} chain – Cage 2

Self Assembly

In a previous section, it was demonstrated that balancing the hydrophilicity and the hydrophobicity of the $Fe^{II}_4L_4$ tetrahedron was a crucial point to enable a phase transfer. Here, **cage 1** with (NTf_2^-) anions serves as a scaffold upon which **cage 2** is built. The hydrophilicity of **cage 2** at ambient temperature was enhanced by self-assembling a cage with the PEG_{SHORT} imidazolium subcomponent **A** (*scheme 9*).

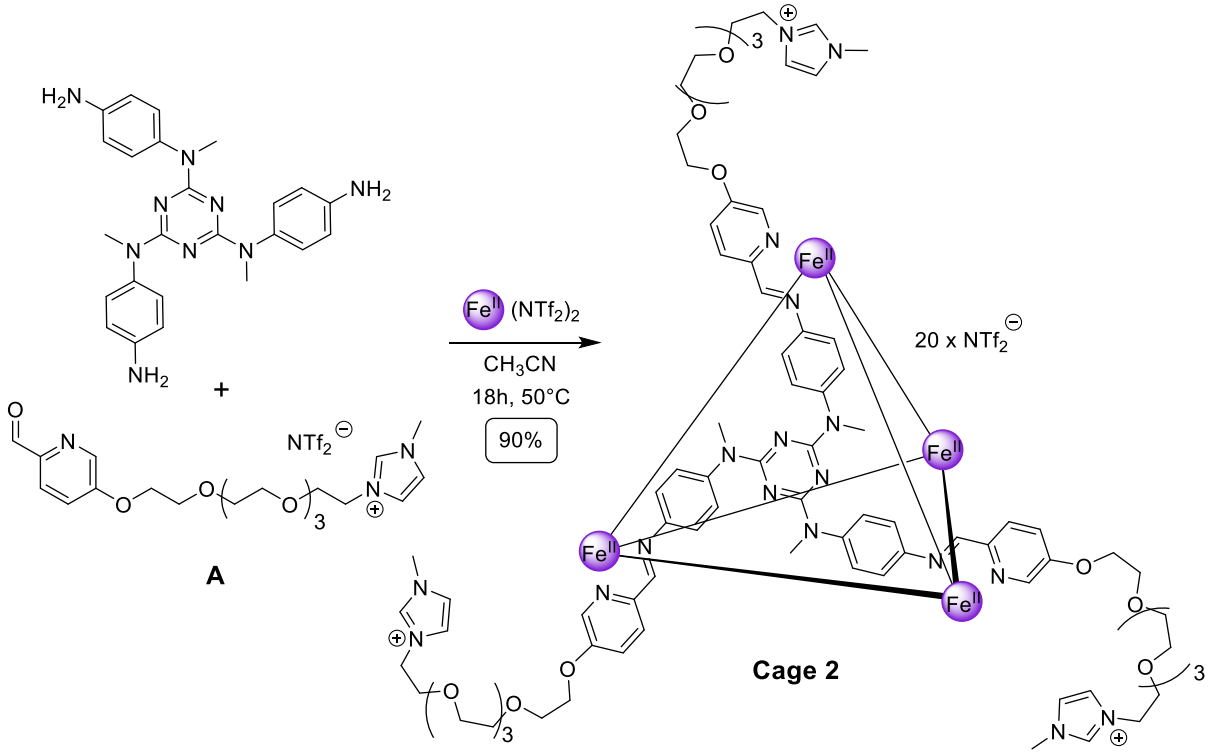

Scheme 9 : Self-assembly of cage 2 in acetonitrile.

The complex formed was characterised by ^{1}H-NMR, ^{19}F-NMR, ^{13}C-NMR spectroscopies and ESI-MS. The ESI-MS spectrum shows peaks of an M_4L_4 species. Peaks corresponding to species between the +7 and the +19 were assigned (*appendix fig S34*). **Cage 2** was obtained to carry on partitioning experiments between water and EtOAc in the presence and the absence of **ILA**.

Partitioning experiments

Partitioning experiments were performed with **cage 2** to study the ability to transfer across an interface upon a temperature change. Multiphasic systems of **cage 2**, water and EtOAc were prepared and the effects of mixing and the temperature were studied (*fig 22*).

Cage 2 (1.5 mg, 0.12 µmol) was weighed in two vials. In Vial 1, water (0.5 mL) was added. In Vial 2, a solution of **ILA** (15%wt., 0.5 mL) in water was added. In both cases, the dark red cage remained undissolved. EtOAc (0.5 mL) was added to both systems and the vials were inverted 3 times. In Vial 1, two layers were formed and the top organic layer became red, thus indicating that the cage was present almost exclusively in the EtOAc phase. Nevertheless, a portion of the cage precipitated out of both layers and remained at the interface of the two phases. In Vial 2, three layers appeared: **cage 2** dissolved in **ILA** composed the bottom layer. Water composed the middle layer and **cage 2** dissolved in EtOAc composed the top layer. Upon heating to 60˚C, the ionic liquid and the cage completely transferred to the organic phase and the bottom layer (water) remained colourless. After cooling down to 10˚C with an ice bath, three layers formed again.

In the absence of ionic liquid, no reversible transfer was observed as the iron cage remained in EtOAc. The presence of the ionic liquid led to partial transfer of **cage 2** between **ILA** and EtOAc. **ILA** also facilitated the dissolution of **cage 2** in EtOAc, as the top layer of Vial 2 was well defined at 60˚C. The ionic liquid did not promote the solubility of **cage 2** in water. Indeed, the aqueous layer remains colourless and the organic layer is dark red throughout both experiments.

Anion exchange was performed in Vial 1 by adding an aqueous solution of tetrabutylammonium sulphate (50%, 0.1 mL). After inverting 3 times, the top layer turned colourless and the bottom phase (water) became dark red, thus establishing the presence of the cage in the water layer. Heating to 60˚C had no effect; both **ILA** and **cage 2** remained in the aqueous layer.

It was found that **cage 2** could follow **ILA** to the EtOAc layer upon heating to 60˚C and back at 10˚C. Nevertheless no water solubility was observed at any stage of the experiment. This result can be rationalised by the assumption that the hydrophilicity of the ethylene glycol chains is not strong enough to compete with hydrophobicity of the anion.

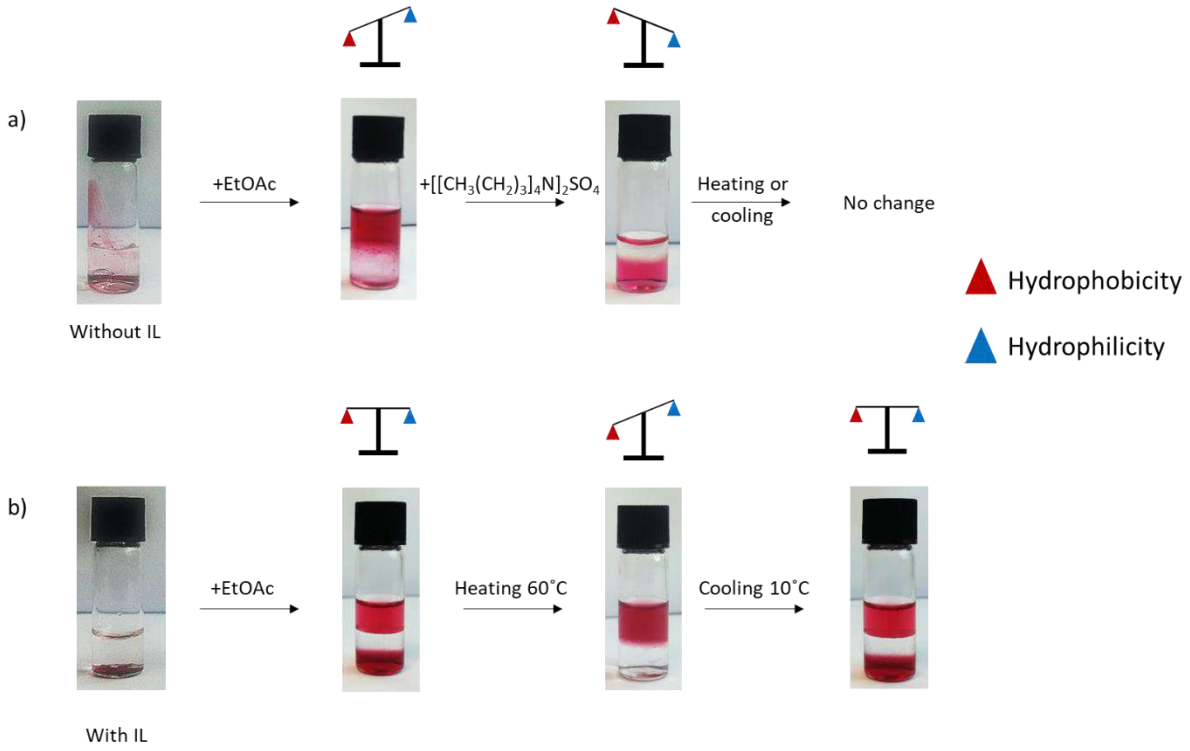

Figure 22 : Partitioning experiments with cage 2 in absence of ionic liquid (top) and in presence of ionic liquid (bottom). In the bottom experiment, a transfer was observed between the ionic liquid and the EtOAc layer.

2.4.2 Tetrahedrons with PEG_{1000} chain – Cages 3, 4 & 5

Self-assembly and stability

To perform a phase transfer as observed for **ILA**, coordination cages with peripheral arms functionalised by PEG-imidazolium chains were synthesised (*fig 23*). As the tetrahedral cage formed with a PEG_{SHORT} chain was not water soluble, longer PEG chain are used to increase the hydrophilicity of the compounds at ambient temperature.

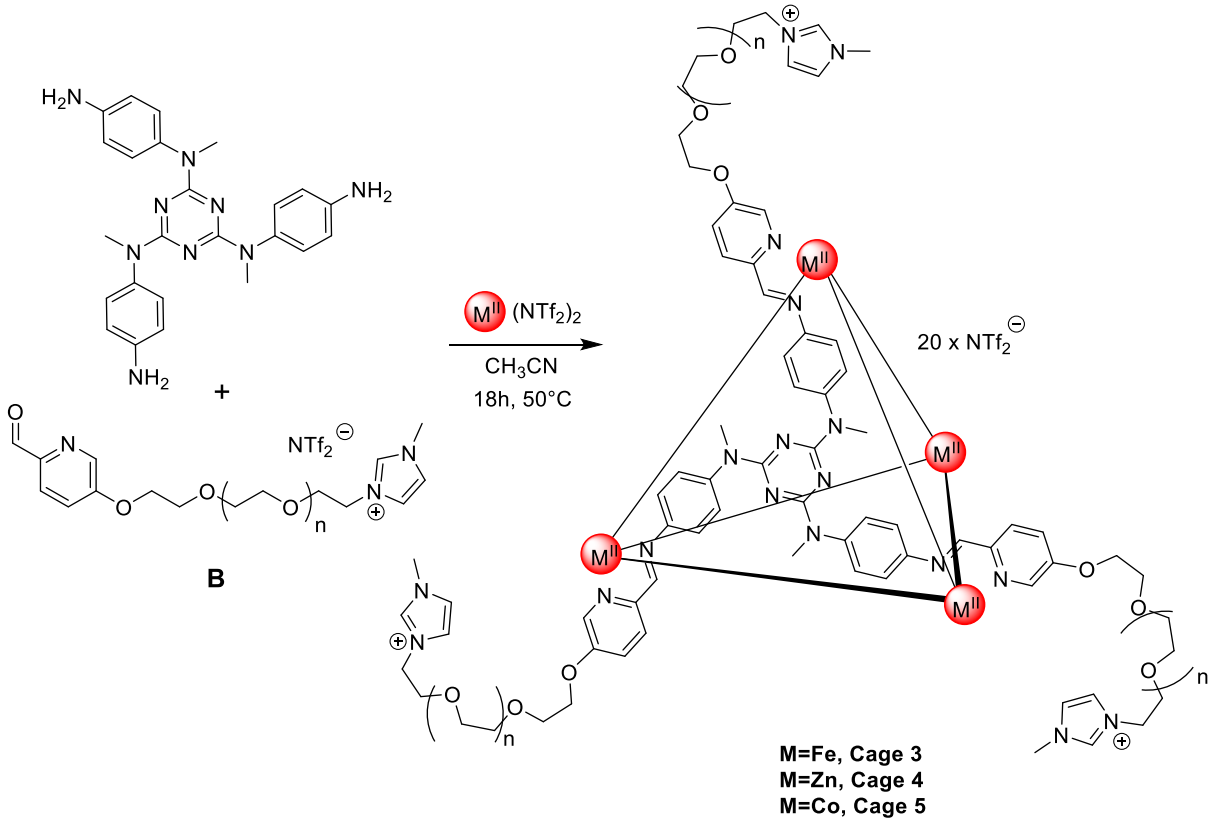

Scheme 9: Self-assembly of cages 3, 4 and 5 in acetonitrile.

Three cages were synthesised with the same C_3-symmetric aniline using different metal salts following the procedure described in section 2.3.3. No ESI-MS could be carried out on the cages with the PEG_{1000} chain because the PEG polymers used for the synthesis of the ligand showed a distribution of lengths. This distribution results in a distribution of cages with varying m/z peaks, which obscures the observation of the charged species by ESI-MS. Instead of discrete peaks for individual charged species, countless small peaks were observed throughout the spectrum.

Final characterization of **cage 3** was done by comparing the spectra of the cages with short and long PEG chains. *Fig 24* compares the aromatic peaks of the ^{1}H-NMR of **cages 2** and **3**. The peak corresponding to proton H_E from the imidazolium shifts upfield for cage 3. This imidazolium proton is known from recent research by Nitschke and coworkers to be highly pH-sensitive. Nevertheless, the proton peaks from the cage have identical chemical shifts for **cage 2** and **cage 3**. **Cage 1** is known to encapsulate the (NTf_2^-) anion, and likewise, encapsulation of (NTf_2^-) by **cages 2** and **3** can be observed in both spectra of a second set of peaks (marked with a *)

Coupled with the ESI-MS of **cage 2**, this spectral comparison establishes that **cage 3** is a tetrahedral cage, isostructural with **cage 2**.

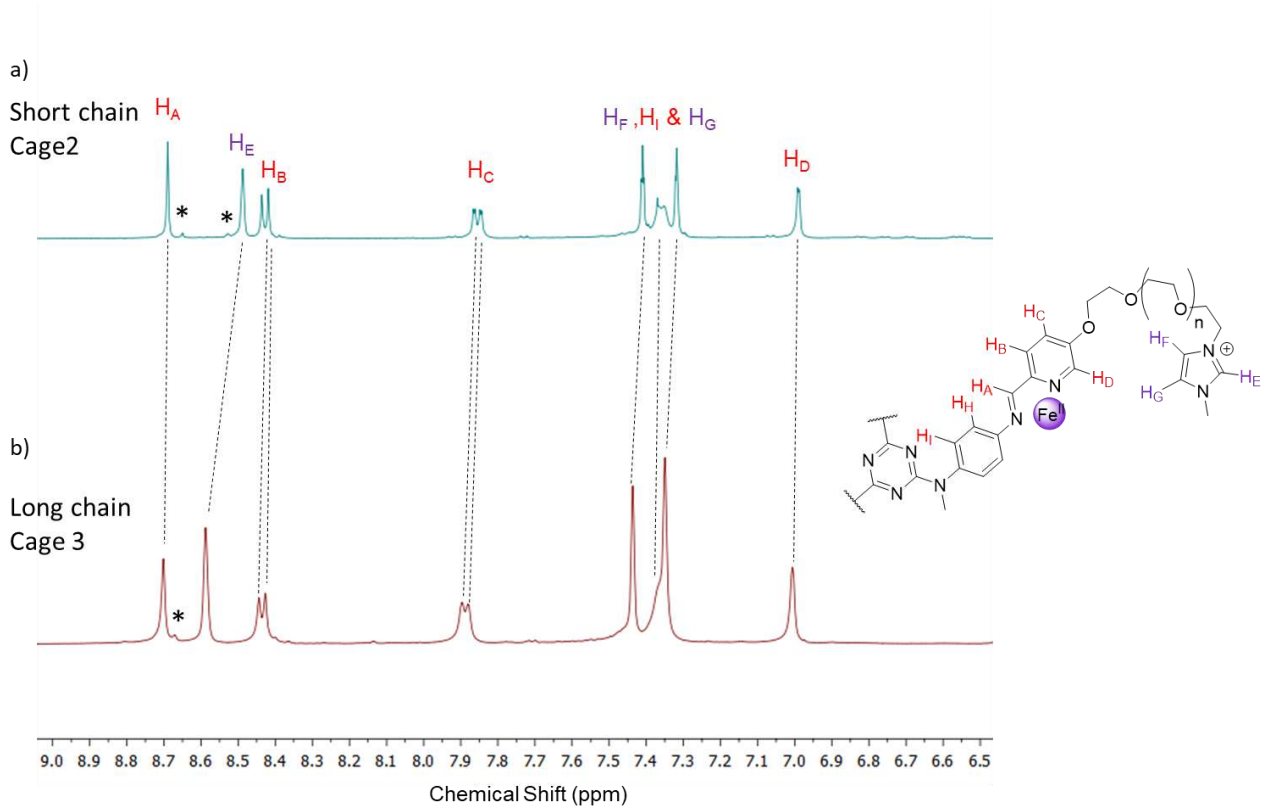

Figure 23 : Direct comparison of the ^{1}H-NMR spectra of cage 2 (top) and cage 3 (bottom) in the aromatic region.

To perform partitioning experiments and observe a phase transfer, the cages must be stable in different solvents. Two types of experiments were performed in order to study the stability of **Cage 3**, **4** and **5**: variable concentration experiments and time stability experiments. An example of UV-Vis characterization of a cage is presented using **cage 3**.

First, a concentration study was performed to investigate the stability of the cages at low concentrations. The stability of **cage 3** at low concentration was studied in acetonitrile and water by UV-Vis experiments at 25°C (*fig 25*).

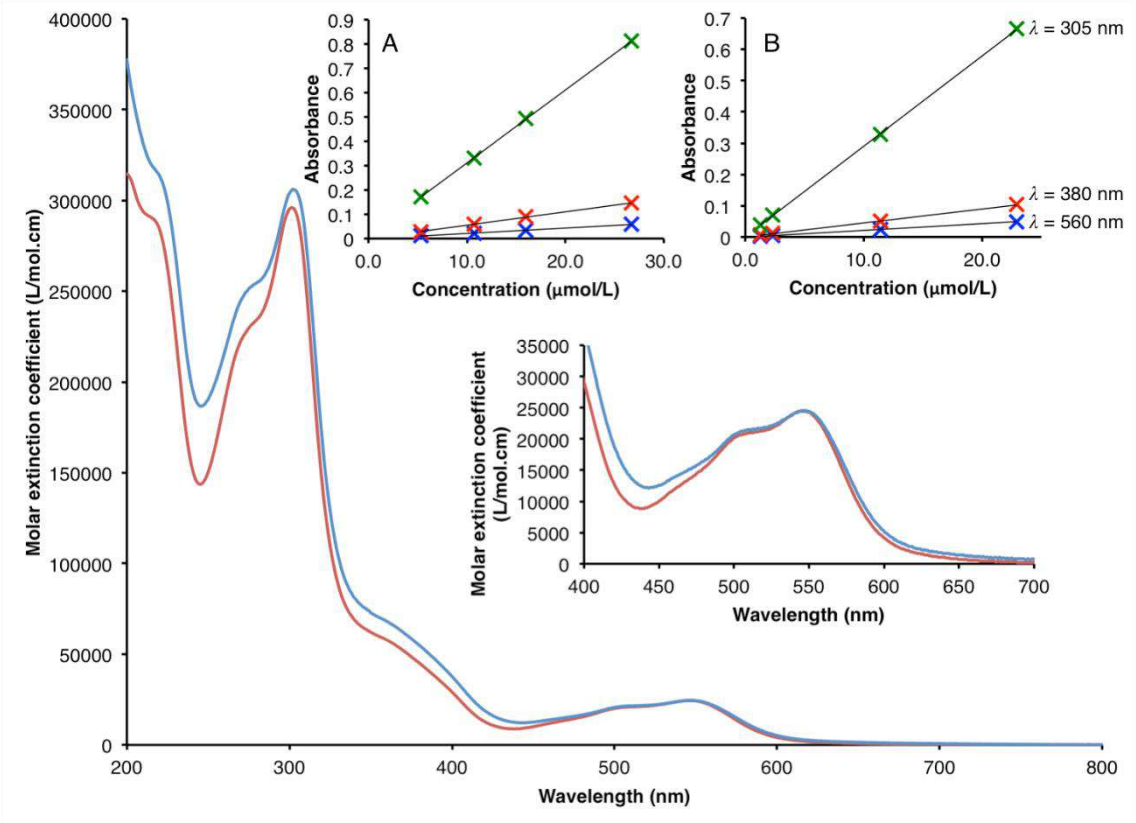

Figure 24 : Absorption spectra of cage 3 at 25°C in CH_3CN (blue) and H_2O (red) at a concentration of 27 µM. The insets (A= CH_3CN, B=H_2O) show the linear increase of absorbance at 560, 380, and 305 nm upon an increase in concentration.

Four different solutions of the cage in acetonitrile (A) and water (B) were prepared by dilution to obtain concentration in cage of 27 µM, 16 µM, 10 µM and 5.1 µM and absorbance was measured in each case between 800 nm and 200 nm.

The spectra in both solvents match and show specific regions: the imidazolium ring absorbance is located between 235 nm and 200 nm. The absorbance shown between 300 nm and 250 nm is characteristic of the pyridine. Finally, the band between 600 nm and 450 nm represents the charge transfer between the metal and the ligand.

As the plot of A versus [C] gives a straight line with good correlation coefficients (coefficients between 0.9964 and 0.9999), the samples follow the Beer-Lambert law

$$A = \varepsilon \cdot l \cdot [C], \qquad [eq.\ 1]$$

with Ɛ: extinction coefficient ($M^{-1}.cm^{-1}$),
l: path length (cm),
[C]: Concentration (M),

These experiments established the stability of **cage 3** in acetonitrile and water at low concentration. **Cages 4** and **5** showed the same behavior and were stable in both water and acetonitrile at low concentration (see appendix *fig S52* and *S57*).

The stability of **cages 3**, **4** and **5** over time was studied. To probe the stability of **cage 3** with time, UV-visible experiments were performed at concentrations of 45 µM and 365 µM (*fig 25*). For each experiment, 80 cycles every 10 min were run at a fixed temperature of 25°C in H_2O and absorbance was measured during the whole duration of the experiments. The absorbance was measured with cuvettes of 1 cm pathway and the band corresponding to the charge transfer between the metal and the ligand was studied. In both cases, the superposition of the UV-Vis spectra shows a decrease in absorbance over time. The plot of absorbance versus time at 550 nm highlights the decrease. At low concentration, after 820 min, the difference in absorbance was evaluated at 13%. It was hypothesised that a decomposition of cage caused this reduction. The concentration effect on the decomposition was studied by running the same experiments in the same conditions at a concentration of 365 µM. At high concentration, the same tendency is observed with a decreased of absorbance with time, although the phenomenon is less important with a difference of 6% after the completion of the experiment. As expected, a higher concentration led to more stability of **cage 3** in water.

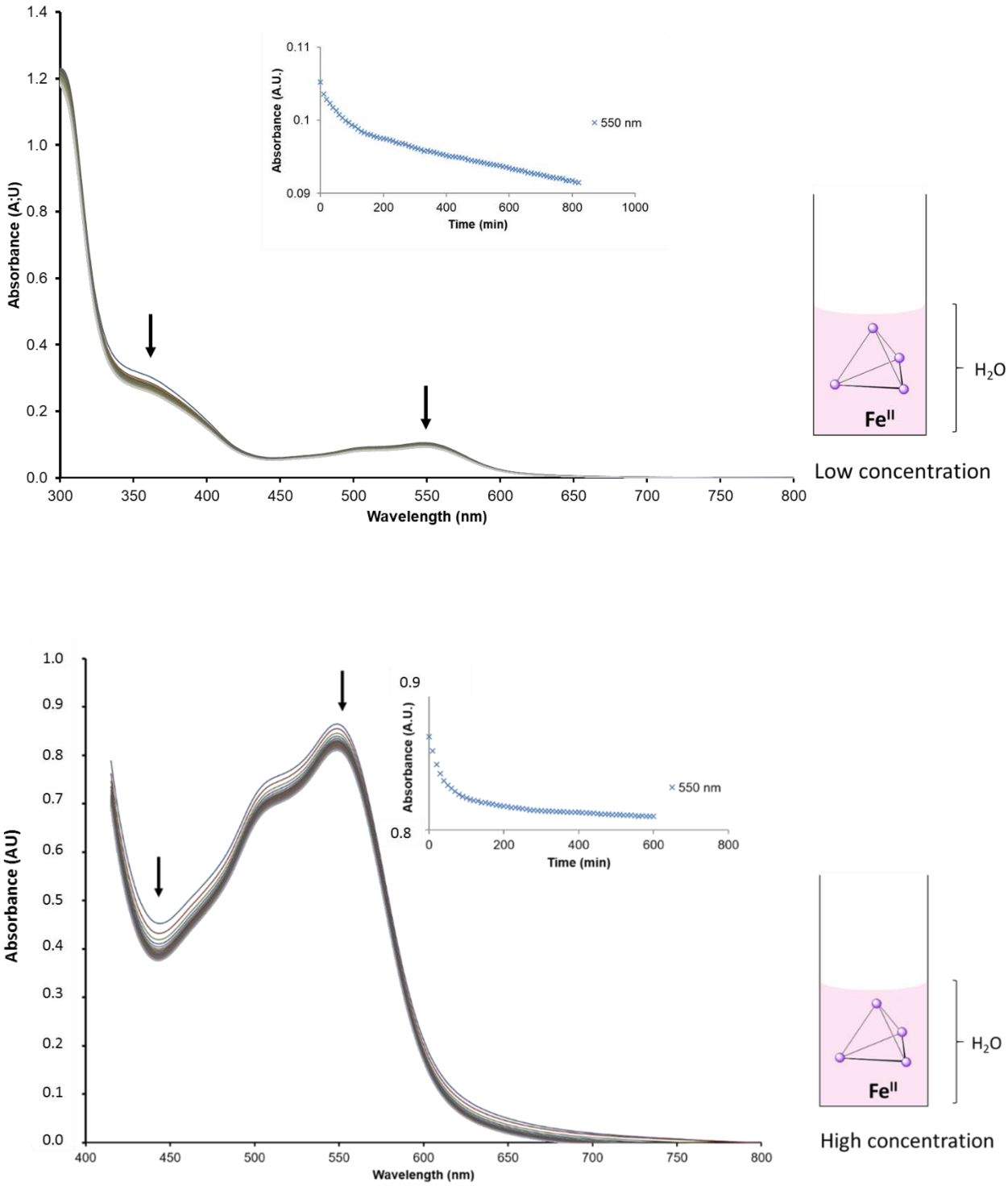

Figure 25 : Absorption spectra of cage 3 at 25°C in H_2O over time for a low concentration (top) and a high concentration (bottom). The insets show the increase in absorbance at 550 nm with time.

As previously discussed, a decrease in absorbance over time was observed for **cage 3** at low and high concentration in water. Comparable experiments were then performed in water for **cage 3** with **ILA** (*fig 26*). The concentration of **ILA** has been fixed at 15%wt in water and two concentrations of cages were studied: 45 µM and 350 µM. UV-Vis experiments were performed with 60 cycles every 10 min at 25°C in water. The absorbance was measured with cuvettes of 1 cm pathway.

Both UV-Vis spectra show very little change in the absorbance. There is a small decrease in the values: 3% for the low concentration and 6% for the high one. This was probably caused by the decomposition of the cage. The decrease in absorbance in these experiments is less important than the previous one with no ionic liquid and it also reaches a plateau by the end of the experiment. The presence of **ILA** thus seems to stabilise the cage in solution.

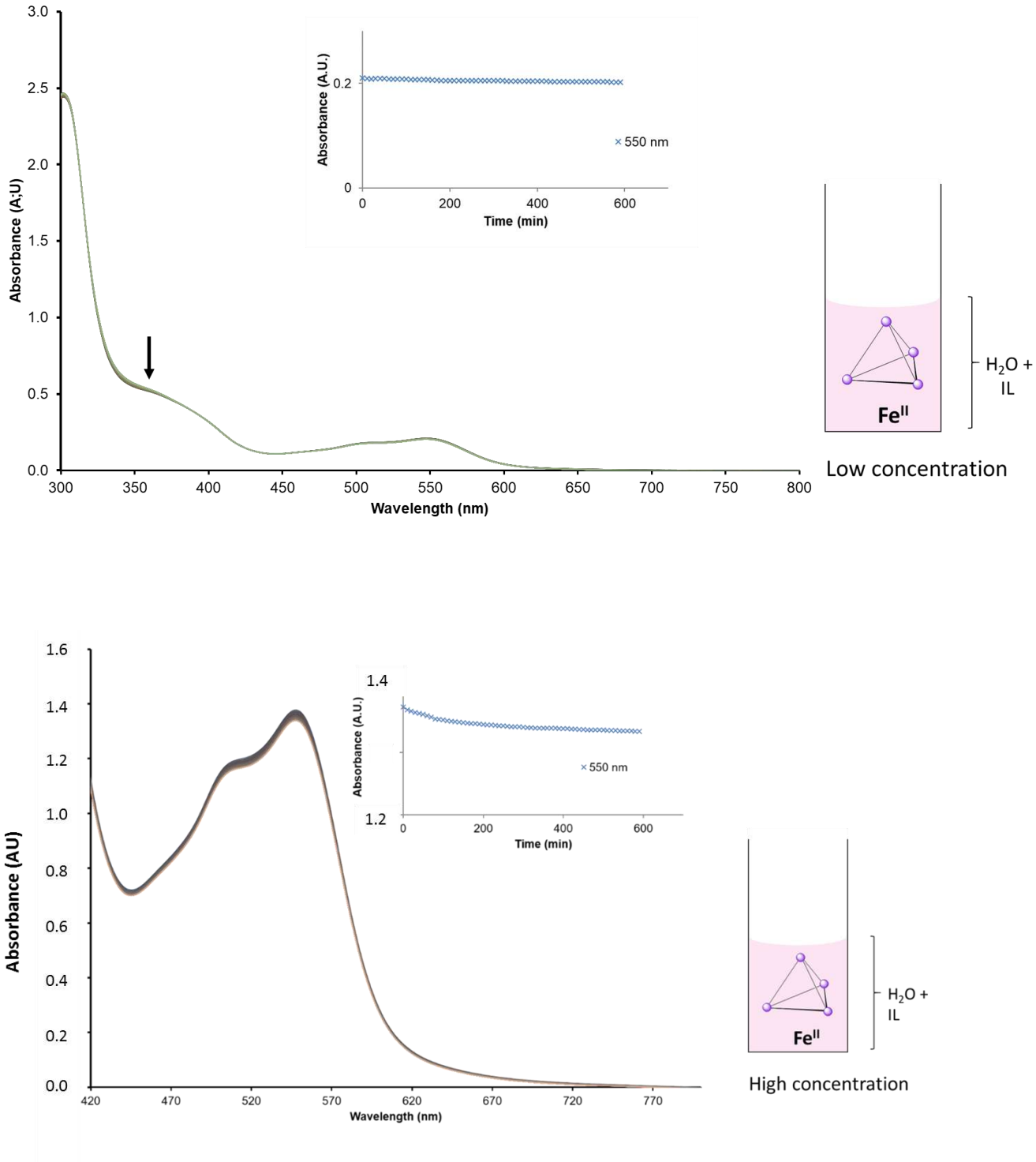

Figure 26 : Absorption spectra of cage 3 at 25°C in H_2O in the presence of 15%wt ionic liquid over time for a low concentration (top) and a high concentration (bottom). The insets show the increase in absorbance at 550 nm with time.

The stability of **cages 4** and **5** in water over time was studied by UV-Vis experiments. The absorbance was studied for both cages at a concentration of 90 µM, in the absence of ionic liquid. For **cage 4**, 90 cycles of measurements every 10 min were carried out at 25°C (*fig 27*). The absorbance around 310 nm and 470 nm decreased drastically. The changes in absorbance were illustrated by the plot over time of the absorbance at different wavelengths. Most of the decomposition happened in the first 170 min of the experiments and the total decomposition of **cage 4** was evaluated at 69% after 890 min. For the cobalt cage, **cage 5**, 60 cycles of measurements every 10 min were recorded at 25°C (*fig 28*). The UV-Vis spectra showed a decrease in absorbance with time. Following the absorbance at 330, 305 and 280 nm emphasized the change in absorption. The phenomenon can be once again explained by a decomposition of **cage 5** in water, estimated at 32% after 590 min of experiment.

From these experiments, it appears that zinc cages and cobalt cages are not stable at these concentrations in water as they begin to decompose immediately. The iron cage (**cage 3**), however, was observed to be the most stable over time and is therefore the most suitable for phase transfer, during which the cage needs to be stable over a long period of time. Because **ILA** helped stabilise **cage 3** in water in this section, partitioning experiments in the following section were performed in the presence of the ionic liquid.

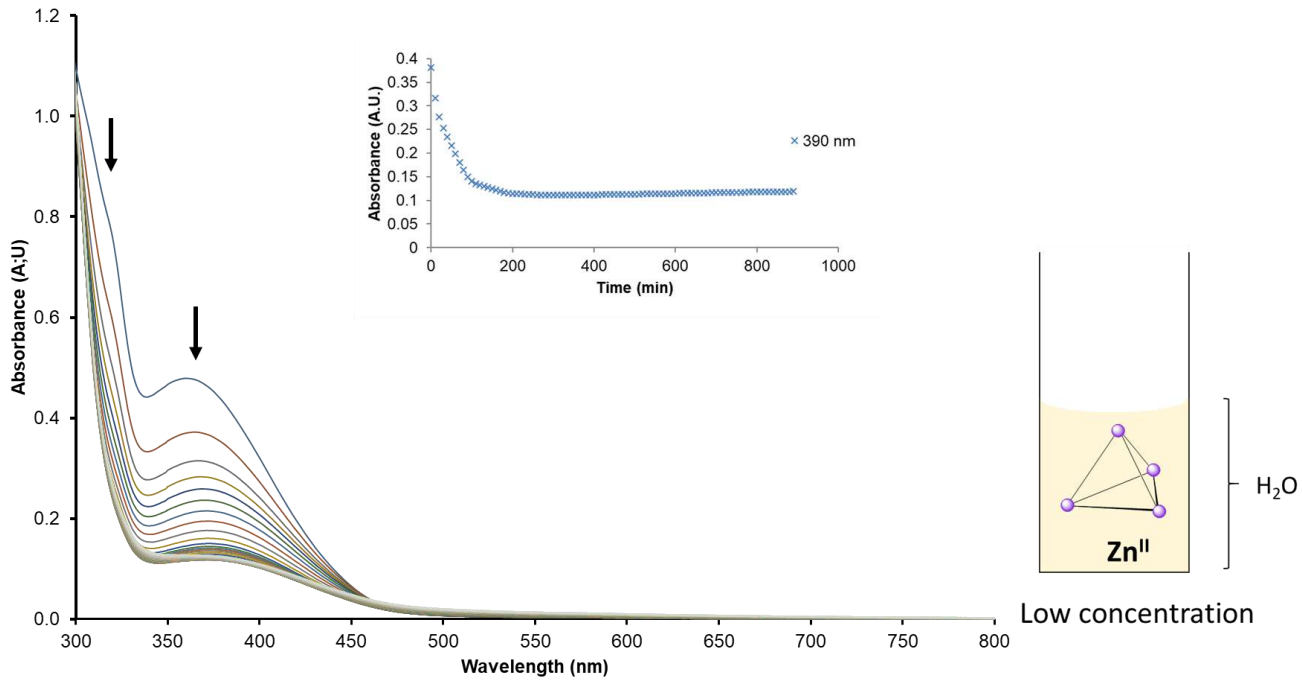

Figure 27 : Absorption spectra of cage 4 at 25°C in H_2O over time for a low concentration. The insets show the increase in absorbance at 390, 315 and 286 nm with time.

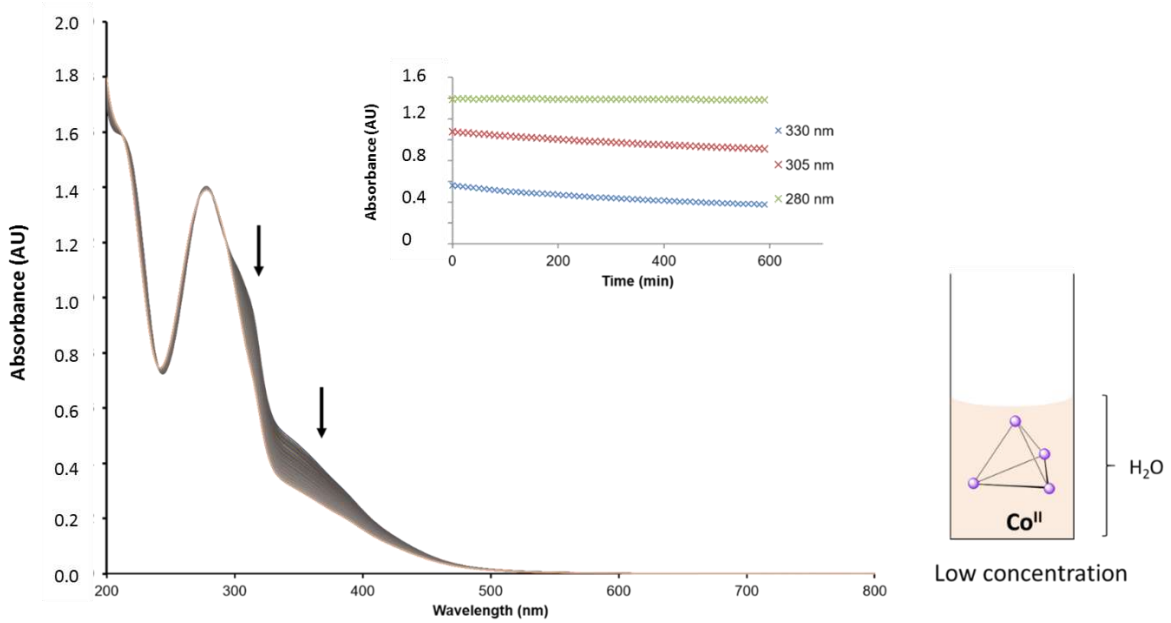

Figure 28 : Absorption spectra of cage 5 at 25°C in H_2O over time for a low concentration. The insets show the increase in absorbance at 330, 305 and 280 nm with time.

Partitioning experiments

Transfer studies were performed to check the ability of the systems {**cage X**+**ILA**} (X=3, 4, 5) to undergo a phase transfer from water to EtOAc and transfer back to water after varying the temperature. A complete study was performed on **cage 3** with three different tests: visual tests, UV-vis experiments and NMR spectroscopy. Partitioning experiments with **cage 4** and **cage 5** were carried out visually.

For the tests, different parameters were modified to determine the best transfer conditions. Low concentration and high concentration in **cage 3** were studied and both showed the ability to transfer with the **ILA**. Different amounts of **ILA** were used to facilitate the transfer. In general, lower concentrations of cage required less ionic liquid to transfer; as a consequence, however, a higher temperature was needed. By using higher %wt., the temperature required for transport to EtOAc can be lowered and the heating time becomes shorter.

Visual experiments

To illustrate the effect of the percentage of ionic liquid, a solution of **cage 3** (0.80 mg, 0.037 µmol, 75 µM) and **ILA** in H_2O (500 µL, 9%wt.) was prepared. EtOAc (500 µL) was added and temperature was alternated between 10°C and 65°C (*fig 29*).

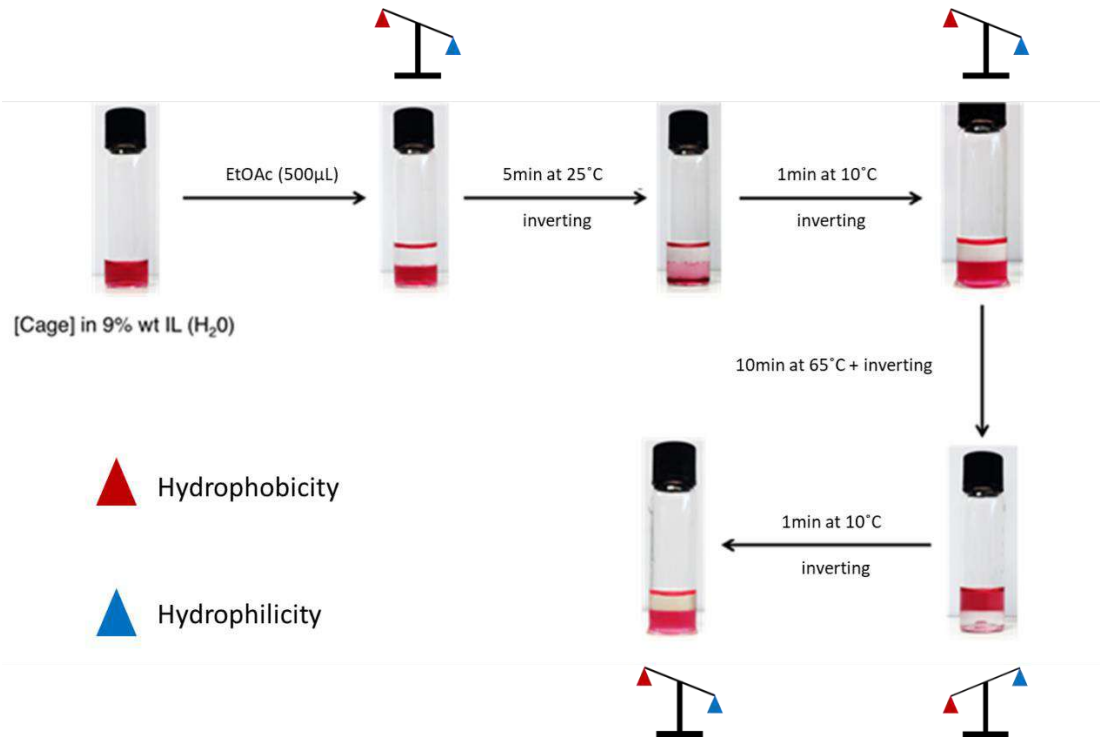

Figure 29 : Visual partitioning experiments of cage 3 in water and EtOAc in presence of 9% wt ILA between 10°C and 65°C; a transfer was observed visually by following the dark red cage.

First, **cage 3** initially dissolved in water, confirming that the PEG_{1000}-imidazolium chain renders the cage hydrophilic at ambient temperature. EtOAc (500 µL) was added, which caused the ionic liquid to separate out from the water layer, thus generating 3 layers. The majority of **cage 3** remained in the IL layer (bottom) but some is soluble in the aqueous middle phase. The whole system was cooled with an ice bath in order to solubilise the IL in the water. At 10°C, only two phases were observed. The bottom phase appeared dark red thus indicating the presence of the cage. The two phases were heated at 65˚C for 10 min and the vial inverted 3 times leading to a transfer of the colour from water to EtOAc. Indeed, the water layer became colourless and the EtOAc became dark red. The increase in temperature drove a phase transfer of the system {**Cage 3**+**ILA**} from the water to the organic EtOAc phase. Cooling at 10°C allowed a reversible transfer of the cage and the IL back to the water phase. The same experiment was performed with a more concentrated solution of cage in water (450 µM) with 15% of IL. The temperature of transfer could be lowered to 60°C and the same results were observed with a more intense colour. This experiment shows that, upon changes in temperature, **cage 3** is able to undergo a reversible phase transfer between water and EtOAc with the aid of ionic liquid **ILA**.

Partitioning experiments were carried out with **cages 4** and **5**, both having PEG_{1000}-imidazolium chains at the vertices (*fig 30*). The apparatus and method used was the same as for **cage 3**. Solutions of **ILA** in H_2O (500 µL, 15%wt.) were prepared and **cages 4** (0.81 mg, 0.038 µmol, 75 µM)and **5** (0.80 mg, 0.037 µmol, 75 µM) were added. In all cases the cages were entirely dissolved in the aqueous solution at ambient temperature. EtOAc (500 µL) was added in both solutions and the systems were cooled using an ice bath. At low temperature, the top phases were observed to be transparent and colourless whereas the bottom phases were coloured. This indicates that the systems {cage+ionic liquid} were located in the aqueous layer. Upon heating to 60°C, the colour moved from water to EtOAc thus indicating that the cages and the ionic liquid transferred from water to EtOAc upon reaching the high temperature. The systems were then cooled down and a reversible transfer from the organic phase to the water was observed. In all cases, it was possible to observe a reversible transfer of the cage triggered by a change in temperature.

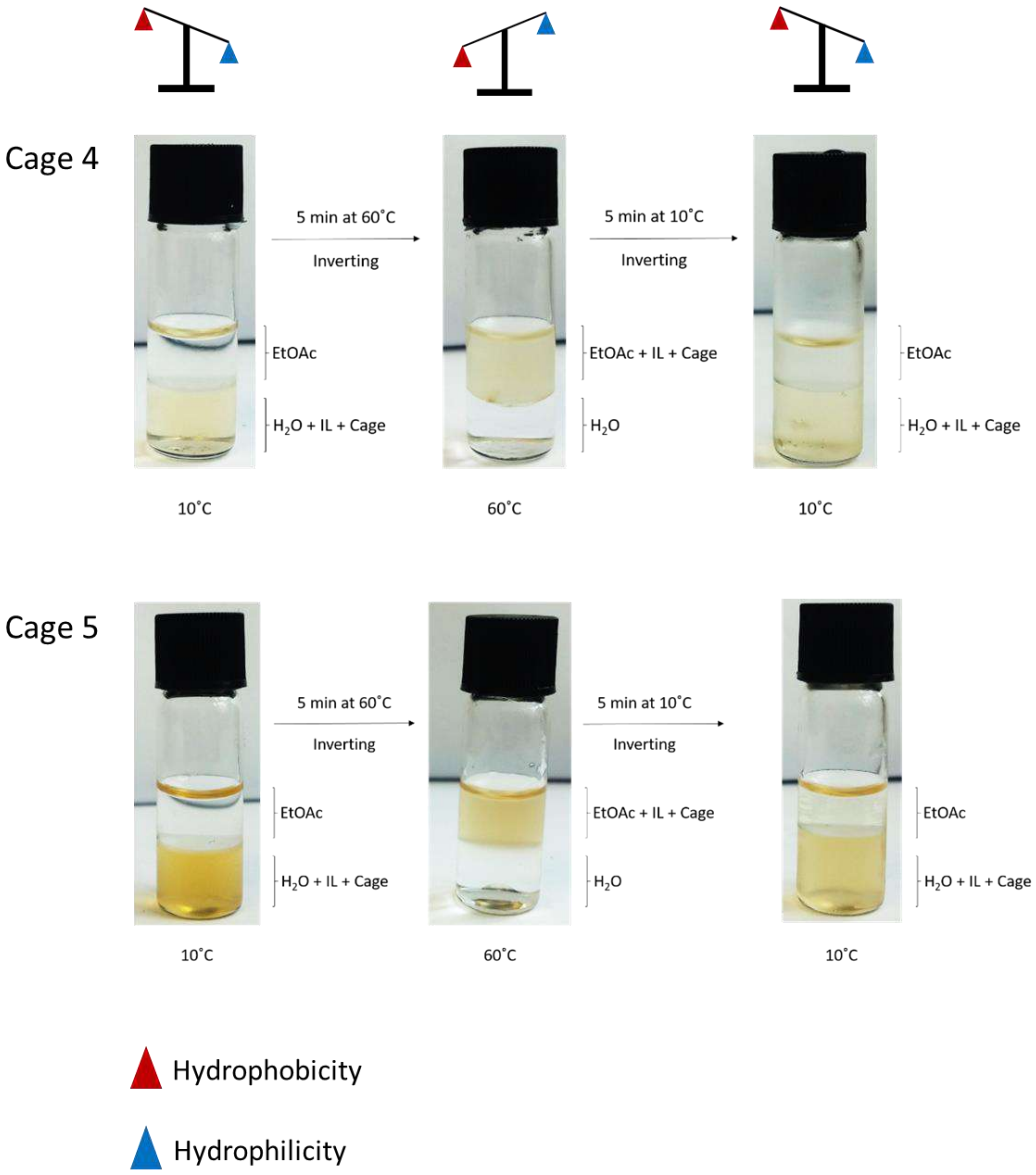

Figure 30: Partitioning experiments of cages 4 and 5 in water and EtOAc in presence of 15% wt ILA. A transfer was observed between 10°C and 60°C by following the transfer of the colored cages.

UV-Vis study

UV-Vis spectroscopy was used to characterise the phase transfer of **cage 3**. Experiments were performed with an aqueous solution **ILA** (400 µL, 15%wt.) to which **cage 3** (3.5 mg, 0.16 µmol, 400 µM) and EtOAc (400 µL) were added. UV-Vis absorbance of each phase was measured at 10˚C and at 60˚C between 800 nm and 380 nm (*fig 31*).

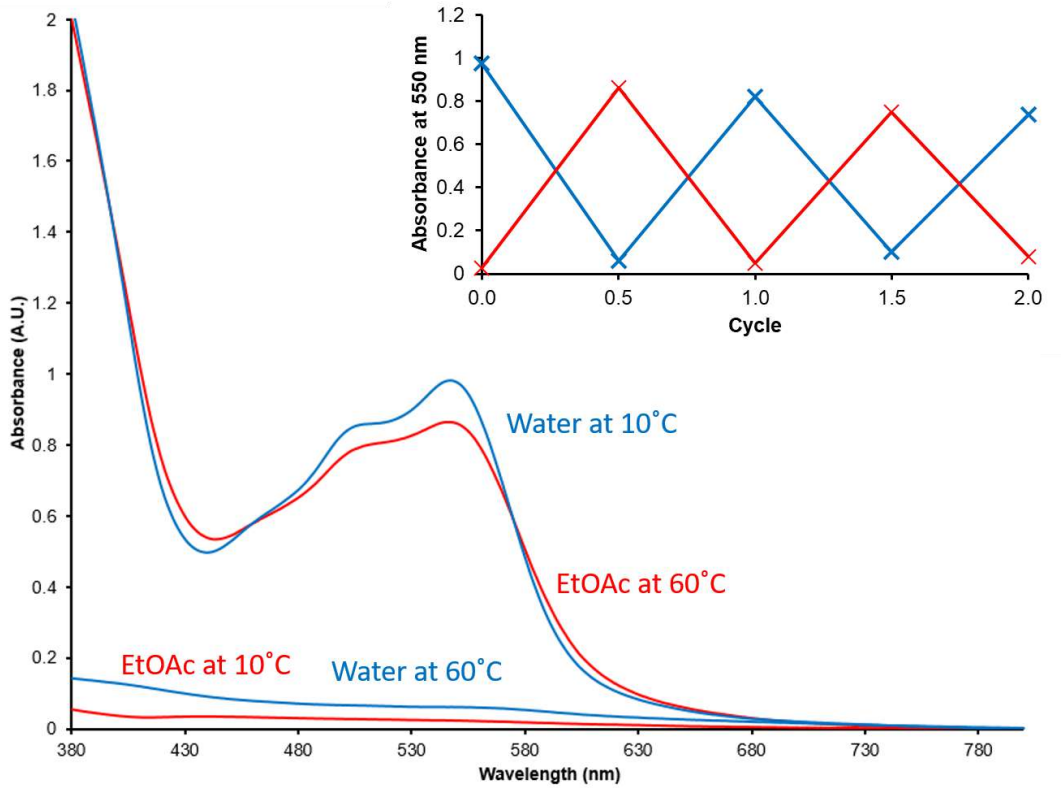

Figure 31 : Absorption spectra at 10°C and at 60°C of the H_2O phase and EtOAc phase during a partitioning experiment. The insets show fatigue study over 2 cycles of heating and cooling.

First measurements at 10˚C showed no absorption of the organic phase and an absorbance pattern corresponding to the cage in the aqueous layer. At 60˚C, **cage 3** was transferred to the organic layer and the absorbance in the water is close to 0. Two cycles of heating and cooling the system were carried out to study the fatigue of the system. After 2 cycles, a fatigue of 24% was observed, as some of the {**cage 3**+**ILA**} system remained in the EtOAc. Nevertheless, these UV-Vis experiments confirmed the transfer of {**cage 3** + **ILA**} from water to EtOAc upon heating to 60˚C and back to the water upon cooling to 10˚C.

2.4.3 $Fe_4^{II}L_6$ tetrahedrons – Cages 6 & 7

Self-assembly and stability

The previous section established the formation of cages **3**, **4** and **5** functionalised with PEG_{1000}-imidazolium peripheral arms. These cages, in presence of **ILA** underwent a reversible phase transfer between water and EtOAc upon temperature changes. In this section, the generality of thermoswitchable phase transfer will be. For this reason a different aniline was investigated for the self-assembly of coordination cages. A C_2-symmetric aniline was used for the formation of coordination cages, as shown in *fig 32*.

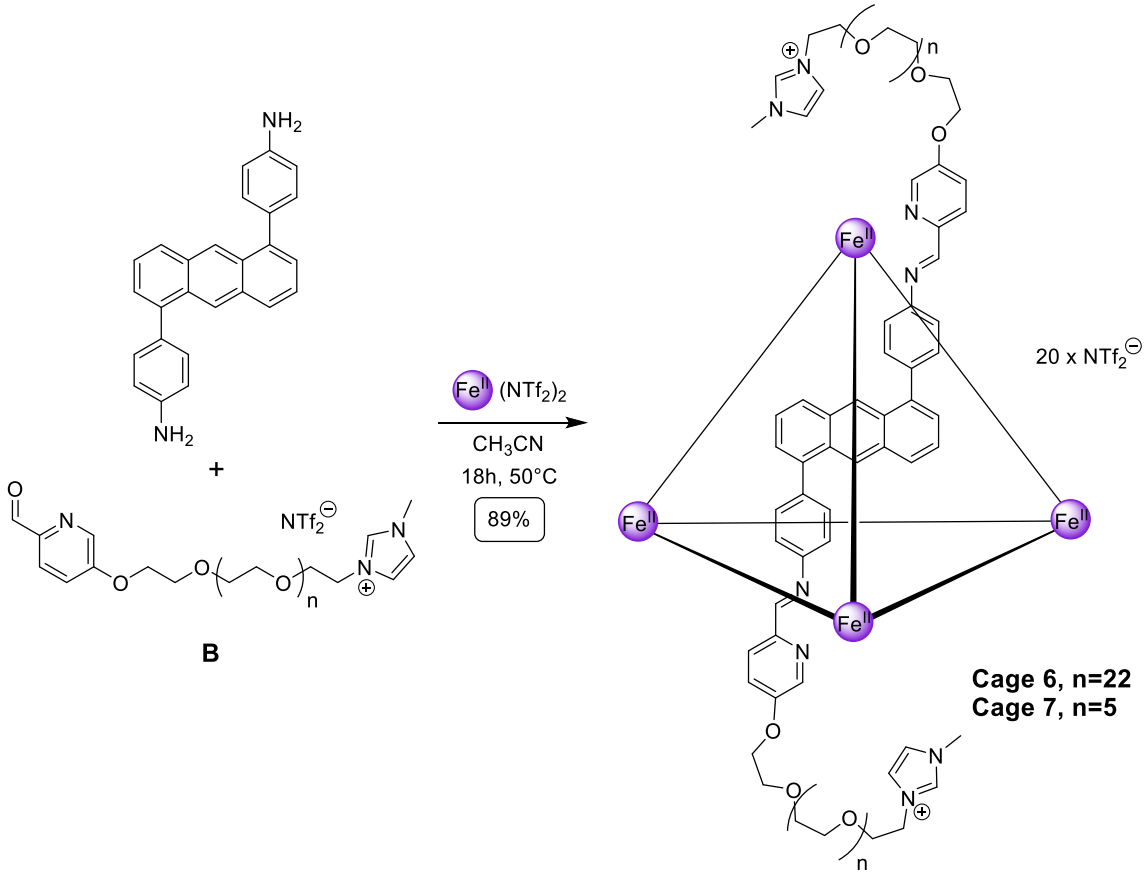

Figure 32 : Self-assembly of cage 6 in acetonitrile.

As for cage 3, it was not possible to characterise **cage 6** by ESI-MS so the structure was confirmed after comparison with **cage 7** which was characterised by both ^{1}H-NMR spectroscopy and ESI-MS. The ^{1}H-NMR spectra from **cages 6** and **7** are comparable with a typical doublet at 6 ppm and the imine singlet around 9 ppm (*fig 33*). Coupled with the ESI-MS of **cage 7** (*appendix fig S74*), this spectral comparison establishes that **cage 6** is a tetrahedral cage, isostructural with **cage 7**.

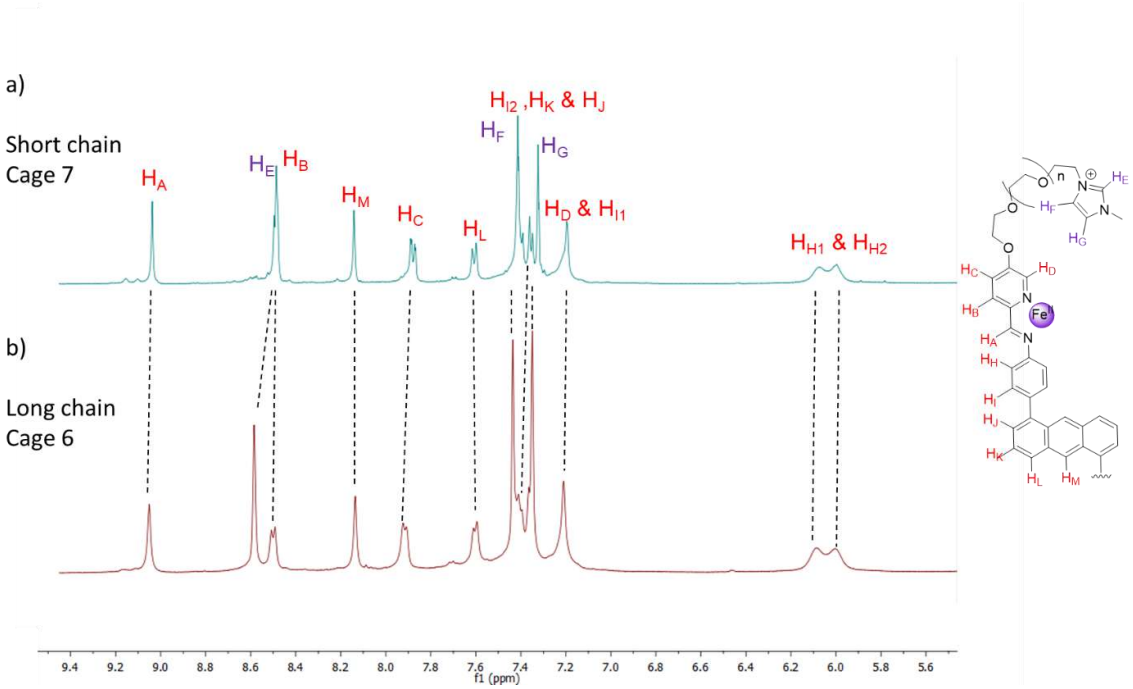

Figure 33 : Direct comparison of the ^{1}H-NMR spectra of cages 6 (bottom) and 7 (top) in the aromatic region.

The stability of **cage 6** at low concentration (27 µM) in water and acetonitrile was studied by UV-Vis at 25˚C (*fig 34*). The cage behaves similarly in both solvents. The absorbance was measured at lower concentrations and the plot of the absorbance versus the concentration for 3 different wave lengths resulted in straight lines. **Cage 6** follows the Beer-Lambert low and thus is stable at low concentration.

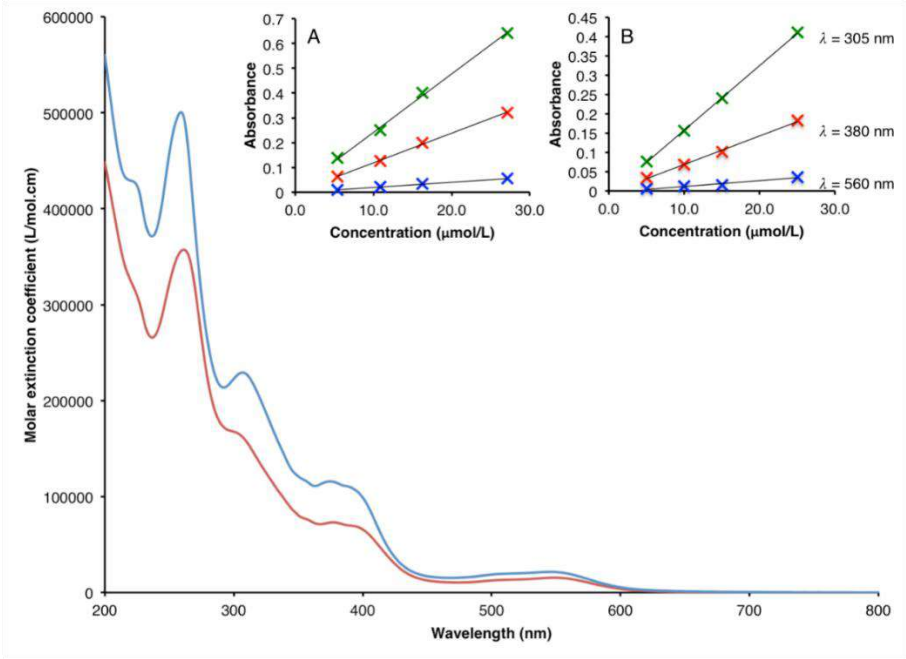

Figure 34: Absorption spectra of the cage 6 at 298K in EtOAc (blue line) and H_2O (red line) at 27 µM. The insets (A: CH_3CN, B: H_2O) show the linear increase of absorbance at 460, 380 and 305 nm upon the increase of the concentration (r^2= 0.998, 0.9988 and 0.9993 in CH_3CN and r^2= 0.9997, 0.998 and 0.9911 in H_2O).

Partitioning experiments

Visual partitioning experiments were performed in order to determine if **cage 6** could undergo a phase transfer as the other cages presented previously (*fig 35*). A solution of **ILA** in water (500 µL, 15%wt.) with **cage 6** (0.82 mg, 0.038 µmol, 75 µM) was prepared. The cage was readily dissolved in the aqueous solution of **ILA**. EtOAc (500 µL) was added and the solution was cooled down to 10˚C with an ice bath. After inverting 3 times, the bottom layer appeared dark red and the top layer was colourless. The system {**cage 6** + **ILA**} was thus present in the water layer. The vial was heated to 60˚C and inverted 3 times. The colour migrated from the water phase to the EtOAc phase. Indeed, the bottom phase became colourless as the organic phase became dark red, thus indicating the transfer of the {**cage 6** + **ILA**} to the EtOAc phase. After cooling the system to 10˚C, the system {**cage 6** + **ILA**} transferred back to the aqueous phase. As for cages **3**, **4** and **5**, **cage 6** was thus capable of reversible phase transfer between water and EtOAc upon temperature changes.

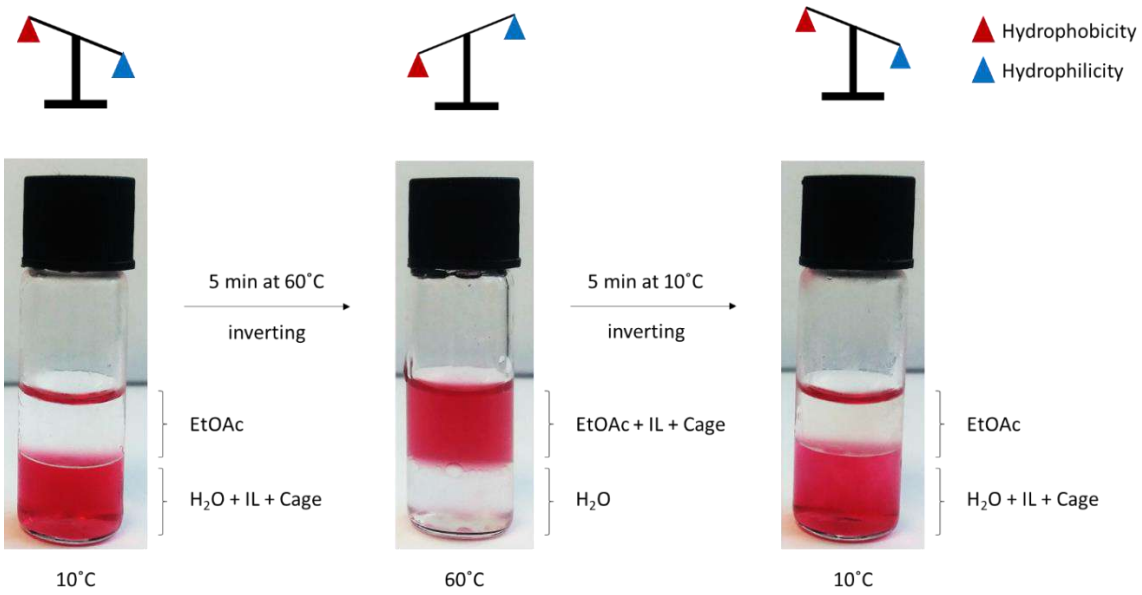

Figure 35: Partitioning experiments of cage 6 in water (bottom) and EtOAc (top) in presence of 15%wt. ILA. A transfer was observed between 10°C and 60°C by following th dark red cage.

2.5 - Conclusion

A library of PEG-imidazolium functionalised tetrahedral coordination cages were synthesised by self-assembly. Parameters such as the length of the PEG chain, the metal atom and the aniline subcomponent have been studied regarding phase transfer.

Table 3: Summary of transport experiments carried out with cages 1-7.

Cages	No IL	IL
Non-functionalised	No transport	No transport
PEG_{SHORT} chain functionalised	No transport	No transport between H_2O and EtOAc
PEG_{1000} chain functionalised	Transfer between H_2O and EtOAc with difficulties	Phase transfer between H_2O and EtOAc

Fe^{2+} **Cage 2** with PEG_{SHORT}-imidzolium confirmed that the cage and **ILA** exhibited limited mobility between a neat IL layer and EtOAc, instead of between H_2O and EtOAc. Nevertheless, the hydrophilicity of the PEG chain was not sufficient to make **cage 2** water soluble at ambient temperature and **cage 2** could not transfer between water and EtOAc.

It was hypothesised that increasing the length of the PEG chain would increase the hydrophilicity of the cage at 25˚C and facilitate the phase transfer. **Cages 3**, **4** and **5** were self-assembled with PEG_{1000} imidazolium arms. It was established that three cages were soluble in water at ambient temperature, yet it appeared the iron cage was more stable than the zinc and cobalt analogues at low concentrations. According to UV-Vis experiments, **cage 3** decomposed slower than **cage 4** and **cage 5**, and the phenomenon was lessened in the presence of the ionic liquid. Partitioning experiments were carried out on these three cages to study their ability to undergo a phase transfer between water and EtOAc. Visual experiments (for **cages 3**, **4** and **5**) and UV-Vis experiments (for **cage 3**) showed successful transfer of the systems {cage + ionic liquid}. By heating at 60°C, the ionic liquid which interacts with the functionalised cages facilitated the phase transfers. Upon cooling down, the systems became hydrophilic and both the ionic liquid and the cages transferred back to the water layer.

To investigate the generality of this transfer strategy, an anthracene derivative was used to self-assemble **cages 6** and **7**. The PEG_{1000}-imidazolium chains made the cage water soluble at room temperature. The cage underwent reversible phase transfer between water and EtOAc in the presence of **ILA** under the same conditions as **cages 3**, **4** and **5**.

The combination of PEG_{1000}-imidazolium chains and $(NTf_2)^-$ anions was shown to be an efficient way to reversibly transfer coordination cages between water and EtOAc upon temperature changes.

3-Future work

So far, 6 cages have been synthesised with PEG imidazolium arms, 4 with PEG_{1000} chains that undergo visual phase transfer between an aqueous layer an an organic layer with variations in the temperature.

Nevertheless, to fully characterise the transfer, the study needs to be completed by performing slice-selective ^{19}F-NMR on all the coordination cages formed. The major problem occurring with this technique is a concentration problem. Indeed, the phase transfer is carried out in the presence of the ionic liquid in high concentration (15% wt. In water) so the intensity of the peaks of the ionic liquid protons saturate the detector, decrease the sensitivity of ^{1}H-NMR experiments, and therefore frustrate attempts to observe cage peaks. It is then impossible to distinguish the peaks of the ionic liquid from the peaks of the cage in the aromatic region for example. Nevertheless, there is precedent in the literature[37] for the transfer study of the system through a fluorinated guest. Indeed, if the tetrahedral iron complex manages to encapsulate a fluorinated guest, it is possible to follow the peaks of the guest by ^{19}F-slice selective NMR. If the peaks of the guest have a different chemical shift than the one from the ionic liquid (NTf_2^-), NMR experiments then show the evolution of the system by following a characteristic peak of the guest in both phases at different temperature. 1-Fluoroadamantane can be used for the $M^{II}_4L_4$ tetrahedrons. For the $M^{II}_4L_6$ tetrahedral cage formed with an anthracene motif, a fluoro[60]fullerene can be tested as a guest, as it was previously established by Nitschke and coworkers that anthracene-edged cages could encapsulate C_{60} molecules.[46] The NMR studies would be performed on the same principle as for the ionic liquid of the $Fe^{II}_4L_4$ cage already characterised: slices on the two phases would be analysed at 10°C and 60°C.

Once the characterisation is done, the cages can be used to create a pumping system with the aim of transporting a cage and its cargo against a concentration gradient. For these experiments, special apparatus are needed: a heating and a cooling devices that are acting locally to increase the temperature to 60°C or decrease it to 10°C, and a tube with alternated solvent slices to transport the system of cage and ionic liquid (*fig 36*).

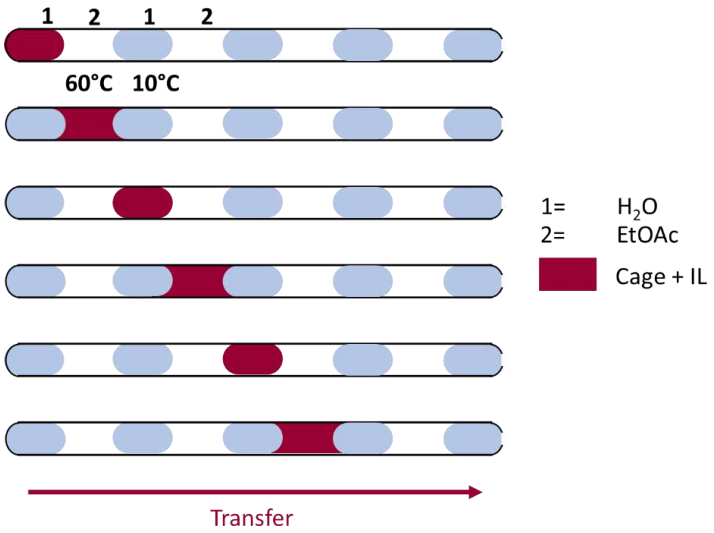

Figure 36: Pumping system with a cage (red) and ILA transferring between alternated water and EtOAc layers with temperature changes.

With this system, cooling and heating slices two by two will result in multiple and successive phase transfer along the tube. A cage such as the ones described in this thesis and its cargo could be transferred from one end of the tube to the other by changing the temperature and no other stimulus. The pumping system can also be used as a separating system. Indeed, it is possible to imagine a 3-directional system with three guests and three cages undergoing thermodriven phase transfer. Each cage would encapsulate a specific guest and the three host-guest complexes could be separated by cooling and heating the arms of the chamber.

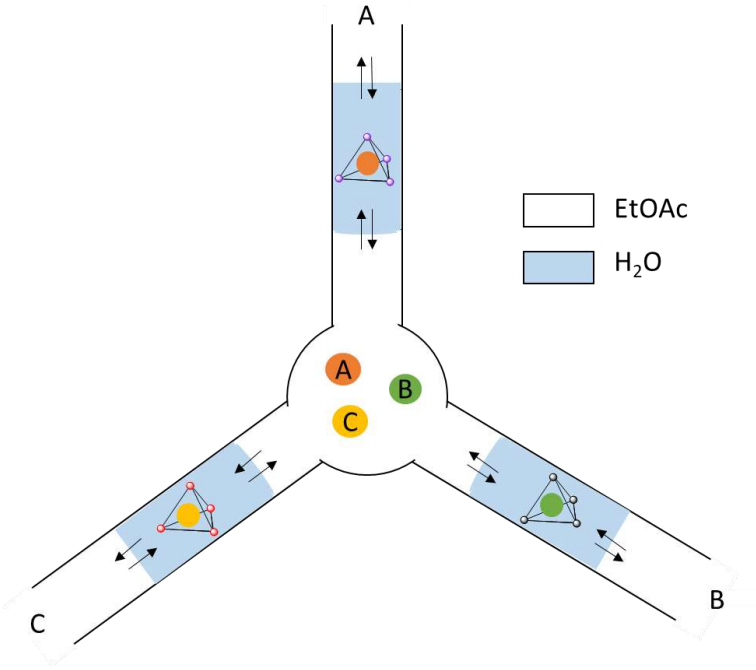

Figure 37: Separating system bases on phase transfer of the cage and ILA in water and EtOAc. A, B and C are guests that can be encapsulated by a specific cage.

It is also interesting to widen the scope of cages with the ability of transferring between phase. It is possible to investigate other anilines like anilines with pyrene motif to obtain another tetrahedron or a porphyrin motif to obtain a cubic cage. Other geometry can also be investigated such as helicates or barrels. This study could reveal the solubility properties that the PEG_{1000} imidazolium ligand gives to the coordination complexes formed and establish new phase transfer abilities.

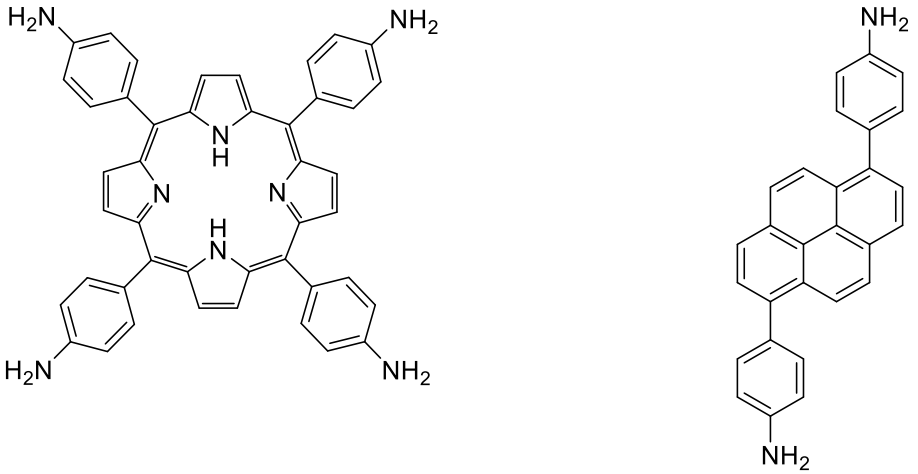

Figure 38: Structure of possible anilines to be investigated for the self-assembly of cages: 5,10,15,20-tetrakis(4-aminophenyl)-21*H*,23*H*-porphine (left) and 1,6-bis(4-aminophenyl)pyrene (right).

APPENDIX-Experimental

A-General

Materials and methods

All reagents and solvents were purchased from commercial sources and used as received. CH_3CN (or CD_3CN) for Iron(II) cage syntheses were degassed by 3-4 evacuation/N_2 fill cycles prior to use. 5-(hydroxyl)picolinaldehyde,[47] 1,14-Bis(tosyloxy)-3,6,9,12-tetraoxatetradecane,[48] N2,N4,N6-tris(4-aminophenyl)-N2,N4,N6-trimethyl-1,3,5-triazine-2,4,6-triamine,[28] 1,5-bis(4-aminophenyl)anthracene,[46] $[PEG(mim)_2][NTf_2]_2$,[38] $Co(NTf_2)_2•6H_2O$[27] and $Fe(NTf_2)_2•6H_2O$[49] were prepared by literature procedures.

Nuclear Magnetic Resonance (NMR)

^{1}H-NMR spectra were all recorded either at 500 MHz on a Bruker AVC-500 spectrometer with an ATM BB probe or at 400 MHz on a Bruker AVC-400 spectrometer with a QNP probe. $^{13}C\{^1H\}$ NMR spectra were recorded at 100 MHz on a Bruker AVC-400 spectrometer with a QNP probe. $^{19}F\{^1H\}$ NMR spectra were recorded either at 471 MHz on a Bruker AVC-500 spectrometer with an ATM BB probe or at 376 MHz on a Bruker AVC-400 spectrometer with a QNP probe. ^{1}H chemical shifts (δ_H) are expressed in parts per million (ppm) and reported relative to the resonance of the residual protons of $CDCl_3$ (δ_H = 7.26 ppm), CD_3CN (δ_H = 1.94 ppm), or relative to the internal standard acetone (δ_H = 2.22 ppm) for samples in D_2O. ^{13}C chemical shifts (δ_C) are expressed in ppm and reported relative to the resonance of the carbons in $CDCl_3$ (δ_C = 77.16 ppm) or CD_3CN (δ_c = 118.26 and 1.32 ppm). In organic solvents and water, ^{19}F chemical shifts (δ_F) are reported relative the external standard (contained in a coaxial capillary) trifluoroacetic acid in $(CD_3)_2CO$ (δ_F = -76.00 ppm) or C_6F_6 in CD_3CN, CD_2Cl_2 or $CDCl_3$ (δ_F = -164.9 ppm). All measurements were carried out at 298 K unless stated differently. Abbreviations used in the description of NMR data are as follows: bs: broad singlet; s: singlet; d: doublet; t: triplet; dd: doublet of doublets; m: multiplet. Coupling constants (*J*) are given in hertz (Hz).

Diffusion Ordered (DOSY) NMR experiments were performed on a Bruker AVC-400 spectrometer with a QNP probe. Maximum gradient strength was 6.57 G/cmA. The standard Bruker pulse program, ledbpgp2s, employing a stimulated echo and longitudinal eddy-current delay (LED) using bipolar gradient pulses for diffusion using 2 spoil gradients was utilised. Rectangular gradients were used with a total duration of 1.5 ms. Gradient recovery delays were 875-1400 µs. Diffusion times (Δ and δ) are quoted for each experiment below. Individual rows of the S4 quasi-2D diffusion databases were phased and baseline corrected.

Mass spectrometry (MS)

Low resolution electrospray ionisation (LR-ESI) mass spectrometry was undertaken on a Micromass Quattro LC mass spectrometer (cone voltage 10-30 eV; desolvation temp. 313 K; ionization temp. 313 K) infused from a Harvard syringe pump at a rate of 10 µL min^{-1}.

UV-Vis spectroscopy

UV-Visible absorption spectroscopy was performed using a Varian Cary 5000 UV-Vis-NIR spectrophotometer fitted with a Peltier temperature controller accessory. Spectra were obtained in double beam mode using only the (front) analyte beam to record spectra, with solvent in the (rear) reference path. A background spectrum of the neat solvent was recorded using the analyte beam prior to each experiment series and baseline correction applied using the Cary WinUV software suite. Samples were analysed using quartz cuvettes with optical path lengths of 10 mm.

Additional Discussion of Characterisation Techniques

At the maximum concentration of cages in ionic liquids used in this paper, ^{1}H signals from the ionic liquid saturate the detector, decrease the sensitivity of NMR experiments, and therefore frustrate attempts to observe cage peaks. Mass spectrometry is similarly not useful; signals from the ionic liquid swamp the spectrum. Additionally, ^{1}H-NMR peaks from imidazolium ionic liquids occur throughout the spectral range, overlapping with potential cage peaks and rendering futile the use of selective pulse sequences for solvent suppression. Likewise, using ^{1}H DOSY to separate ionic liquid signals from solute signals is not feasible – as observed by Giernoth *et al*.,[50] the diffusion coefficients of the ionic liquid and large solutes are too similar. We also attempted using ^{19}F DOSY NMR to distinguish encapsulated from free fluorinated guests. In all cases, the encapsulated guest peaks lacked sufficient intensity to be observed by DOSY after measuring 16 increments of 1600 scans each. In previous work,[36,37] however, we demonstrated the similarity between ^{19}F NMR and UV-Vis spectra of comparable host-guest complexes in acetonitrile and 15% wt $[PEG_{1000}(mim)_2][NTf_2]_2$ in water. UV-Vis alone could not be used to distinguish between empty cage and cages which host an encapsulated guest.

B-Synthesis and characterisation

1. Characterisation of ILA

$[PEG_{1000}(mim)_2][NTf_2]_2$ was prepared by literature procedures.[38]

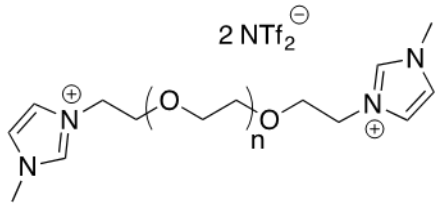

Figure S1: Structure de l'ionic liquid $PEG(mim)_2][NTf_2]_2$.

^{1}H NMR (400 MHz, 298 K, $CDCl_3$): δ 8.84 (s, 2H, H_A), 7.53 (s, 2H, $H_{B\text{-}C}$), 7.40 (s, 2H, $H_{B\text{-}C}$), 4.35 (t, J = 4 Hz, 4H, H_a), 3.93 (s, 6H, H_c), 3.83 (t, J = 4 Hz, 4H, H_b), 3.61 – 3.56 (m, 96H, $H_{aliphaticPEG}$).

^{19}F NMR (376.5 MHz, 298 K, $CDCl_3$): δ -81.9.

LR-ESI-MS (MeOH): $[M - 2NTf_2]^{2+}$ for n = 13-30: *m/z* = 260.1; 382.1; 404.1; 426.1; 448.2; 470.2; 492.3; 514.4; 536.2; 558.3; 580.3; 602.3; 624.3; 646.3; 668.4; 690.4; 712.4; 734.4 $[M - NTf_2]^+$ for n = 15-30: *m/z* = 956.2; 1000.3; 1044.3; 1088.3; 1132.3; 1176.3; 1220.4; 1264.4; 1308.4; 1352.4; 1396.5; 1440.5; 1484.5; 1528.6; 1572.6; 1616.6; 1660.7.

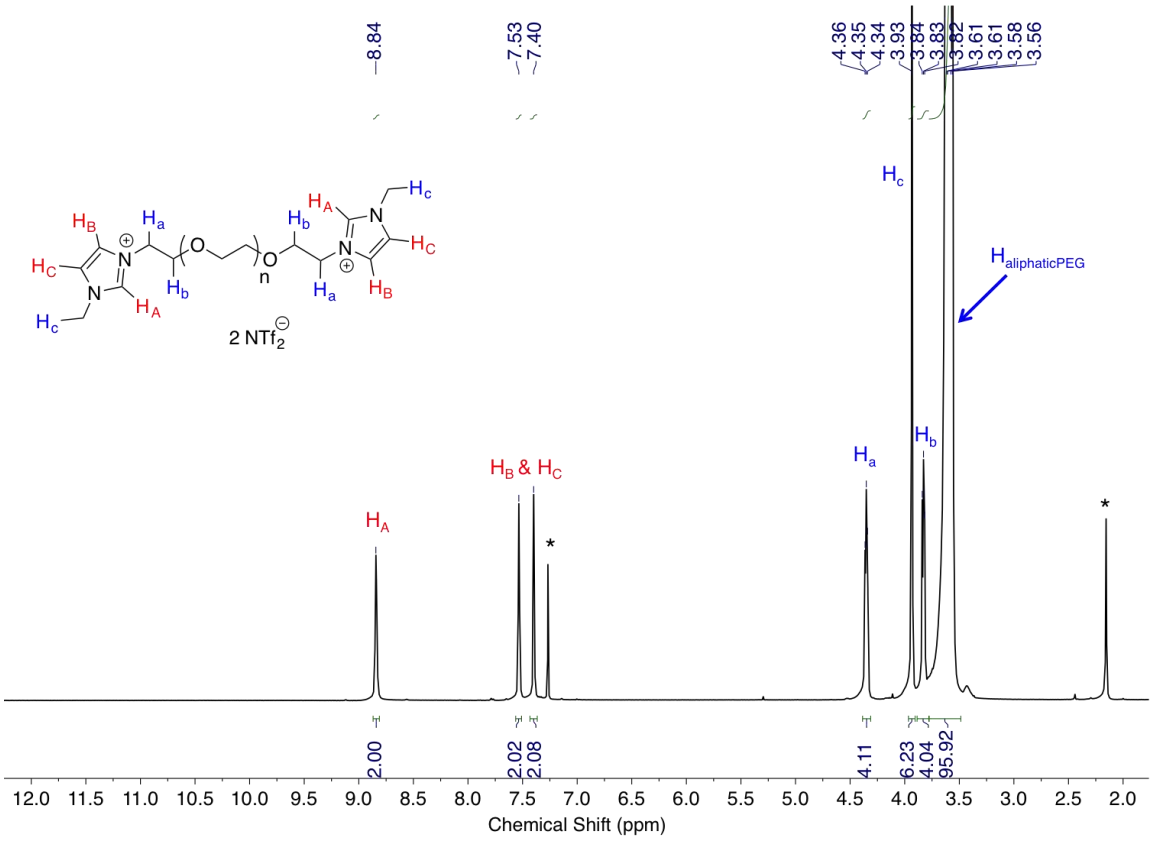

Figure S2. ^{1}H NMR spectrum of ILA in $CDCl_3$ at 298K on a 400 MHz spectrometer. (* Corresponds to residual solvents: chloroform and acetone).

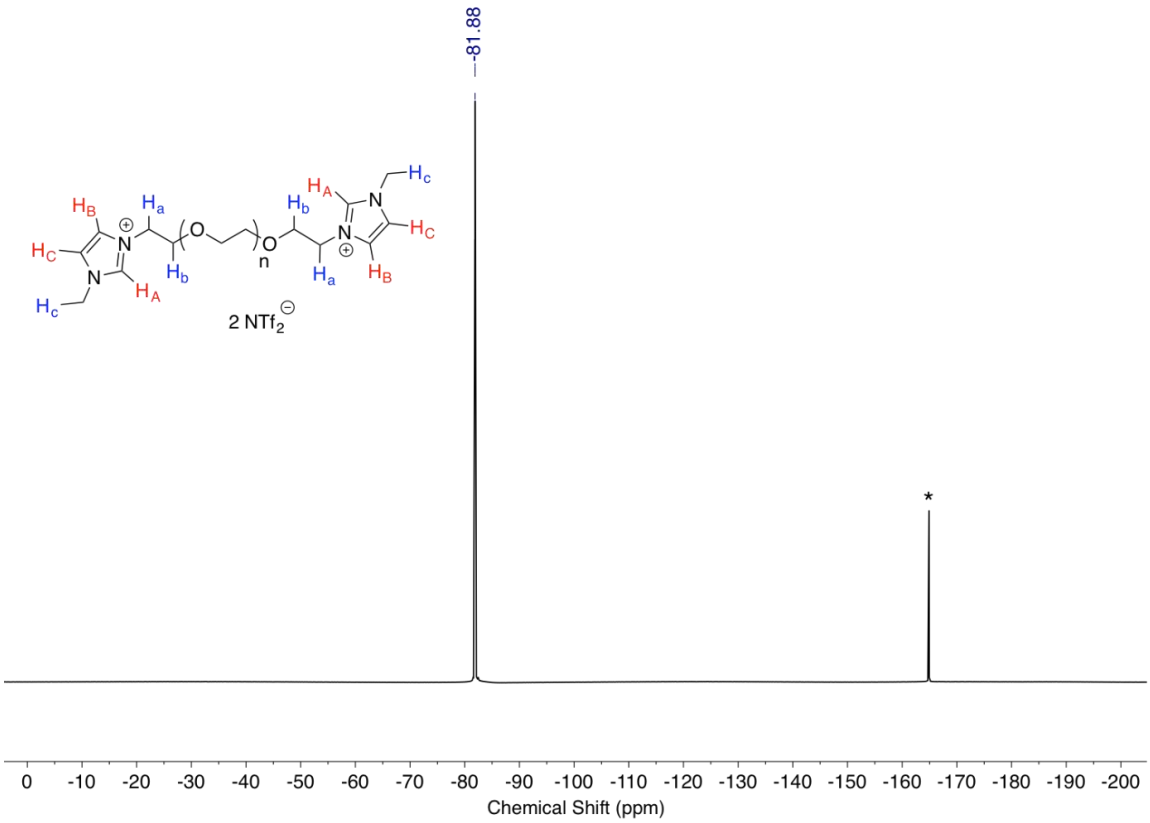

Figure S3. ^{19}F NMR spectrum of ILA in $CDCl_3$ at 298K on a 400 MHz spectrometer. (* Corresponds to the external standard C_6F_6).

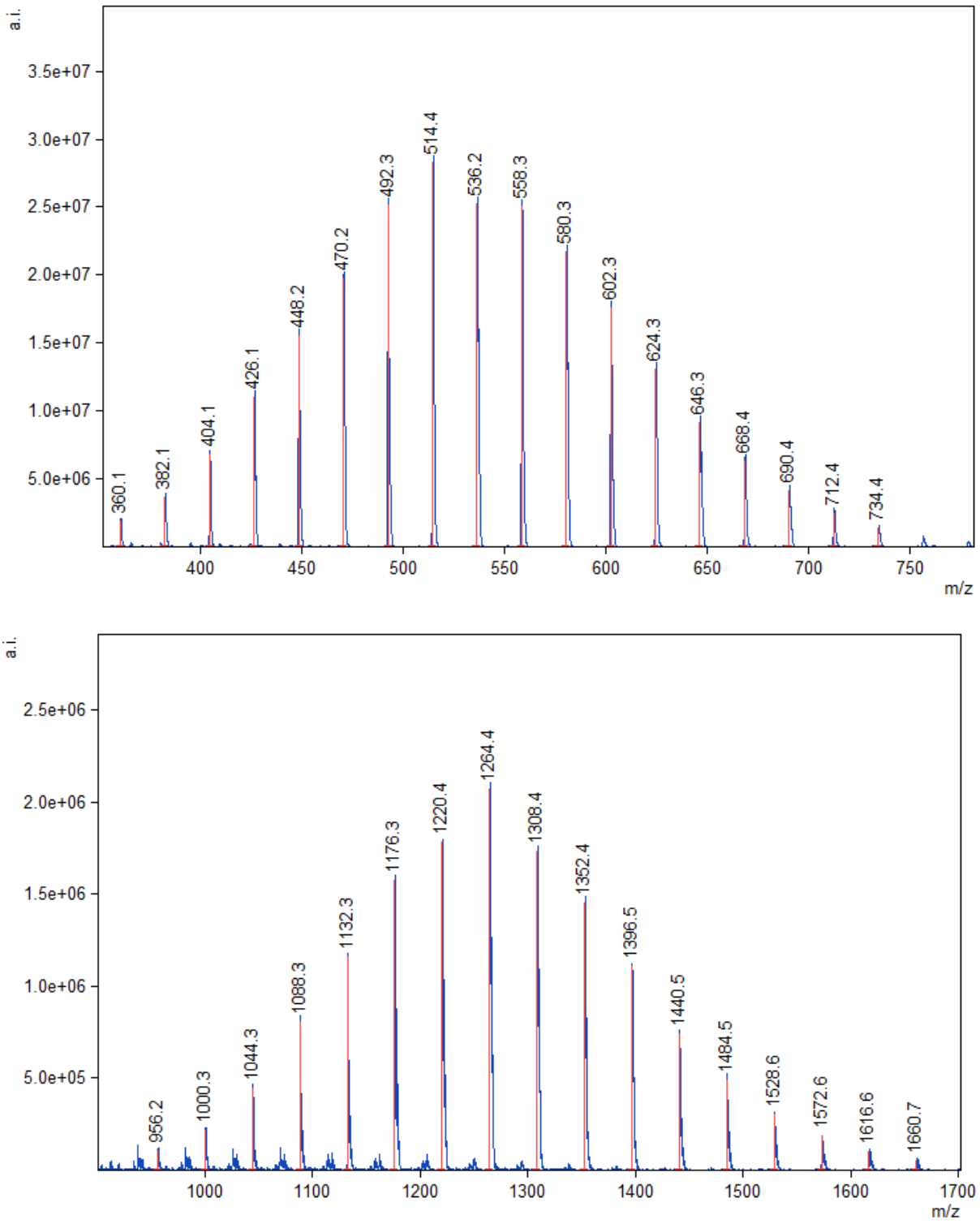

Figure S4. Low resolution ESI mass spectrum of ILA, showing the observed *z* = +2 charge (top) and the observed *z* = +1 charge (bottom).

2. Preparation and characterisation of subcomponent A

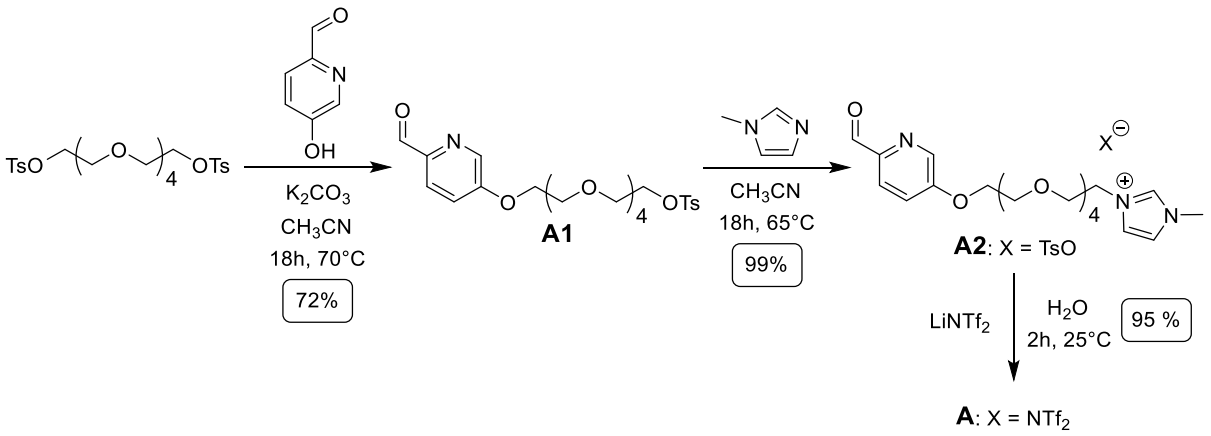

Figure S5. Protocol for the synthesis of subcomponent A.

Precursor A1: A solution of 1,14-Bis(tosyloxy)-3,6,9,12-tetraoxatetradecane (6.66 g, 12.2 mmol, 10 eq.), 5-(hydroxyl)picolinaldehyde (150 mg, 1.22 mmol, 1 eq.) and potassium carbonate (670 mg, 4.88 mmol, 4 eq.) in dry acetonitrile (20 mL) was heated at 70°C under N_2 for 18h. The beige suspension was filtered off and washed with acetonitrile (30 mL) and the solvent was removed by rotary evaporation. The residue was extracted with chloroform (3 × 25 mL). The organic phase was washed with water (3 × 10 mL). The organic layer was dried over $MgSO_4$ then filtered and the solvent was removed by rotary evaporation. The crude product was purified by flash column chromatography (C18, water/acetonitrile 60:40 to 50:60, *v*/*v*) afforded the desired product **A1** (437 mg, 72%) as yellow oil.

^{1}H NMR (400 MHz, 298 K, $CDCl_3$): δ 9.98 (s, 1H, H_A), 8.45 (d, J = 4 Hz, 1H, H_D), 7.95 (d, J = 8 Hz, 1H, H_B), 7.79 (d, J = 8 Hz, 2H, H_1), 7.35-7.32 (m, 3H, H_C and H_2), 4.27 (t, J = 4 Hz, 2H, H_a), 4.15 (t, J = 4 Hz, 2H, H_b), 3.91 (t, J = 4 Hz, 2H, H_d), 3.74 – 3.58 (m, 92H, H_c; $H_{aliphaticPEG}$), 2.45 (s, 3H, H_3).

Precursor A2: 1-Methylimidazole (0.046 mL, 0.579 mmol, 3 eq.) was added to solution of precursor **A1** (96 mg, 0.193 mmol, 1 eq.) in acetonitrile (5 mL) under N_2. The mixture was heated at 65°C under N_2 for 18h. The solvent was removed by rotary evaporation and the residue was washed with diethyl ether (3 × 75 mL). The bottom layer was dried under vacuum, to afford the desired product **A2** (112 mg, 99%) as yellow oil.

^{1}H NMR (400 MHz, 298 K, $CDCl_3$): δ 9.97 (s, 1H, H_A), 9.85 (s, 1H, H_E), 8.43 (d, J = 4 Hz, 1H, H_D), 7.93 (d, J = 8 Hz, 1H, H_B), 7.78 (d, J = 8 Hz, 2H, H_1), 7.53 (t, J = 2 Hz, 1H, H_F), 7.34 (dd, J = 8 and 4 Hz, 1H, H_C), 7.18 (t, J = 2 Hz, 1H, H_G), 7.14 (d, J = 8 Hz, 2H, H_2), 4.50 (t, J = 4 Hz, 2H, H_d), 4.25 (t, J = 4 Hz, 2H, H_a), 3.98 (s, 3H, H_e), 3.88 (t, J = 4 Hz, 2H, H_b), 3.86 (t, J = 4 Hz, 2H, H_c), 3.72 – 3.60 (m, 12H, $H_{aliphaticPEG}$), 2.34 (s, 3H, H_3). **^{13}C NMR** (100 MHz, 298 K, CD_2Cl_2): δ 192.1; 158.5; 146.5; 143.7; 139.5; 139.2; 138.7; 128.8; 126.0; 123.7; 122.6; 122.4; 120.9; 71.0; 70.7; 70.6; 70.5; 70.4; 70.3; 69.5; 69.3; 68.4; 49.9; 36.5; 21.5. **HRMS (ESI)** calcd for $C_{20}H_{30}N_3O_6$ m/z = 408.2129 $[M - OTs]^+$, found m/z = 408.2124 $[M - OTs]^+$.

Ligand A: Bis(trifluoromethane)sulfonimide lithium salt (80 mg, 0.279 mmol, 1.5 eq.) was added to solution of precursor **A2** (108 mg, 0.186 mmol, 1 eq.) in water (5 mL). The mixture was stirred for 2h at room temperature. Dichloromethane (60 mL) was added and the organic phase was washed with water (3 × 25 mL). The organic layer was dried over $MgSO_4$ then filtered and the solvent was removed by rotary evaporation, to afford the desired ligand **A** (110 mg, 86%) as yellow oil.

^{1}H NMR (400 MHz, 298 K, $CDCl_3$): δ 9.93 (s, 1H, H_A), 8.78 (s, 1H, H_E), 8.40 (d, J = 4 Hz, 1H, H_D), 7.91 (d, J = 8 Hz, 1H, H_B), 7.47 (t, J = 2 Hz, 1H, H_F), 7.33 (dd, J = 8 and 4 Hz, 1H, H_C), 7.26 (t, J = 2 Hz, 1H, H_G), 4.31 (t, J = 4 Hz, 2H, H_d), 4.23 (t, J = 4 Hz, 2H, H_a), 3.90 (s, 3H, H_e), 3.85 (t, J = 4 Hz, 2H, H_b), 3.79 (t, J = 4 Hz, 2H, H_c), 3.69 – 3.57 (m, 12H, $H_{aliphaticPEG}$). **^{19}F NMR** (376.5 MHz, 298 K, $CDCl_3$): δ -81.9. **^{13}C NMR** (100 MHz, 298 K, $CDCl_3$): δ 192.0; 158.5; 146.3; 139.2; 136.7; 123.9; 123.6; 123.2; 121.5 & 118.3 (d, J = 120 Hz, C_{NTf2}); 120.7; 70.9; 70.5; 70.4; 70.4; 70.3: 70.2; 69.3; 68.5; 68.4; 49.9; 36.3. **HRMS (ESI)** calcd for $C_{20}H_{30}N_3O_6$ m/z = 408.2129 $[M - NTf_2]^+$, found m/z = 408.2126 $[M – NTf_2]^+$.

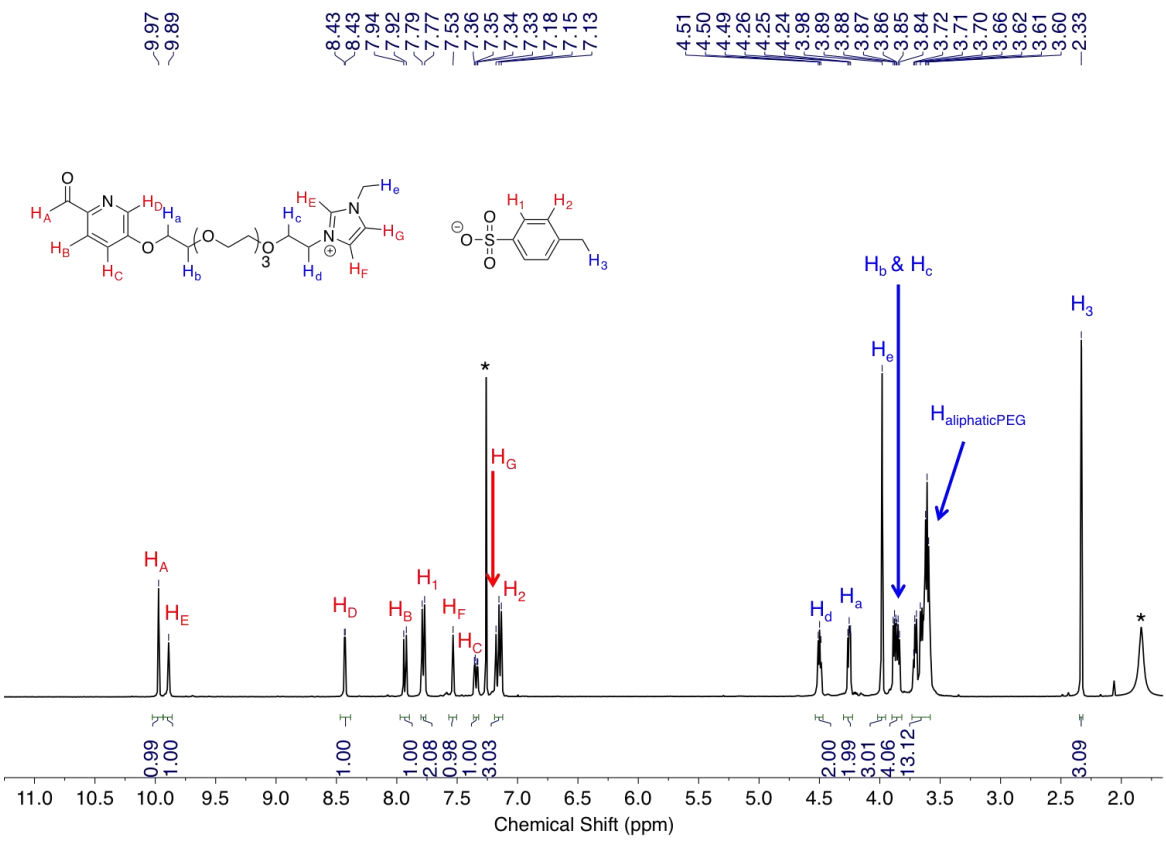

Figure S6. ^{1}H NMR spectrum of the precursor A2 in $CDCl_3$ at 298K on a 400 MHz spectrometer. (* Corresponds to residual solvents: chloroform and water).

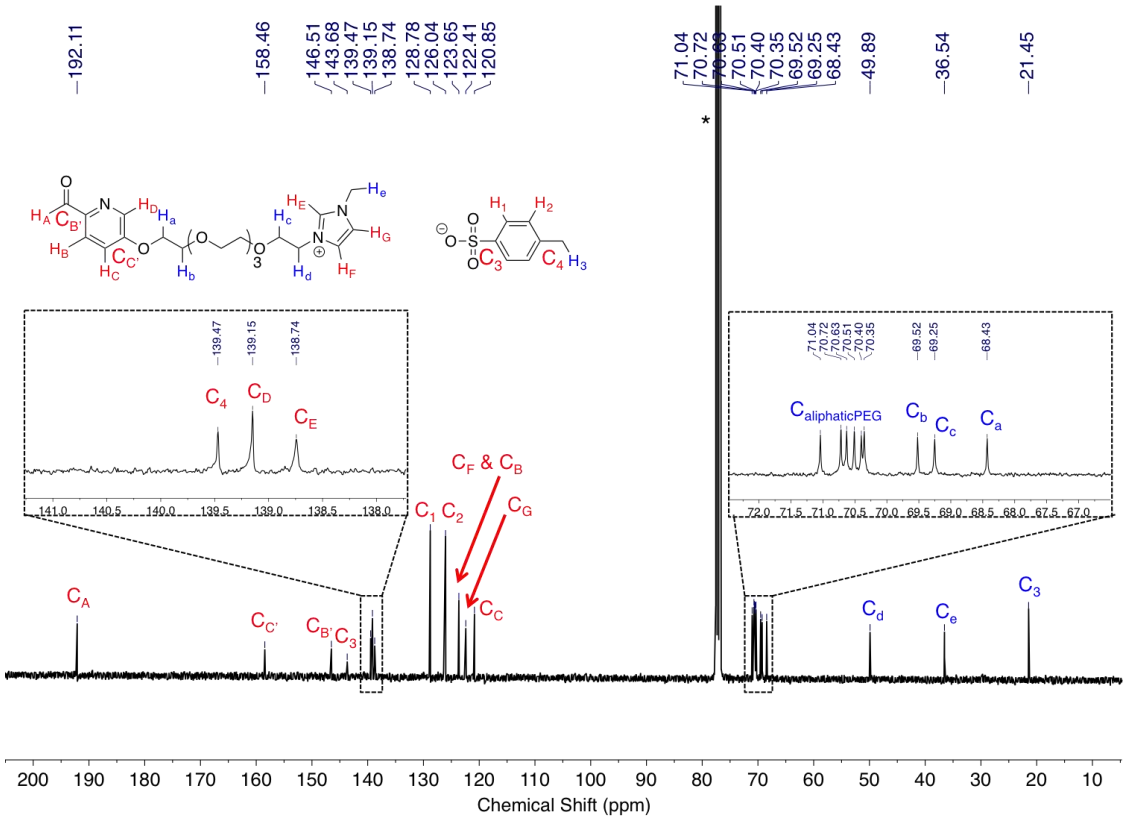

Figure S7. ^{13}C NMR spectrum of the precursor A2 in $CDCl_3$ at 298K on a 400 MHz spectrometer. (* Corresponds to residual solvent: chloroform).

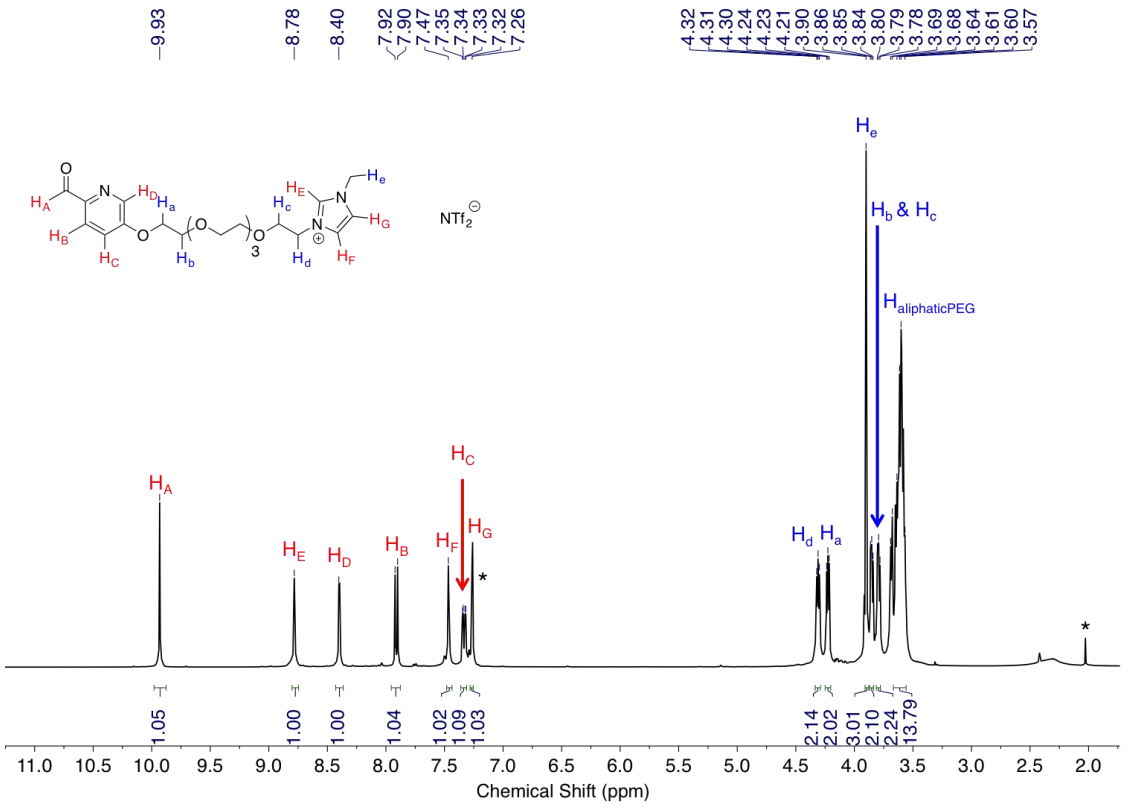

Figure S8. ^{1}H NMR spectrum of the precursor A in $CDCl_3$ at 298K on a 400 MHz spectrometer. (* Corresponds to residual solvent: chloroform).

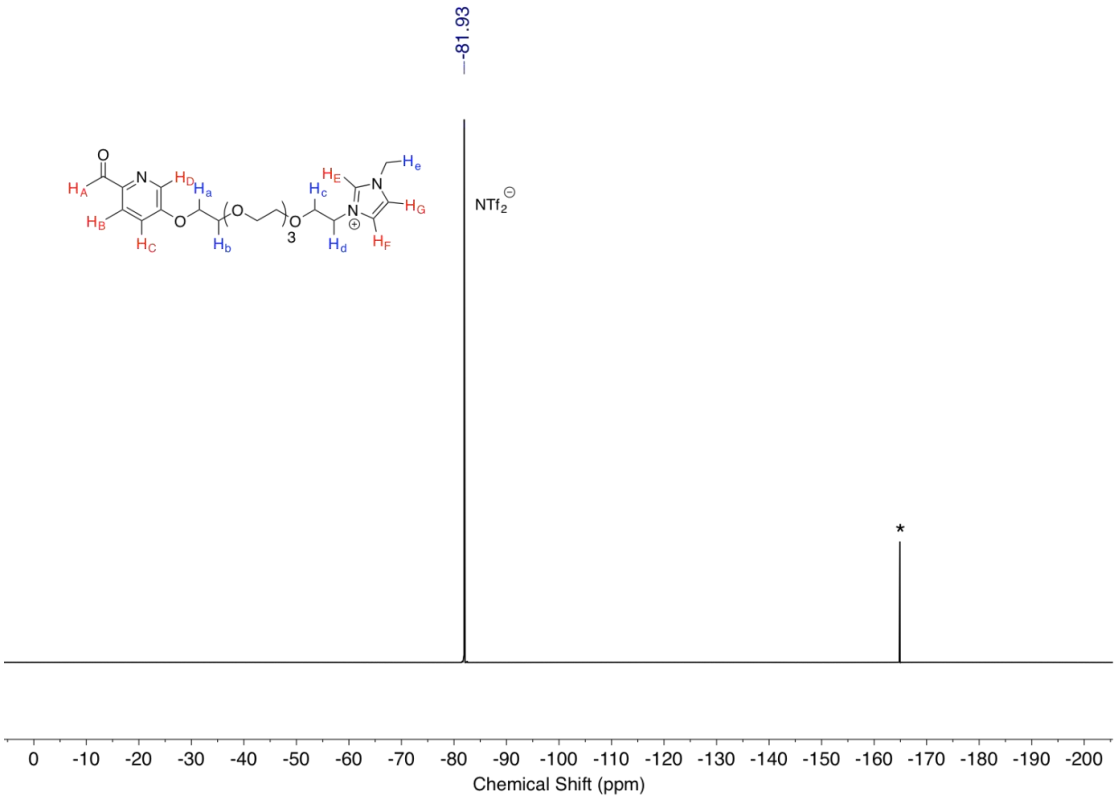

Figure S9. ^{19}F NMR spectrum of the ligand A in CD_2Cl_2 at 298K on a 400 MHz spectrometer. (* Corresponds to the external standard C_6F_6).

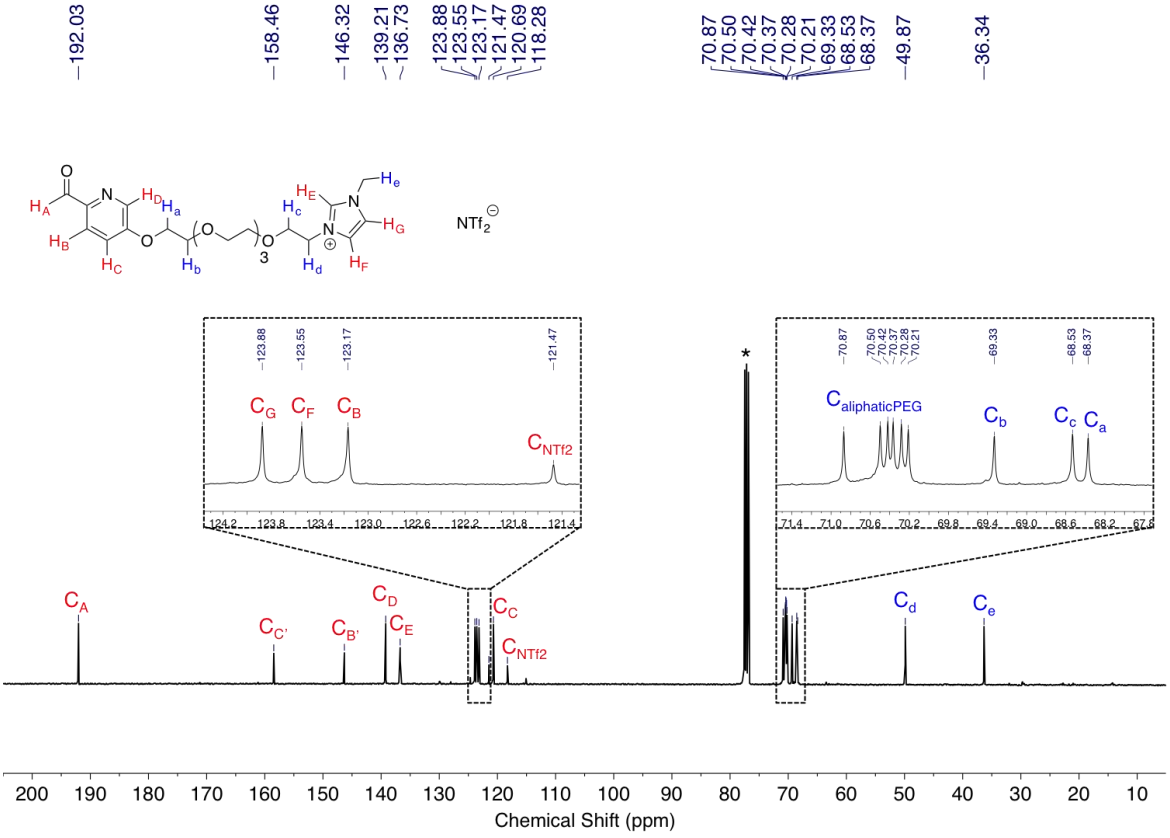

Figure S10. ^{13}C NMR spectrum of the precursor A in $CDCl_3$ at 298K on a 400 MHz spectrometer. (* Corresponds to residual solvent: chloroform).

3. Preparation and characterisation of subcomponent B

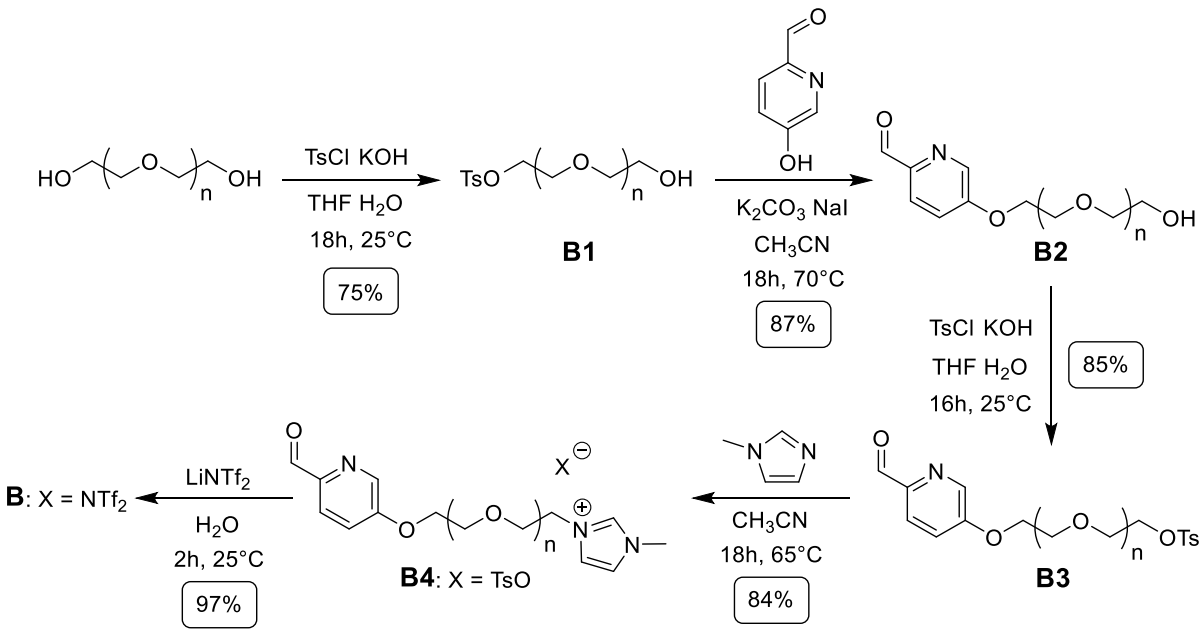

Figure S11. Protocol for the synthesis of subcomponent B.

Precursor B1: A solution of potassium hydroxide (480 mg, 8.57 mmol, 3 eq.) in water (7.5 mL) was added slowly to a solution of polyethylene glycol (RMM = 1000 Da, 21 g, 21 mmol, 7.3 eq.) and 4-toluenesulfonyl chloride (550 mg, 2.89 mmol, 1 eq.) in tetrahydrofuran (250 mL). The mixture was stirred overnight at room temperature. Water (250 mL) was added and the reaction mixture was extracted with dichloromethane (3 × 100 mL). The organic layer was dried over $MgSO_4$ then filtered and the solvent was removed by rotary evaporation. The crude product was purified by flash column chromatography (SiO_2, chloroform/methanol 99:1 to 95:5, *v*/*v*) afforded the desired product **B1** (2.5 g, 75%) as a white wax.

^{1}H NMR (400 MHz, 298 K, $CDCl_3$): δ 7.76 (d, J = 8 Hz, 2H, H_1), 7.31 (d, J = 8 Hz, 2H, H_2), 4.12 (t, J = 4 Hz, 2H, H_a), 3.66 – 3.54 (m, 92H, H_b; H_c; H_d; $H_{aliphaticPEG}$), 2.91 (bs, 1H, H_{OH}), 2.41 (s, 3H, H_3). **^{13}C NMR** (100 MHz, 298 K, $CDCl_3$): δ 144.8, 133.0, 129.9, 128.0, 72.7, 70.6, 69.3, 68.7, 61.7, 21.7. **LR-ESI-MS** (MeOH): $[M + H]^+$ for n = 15-27: *m/z* = 833.1; 877.4; 921.4; 965.3; 1009.2; 1053.3; 1097.4; 1141.3; 1185.1; 1229.5; 1273.2; 1317.6; 1361.1. $[M + Na]^+$ for n = 14-28: *m/z* = 811.1; 855.3; 899.3; 943.4; 987.2; 1031.6; 1075.5; 1119.6; 1163.5; 1207.4; 1251.4; 1295.7; 1339.3; 1383.6; 1405.5.

Precursor B2: A solution of precursor **B1** (820 mg, 0.710 mmol, 1 eq.), 5-(hydroxyl)picolinaldehyde (87 mg, 0.710 mmol, 1 eq.), potassium carbonate (490 mg, 3.55 mmol, 5 eq.) and sodium iodide (20 mg, 0.130, 0.18 eq.) in dry acetonitrile (10 mL) was heated at 70°C under N_2 for 18h. The beige suspension was filtered off and washed with acetonitrile (30 mL) and the solvent was removed by rotary evaporation. The residue was extracted with chloroform (3 × 25 mL). The organic phase was washed with water (3 × 10 mL). The organic layer was dried over $MgSO_4$ then filtered and the solvent was removed by rotary evaporation, to afford the product **B2** (680 mg, 87%) as a yellow wax.

^{1}H NMR (400 MHz, 298 K, $CDCl_3$): δ 9.98 (s, 1H, H_A), 8.45 (d, J = 4 Hz, 1H, H_D), 7.95 (d, J = 8 Hz, 1H, H_B), 7.33 (dd, J = 8 and 4 Hz, 1H, H_C), 4.27 (t, J = 4 Hz, 2H, H_a), 3.90 (t, J = 4 Hz, 2H, H_b), 3.66 – 3.60 (m, 92H, H_c; H_d; $H_{aliphaticPEG}$), 2.69 (bs, 1H, H_{OH}). **^{13}C NMR** (100 MHz, 298 K, $CDCl_3$): δ 192.2; 158.5; 146.5; 139.1; 123.5; 120.9; 72.7; 71.1; 70.7; 70.5; 69.5; 68.4; 61.9. **ESI-MS** (MeOH): $[M + Na]^+$ for n = 15-30: *m/z* = 806.3; 850.3; 894.4; 938.5; 982.5; 1026.5; 1070.4; 114.4; 1158.5; 1202.5; 1246.7; 1290.6; 1334.8; 1378.7; 1422.6; 1466.6.

Precursor B3: A solution of potassium hydroxide (122 mg, 2.17 mmol, 4 eq.) in water (1 mL) was added slowly to a solution of precursor **B2** (600 mg, 0.542 mmol, 1 eq.) and 4-toluenesulfonyl chloride (206 mg, 1.08 mmol, 2 eq.) in tetrahydrofuran (20 mL). The mixture was stirred overnight at room temperature. Water (60 mL) was added and the reaction mixture was extracted with dichloromethane (3 × 25 mL). The organic layer was dried over $MgSO_4$ then filtered and the solvent was removed by rotary evaporation. The crude product was purified by flash column chromatography (SiO_2, chloroform/methanol 100:0 to 90:10, *v*/*v*) afforded the product **B3** (580 mg, 85%) as yellow oil.

^{1}H NMR (400 MHz, 298 K, $CDCl_3$): δ 9.98 (s, 1H, H_A), 8.45 (d, J = 4 Hz, 1H, H_D), 7.95 (d, J = 8 Hz, 1H, H_B), 7.79 (d, J = 8 Hz, 2H, H_1), 7.35-7.32 (m, 3H, H_C and H_2), 4.27 (t, J = 4 Hz, 2H, H_a), 4.15 (t, J = 4 Hz, 2H, H_b), 3.91 (t, J = 4 Hz, 2H, H_d), 3.74 – 3.58 (m, 92H, H_c; $H_{aliphaticPEG}$), 2.45 (s, 3H, H_3). **^{13}C NMR** (100 MHz, 298 K, $CDCl_3$): δ 192.1; 158.5; 146.5; 144.9; 139.0; 133.1; 129.9; 128.1; 123.4; 120.8; 71.1; 70.9; 70.7; 69.5; 69.4; 68.8; 68.4; 21.8. **LR-ESI-MS** (MeOH): $[M + H]^+$ for n = 15-25: *m/z* = 938.3; 982.5; 1026.5; 1070.4; 1114.5; 1158.4; 1202.4; 1246.5; 1290.3; 1334.5; 1378.4. $[M + Na]^+$ for n = 14-29: *m/z* = 916.2; 960.4; 1004.5; 1048.4; 1092.3; 1136.4; 1180.3; 1224.5; 1268.5; 1312.4; 1356.5; 1400.3; 1444.5; 1488.3; 1532.5; 1576.5.

Precursor B4: 1-Methylimidazole (0.11 mL, 1.33 mmol, 3 eq.) was added to solution of precursor **B3** (560 mg, 0.445 mmol, 1 eq.) in acetonitrile (5 mL) under N_2. The mixture was heated at 65°C under N_2 for 18h. The solvent was removed by rotary evaporation and the residue was washed with diethyl ether (3 × 75 mL). The bottom layer was dried under vacuum, to afford the desired product **B4** (500 mg, 84%) as yellow oil.

^{1}H NMR (400 MHz, 298 K, CD_2Cl_2): δ 9.92 (s, 1H, H_A), 9.65 (s, 1H, H_E), 8.44 (d, J = 4 Hz, 1H, H_D), 7.92 (d, J = 8 Hz, 1H, H_B), 7.67 (d, J = 8 Hz, 2H, H_1), 7.60 (t, J = 2 Hz, 1H, H_F), 7.36 (dd, J = 8 and 4 Hz, 1H, H_C), 7.28 (t, J = 2 Hz, 1H, H_G), 7.15 (d, J = 8 Hz, 2H, H_2), 4.45 (t, J = 4 Hz, 2H, H_d), 4.27 (t, J = 4 Hz, 2H, H_a), 3.95 (s, 3H, H_e), 3.87 (t, J = 4 Hz, 2H, H_b), 3.83 (t, J = 4 Hz, 2H, H_c), 3.70 – 3.57 (m, 88H, $H_{aliphaticPEG}$), 2.34 (s, 3H, H_3). **^{13}C NMR** (100 MHz, 298 K, CD_2Cl_2): δ 192.4; 158.8; 146.9; 145.0; 139.5; 139.3; 138.6; 128.9; 126.1; 123.9; 123.5; 123.1; 121.0; 71.3; 70.9; 70.7; 70.7; 70.6; 69.7; 69.4; 68.8; 50.0; 36.6; 21.4. **LR-ESI-MS** (CH_2Cl_2): $[M - OTs + H]^{2+}$ for n = 17-30: m/z = 468.9; 490.9; 512.9; 512.9; 534.9; 556.9; 578.9; 600.9; 622.9; 644.9; 666.8; 688.9; 710.9; 732.7; 754.9. $[M - OTs]^{+}$ for n = 14-30: m/z = 804.2; 848.4; 892.2; 936.5; 980.4; 1024.6; 1068.6; 1112.5; 1156.6; 1200.6; 1244.7; 1288.7; 1332.8; 1376.7; 1420.7; 1464.8; 1508.8; 1552.7.

Ligand B: Bis(trifluoromethane)sulfonimide lithium salt (148 mg, 0.515 mmol, 1.5 eq.) was added to solution of precursor **B4** (460 mg, 0.343 mmol, 1 eq.) in water (5 mL). The mixture was stirred for 2h at room temperature. Dichloromethane (60 mL) was added and the organic phase was washed with water (3 × 25 mL). The organic layer was dried over $MgSO_4$ then filtered and the solvent was removed by rotary evaporation, to afford the desired ligand B (480 mg, 97%) as yellow oil.

^{1}H NMR (400 MHz, 298 K, CD_2Cl_2): δ 9.94 (s, 1H, H_A), 8.90 (s, 1H, H_E), 8.44 (d, J = 4 Hz, 1H, H_D), 7.92 (d, J = 8 Hz, 1H, H_B), 7.46 (dd, J = 8 and 4 Hz, 1H, H_C), 7.44 (t, J = 2 Hz, 1H, H_F), 7.35 (t, J = 2 Hz, 1H, H_G), 4.29-4.26 (m, 4H, H_d & H_a), 3.84 (s, 3H, H_e), 3.83 (t, J = 4 Hz, 2H, H_b), 3.79 (t, J = 4 Hz, 2H, H_c), 3.70 – 3.53 (m, 88H, $H_{aliphaticPEG}$). **^{1}H NMR** (400 MHz, 298 K, CD_3CN): δ 9.91 (s, 1H, H_A), 8.60 (s, 1H, H_E), 8.45 (d, J = 4 Hz, 1H, H_D), 7.92 (d, J = 8 Hz, 1H, H_B), 7.52 (t, J = 2 Hz, 1H, H_F), 7.37 (t, J = 2 Hz, 1H, H_G), 7.36 (dd, J = 8 and 4 Hz, 1H, H_C), 4.36 (t, J = 4 Hz, 2H, H_d), 4.27 (t, J = 4 Hz, 2H, H_a), 3.94 (s, 3H, H_e), 3.87 (t, J = 4 Hz, 2H, H_b), 3.85 (t, J = 4 Hz, 2H, H_c), 3.65 – 3.52 (m, 88H, $H_{aliphaticPEG}$). **^{19}F NMR** (376.5 MHz, 298 K, CD_2Cl_2): δ -82.5. **^{13}C NMR** (100 MHz, 298 K, CD_2Cl_2): δ 192.4; 158.8; 146.9; 139.3; 137.6; 123.7; 123.6; 123.5; 121.9 & 118.7 (d, J = 120 Hz, C_{NTf2}); 121.0; 71.3; 70.9; 70.6; 69.7; 68.9; 68.8; 50.3; 36.7. **LR-ESI-MS** (CH_2Cl_2): $[M - NTf_2]^{+}$ for n = 13-29: m/z = 760.3; 804.3; 848.4; 892.4; 936.5; 980.5; 1024.6; 1068.6; 1112.6; 1156.8; 1200.6; 1244.7; 1288.7; 1332.7; 1376.7; 1420.7; 1464.8.

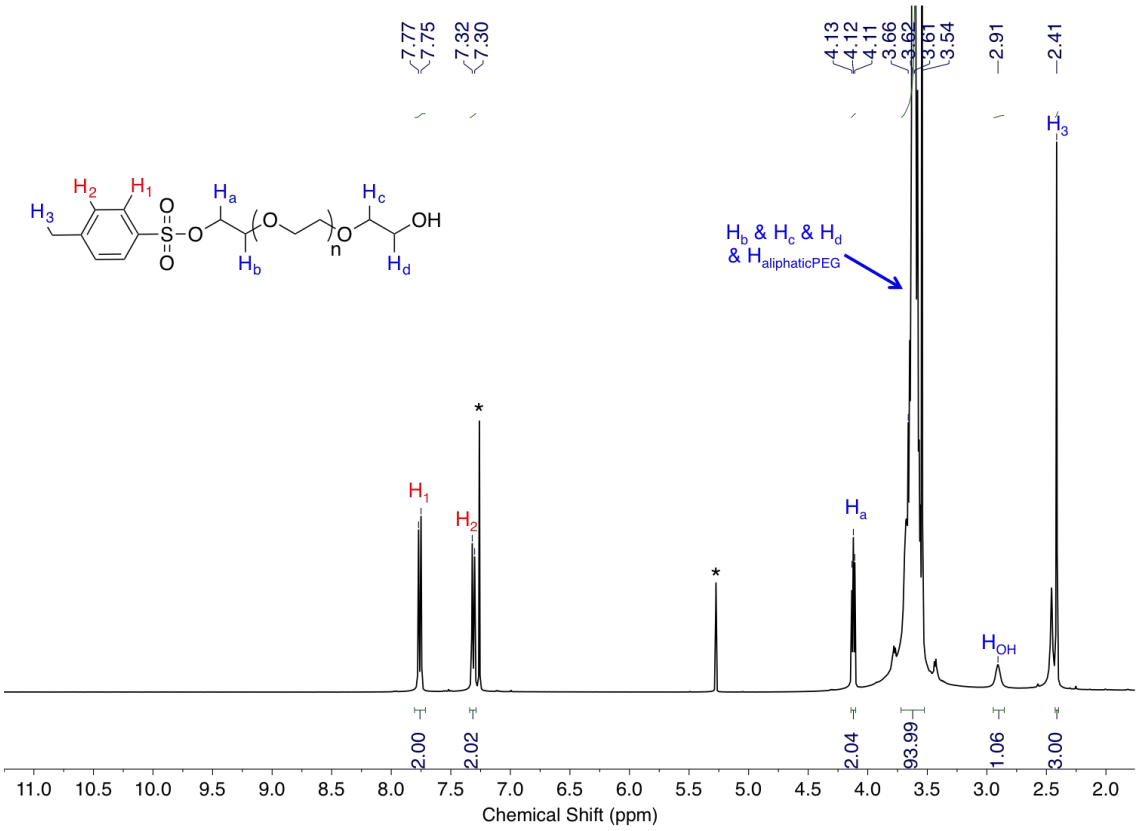

Figure S12. ^{1}H NMR spectrum of the precursor B1 in $CDCl_3$ at 298K on a 400 MHz spectrometer. (* Corresponds to residual solvents: chloroform and dichloromethane).

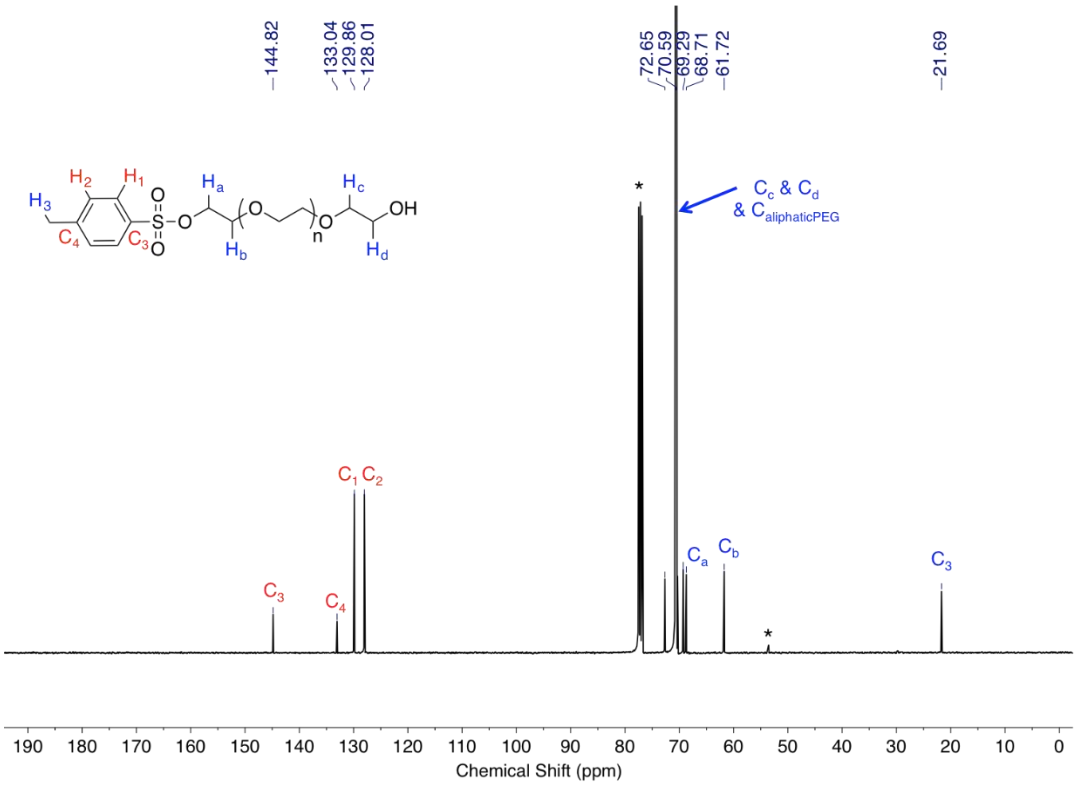

Figure S13. ^{13}C NMR spectrum of the precursor B1 in $CDCl_3$ at 298K on a 400 MHz spectrometer. (* Corresponds to residual solvents: chloroform and dichloromethane).

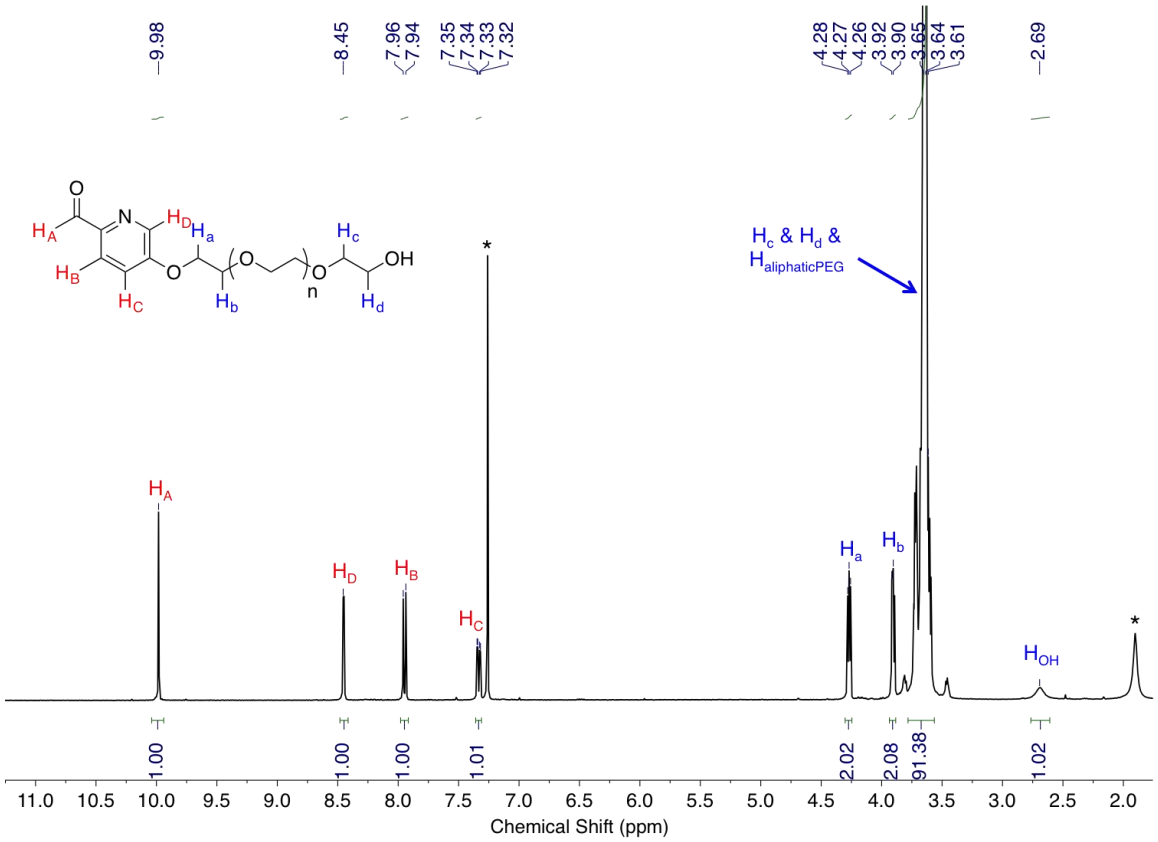

Figure S14. ^{1}H NMR spectrum of the precursor B2 in $CDCl_3$ at 298K on a 400 MHz spectrometer. (* Corresponds to residual solvents: chloroform).

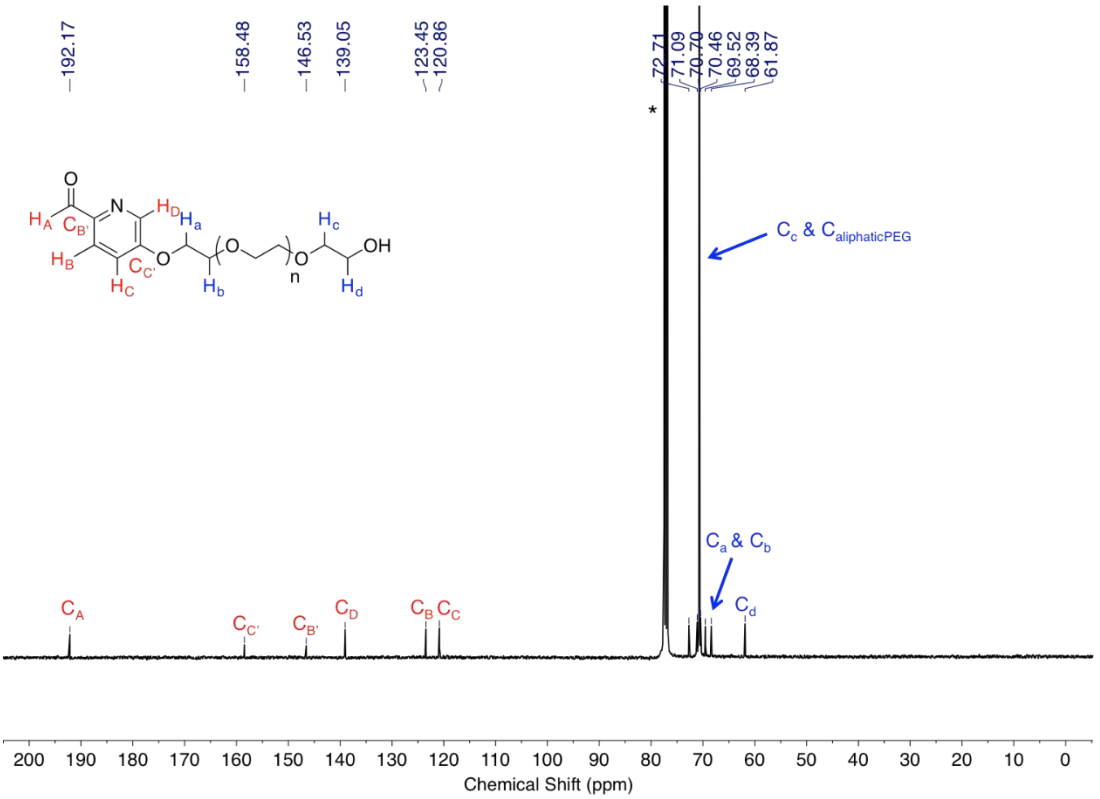

Figure S15. ^{13}C NMR spectrum of the precursor B2 in $CDCl_3$ at 298K on a 400 MHz spectrometer. (* Corresponds to residual solvent: chloroform).

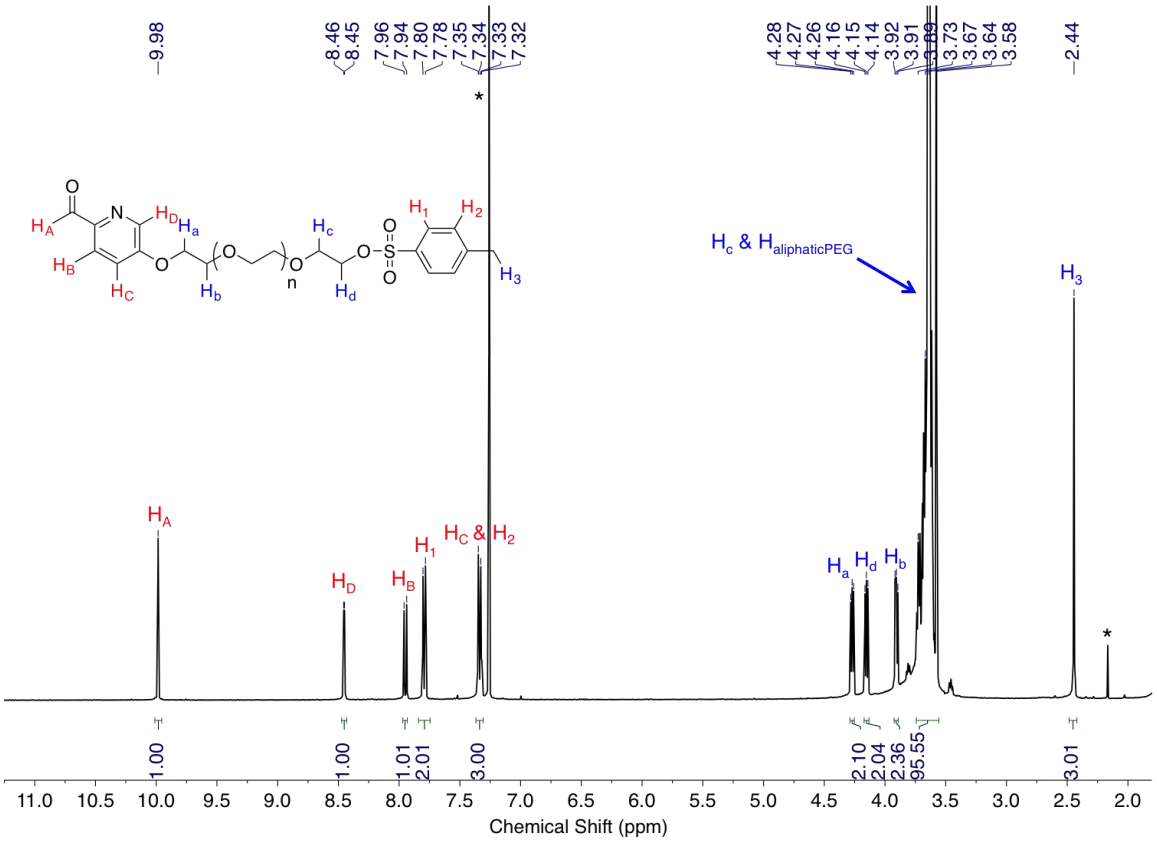

Figure S16. ^{1}H NMR spectrum of the precursor B3 in $CDCl_3$ at 298K on a 400 MHz spectrometer. (* Corresponds to residual solvents: chloroform and acetone).

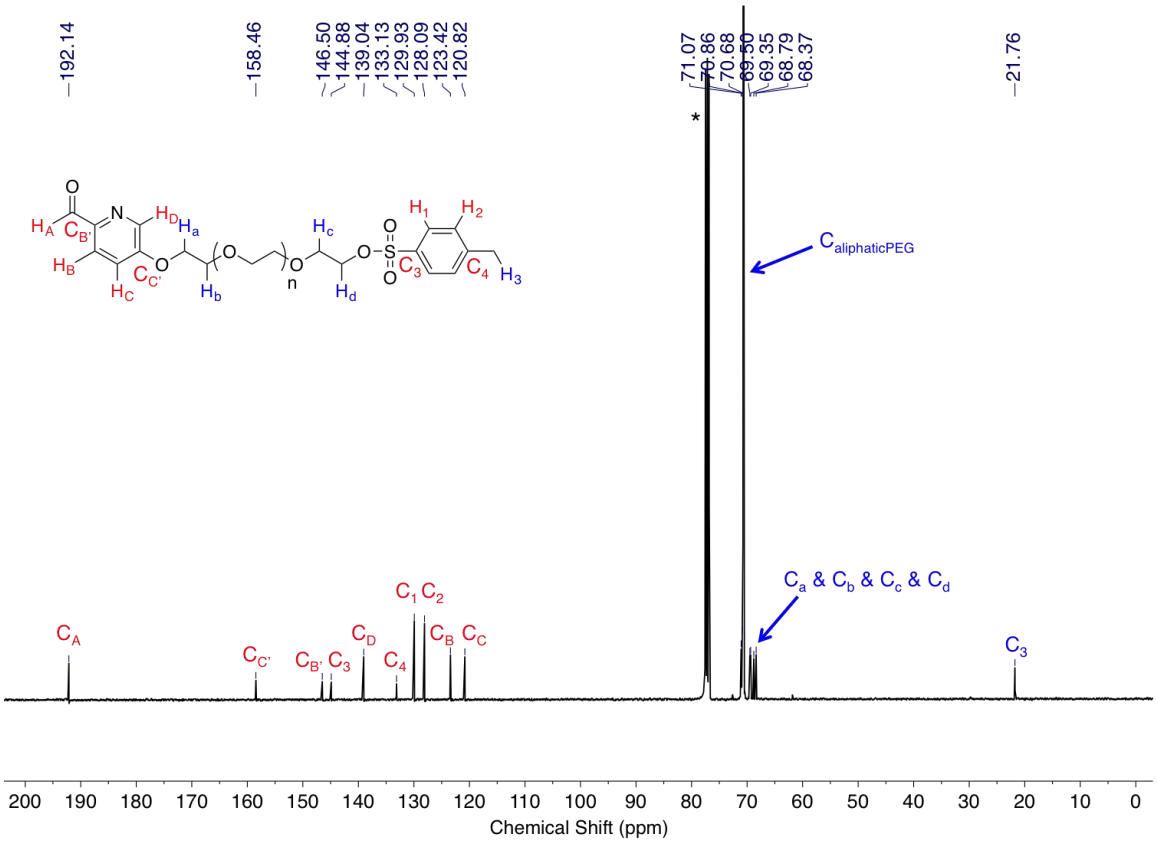

Figure S17. ^{13}C NMR spectrum of the precursor B3 in $CDCl_3$ at 298K on a 400 MHz spectrometer. (* Corresponds to residual solvent: chloroform).

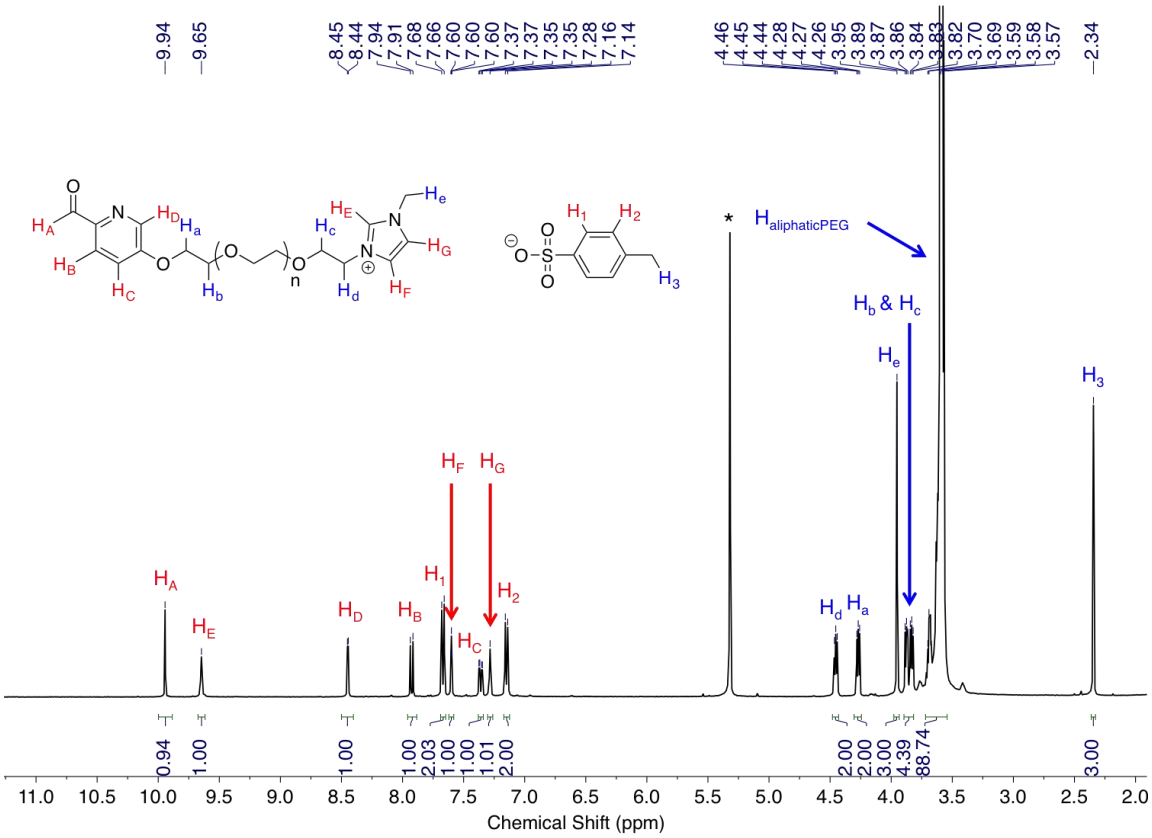

Figure S18. ^{1}H NMR spectrum of the precursor B4 in CD_2Cl_2 at 298K on a 400 MHz spectrometer. (* Corresponds to residual solvent: dichloromethane).

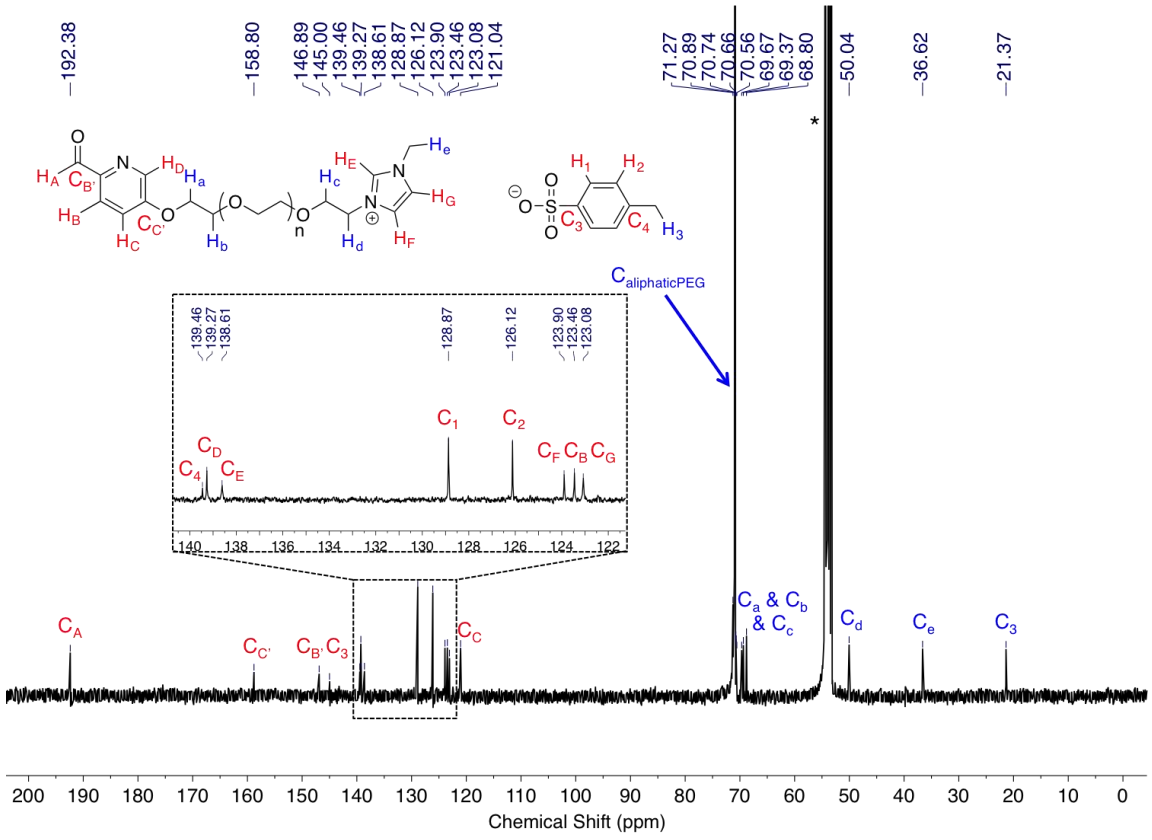

Figure S19. ^{13}C NMR spectrum of the precursor B4 in CD_2Cl_2 at 298K on a 400 MHz spectrometer. (* Corresponds to residual solvent: dichloromethane).

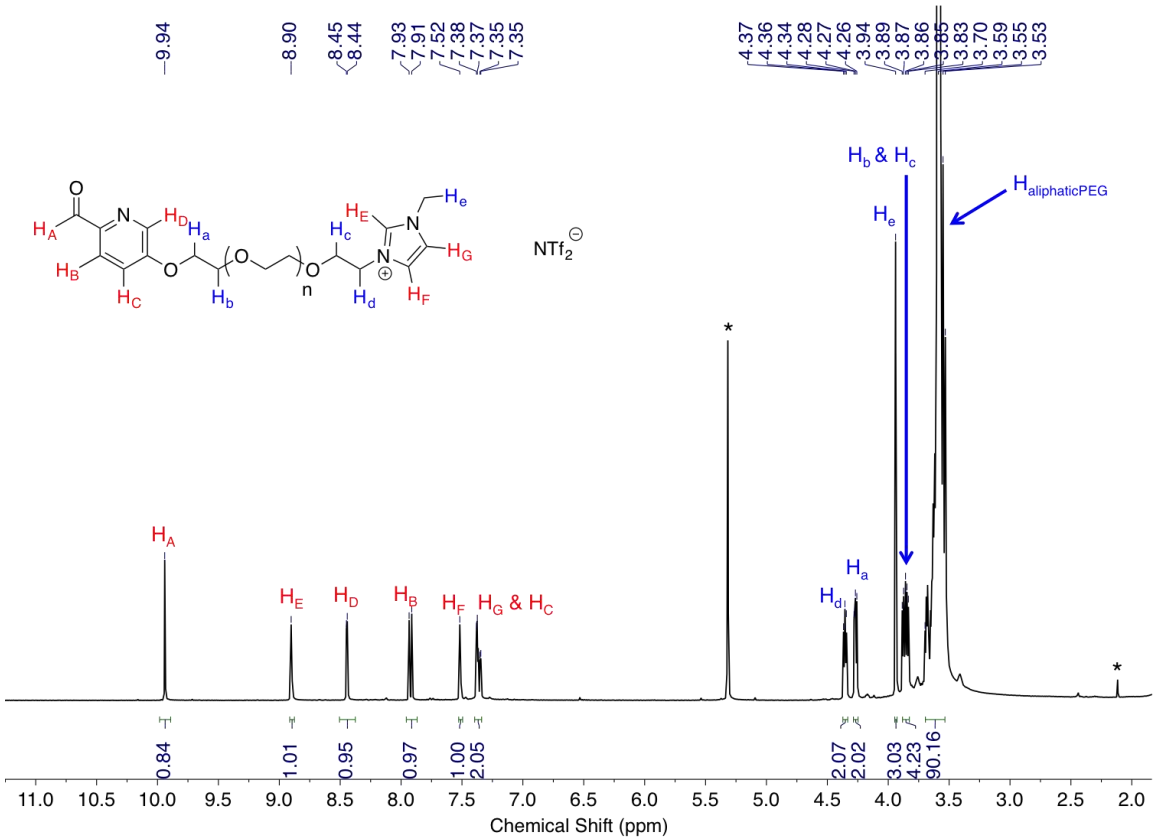

Figure S20. ^{1}H NMR spectrum of the ligand B in CD_2Cl_2 at 298K on a 400 MHz spectrometer. (* Corresponds to residual solvents: dichloromethane & acetone).

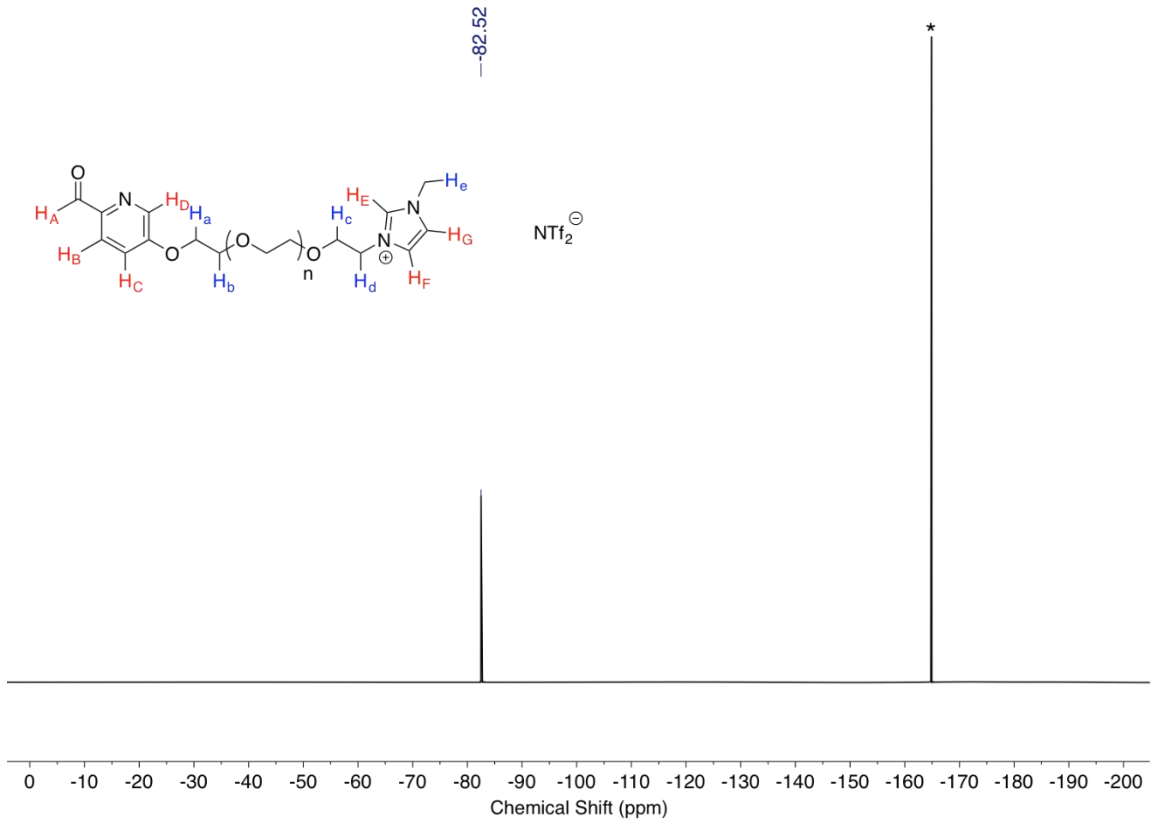

Figure S21. ^{19}F NMR spectrum of the ligand B in CD_2Cl_2 at 298K on a 400 MHz spectrometer. (* Corresponds to the external standard C_6F_6).

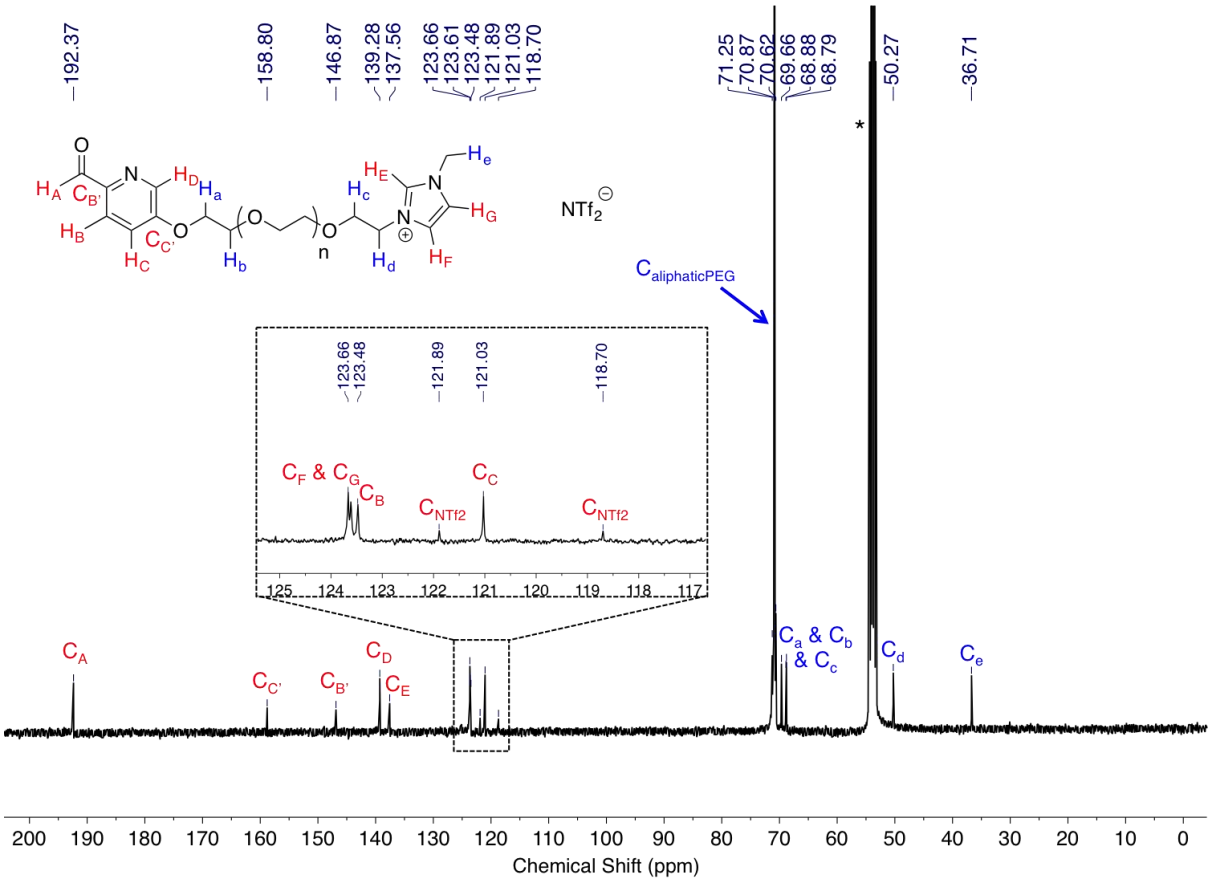

Figure S22. ^{13}C NMR spectrum of the ligand B in CD_2Cl_2 at 298K on a 400 MHz spectrometer. (* Corresponds to residual solvent: dichloromethane).

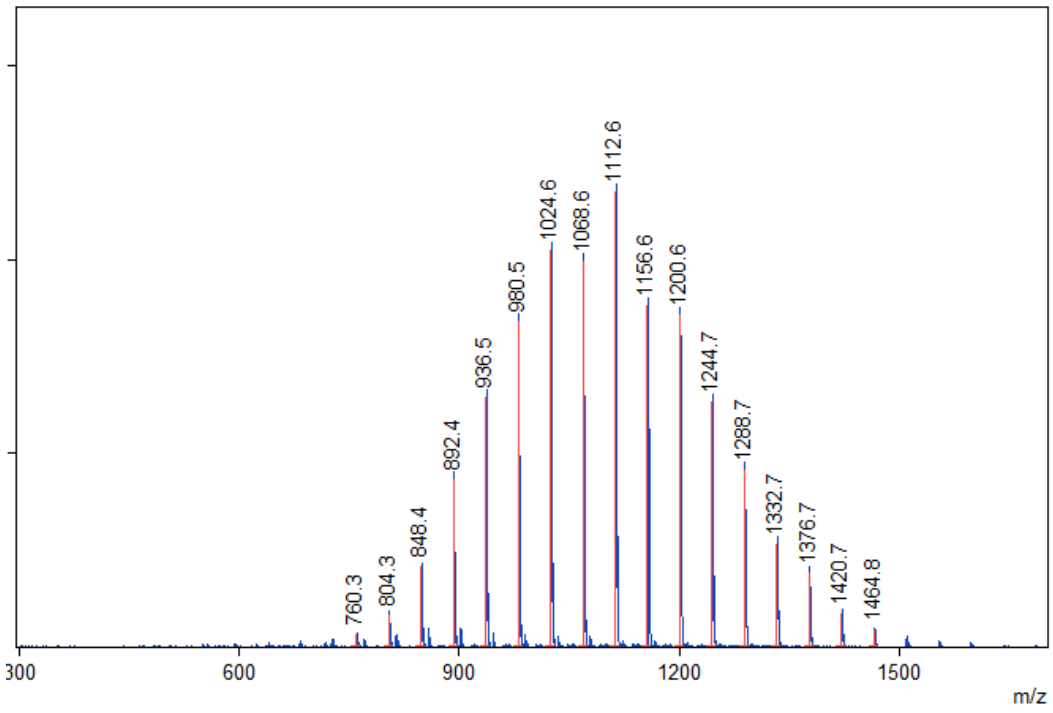

Figure S23. Low resolution ESI mass spectrum of the ligand B, showing the observed *z* = +1 charge.

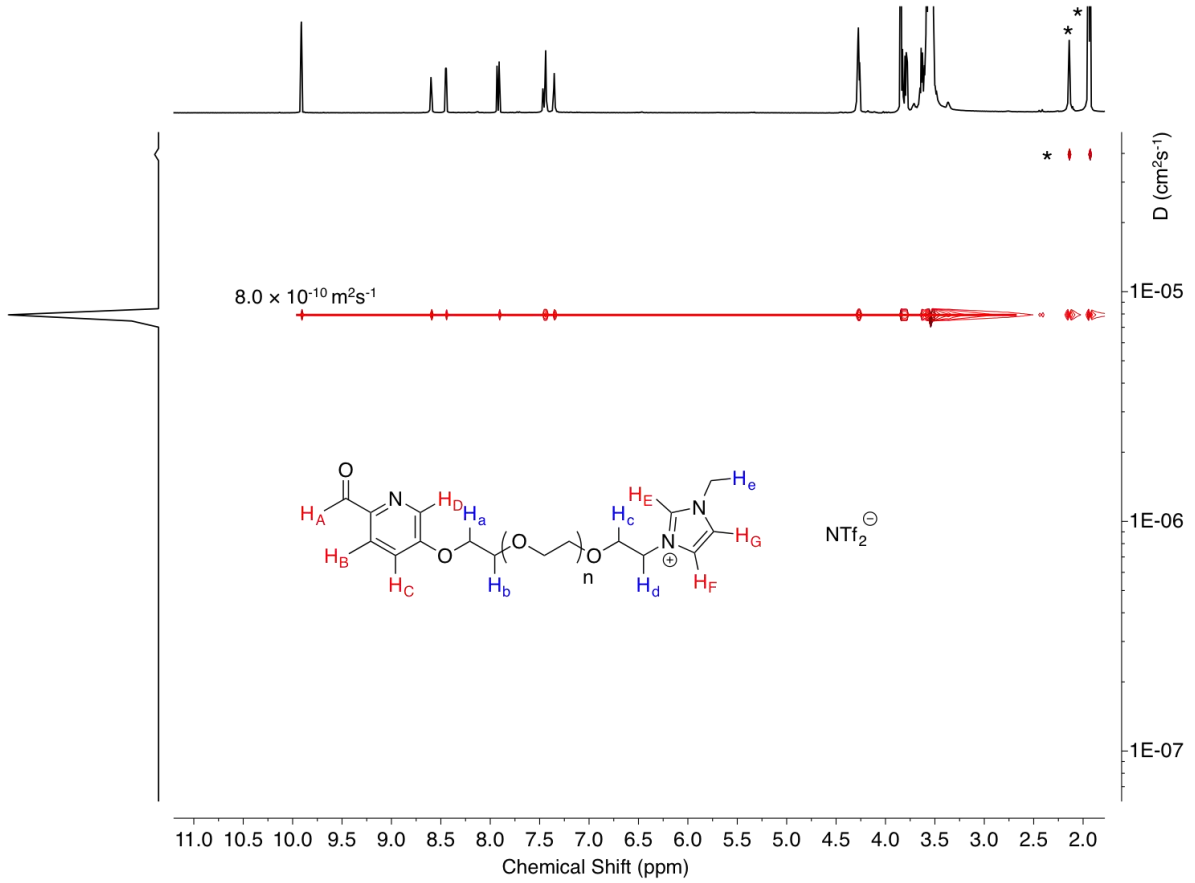

Figure S24. Diffusion Ordered NMR spectra recorded in CD_3CN at a concentration of 1.5 mM of the ligand B at 298K on a 400 MHz spectrometer. The diffusion coefficient was measured to be 8.0×10^{-10} m^2s^{-1}. (* Corresponds to residual solvents: acetonitrile and water).

4. Preparation and characterisation of cage 1

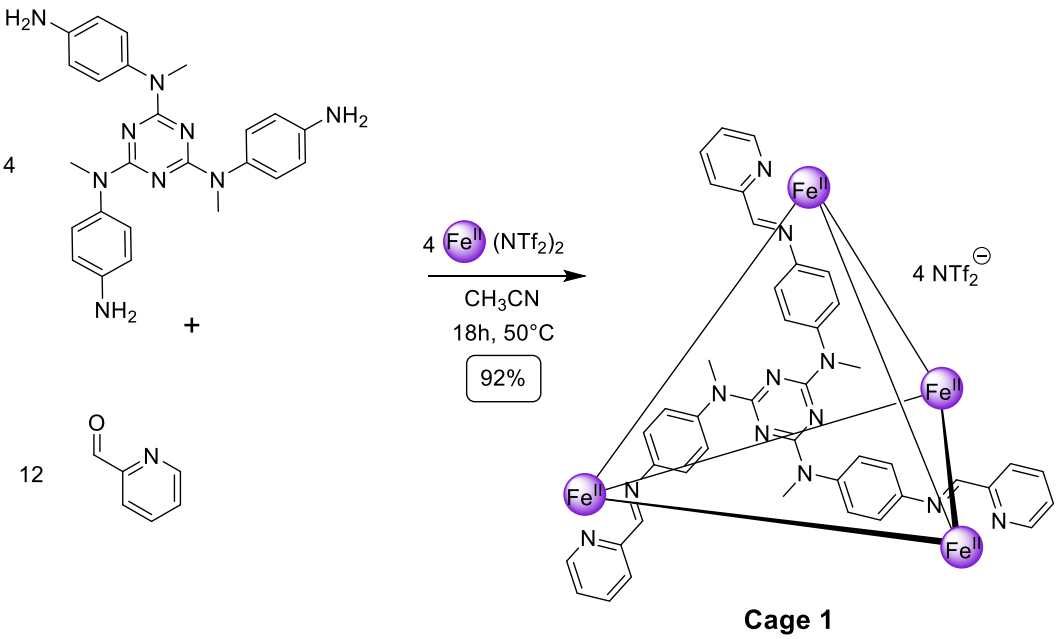

Figure S25: Self-assembly of cage 1.

Cage 1. N2,N4,N6-tris(4-aminophenyl)-N2,N4,N6-trimethyl-1,3,5-triazine-2,4,6-triamine (1.71 mg, 3.87 µmol, 4 eq.), 2-pyridinecarboxaldehyde (1.3 µL, 11.6 µmol, 12 eq.) were combined in dry acetonitrile (400 µL). The solution was subjected to three evacuation/nitrogen fill cycles and $Fe(NTf_2)_2 \bullet 6H_2O$ (2.66 mg, 3.87 µmol, 4 eq.) was added. The mixture was heated at 50 °C for 18h. The solvent was evaporated and the solid triturated with diethyl ether to yield **cage 1** (13 mg, 92%) as a purple solid.

^{1}H NMR (500 MHz, 298 K, CD_3CN): δ 8.83 (s, 1H, H_A), 8.49 (d, *J* = 7.6 Hz, 1H, H_B), 8.39 (t, *J* = 7.7 Hz, 1H, H_C), 7.77 – 7.70 (m, 3H, H_I & H_D), 5.10 (s, 2H, H_H), 3.40 (s, 3H, H_f).

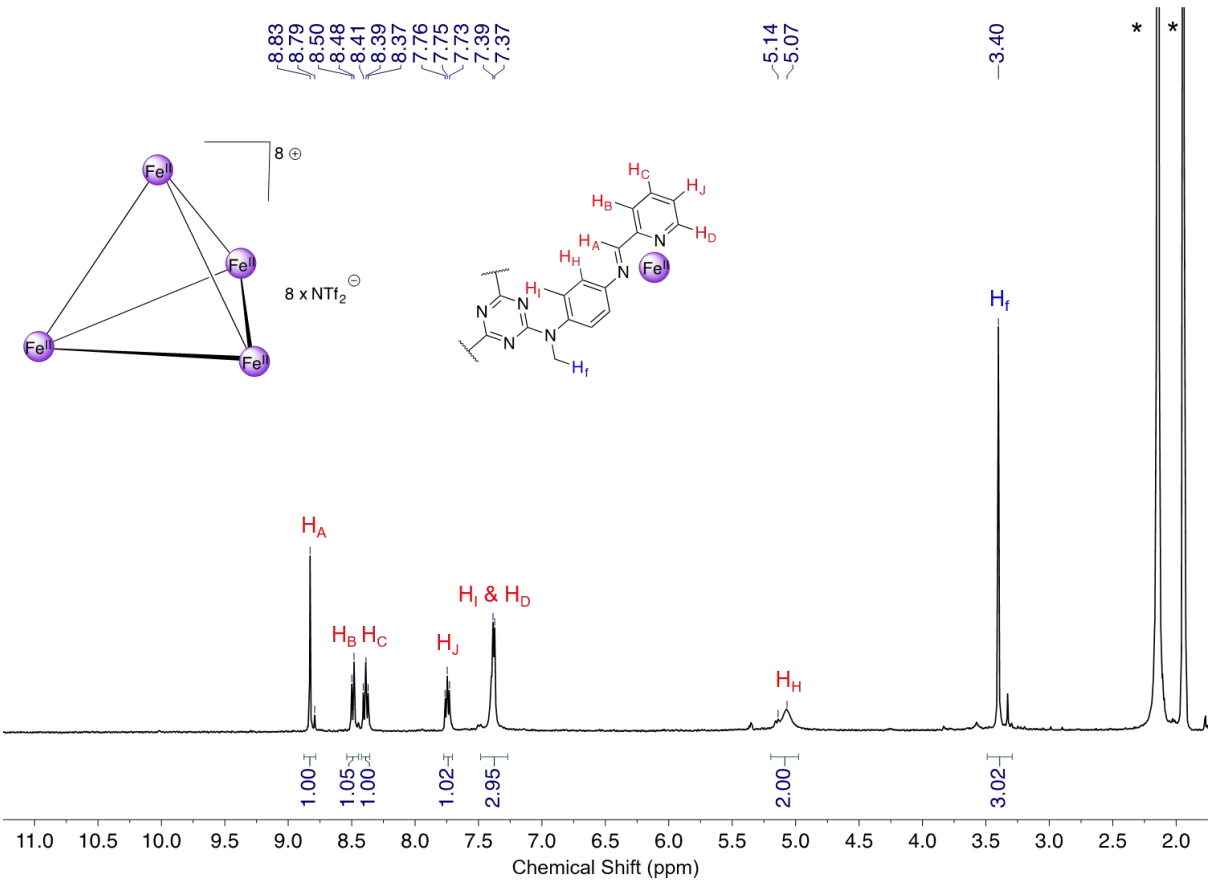

Figure S26. ^{1}H NMR spectrum of the cage 1 in CD_3CN at 298K on a 500 MHz spectrometer. (* Corresponds to residual solvents: acetonitrile and water).

5. Preparation and characterisation of cage 2

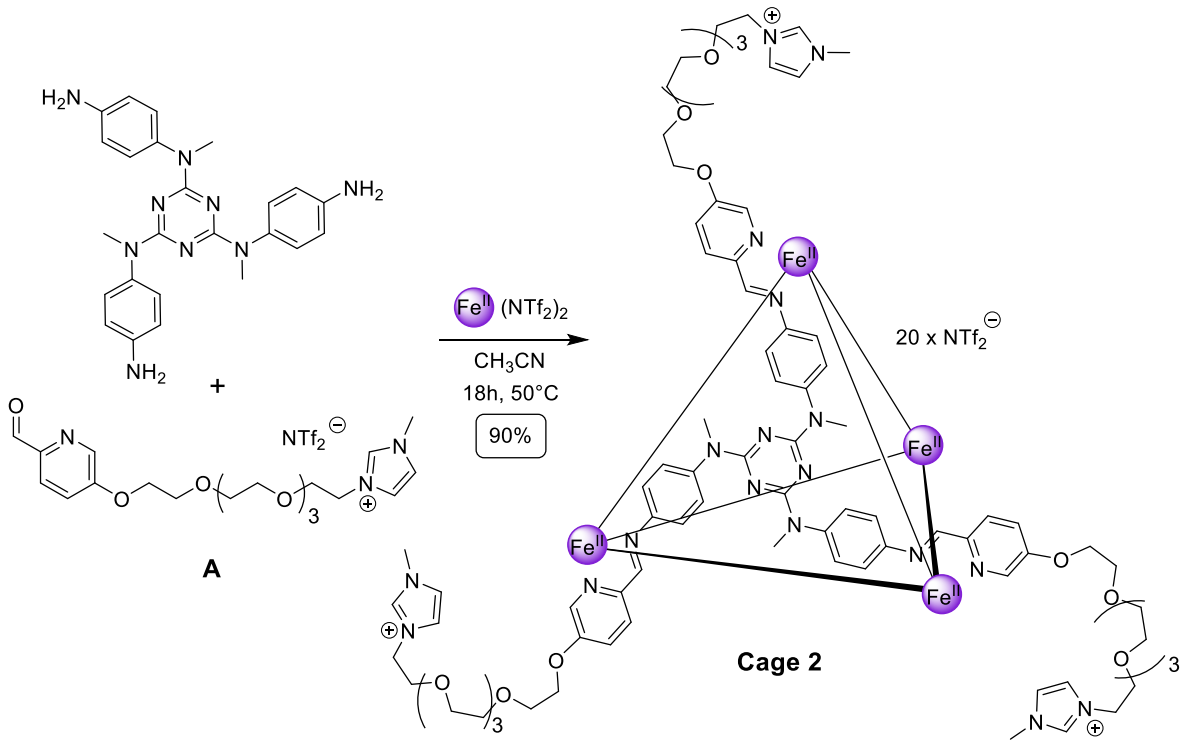

Figure S27: Self-assembly of cage 2.

Cage 2. N2,N4,N6-tris(4-Aminophenyl)-N2,N4,N6-trimethyl-1,3,5-triazine-2,4,6-triamine (0.78 mg, 1.76 µmol, 4 eq.), ligand **A** (3.64 mg, 5.29 µmol, 12 eq.) were combined in dry acetonitrile (400 µL). The solution was subjected to three evacuation/nitrogen fill cycles and $Fe(NTf_2)_2 \bullet 6H_2O$ (1.21 mg, 1.76 µmol, 4 eq.) was added. The mixture was heated at 50 °C for 18h. The solvent was evaporated and the solid triturated with diethyl ether to yield **cage 2** (7 mg, 90%) as a dark red sticky solid.

^{1}H NMR (500 MHz, 298 K, CD_3CN): δ 8.69 (s, 1H, H_A), 8.49 (s, 1H, H_E), 8.43 (d, *J* = 8.8 Hz, 2H, H_B), 7.85 (dd, *J* = 8.9, 2.4 Hz, 2H, H_C), 7.49 – 7.26 (m, 4H, H_F, H_G & H_I), 6.99 (d, *J* = 2.2 Hz, 1H, H_D), 5.08 (s, 2H, H_H), 4.35 – 4.14 (m, *J* = 8.5, 3.6 Hz, 4H, H_a & H_d), 3.82 (s, 3H, H_e), 3.80 – 3.73 (m, *J* = 9.6 Hz, 4H, H_b & H_c), 3.67 – 3.49 (m, 10H, $H_{aliphatic}$, H_f).

^{19}F NMR (376.5 MHz, 298 K, CD_3CN): *δ* -80.4 (*exo* NTf_2).

^{13}C NMR (125 MHz, 298 K, CD_3CN): δ 173.70, 165.41, 159.90, 151.71, 146.50, 145.03, 137.35, 132.50, 125.87, 124.68, 124.18, 123.89, 123.44, 122.13, 71.19, 71.01, 70.95, 70.76, 70.16, 69.55, 69.16, 50.39, 37.97, 36.83.

LR-ESI-MS (CH_3CN):m/z $[M\text{-}NTf_2]^{19+}$: 365.98, $[M\text{-}2(NTf_2)]^{18+}$: 402.07, $[M\text{-}3(NTf_2)]^{17+}$: 442.16, $[M\text{-}4(NTf_2)]^{16+}$: 487.01, $[M\text{-}5(NTf_2)]^{15+}$: 537.35, $[M\text{-}6(NTf_2)]^{14+}$: 597.19, $[M\text{-}7(NTf_2)]^{13+}$: 663.66, $[M\text{-}8(NTf_2)]^{12+}$: 742.51, $[M\text{-}9(NTf_2)]^{11+}$:836.06, $[M\text{-}10(NTf_2)]^{10+}$: 947.13, $[M\text{-}11(NTf_2)]^{9+}$: 1084.41, $[M\text{-}12(NTf_2)]^{8+}$:1254.59.

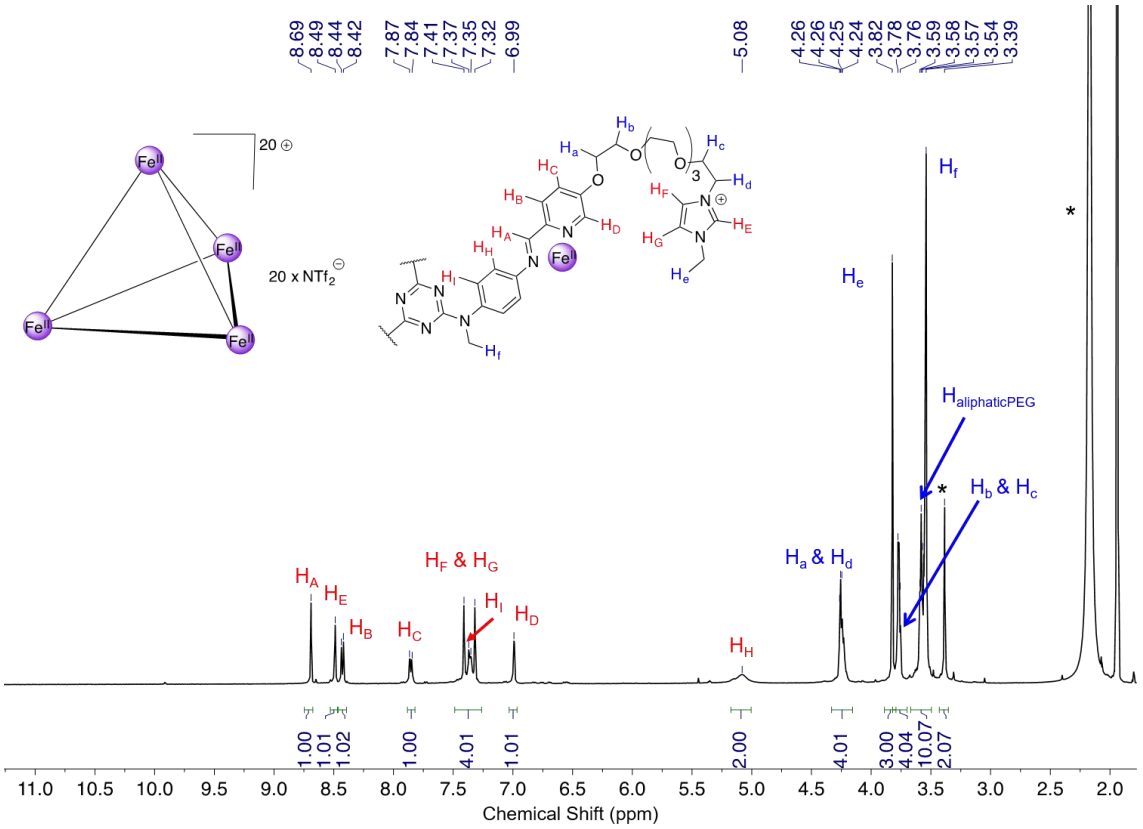

Figure S28. ^{1}H NMR spectrum of the cage 2 in CD_3CN at 298K on a 500 MHz spectrometer. (* Corresponds to residual solvents: acetonitrile and water).

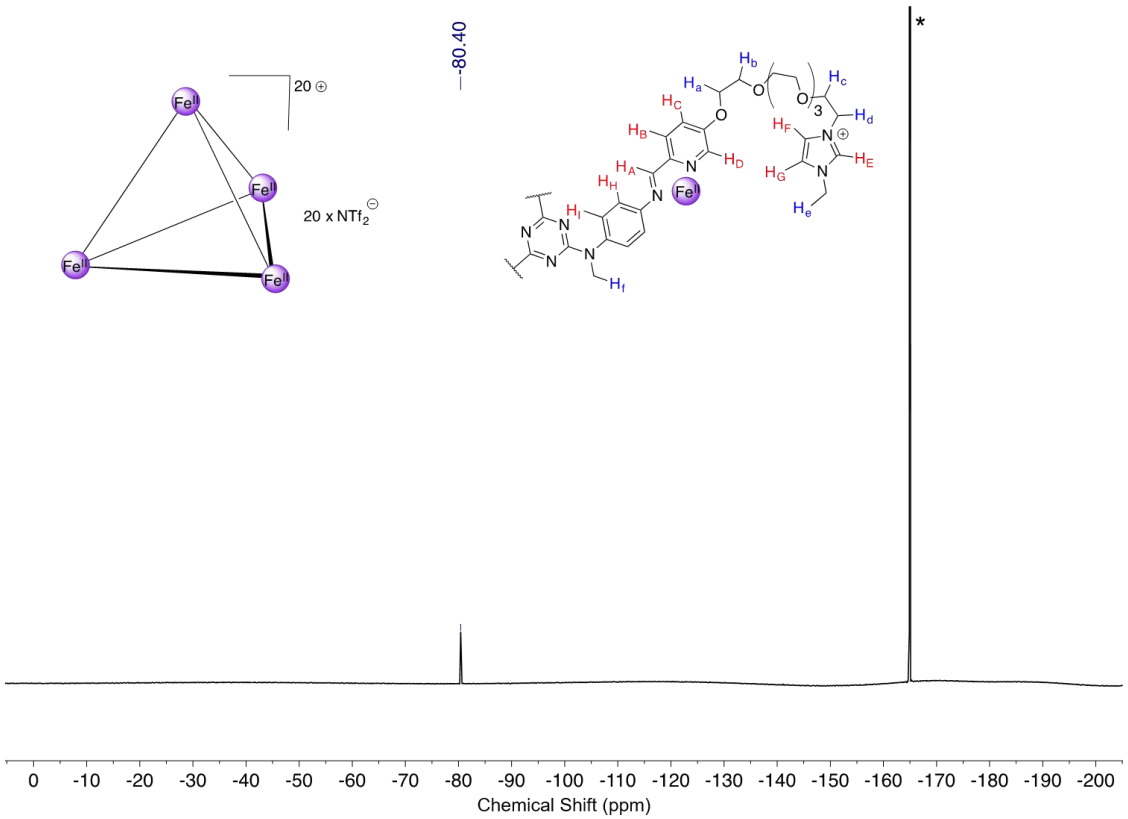

Figure S29. ^{19}F NMR spectrum of the cage 2 in CD_3CN at 298K on a 400 MHz spectrometer. (* Corresponds to the external standard C_6F_6).

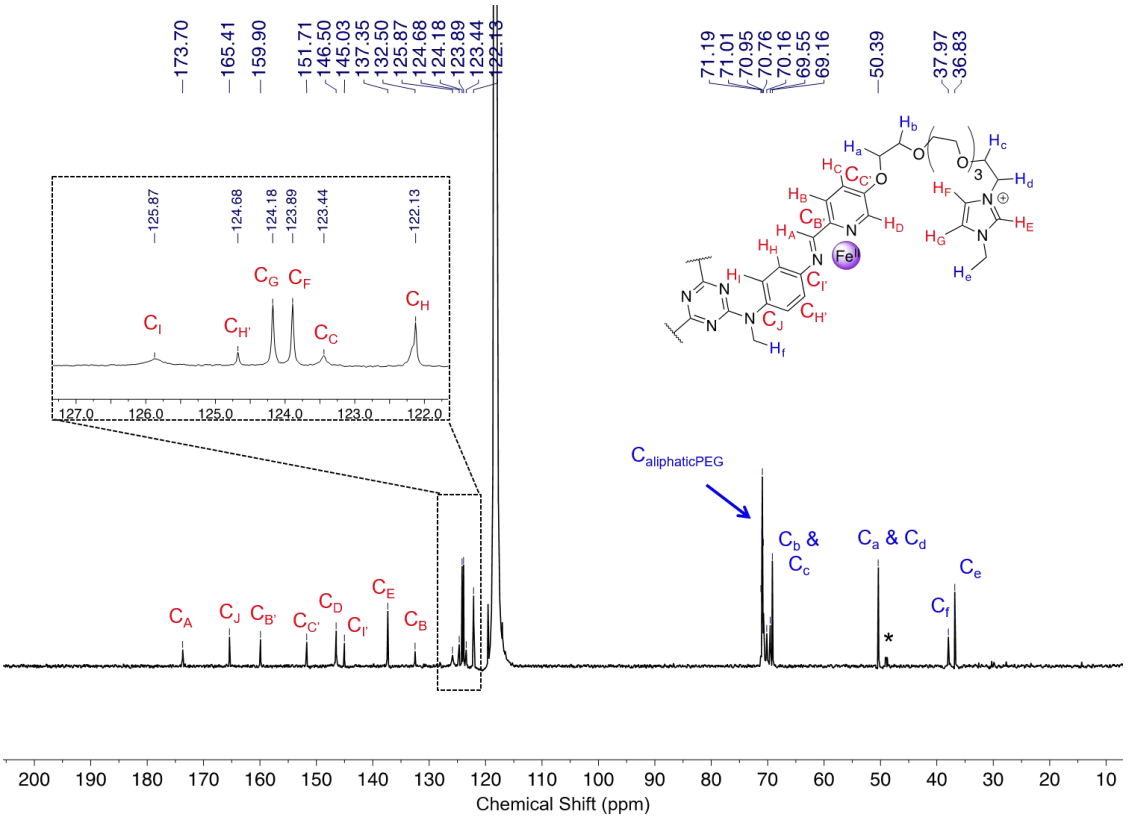

Figure S30. ^{13}C NMR spectrum of the cage 2 in CD_3CN at 298K on a 500 MHz spectrometer. (* Corresponds to residual solvents: acetonitrile and diethyl ether).

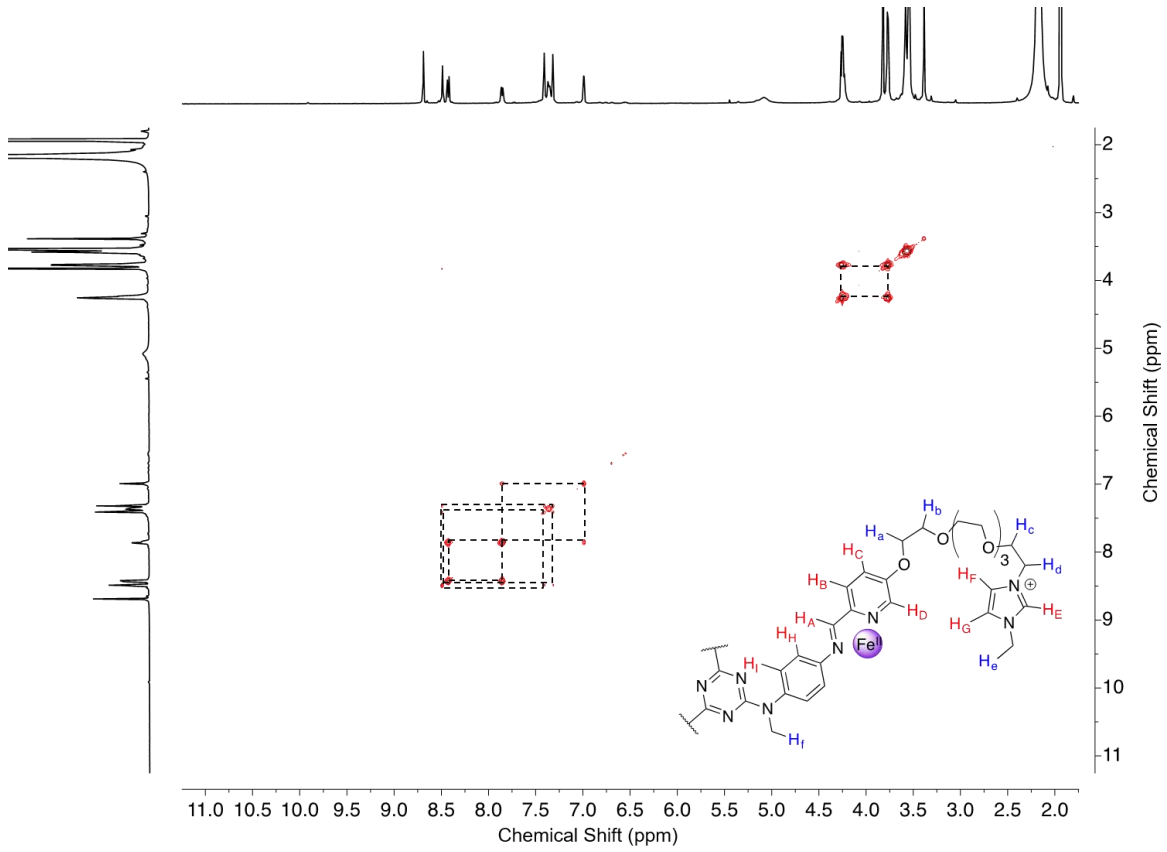

Figure S31. ^{1}H-^{1}H COSY NMR 2D spectrum of the cage 2 in CD_3CN at 298K on a 400 MHz spectrometer.

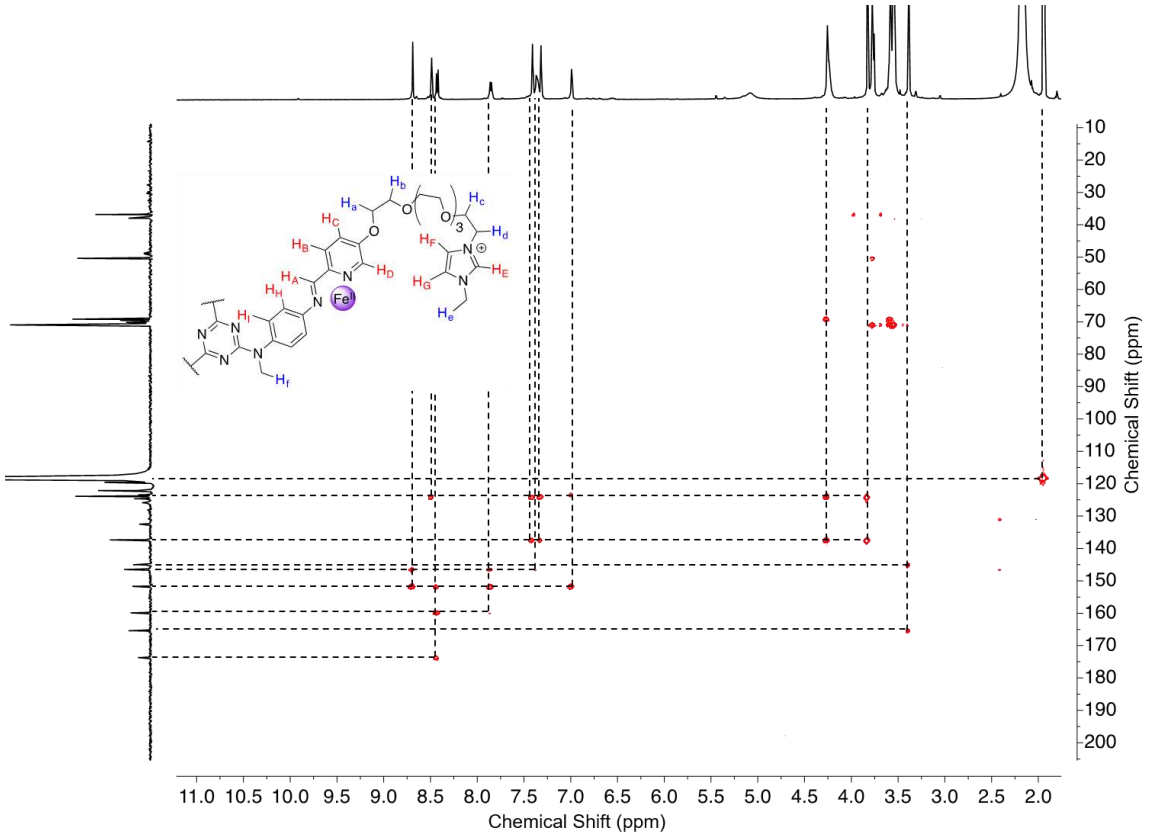

Figure S32. ^{1}H-^{13}C HSQC NMR 2D spectrum of the cage 2 in CD_3CN at 298K on a 500 MHz spectrometer.

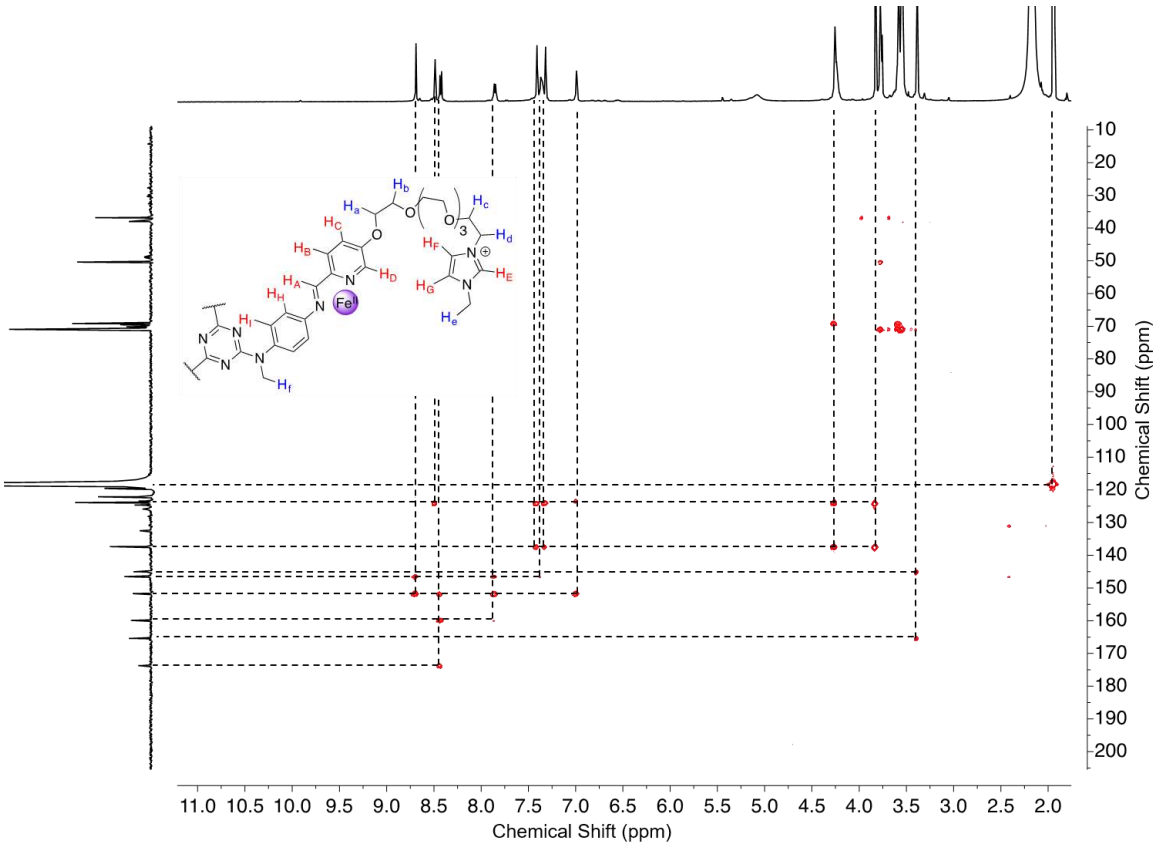

Figure S33. ^{1}H-^{13}C HMBC NMR 2D spectrum of the cage 2 in CD_3CN at 298K on a 500 MHz spectrometer.

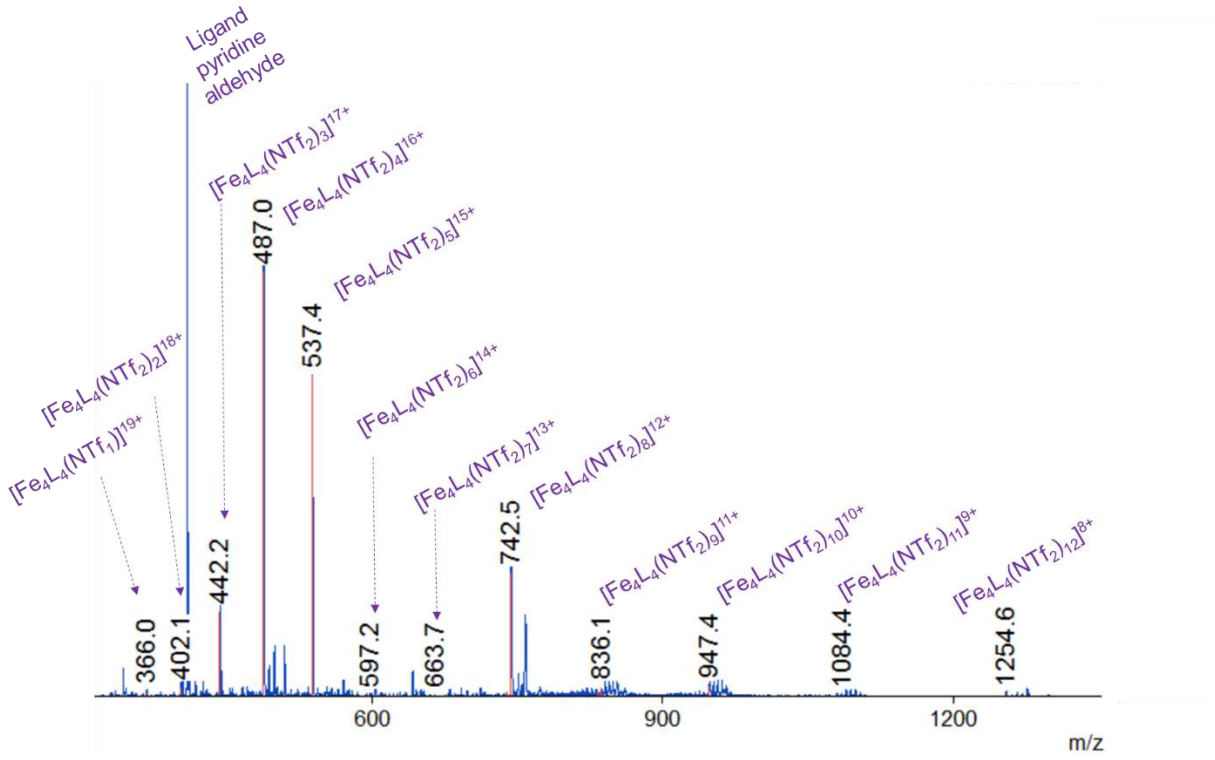

Figure S34. Low resolution ESI mass spectrum of the cage 3 in CH3CN, showing the observed *z* = +8 to +19 species.

6. Preparation and characterisation of cage 3

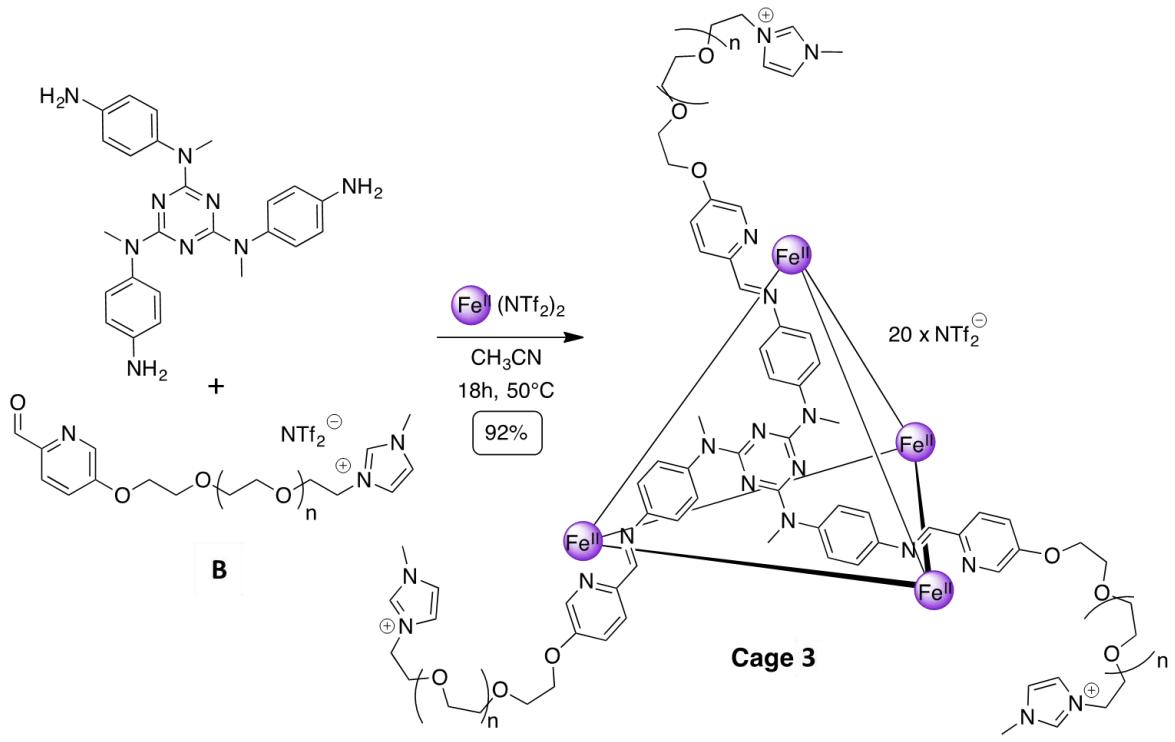

Figure S35: Self-assembly of cage 3.

Cage 3. N2,N4,N6-tris(4-Aminophenyl)-N2,N4,N6-trimethyl-1,3,5-triazine-2,4,6-triamine (1.17 mg, 2.66 µmol, 4 eq.), ligand **B** (11.5 mg, 7.99 µmol, 12 eq.) were combined in dry acetonitrile (400 µL). The solution was subjected to three evacuation/nitrogen fill cycles and $Fe(NTf_2)_2$·$6H_2O$ (1.83 mg, 2.66 µmol, 4 eq.) was added. The mixture was heated at 50 °C for 18h. The solvent was evaporated and the solid triturated with diethyl ether to yield **cage 1** (13 mg, 92%) as a dark red sticky solid.

^{1}H NMR (500 MHz, 298 K, CD_3CN): δ 8.70 (s, 12H, H_A), 8.59 (s, 12H, H_E), 8.43 (d, J = 10 Hz, 12H, H_B), 7.89 (d, J = 10 Hz, 12H, H_C), 7.44 (s, 12H, H_F), 7.35 (m, 36H, H_G & H_I), 7.01 (s, 12H, H_D) 5.09 (bs, 24H, H_H), 4.27 (t, J = 5 Hz, 48H, H_a & H_d), 3.84 (s, 36H, H_e), 3.79 (t, J = 5 Hz, 48H, H_b & H_c), 3.62 – 3.54 (m, 1056H, $H_{aliphaticPEG}$), 3.39 (s, 36H, H_f).

^{19}F NMR (376.5 MHz, 298 K, CD_3CN): δ -75.4 (*endo* NTf_2); -80.4 (*exo* NTf_2).

^{13}C NMR (125 MHz, 298 K, CD_3CN): δ 173.7; 165.4; 160.0; 151.6; 146.5; 145.0; 137.6; 132.6; 125.9; 124.7; 124.2; 123.9; 123.6; 122.1; 71.0; 70.8; 69.7; 69.1; 50.4; 38.0; 36.8

UV-vis (**H_2O**): 545 (ε = 24,440 L.mol^{-1}.cm^{-1}); 390 (ε = 37,420 L.mol^{-1}.cm^{-1}); 301 (ε = 295,990 L.mol^{-1}.cm^{-1}); 275 (ε = 229,720 L.mol^{-1}.cm^{-1}); (**CH_3CN**) : 545 (ε = 24,490 L.mol^{-1}.cm^{-1}); 390 (ε = 46,730 L.mol^{-1}.cm^{-1}); 301 (ε = 305,290 L.mol^{-1}.cm^{-1}); 275 (ε = 251,450 L.mol^{-1}.cm^{-1}).

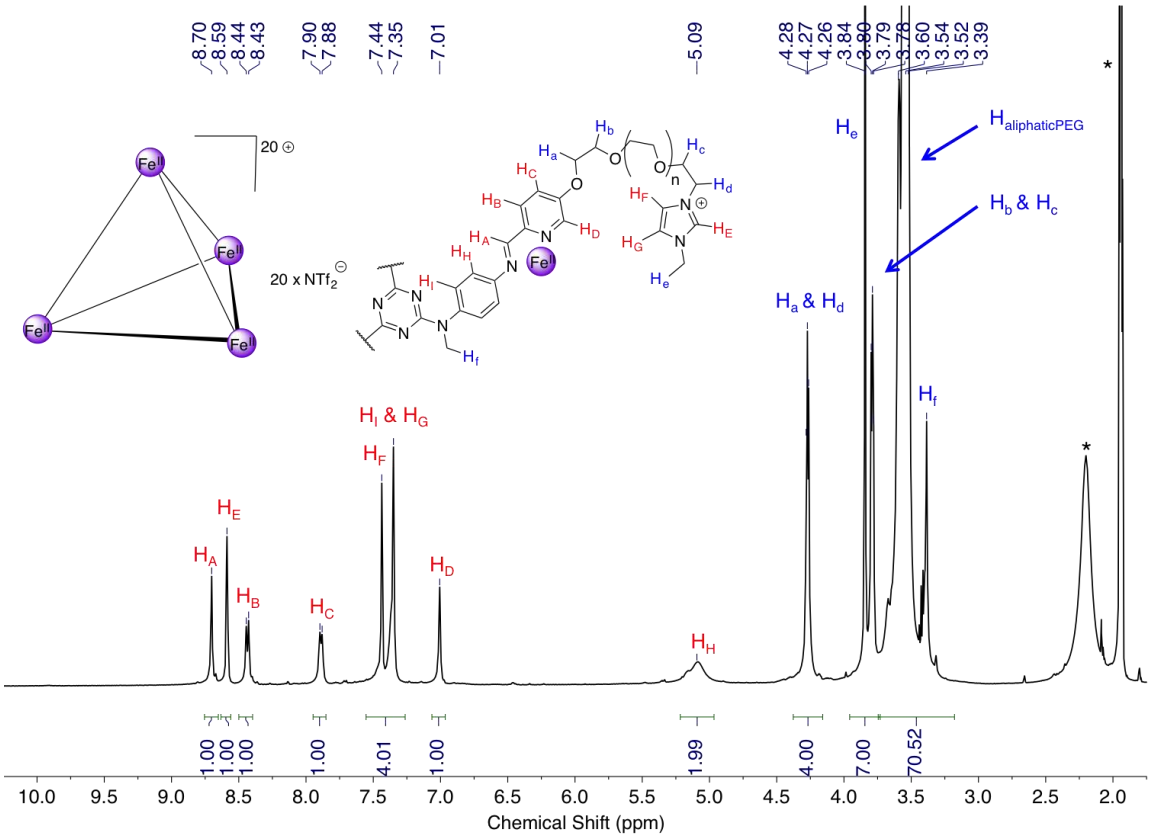

Figure S36. ^{1}H NMR spectrum of the cage 3 in CD_3CN at 298K on a 500 MHz spectrometer. (* Corresponds to residual solvents: acetonitrile and water).

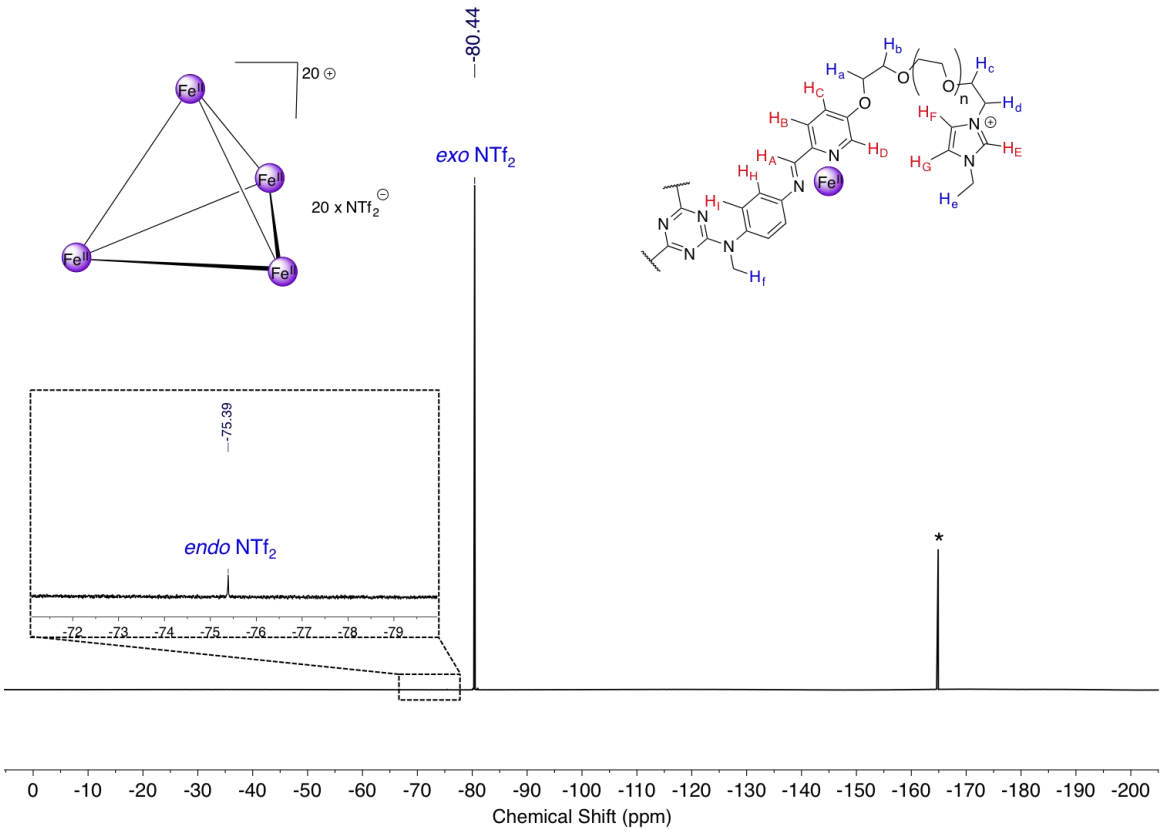

Figure S37. ^{19}F NMR spectrum of the cage 3 in CD_3CN at 298K on a 400 MHz spectrometer. (* Corresponds to the external standard C_6F_6).

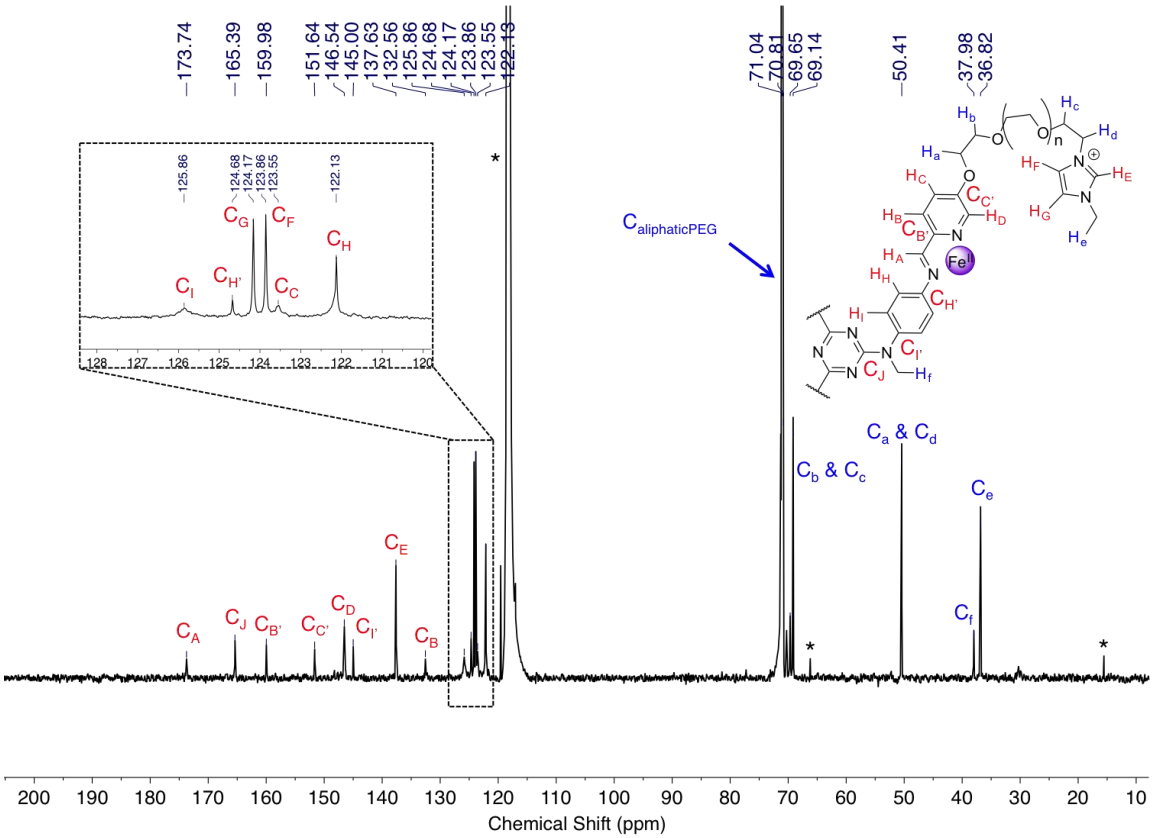

Figure S38. ^{13}C NMR spectrum of the cage 3 in CD_3CN at 298K on a 500 MHz spectrometer. (* Corresponds to residual solvents: acetonitrile and diethyl ether).

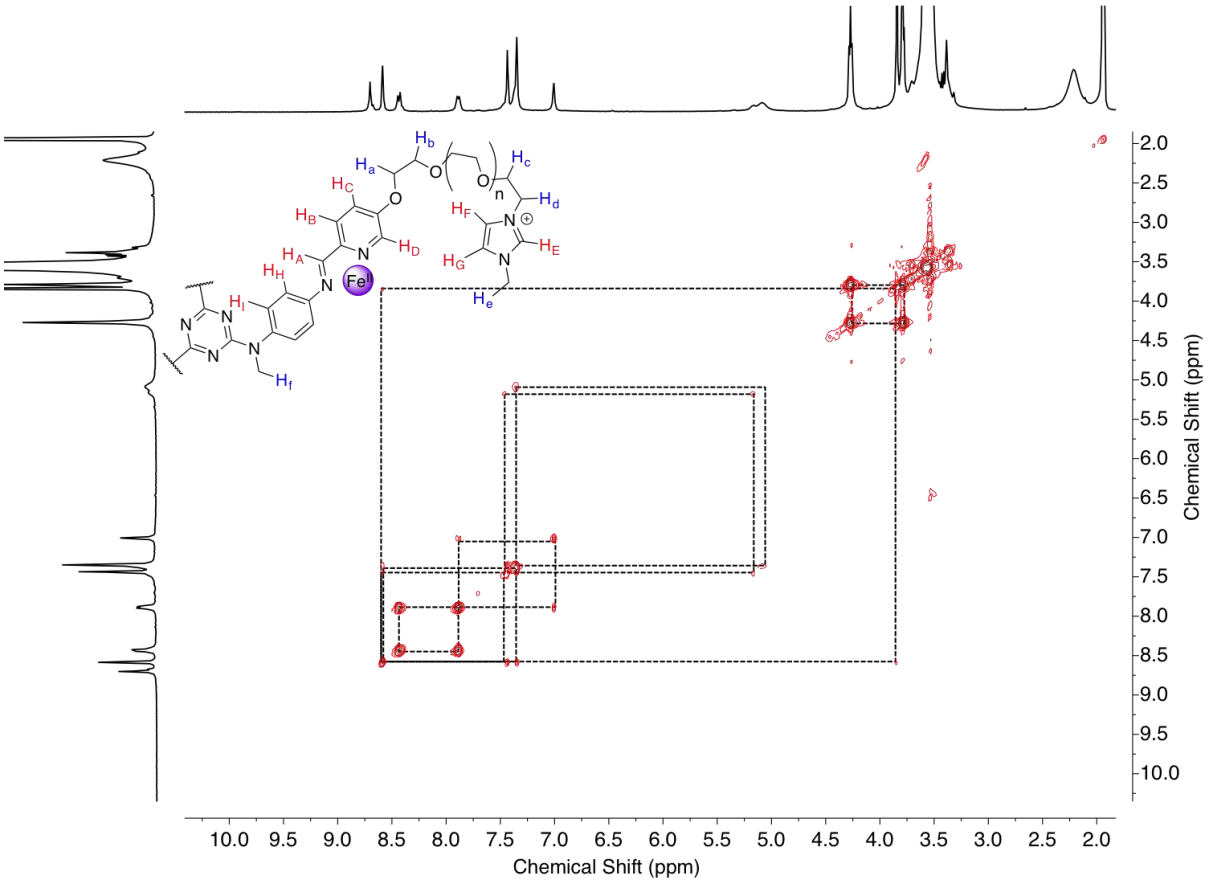

Figure S39. ^{1}H-^{1}H COSY NMR 2D spectrum of the cage 3 in CD_3CN at 298K on a 400 MHz spectrometer.

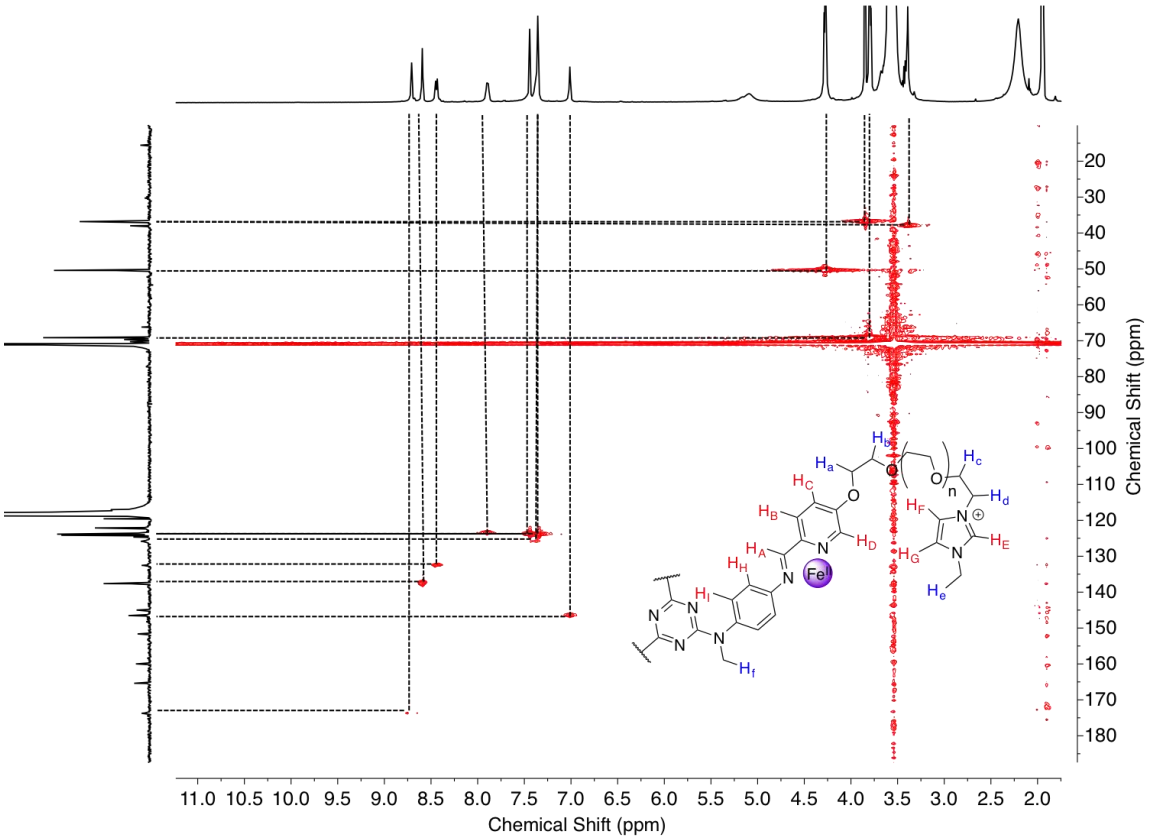

Figure S40. ^{1}H-^{13}C HSQC NMR 2D spectrum of the cage 3 in CD_3CN at 298K on a 500 MHz spectrometer.

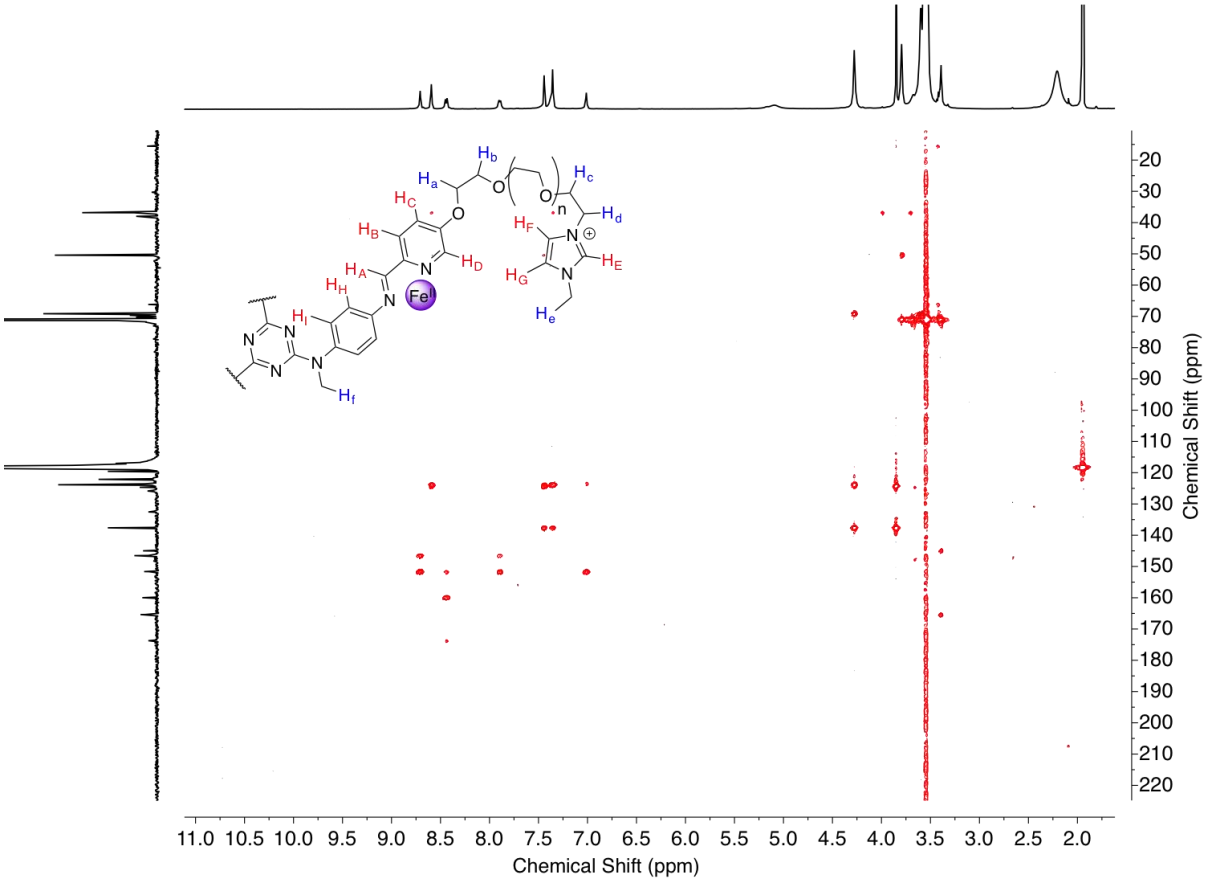

Figure S41. ^{1}H-^{13}C HMBC NMR 2D spectrum of the cage 3 in CD_3CN at 298K on a 500 MHz spectrometer.

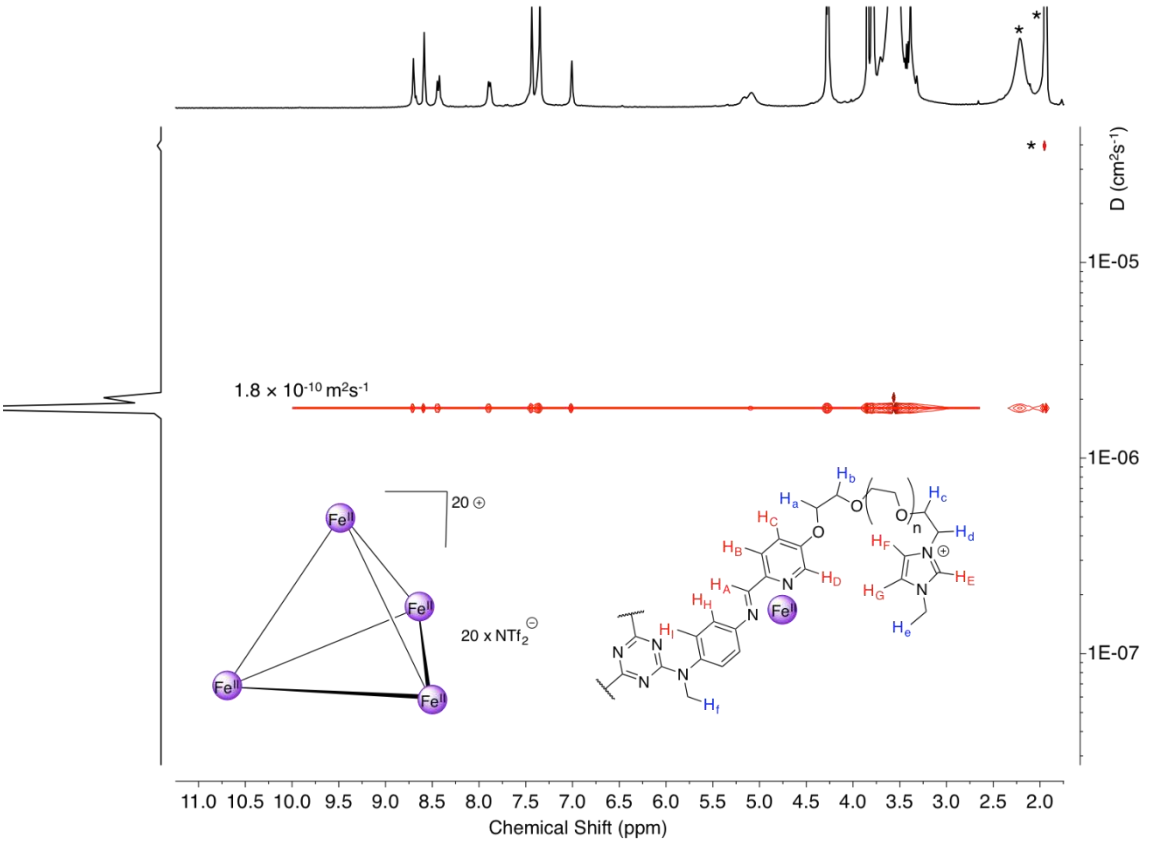

Figure S42. Diffusion Ordered NMR spectrum recorded in CD_3CN at a concentration of 1.5 mM of the cage 3 at 298K on a 400 MHz spectrometer. The diffusion coefficient was measured to be 1.8×10^{-10} m^2s^{-1}. (* Corresponds to residual solvents: acetonitrile and water)

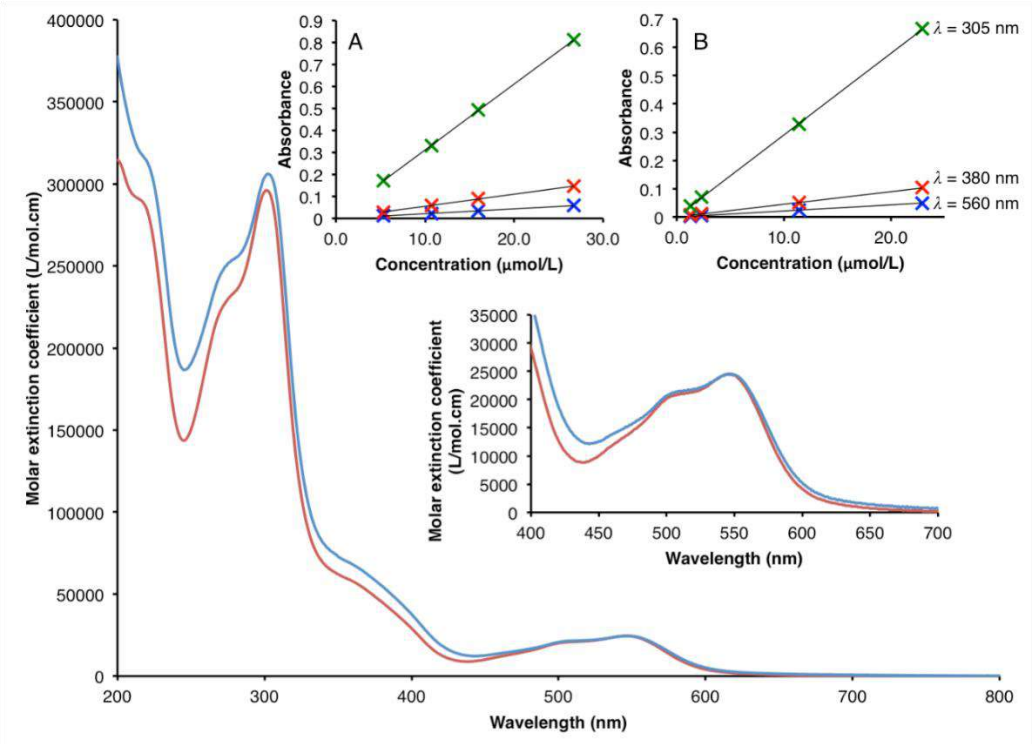

Figure S43. Asorption spectra of the cage 3 at 298K in CH_3CN (blue line) and in H_2O (red line). The insets (A: CH_3CN, B: H_2O) show the linear increase of absorbance at 560, 380 and 305 nm with the concentration.

7. Preparation and characterisation of cage 4

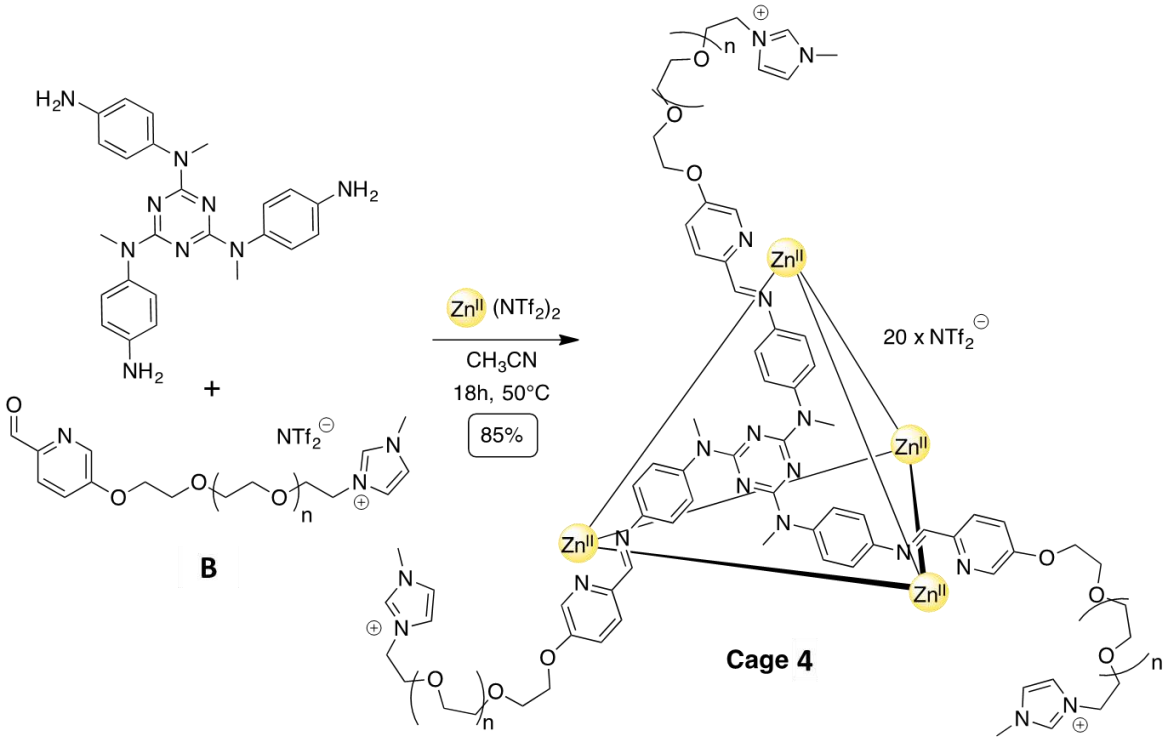

Figure S44: Self-assembly of cage 4.

Cage 4. N2,N4,N6-tris(4-Aminophenyl)-N2,N4,N6-trimethyl-1,3,5-triazine-2,4,6-triamine (1.17 mg, 2.66 µmol, 4 eq.), ligand **B** (11.5 mg, 7.99 µmol, 12 eq.) and $Zn(NTf_2)_2 \bullet xH_2O$ (1.66 mg, 2.66 µmol, 4 eq.) were combined in dry acetonitrile (400 µL). The mixture was heated at 50 °C for 18h. The solvent was evaporated and the solid triturated with diethyl ether to yield **cage 4** (11 mg, 85%) as a yellow sticky solid.

^{1}H NMR (500 MHz, 298 K, CD_3CN): δ 8.59 (s, 12H, H_E), 8.41 (s, 12H, H_A), 8.18 (d, J = 10 Hz, 12H, H_B), 7.91 (d, J = 10 Hz, 12H, H_C), 7.81 (s, 12H, H_D), 7.44 (m, 36H, H_F & H_I), 7.35 (s, 12H, H_G), 5.54 (d, J = 10 Hz, 24H, H_H), 4.33 (bs, 24H, H_a) 4.27 (t, J = 5 Hz, 24H, H_d), 3.84 (m, 60H, H_e & H_b), 3.79 (t, J = 4 Hz, 24H, H_c), 3.78 – 3.52 (m, 1056H, $H_{aliphaticPEG}$), 3.41 (s, 36H, H_f).

^{19}F NMR (376.5 MHz, 298 K, CD_3CN): δ -80.5.

^{13}C NMR (125 MHz, 298 K, CD_3CN): δ 165.5; 164.0; 161.5; 144.8; 144.3; 141.2; 140.0; 137.7; 132.7; 126.4; 125.2; 124.7 & 122.1 (d, J = 124 Hz, C_{NTf2}); 124.2; 123.9; 121.7; 71.1; 70.4; 69.7; 69.2; 50.5; 38.0; 36.9.

UV-vis (**H_2O**): 380 (ε = 26,030 $L.mol^{-1}.cm^{-1}$); 275 (ε = 304,580 $L.mol^{-1}.cm^{-1}$).

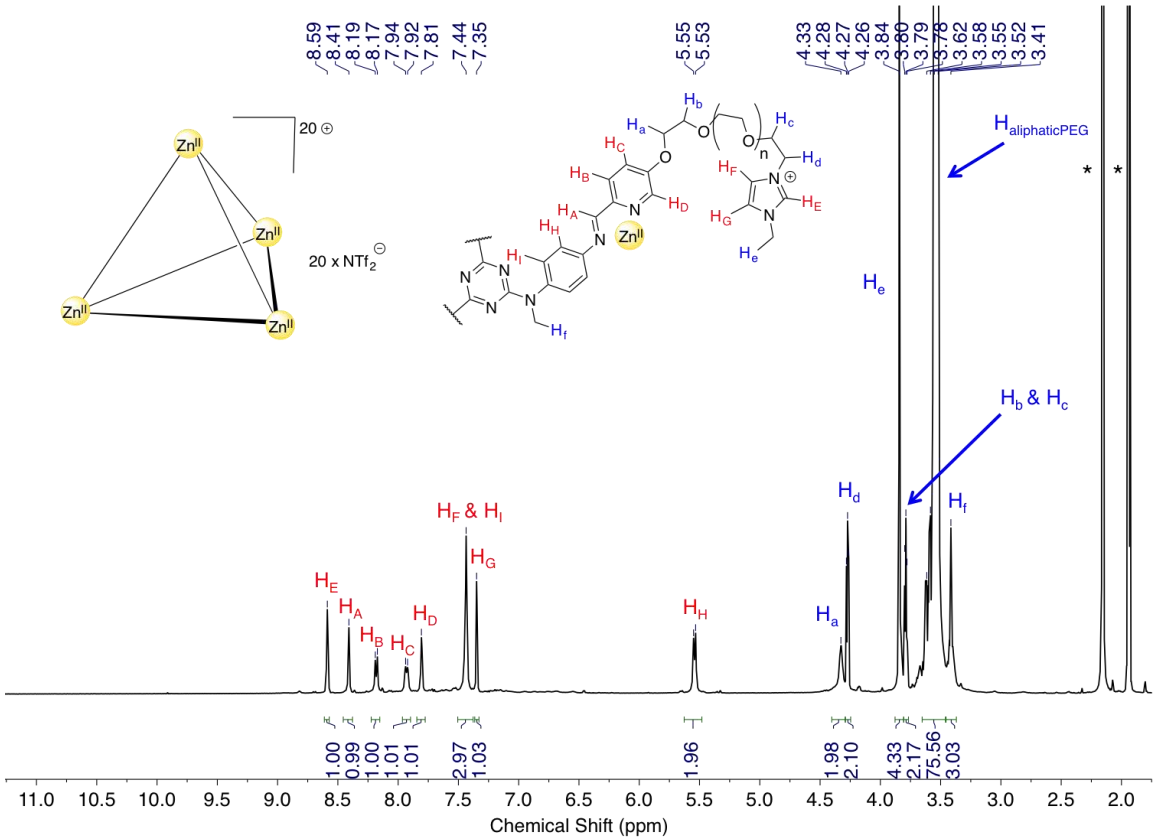

Figure S45. ^{1}H NMR spectrum of the cage 4 in CD_3CN at 298K on a 500 MHz spectrometer. (* Corresponds to residual solvents: acetonitrile and water).

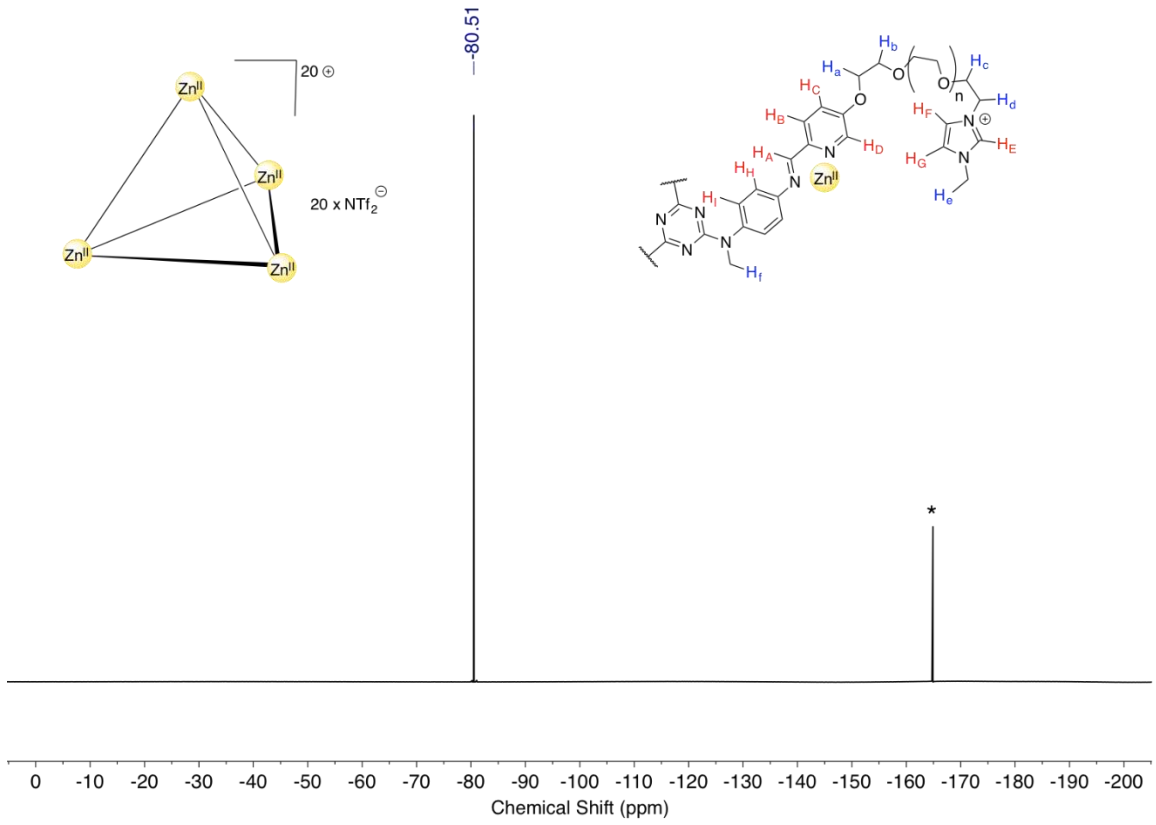

Figure S46. ^{19}F NMR spectrum of the cage 4 in CD_3CN at 298K on a 400 MHz spectrometer. (* Corresponds to the external standard C_6F_6)

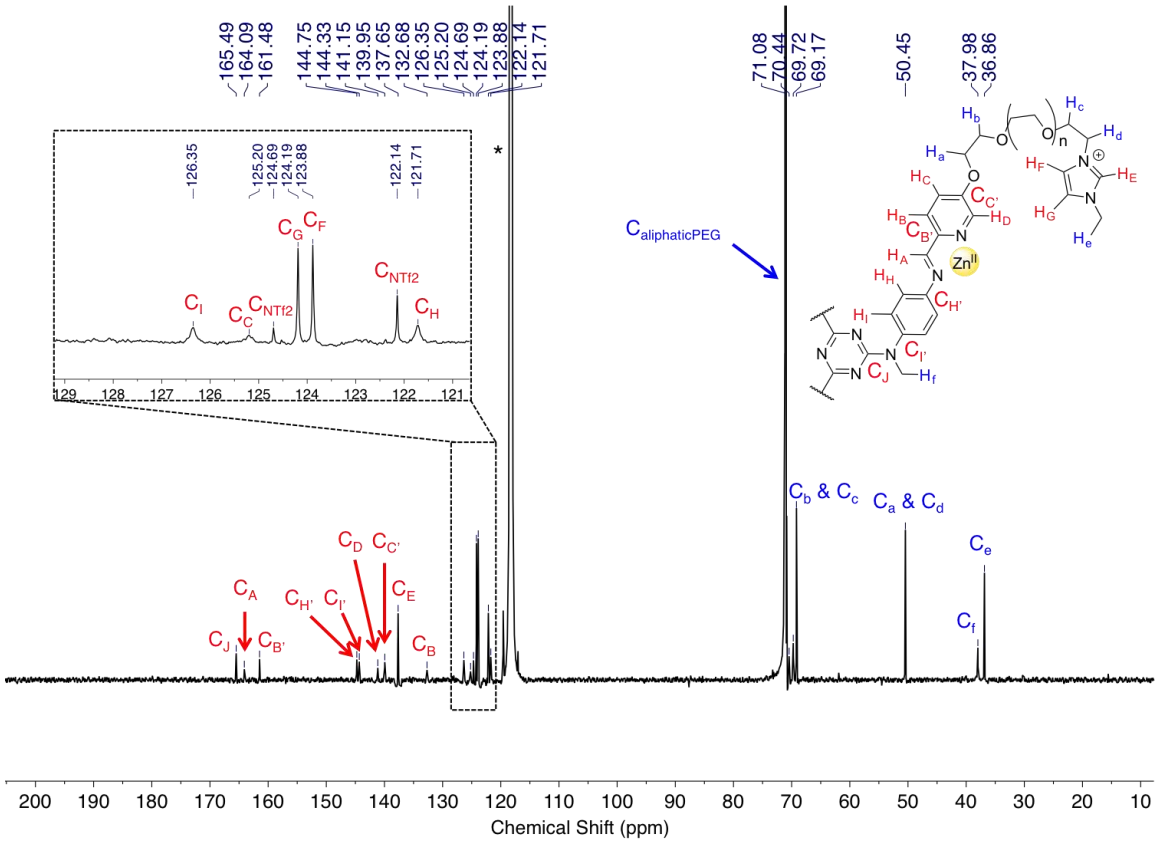

Figure S47. ^{13}C NMR spectrum of the cage 4 in CD_3CN at 298K on a 500 MHz spectrometer.

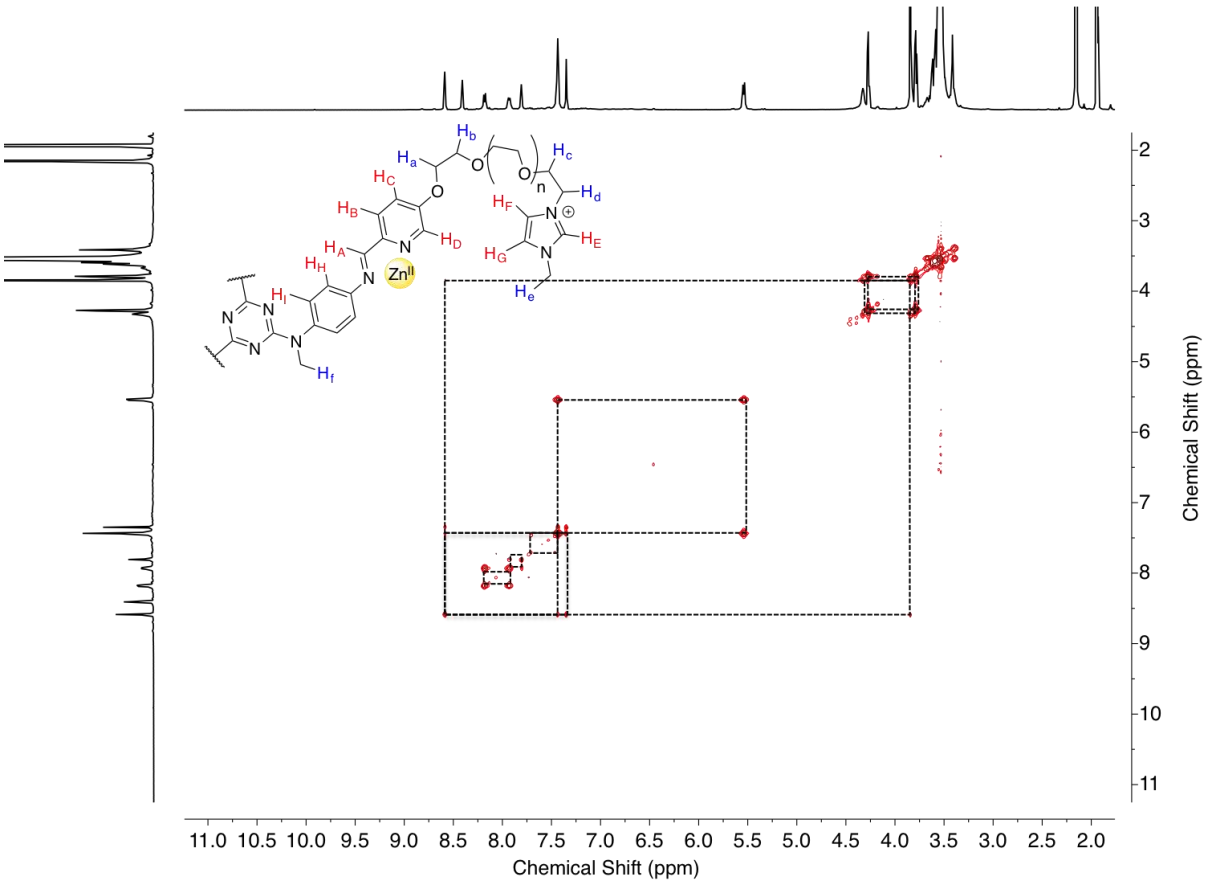

Figure S48. ^{1}H-^{1}H COSY NMR 2D spectrum of the cage 4 in CD_3CN at 298K on a 500 MHz spectrometer.

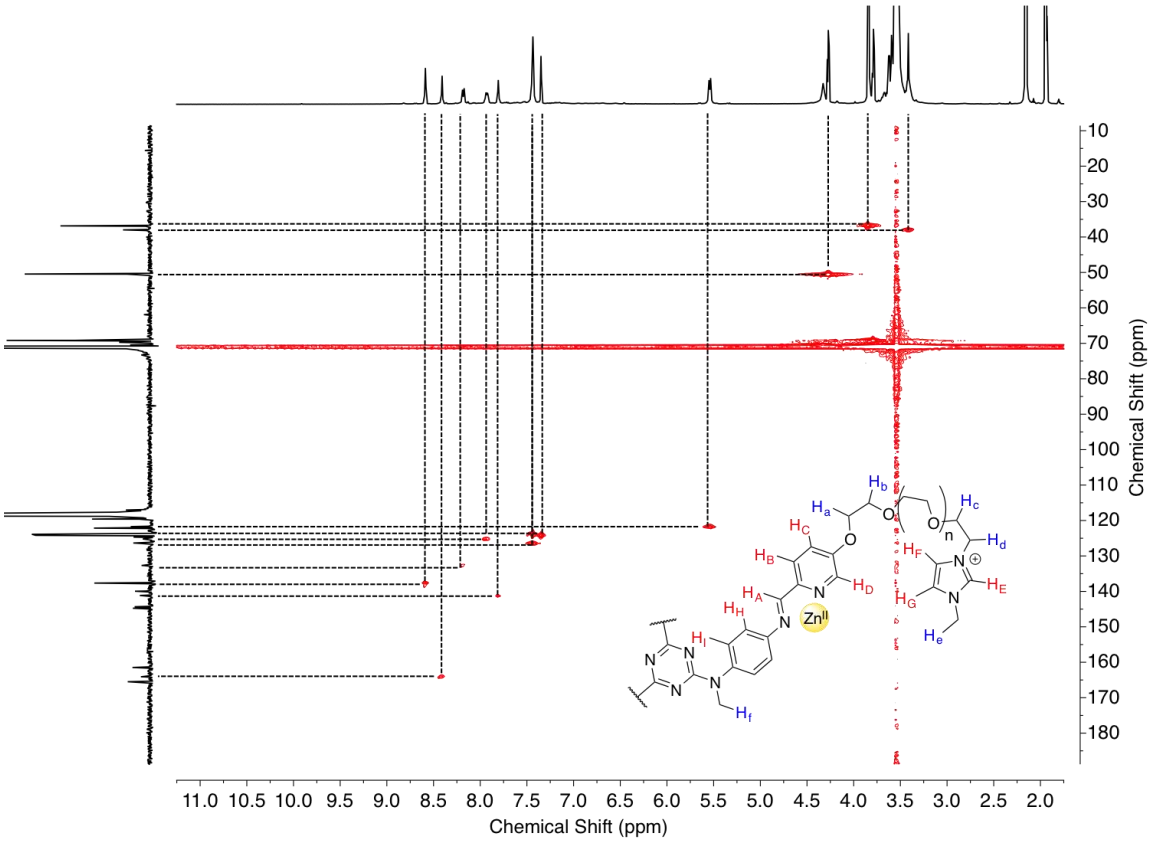

Figure S49. ^{1}H-^{13}C HSQC NMR 2D spectrum of the cage 4 in CD_3CN at 298K on a 500 MHz spectrometer.

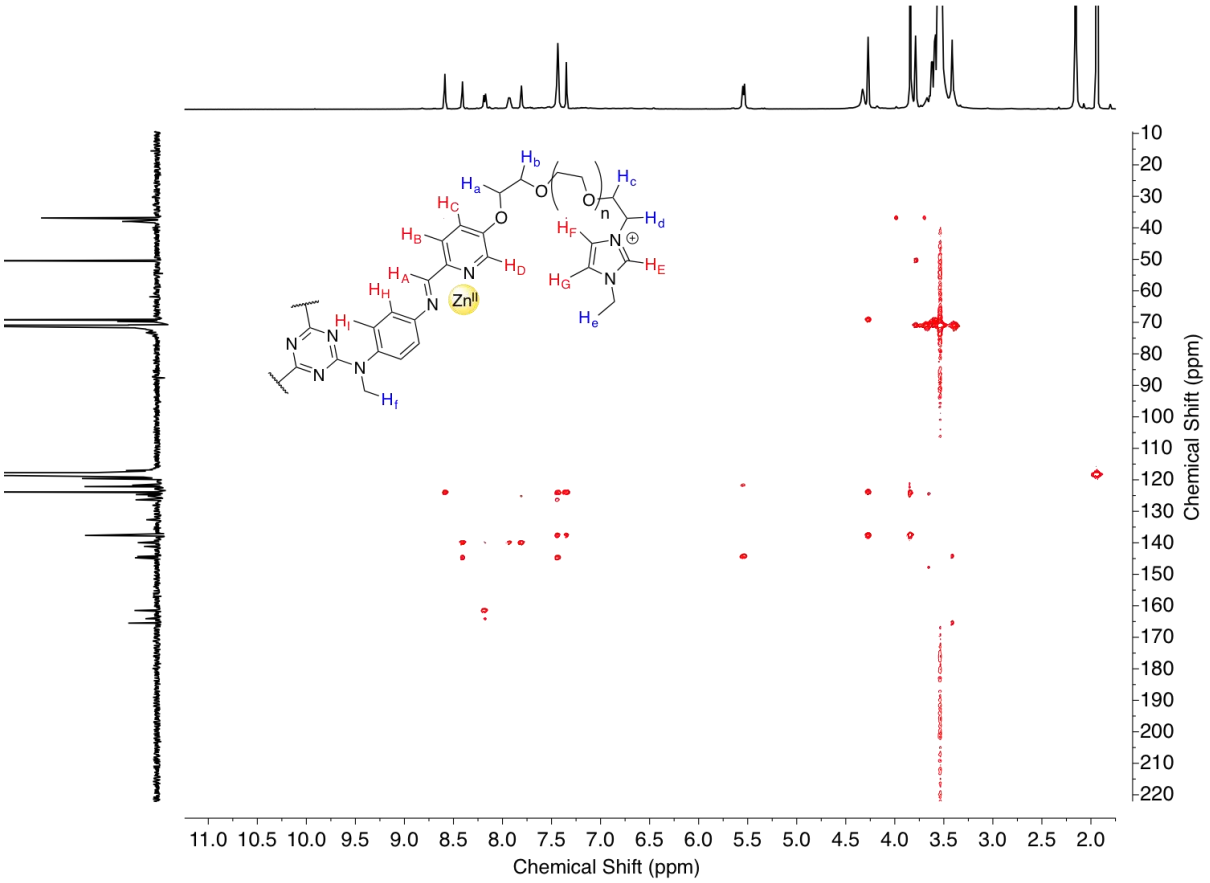

Figure S50. ^{1}H-^{13}C HMBC NMR 2D spectrum of the cage 4 in CD_3CN at 298K on a 500 MHz spectrometer.

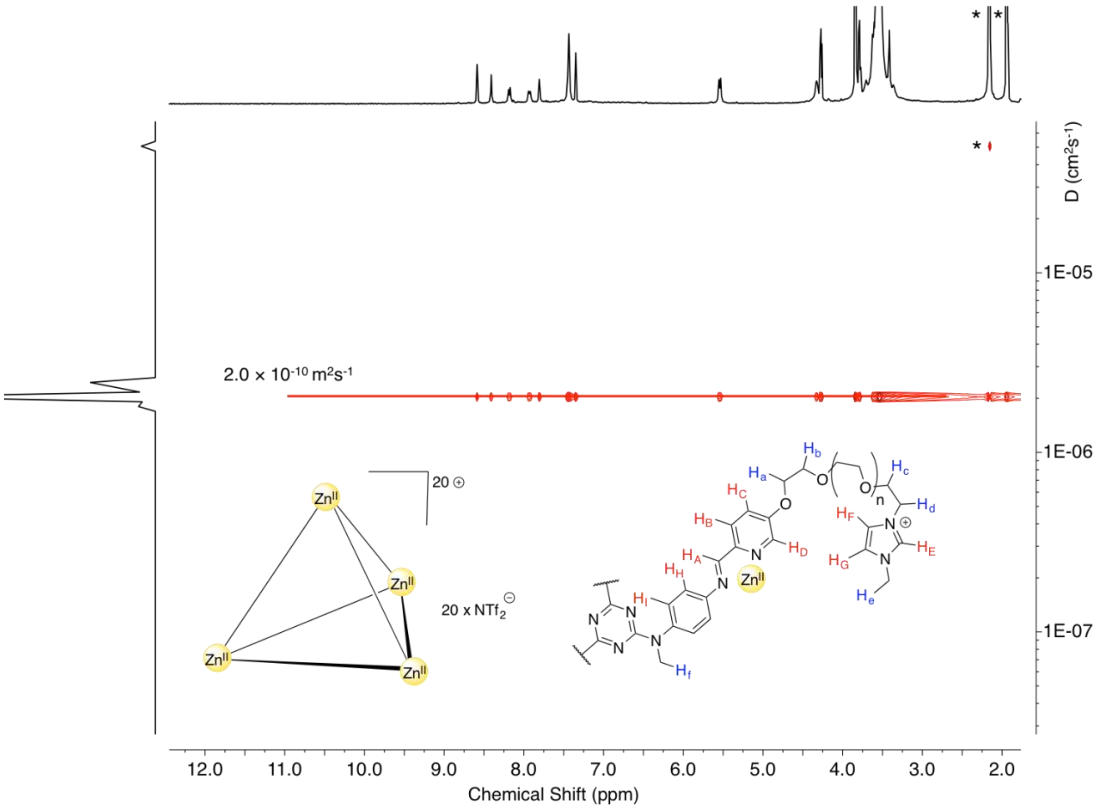

Figure S51. Diffusion Ordered NMR spectrum recorded in CD_3CN at a concentration of 1.5 mM of the cage 4 at 298K on a 400 MHz spectrometer. The diffusion coefficient was measured to be 2.0×10^{-10} m^2s^{-1}. (* Corresponds to residual solvents: acetonitrile and water).

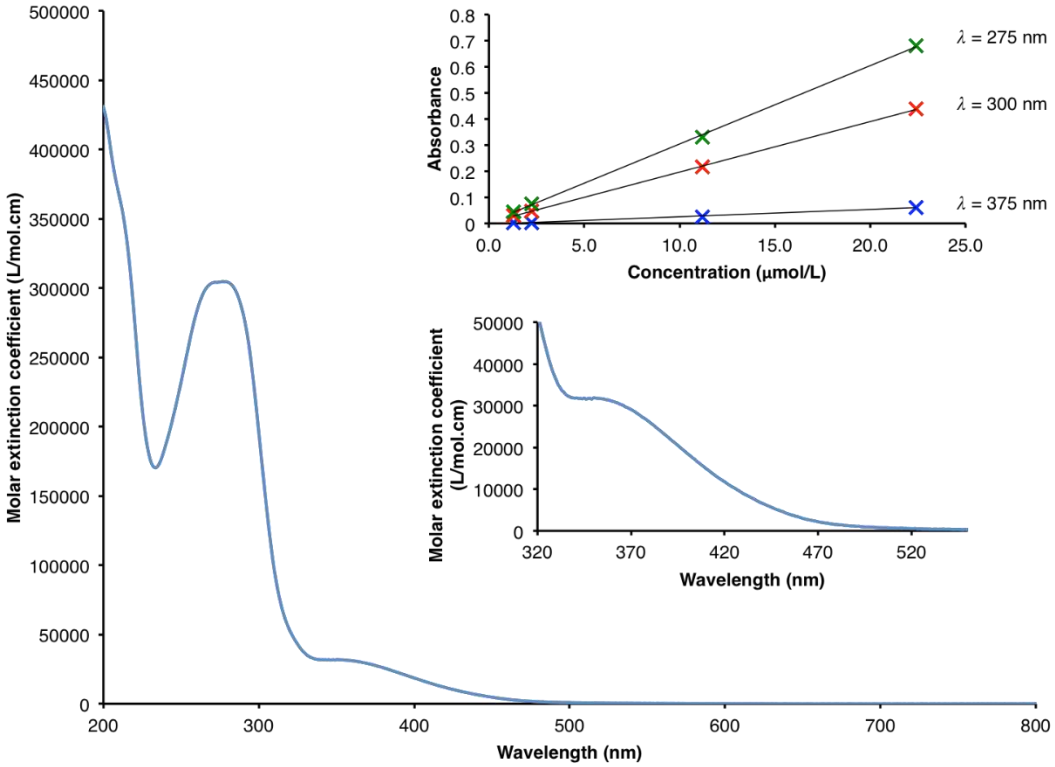

Figure S52.Absorption spectra of the cage 4 at 298K in H_2O. The inset shows the linear increase of absorbance at 375, 300 and 275 nm upon the increase of the concentration (r^2= 0.993, 0.9998 and 0.9994 respectively).

8. Preparation and characterisation of cage 5

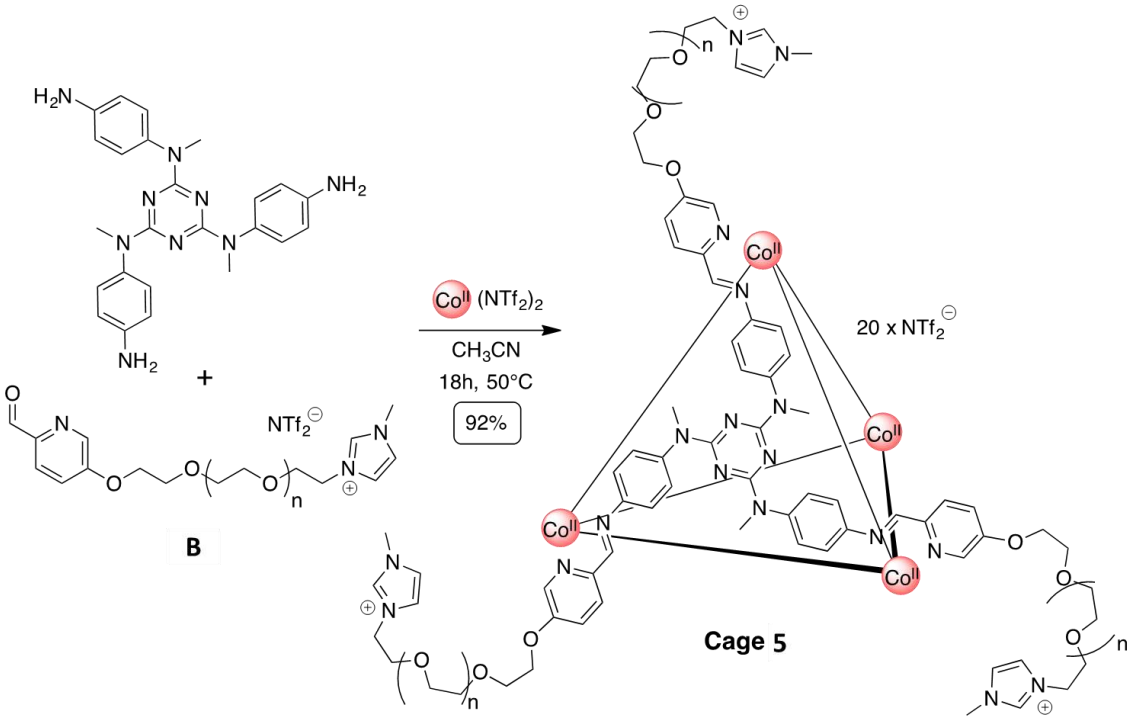

Figure S53:Self-assembly of cage 5.

Cage 5. N2,N4,N6-tris(4-Aminophenyl)-N2,N4,N6-trimethyl-1,3,5-triazine-2,4,6-triamine (1.17 mg, 2.66 µmol, 4 eq.), ligand **B** (11.5 mg, 7.99 µmol, 12 eq.) and $Co(NTf_2)_2 \bullet 6H_2O$ (1.84 mg, 2.66 µmol, 4 eq.) were combined in dry acetonitrile (400 µL). The mixture was heated at 50 °C for 18h. The solvent was evaporated and the solid triturated with diethyl ether to yield **cage 5** (13 mg, 92%) as an orange sticky solid.

^{1}H NMR (400 MHz, 298 K, CD_3CN): δ 251.7; 106.7; 82.0; 12.5; 8.8; 7.6; 4.5; 3.8; 2.9; 2.1; 1.4; 1.1; -0.2; -0.5; -4.9; -23.7.

^{19}F NMR (376.5 MHz, 298 K, CD_3CN): δ -79.7.

^{13}C NMR (125 MHz, 298 K, CD_3CN): δ 166.1; 137.7; 125.2; 124.2; 123.9; 122.6; 88.2; 71.2; 70.6; 70.2; 69.9; 69.2; 69.1; 68.9; 50.5; 36.9.

UV-vis (H_2O): 370 (ε = 71,370 $L.mol^{-1}.cm^{-1}$); 305 (ε = 216,110 $L.mol^{-1}.cm^{-1}$); 280 (ε = 273,040 $L.mol^{-1}.cm^{-1}$). (**CH_3CN**): 370 (ε = 109,450 $L.mol^{-1}.cm^{-1}$); 305 (ε = 204,240 $L.mol^{-1}.cm^{-1}$); 280 (ε = 289,330 $L.mol^{-1}.cm^{-1}$).

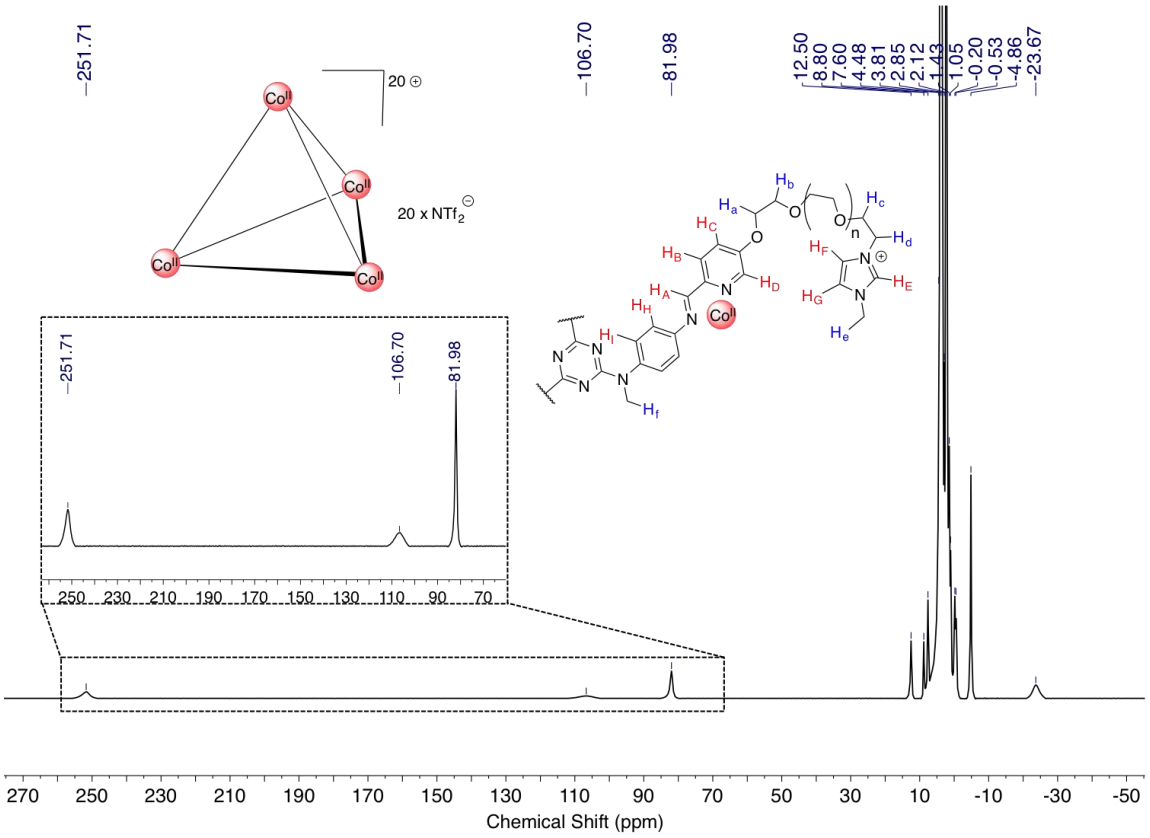

Figure S54. ^{1}H NMR spectrum of the cage 5 in CD_3CN at 298K on a 400 MHz spectrometer.

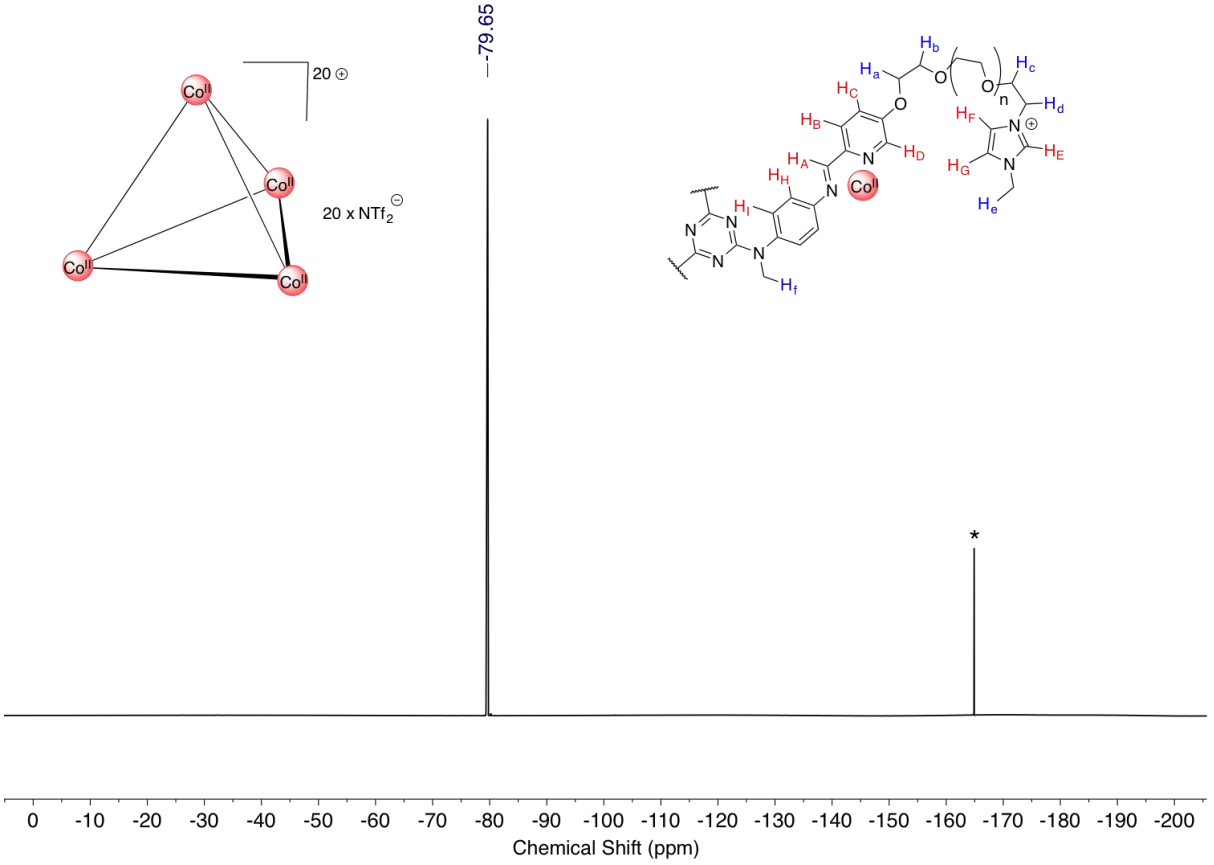

Figure S55. ^{19}F NMR spectrum of the cage 5 in CD_3CN at 298K on a 400 MHz spectrometer. (* Corresponds to the external standard C_6F_6).

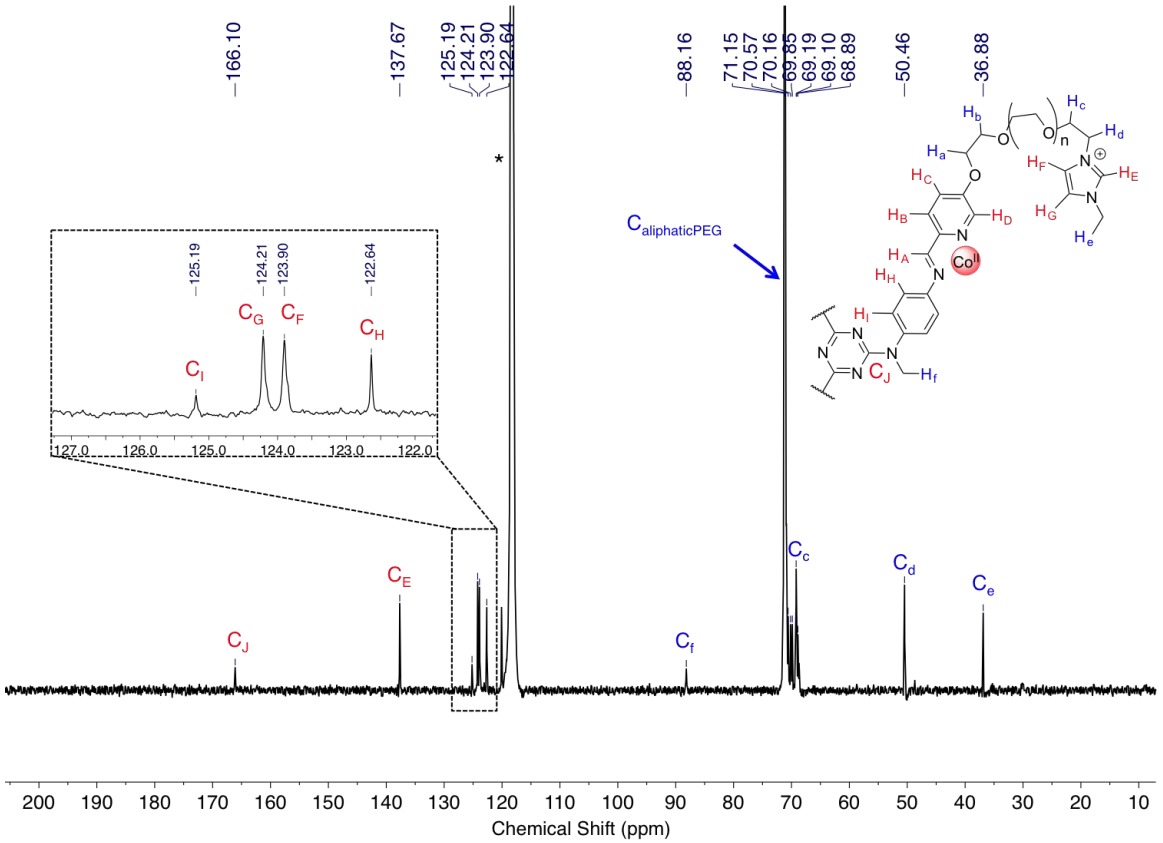

Figure S56. ^{13}C NMR spectrum of the cage 5 in CD_3CN at 298K on a 500 MHz spectrometer. (* Corresponds to residual solvent: acetonitrile).

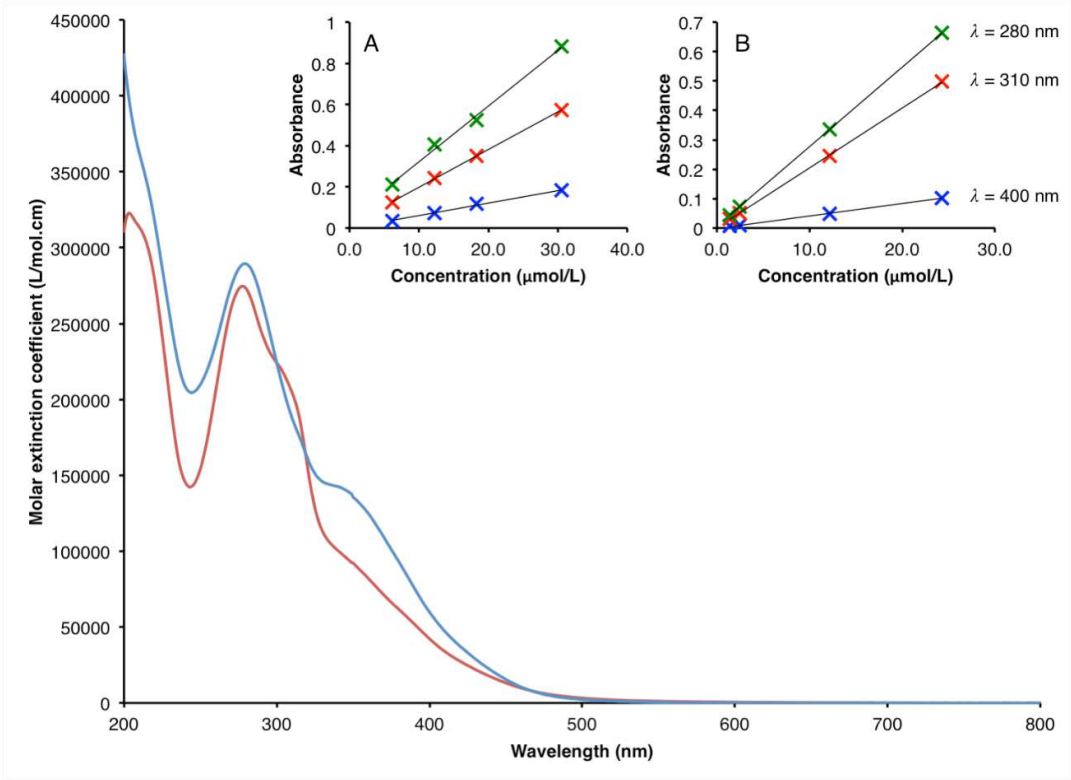

Figure S57. Electronic absorption spectra of the cage 5 at 298K in CH_3CN (blue line) and in H_2O (red line). The insets (A: CH_3CN, B: H_2O) show the linear increase of absorbance at 400, 310 and 280 nm upon the increase of the concentration (r^2=0.9956, 0.995 and 0.9994 in CH_3CN and r^2= 0.9997, 0.9956 and 0.9957 in H_2O).

9. Preparation and characterisation of cage 6

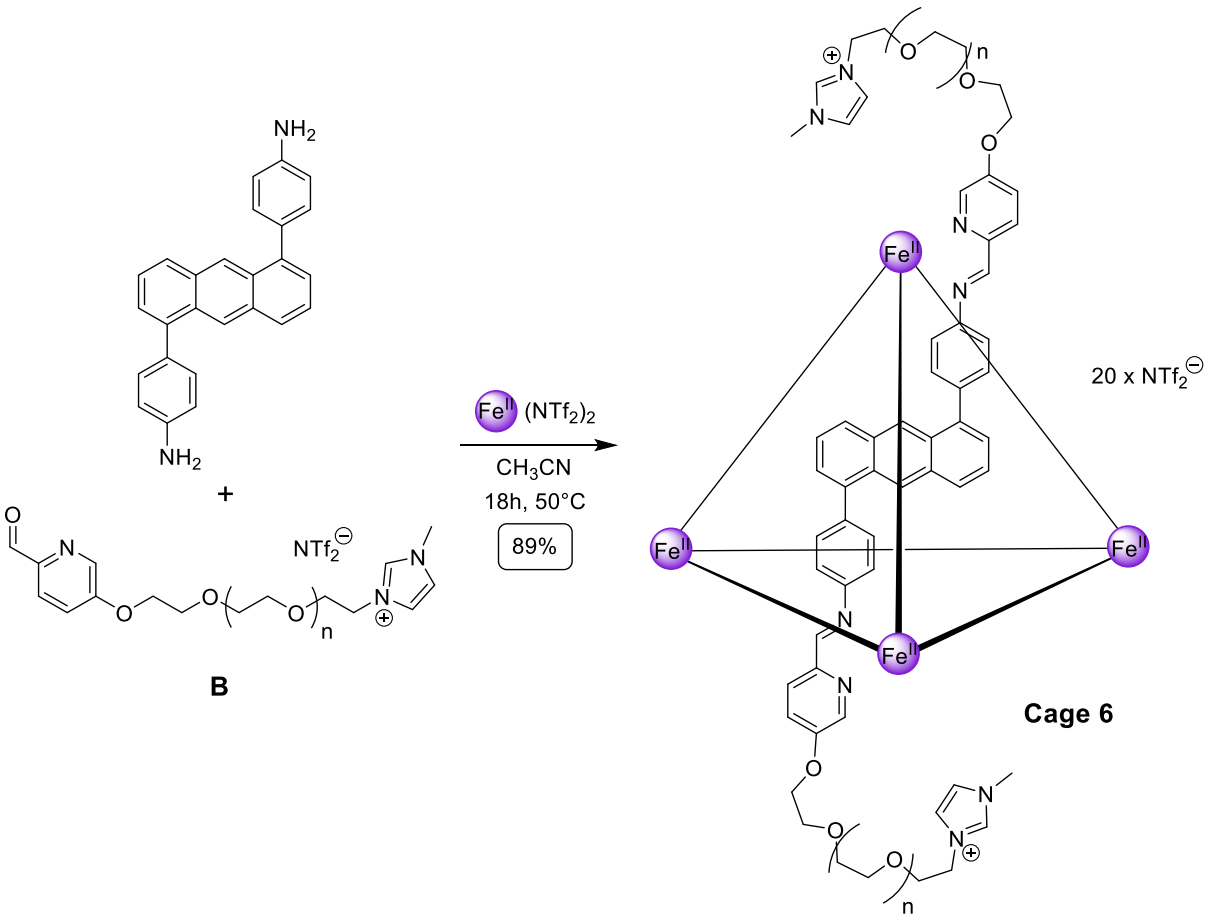

Figure S58: Self-assembly of cage 6.

Cage 6. 1,5-bis(4-aminophenyl)anthracene (1.34 mg, 3.72 µmol, 6 eq.), ligand **B** (10.8, 7.5µmol, 12 eq.) were combined in dry acetonitrile (400 µL). The solution was subjected to three evacuation/nitrogen fill cycles and $Fe(NTf_2)_2 \bullet 6H_2O$ (1.71 mg, 2.49 µmol, 4 eq.) was added. The mixture was heated at 50 °C for 18h. The solvent was evaporated and the solid triturated with diethyl ether to yield **cage 6** (12 mg, 89%) as a dark red sticky solid.

^{1}H NMR (500 MHz, 298 K, CD_3CN): δ 9.05 (s, 12H, H_A), 8.58 (s, 12H, H_E), 8.50 (d, J = 10 Hz, 12H, H_B), 8.14 (s, 12H, H_M), 7.91 (d, J = 5 Hz, 12H, H_C), 7.60 (d, 12H, H_L), 7.44 (s, 12H, H_F), 7.41-7.36 (m, 36H, H_K & H_J & H_{I2}), 7.35 (s, 12H, H_G), 7.21 (m, 24H, H_D & H_{I1}), 6.04 (m, 24H, H_{H1} & H_{H2}), 4.31 (bs, 24H, H_a) 4.27 (t, J = 5 Hz, 24H, H_d), 3.84 (m, 60H, H_e & H_b), 3.79 (t, J = 4 Hz, 24H, H_c), 3.78 – 3.52 (m, 1056H, $H_{aliphaticPEG}$).

^{19}F NMR (376.5 MHz, 298 K, CD_3CN): δ -80.4.

^{13}C NMR (125 MHz, 298 K, CD_3CN): δ 174.2; 160.6; 151.7; 151.3; 146.7; 141.9; 139.7; 137.2; 133.0; 132.1; 130.7; 129.2; 127.4; 125.8; 125.4; 124.7; 124.2; 123.9; 123.6; 122.1; 71.3; 71.0; 70.8; 70.4; 69.7; 69.2; 50.4; 36.8.

UV-vis (**H_2O**): 545 (ε = 15,390 $L.mol^{-1}.cm^{-1}$); 390 (ε = 69,750 $L.mol^{-1}.cm^{-1}$); 301 (ε = 167,210 $L.mol^{-1}.cm^{-1}$); 275 (ε = 265,260 $L.mol^{-1}.cm^{-1}$); (**CH_3CN**) : 545 (ε = 21,510 $L.mol^{-1}.cm^{-1}$); 390 (ε = 109,970 $L.mol^{-1}.cm^{-1}$); 301 (ε = 224,530 $L.mol^{-1}.cm^{-1}$); 275 (ε = 309,440 $L.mol^{-1}.cm^{-1}$).

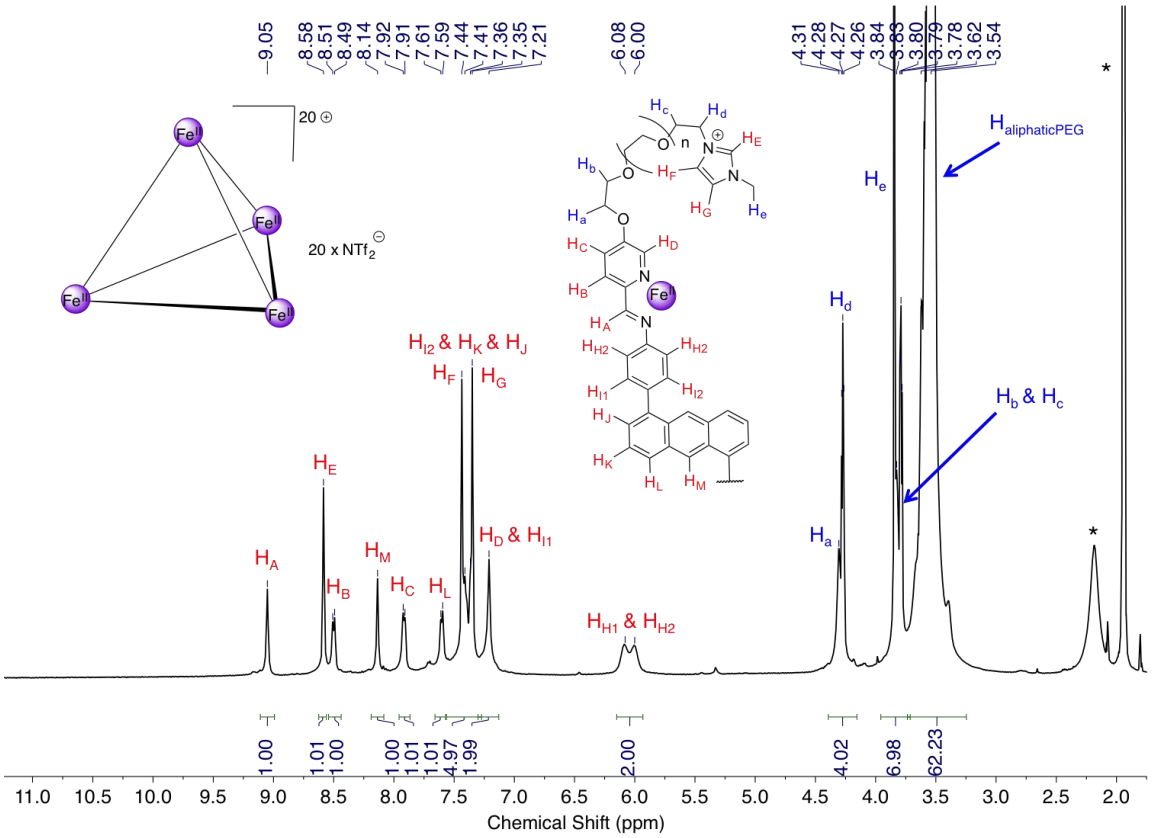

Figure S59. ^{1}H NMR spectrum of the cage 6 in CD_3CN at 298K on a 500 MHz spectrometer. (* Corresponds to residual solvents: acetonitrile and water).

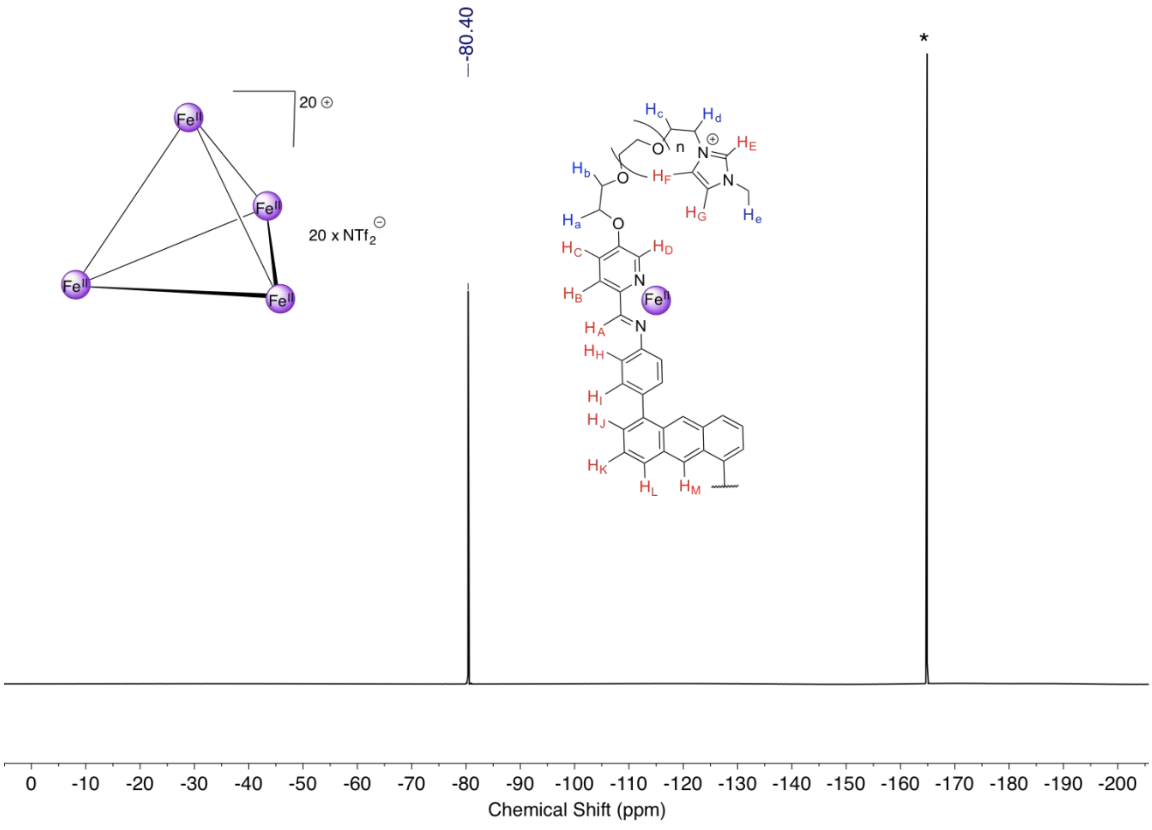

Figure S60. ^{19}F NMR spectrum of the cage 6 in CD_3CN at 298K on a 400 MHz spectrometer. (* Corresponds to the external standard C_6F_6).

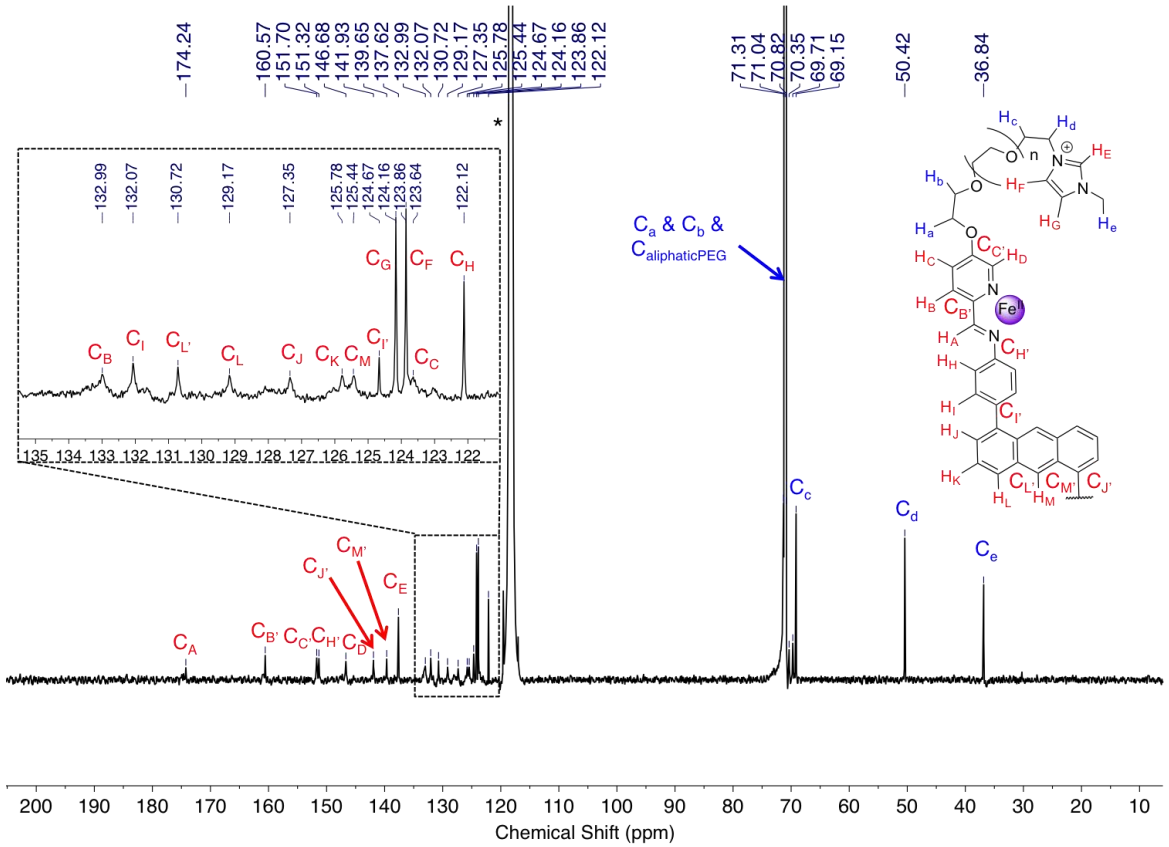

Figure S61. ^{13}C NMR spectrum of the cage 6 in CD_3CN at 298K on a 500 MHz spectrometer.

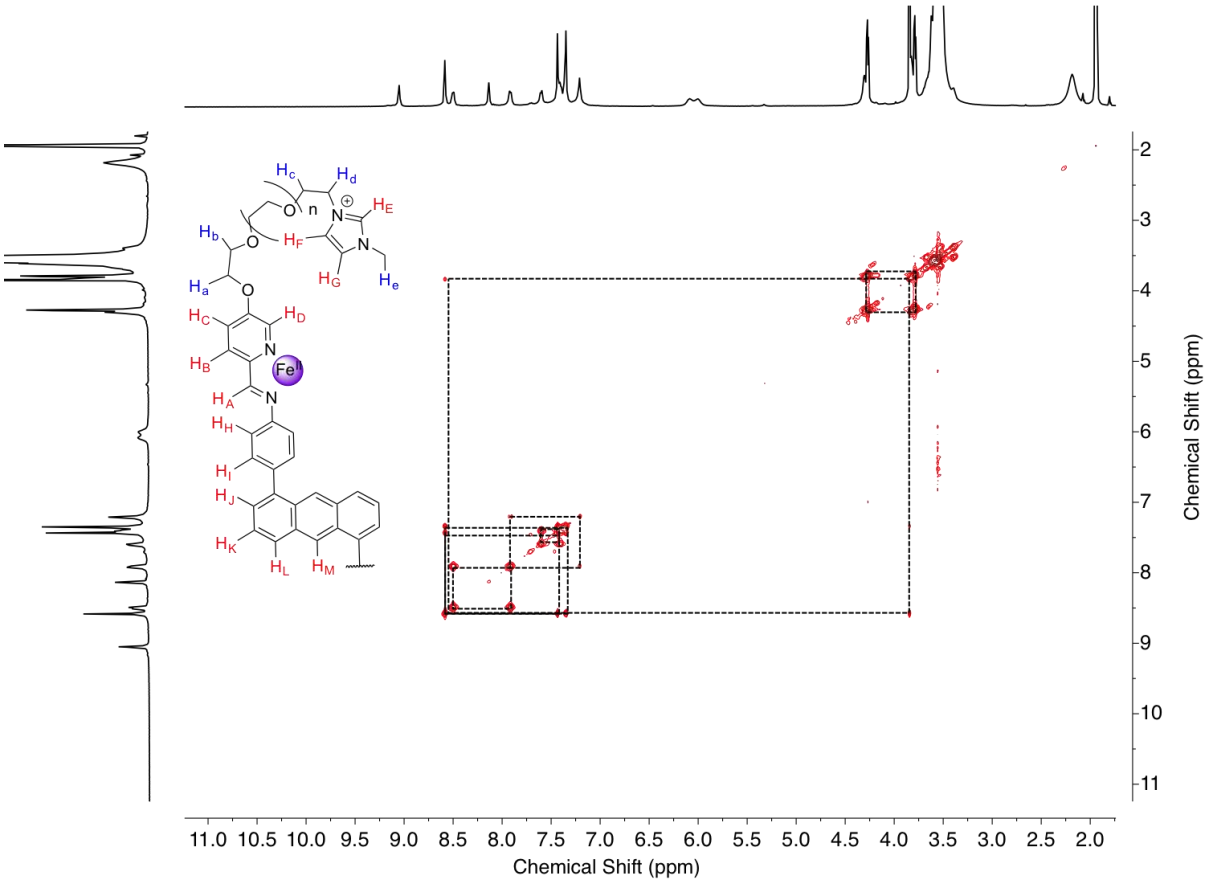

Figure S62. ^{1}H-^{1}H COSY NMR 2D spectrum of the cage 6 in CD_3CN at 298K on a 500 MHz spectrometer.

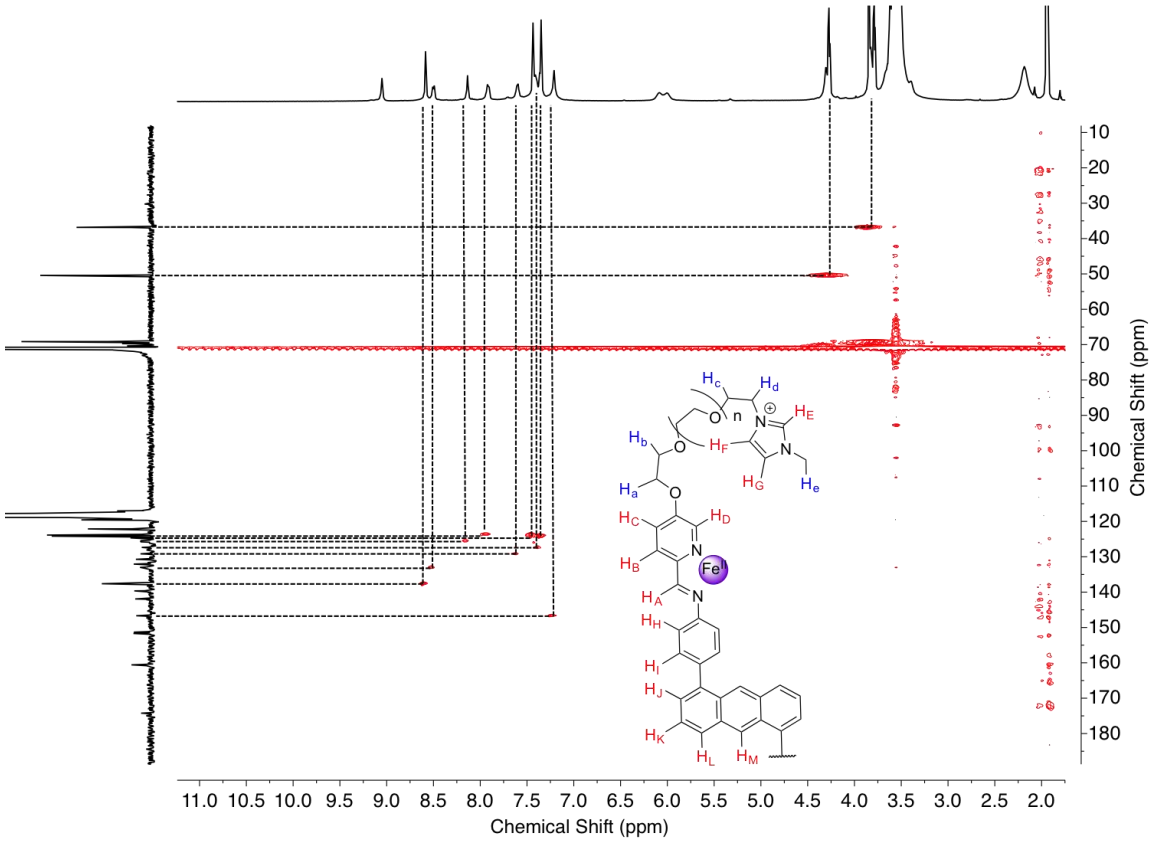

Figure S63. ^{1}H-^{13}C HSQC NMR 2D spectrum of the cage 6 in CD_3CN at 298K on a 500 MHz spectrometer.

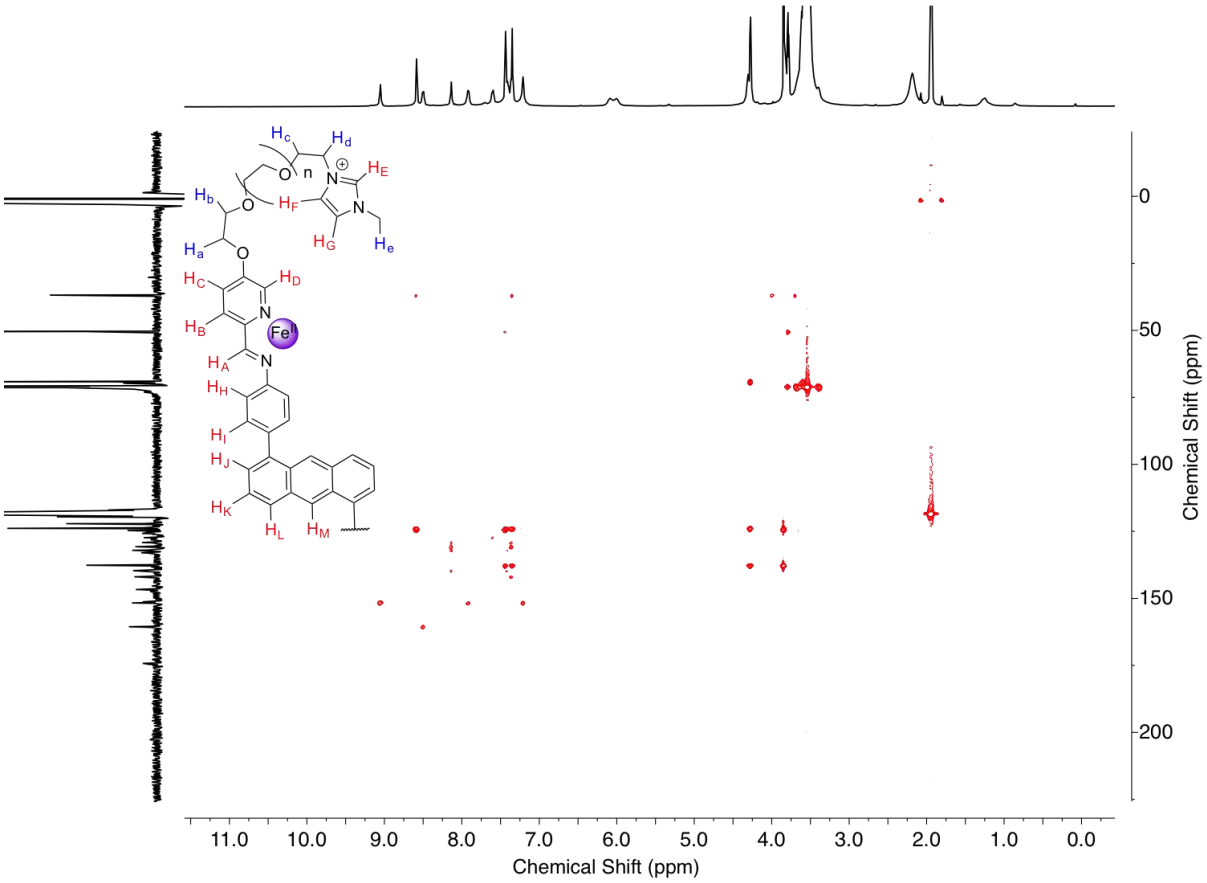

Figure S64. ^{1}H-^{13}C HMBC NMR 2D spectrum of the cage 6 in CD_3CN at 298K on a 500 MHz spectrometer.

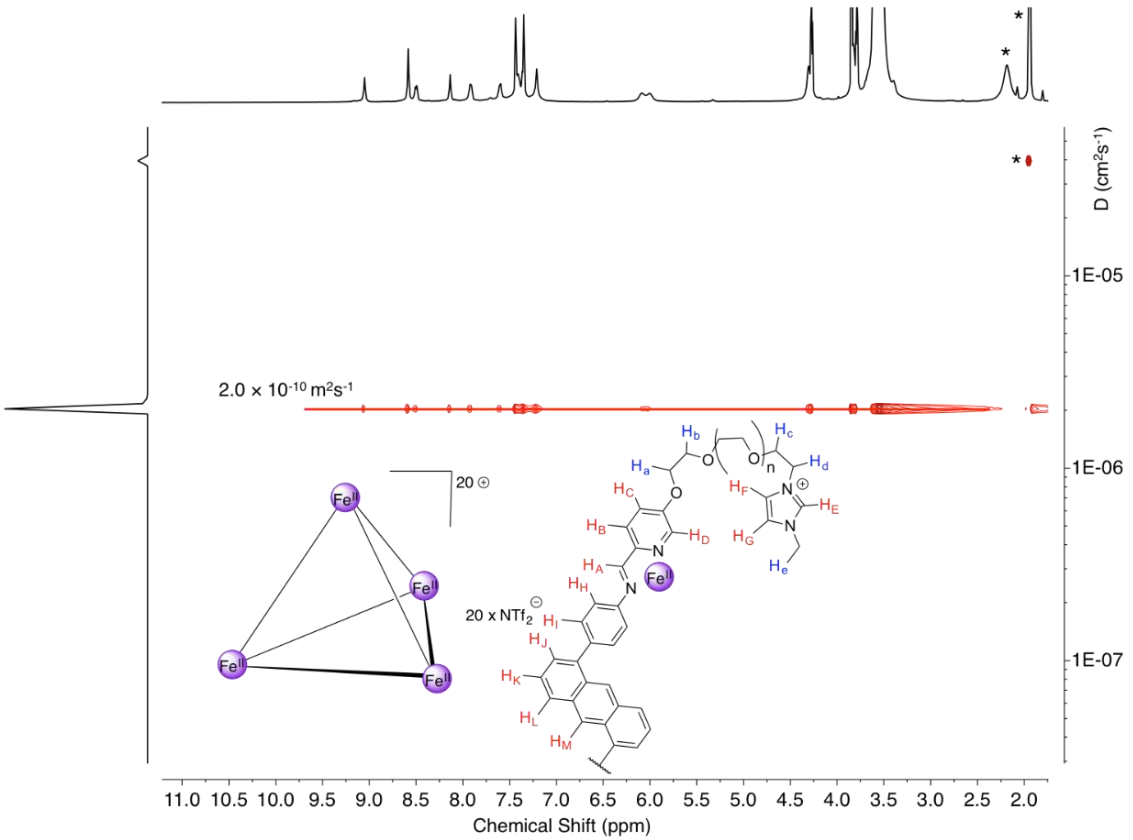

Figure S65. Diffusion Ordered NMR spectrum recorded in CD_3CN at a concentration of 1.5 mM of the cage 6 at 298K on a 400 MHz spectrometer. The diffusion coefficient was measured to be 2.0×10^{-10} m^2s^{-1}. (* Corresponds to residual solvents: acetonitrile and water).

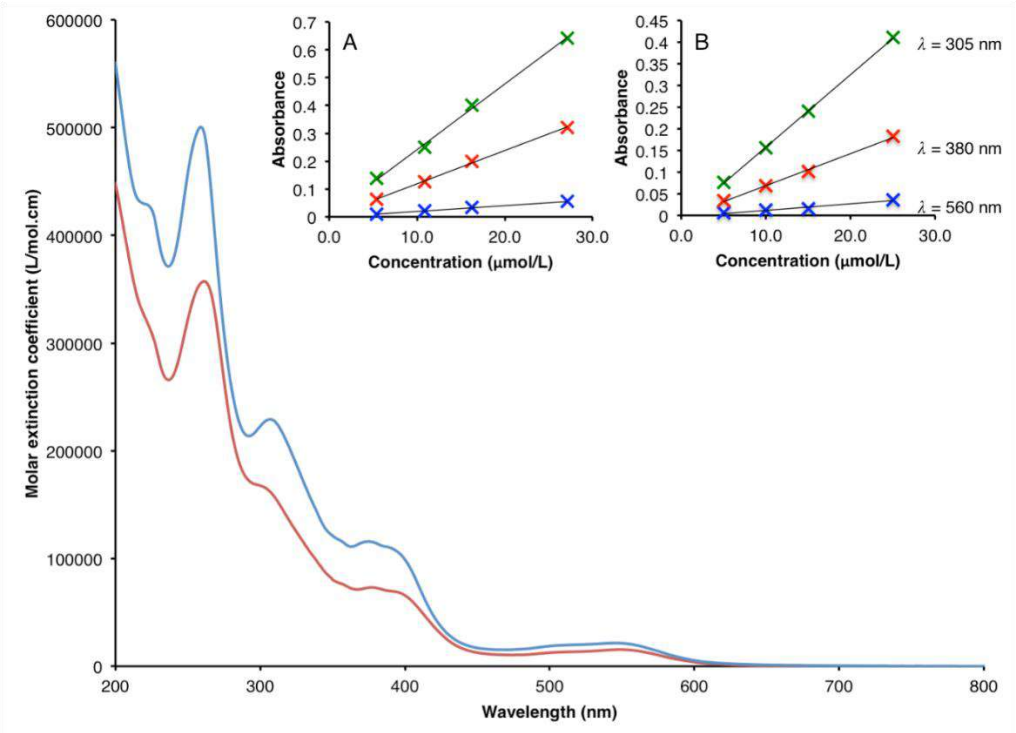

Figure S66. Electronic absorption spectra of the cage 6 at 298K in EtOAc (blue) and H_2O (red). The insets (A: CH_3CN, B: H_2O) show the linear increase of absorbance at 460, 380 and 305 nm upon the increase of the concentration (r^2= 0.998, 0.9988 and 0.9993 in CH_3CN and r^2= 0.9997, 0.998 and 0.9911 in H_2O).

10. Preparation and characterisation of cage 7

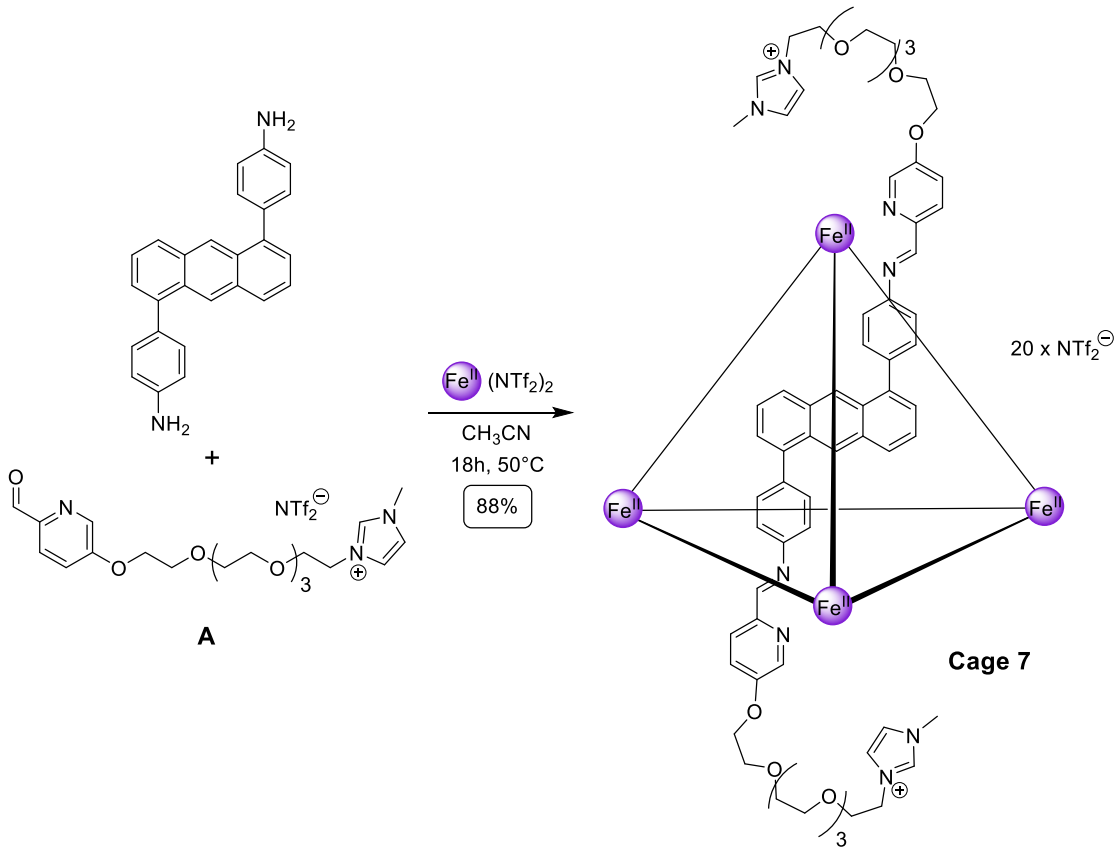

Figure S67: Self-assembly of cage 7.

Cage 7. 1,5-bis(4-aminophenyl)anthracene (1.01 mg, 2.80 µmol, 6 eq.), ligand **A** (3.86 mg, 5.61 µmol, 12 eq.) were combined in dry acetonitrile (400 µL). The solution was subjected to three evacuation/nitrogen fill cycles and $Fe(NTf_2)_2 \bullet 6H_2O$ (1.29 mg, 1.87 µmol, 4 eq.) was added. The mixture was heated at 50 °C for 18h. The solvent was evaporated and the solid triturated with diethyl ether to yield **cage 7** (6.7 mg, 88%) as a dark red sticky solid.

^{1}H NMR (500 MHz, 298 K, CD_3CN): δ 9.04 (s, 1H, H_A), 8.49 (d, *J* = 5.1 Hz, 2H, H_E & H_B), 8.14 (s, 1H, H_M), 7.88 (dd, *J* = 8.9, 2.3 Hz, 1H, H_C), 7.61 (d, *J* = 8.5 Hz, 1H, H_L), 7.47 – 7.28 (m, 5H, H_F, H_G, H_{I2}, H_K, H_J), 7.20 (s, 2H, H_D, H_{I1}), 6.04 (d, *J* = 41.7 Hz, 2H, H_{H1} & H_{H2}), 4.31 – 4.23 (m, 4H, H_a & H_d), 3.85 – 3.73 (m, 7H, H_e, H_b & H_c), 3.65 – 3.48 (m, 12H, $H_{aliphatic}$).

^{19}F NMR (376.5 MHz, 298 K, CD_3CN): *δ* -80.38 (*exo* NTf_2).

^{13}C NMR (125 MHz, 298 K, CD_3CN): δ 174.19, 160.50, 151.78, 151.29, 146.65, 141.99, 139.66, 137.35, 132.96, 132.08, 130.73, 129.20, 127.34, 125.77, 125.46, 124.67, 124.19, 123.91, 123.54, 122.12, 118.26, 71.23, 71.03, 70.97, 70.78, 70.24, 69.60, 69.18, 50.40, 36.85.

LR-ESI-MS (CH_3CN): m/z $[M\text{-}2(NTf_2)_2]^{18+}$: 423.2, $[M\text{-}6(NTf_2)_2]^{14+}$: 625.9, $[M\text{-}7(NTf_2)_2]^{13+}$: 694.7, $[M\text{-}8(NTf_2)_2]^{12+}$: 776.1, $[M\text{-}9(NTf_2)_2]^{11+}$: 872.0.

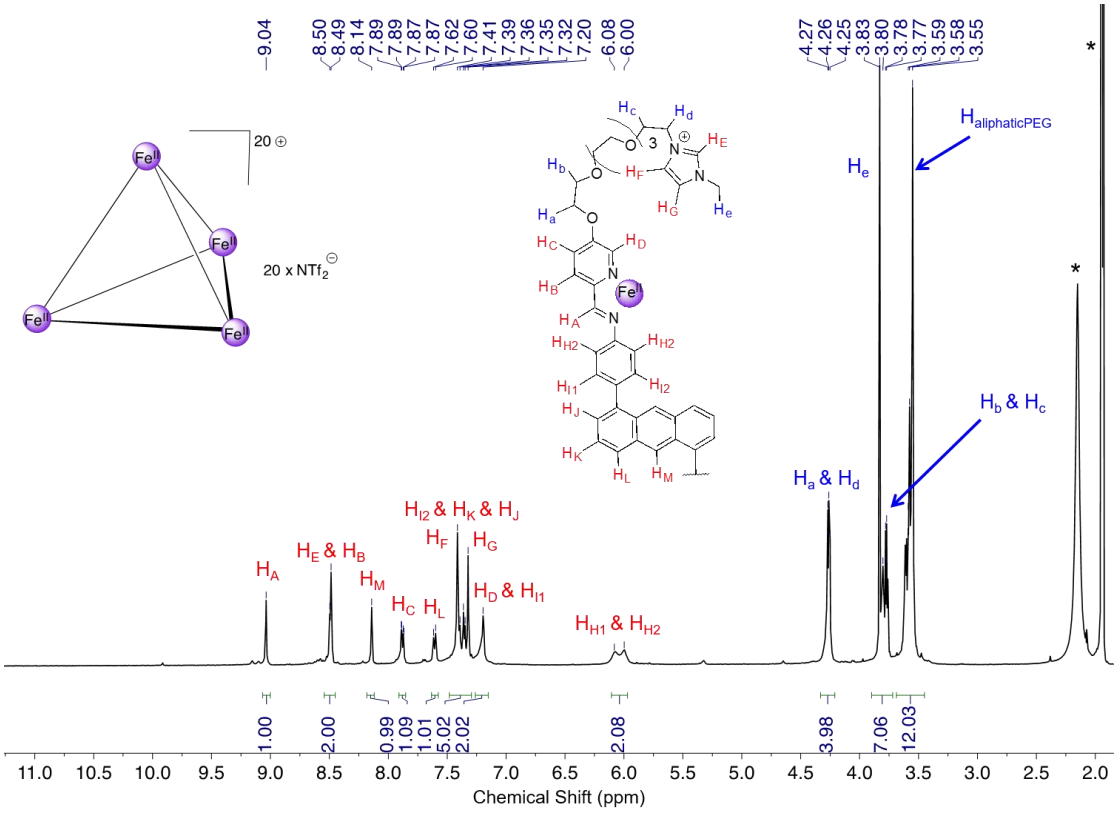

Figure S68. ^{1}H NMR spectrum of the cage 7 in CD_3CN at 298K on a 500 MHz spectrometer. (* Corresponds to residual solvents: acetonitrile and water).

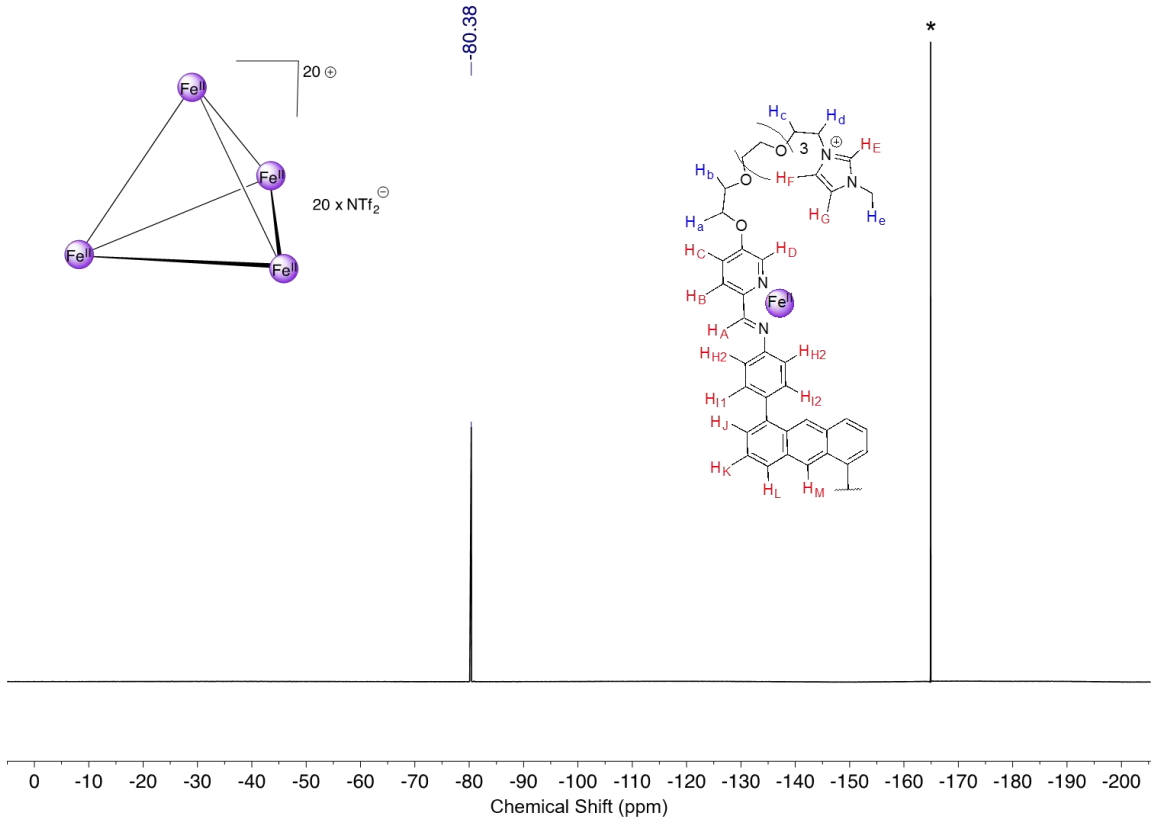

Figure S69. ^{19}F NMR spectrum of the cage 7 in CD_3CN at 298K on a 400 MHz spectrometer. (* Corresponds to the external standard C_6F_6).

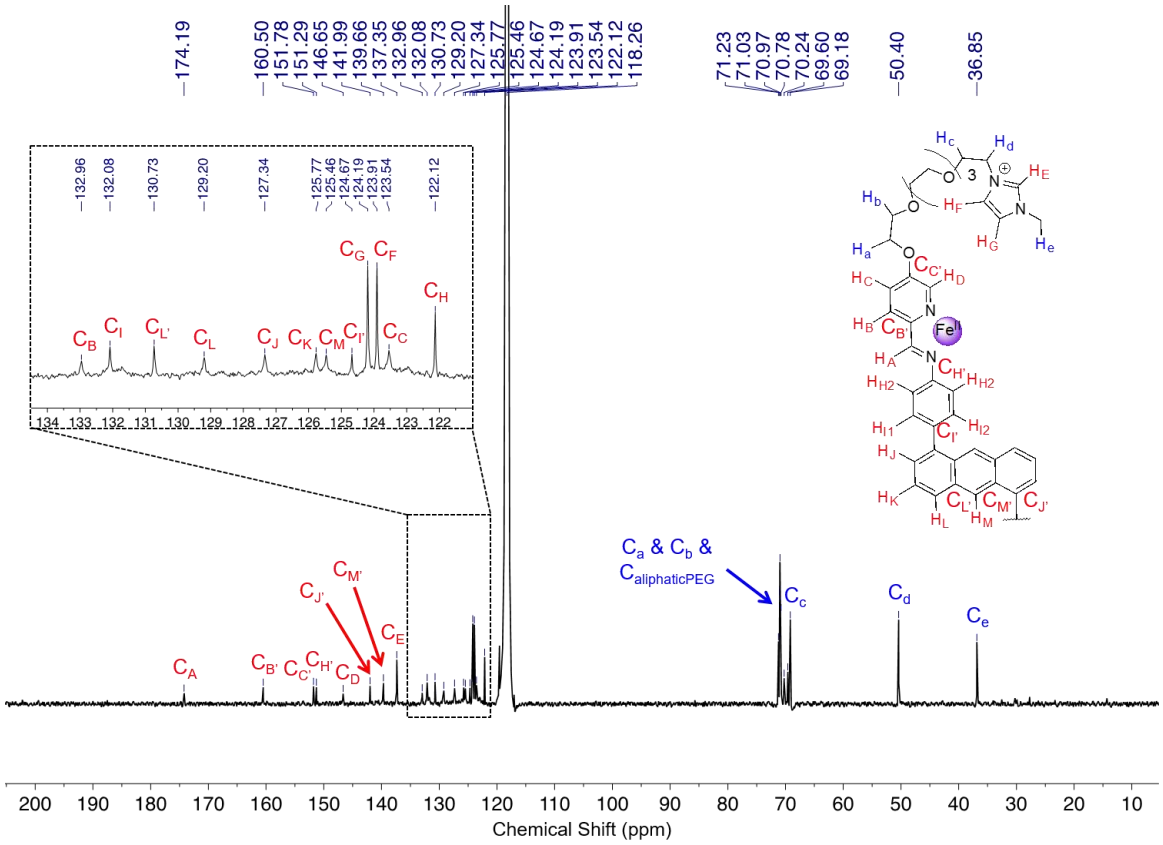

Figure S70. ^{13}C NMR spectrum of the cage 7 in CD_3CN at 298K on a 500 MHz spectrometer. (* Corresponds to residual solvents: acetonitrile and diethyl ether).

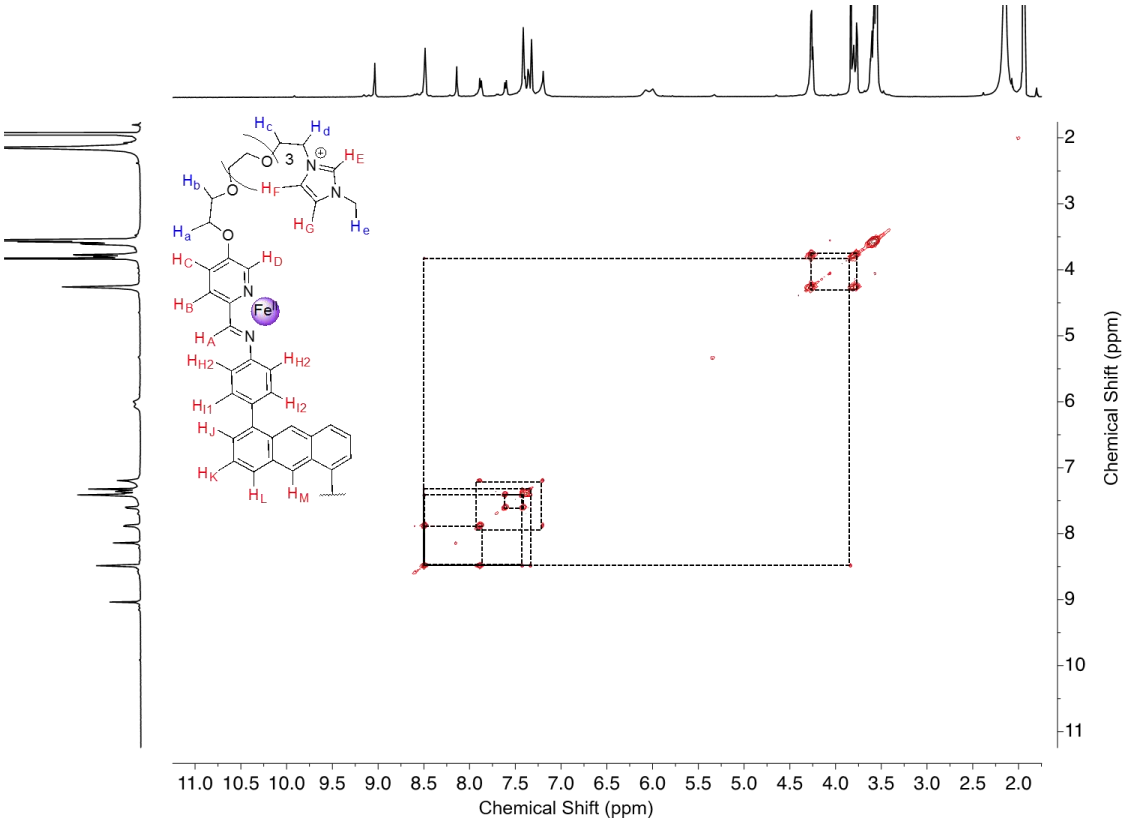

Figure S71. ^{1}H-^{1}H COSY NMR 2D spectrum of the cage 7 in CD_3CN at 298K on a 400 MHz spectrometer.

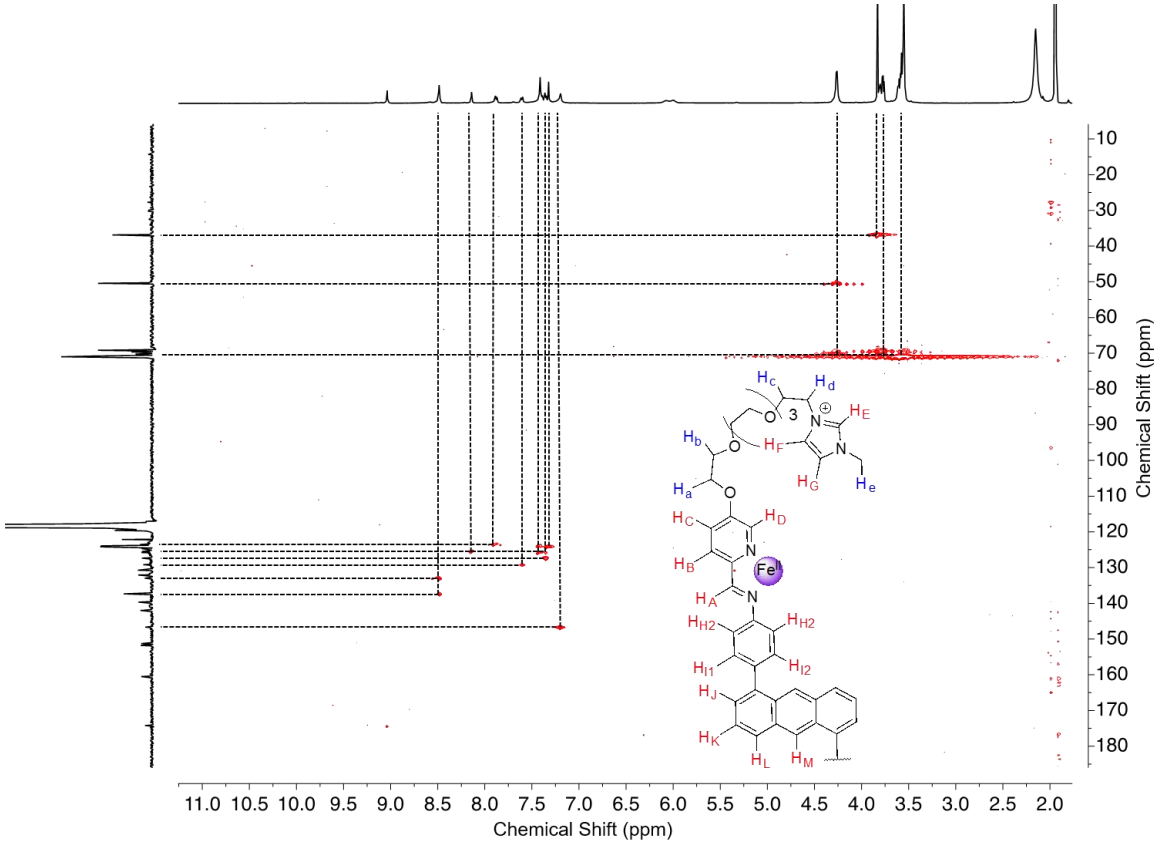

Figure S72. ^{1}H-^{13}C HSQC NMR 2D spectrum of the cage 7 in CD_3CN at 298K on a 500 MHz spectrometer.

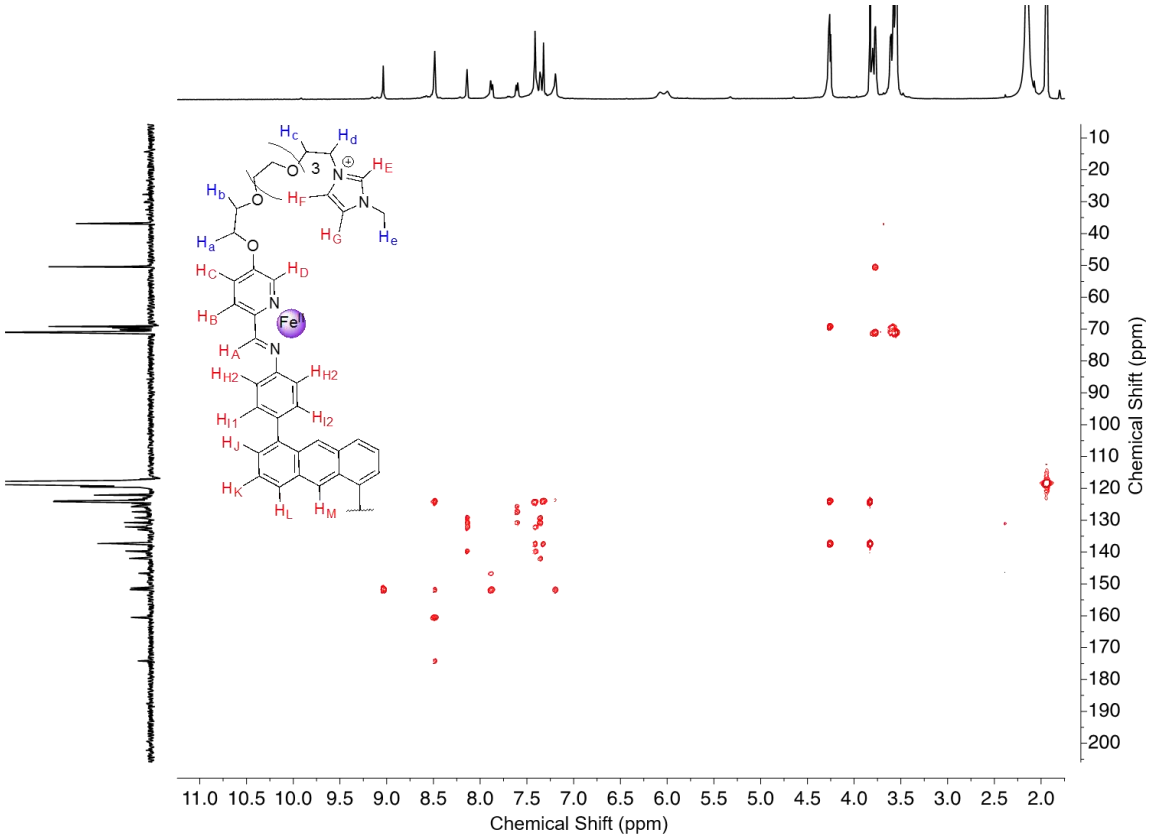

Figure S73. ^{1}H-^{13}C HMBC NMR 2D spectrum of the cage 7 in CD_3CN at 298K on a 500 MHz spectrometer.

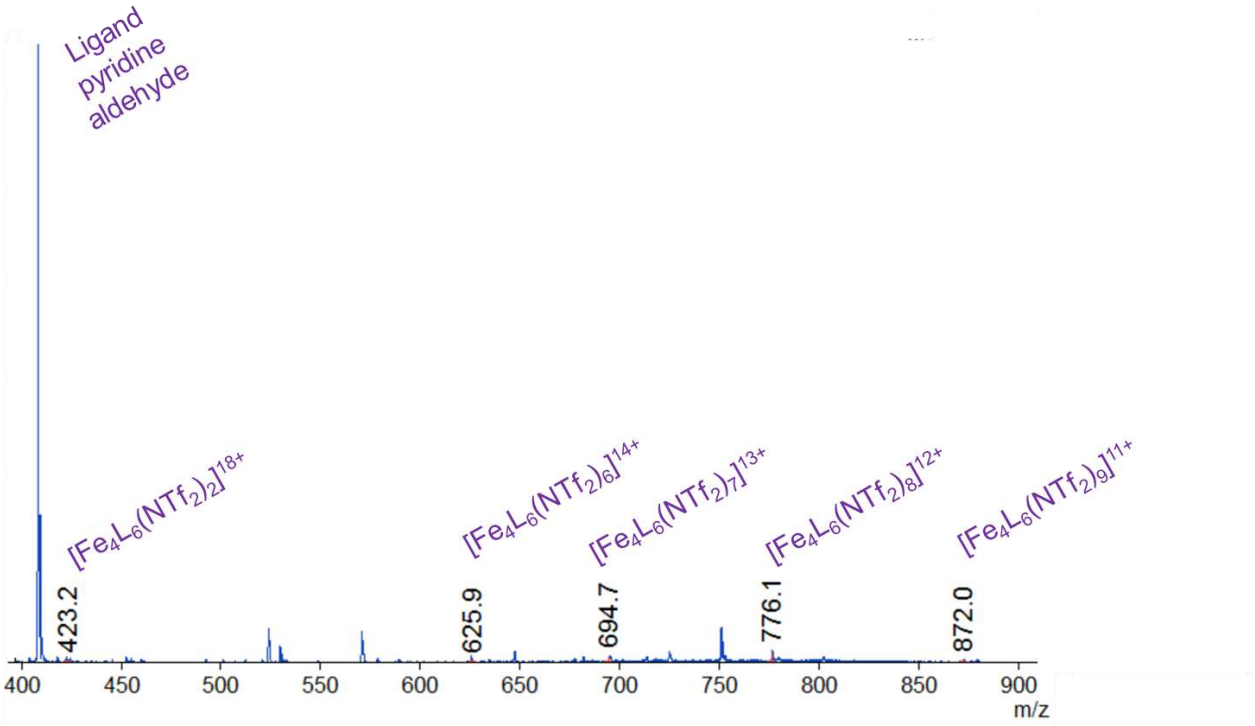

Figure S74. Low resolution ESI-MS of cage 7 in CH_3CN showing peaks corresponding to a tetrahedral architecture.

L

References

(1) Lehn, J.-M. *Angew. Chemie Int. Ed. English* **1988**, *27* (1), 89.

(2) Fischer, E. *Berichte der Dtsch. Chem. Gesellschaft* **1894**, *27* (3), 2985.

(3) Pedersen, C. J. *Angew. Chemie Int. Ed. English* **1988**, *27* (8), 1021.

(4) Cram, D. J. *Angew. Chemie Int. Ed. English* **1988**, *27* (8), 1009.

(5) Leigh, D. A. *Angew. Chemie Int. Ed.* **2016**, *55* (47), 14506.

(6) Zhang, G.; Mastalerz, M.; Fujita, M.; Hagen, S.; Mack, J.; Blank, J.; Wegner, H.; Meijere, A. de; Clarizia, G.; Jansen, J. C.; Steiner, A.; Cooper, A. I.; Steiner, A.; Day, G. M.; Cooper, A. I.; Slawin, A. M. Z.; Steiner, A.; Cooper, A. I. *Chem. Soc. Rev.* **2014**, *43* (6), 1934.

(7) Nyman, M.; Burns, P. C.; Cao, J.; Burns, P. C.; Gagliardi, L.; Cramer, C. J.; Holman, K. T.; Pope, M. T.; Su, Z. M.; Randerath, M.; Menke, C. *Chem. Soc. Rev.* **2012**, *41* (22), 7354.

(8) Paul, R. L.; Bell, Z. R.; Jeffery, J. C.; McCleverty, J. A.; Ward, M. D. *Proc. Natl. Acad. Sci. U. S. A.* **2002**, *99* (8), 4883.

(9) Mal, P.; Breiner, B.; Rissanen, K.; Nitschke, J. R. *Science (80-.).* **2009**, *324* (5935).

(10) Zhang, Q.; Tiefenbacher, K. *Nat. Chem.* **2015**, *7* (3), 197.

(11) Raynal, M.; Ballester, P.; Vidal-Ferran, A.; van Leeuwen, P. W. N. M.; Zhu, J. P.; Guo, X.; Jiang, L.-Q.; Zhang, Z.-Y.; Hu, W.-H.; Ollivier, C.; Liable-Sands, L. M.; Golen, J. D.; Zakharov, L. N.; Rheingold, A. L. *Chem. Soc. Rev.* **2014**, *43* (5), 1660.

(12) Makoto Fujita, *; Masahide Tominaga; Akiko Hori, and; Therrien, B. **2005**.

(13) Dietrich-Buchecker, C. O.; Sauvage, J. P. *Chem. Rev.* **1987**, *87* (4), 795.

(14) Beves, J. E.; Blight, B. A.; Campbell, C. J.; Leigh, D. A.; McBurney, R. T. *Angew. Chemie Int. Ed.* **2011**, *50* (40), 9260.

(15) Ponnuswamy, N.; Cougnon, F. B. L.; Clough, J. M.; Pantos, G. D.; Sanders, J. K. M. *Science (80-.).* **2012**, *338* (6108), 783.

(16) Ashton, P. R.; Ballardini, R.; Balzani, V.; Credi, A.; Dress, K. R.; Ishow, E.; Kleverlaan, C. J.; Kocian, O.; Preece, J. A.; Spencer, N.; Stoddart, J. F.; Venturi, M.; Wenger, S. *Chem. - A Eur. J.* **2000**, *6* (19), 3558.

(17) Chakrabarty, R.; Mukherjee, P. S.; Stang, P. J. *Chem. Rev.* **2011**, *111* (11), 6810.

(18) Fujita, M.; Oguro, D.; Miyazawa, M.; Oka, H.; Yamaguchi, K.; Ogura, K. *Nature* **1995**, *378* (6556), 469.

(19) Cook, T. R.; Zheng, Y.-R.; Stang, P. J. *Chem. Rev.* **2013**, *113* (1), 734.

(20) Caulder, D. L.; Raymond, K. N.; Dupont-Gervais, A.; VanDorsselaer, A.; Charbonniére, L. J.; Williams, A. F.; Ogura, K.; Bill, E.; Müther, M.; Trautwein, A. X.; Thomas, C. D.;

Shaw, W. V.; Harrison, P. M. *J. Chem. Soc. Dalt. Trans.* **1999**, *36* (8), 1185.

(21) Dalgarno, S. J.; Power, N. P.; Atwood, J. L. *Coord. Chem. Rev.* **2008**, *252* (8–9), 825.

(22) Hastings, C. J.; Pluth, M. D.; Bergman, R. G.; Raymond, K. N. *J. Am. Chem. Soc.* **2010**, *132* (20), 6938.

(23) Yoshizawa, M.; Takeyama, Y.; Kusukawa, T.; Fujita, M. *Angew. Chemie Int. Ed.* **2002**, *41* (8), 1347.

(24) Suzuki, K.; Sato, S.; Fujita, M. *Nat. Chem.* **2010**, *2* (1), 25.

(25) Nitschke, J. R. *Angew. Chemie Int. Ed.* **2004**, *43* (23), 3073.

(26) Mal, P.; Schultz, D.; Beyeh, K.; Rissanen, K.; Nitschke, J. *Angew. Chemie Int. Ed.* **2008**, *47* (43), 8297.

(27) Riddell, I. A.; Smulders, M. M. J.; Clegg, J. K.; Nitschke, J. R.; Mendoza, J. de; Maverick, A. W.; Batten, S. R.; Yamaguchi, K.; Fujita, M.; Trautwein, A. X.; Yildirim, T.; Zhou, W. *Chem. Commun.* **2011**, *47* (1), 457.

(28) Bolliger, J. L.; Ronson, T. K.; Ogawa, M.; Nitschke, J. R. *J. Am. Chem. Soc.* **2014**, *136* (41), 14545.

(29) Earle, M. J.; Seddon, K. R. 2002; pp 10–25.

(30) Winterton, N.; Khokhlov, A. R.; Potemkin, I. I.; Ishikawa, M.; Noda, A.; Watanabe, M.; Waymouth, R. M.; Aida, T.; Russell, A. J. *J. Mater. Chem.* **2006**, *16* (44), 4281.

(31) Zhao, H. *J. Chem. Technol. Biotechnol.* **2010**, *85* (7), 891.

(32) Polo-Luque, M. L.; Simonet, B. M.; Valc?rcel, M. *TrAC Trends Anal. Chem.* **2013**, *47*, 99.

(33) Chiappe, C.; Pieraccini, D. *J. Phys. Org. Chem.* **2005**, *18* (4), 275.

(34) Meine, N.; Benedito, F.; Rinaldi, R.; Maupin, P. H.; Long, H. C. De; Truvole, P. C.; Jastorff, B.; DeLong, H. C.; Fox, D. M. *Green Chem.* **2010**, *12* (10), 1711.

(35) Ahrens, S.; Peritz, A.; Strassner, T. *Angew. Chemie Int. Ed.* **2009**, *48* (42), 7908.

(36) Grommet, A. B.; Bolliger, J. L.; Browne, C.; Nitschke, J. R. *Angew. Chemie Int. Ed.* **2015**, *54* (50), 15100.

(37) Grommet, A. B.; Nitschke, J. R. *J. Am. Chem. Soc.* **2017**, *139* (6), 2176.

(38) Yao, W.; Wang, H.; Cui, G.; Li, Z.; Zhu, A.; Zhang, S.; Wang, J. *Angew. Chemie Int. Ed.* **2016**, *55* (28), 7934.

(39) Fenn, E. E.; Moilanen, D. E.; Levinger, N. E.; Fayer, M. D. *J. Am. Chem. Soc.* **2009**, *131* (15), 5530.

(40) Li, X.; Hou, M.; Zhang, Z.; Han, B.; Yang, G.; Wang, X.; Zou, L.; Li, W. J. *Green Chem.* **2008**, *10* (8), 879.

(41) Gurkan, B. E.; Gohndrone, T. R.; McCready, M. J.; Brennecke, J. F.; Nanjo, H.; Kato, M.; Brennecke, J. F.; Wu, H.; Glaser, M. F.; Shah, J. K.; Maginn, E. J.; Brennecke, J. F.; Schneider, W. F. *Phys. Chem. Chem. Phys.* **2013**, *15* (20), 7796.

(42) Mitrev, Y. N. *Bulg. Chem. Commun.* **2017**, *49*, 65.

(43) Krachkovskiy, S. A.; Pauric, A. D.; Halalay, I. C.; Goward, G. R. *J. Phys. Chem. Lett.* **2013**, *4* (22), 3940.

(44) Niklas, T.; Stalke, D.; John, M.; John, M.; Eyring, E. M.; John, M.; Mata, R. A.; Stalke, D. *Chem. Commun.* **2015**, *51* (7), 1275.

(45) Evans, R.; Sandhu, A.; Bridgwater, T.; Chong, K. *Energy & Fuels* **2017**, *31* (4), 4135.

(46) Ronson, T. K.; Pilgrim, B. S.; Nitschke, J. R. *J. Am. Chem. Soc.* **2016**, *138* (33), 10417.

(47) M. Seredyuk, †; A. B. Gaspar, *,‡; V. Ksenofontov, †; Y. Galyametdinov, §; J. Kusz, ‖ and; P. Gütlich*, †. **2008**.

(48) Ji, L.; Yang, Z.; Zhao, Y.; Sun, M.; Cao, L.; Yang, X.-J.; Wang, Y.-Y.; Wu, B.; Janiak, C.; Zhang, Z.; Wang, Y.-Y.; Wu, B. *Chem. Commun.* **2016**, *52* (45), 7310.

(49) Clegg, J. K.; Cremers, J.; Hogben, A. J.; Breiner, B.; Smulders, M. M. J.; Thoburn, J. D.; Nitschke, J. R. *Chem. Sci.* **2013**, *4* (1), 68.

(50) Giernoth, R.; Bankmann, D. *European J. Org. Chem.* **2005**, *2005* (21), 4529.